

TECHNISCHE UNIVERSITÄT MÜNCHEN

Lehrstuhl für Lebensmittelchemie und Molekulare Sensorik

**Activity-guided discovery of antioxidants
in processed garlic extracts**

Junichiro Wakamatsu

Vollständiger Abdruck der von der Fakultät Wissenschaftszentrum
Weihenstephan für Ernährung, Landnutzung und Umwelt der Technischen
Universität München zur Erlangung des akademischen Grades eines

Doktors der Naturwissenschaften

genehmigten Dissertation.

Vorsitzender:

Prof. Dr. Wilfried Schwab

Prüfer der Dissertation:

1. Prof. Dr. Thomas F. Hofmann

2. Prof. Dr. Michael Rychlik

Die Dissertation wurde am 20.11.2017 bei der Technischen Universität
München eingereicht und durch die Fakultät Wissenschaftszentrum
Weihenstephan für Ernährung, Landnutzung und Umwelt am 03.05.2018
angenommen.

Acknowledgment

The experimental work of this Ph.D thesis has been carried out under the supervision of Professor Dr. Thomas Hofmann between 2012 and 2016 at the chair of food chemistry and molecular sensory science, Germany.

First, I would like to show the deepest appreciation to Professor Dr. Thomas Hofmann for his acceptance of a research seed which I proposed and his direction for my research. His great superintendence and fruitful mentorship for four years enabled me to achieve a series of my research regarding this thesis.

Next, I would like to express my sincere gratitude to my mentor Dr. Timo D. Stark for his great support on my research as well as my private life in Germany. My family and I could not reach the current situation without his support and cooperation. In addition, I appreciate to all members of the institute. In particular, Dr. Oliver Frank and his working group had made a great effort to measure NMR spectra of my analytical samples, Mr. Ludwig Friedrich gave me a special cooperation on data interpretation, and the lab 4-mates have kept a very good atmosphere in our working places everyday.

I would like to show deep appreciation to President Mr. Kanji Wakunaga and Vice President Mr. Hironobu Wakunaga of Wakunaga Pharmaceutical Co., Ltd, Japan for giving me an opportunity to do this research at TUM. Dr. Takami Oka had been giving me constructive comments and warm encouragement.

I am deeply grateful to Dr. Yoshihide Ikeuchi, Dr. Ryuichi Tatsumi, and Dr. Wataru Mizunoya for coaching me how to do research during my undergraduate and graduate education at Kyushu University in Japan. All experiences that I had taken in the time greatly contribute to the bottom of my current working style.

Finally, I want to thank my parents, sons, wife, and all relatives for their daily support. Especially, my wife's advice regarding organic chemistry and NMR interpretation were very precious and helpful for me to achieve my research.

Publication

Wakamatsu, J.; Stark, T.D.; Hofmann, T. Investigations on structure-activity relationship of new Maillard reaction products generated from *S*-allyl-L-cysteine and D-glucose. 11th Wartburg symposium, **2016**, poster presentation.

Wakamatsu, J.; Stark, T.D.; Hofmann, T. Taste-active Maillard reaction products in roasted garlic (*Allium sativum*). *J. Agric. Food Chem.* **2016**, 64, 5845—5854.

1 Introduction

1.1 Reactive oxygen species and antioxidants

1.2 Maillard reaction and antioxidative products

1.3 Garlic

1.3.1 Botany and use of garlic

1.3.2 Chemical composition of garlic

1.3.3 Taste and pharmacological activities of garlic constituents

1.4 Garlic preparations

1.4.1 Non-thermally processed garlic preparations

1.4.2 Thermally processed garlic preparation

1.5 Objectives

2 Results and discussion

2.1 Influence of thermal processing on the antioxidant activity of AGE

2.1.1 Influence of heating time and temperature on antioxidant activity of AGE

2.1.2 Influence of pH on antioxidant activity of processed AGE

2.1.3 Optimization of heating temperature and time for generation of increased antioxidative activity

2.2 Activity-guided fractionation of processed AGE and identification of antioxidants

2.2.1 Separation of processed AGE by means of ultrafiltration.

2.2.2 MPLC separation of low molecular weight fraction of the pAGE

2.2.3 Isolation and structure elucidation of antioxidants in MPLC fraction No.4

2.2.4 Isolation and structure elucidation of antioxidants in MPLC fraction No.5

2.2.5 Isolation and structure elucidation of antioxidants in MPLC fraction No.6

2.2.6 Isolation and structure elucidation of antioxidants in MPLC fraction No.7

2.3 Generation, isolation and identification of sulfur-containing compounds, spiro-alkaloids, and a pyrrole derivative in model systems

2.3.1 Development of a model reaction between S-allyl-L-cysteine and D-glucose

2.3.2 Isolation and structure determination of sulfur-containing compounds, spiro-alkaloids, and a new pyrrole derivative (27—35)

2.3.3 Identification of isolated compounds **27—35** in pAGE

2.4 Proposed reaction pathways governing the formation of compounds 1—37

2.4.1 Formation of pyrazine derivatives **1, 2, 4, 5, 7, 17, 22** and **25**

2.4.2 Formation of amino acid pyrrole derivatives **3, 11, 13, 19, 23, 26,** and **32—37**

- 2.4.3 Formation of a citric acid derivative, spiro-alkaloids and a pyrrole derivative (compounds **21** and **27—31**)
- 2.4.4 Formation of compounds **8, 12** and **14**
- 2.4.5 Formation of glutamic acid derivatives **15** and **20**
- 2.4.6 Formation of the pyridine derivative **24**

2.5 Identification of known compounds in pAGE by means of LC-MS/MS

2.6 Quantitative analysis of the identified compounds

- 2.6.1 Quantitative analysis of all compounds identified on the processed and non-processed AGE powder
- 2.6.2 Quantitation of compounds **27—35** in garlic preparations
- 2.6.3 Influence of processing conditions on the generation of thermally produced compounds **1—35** in pAGE

2.7 Antioxidant, taste, and pharmacological activities of the identified compounds

- 2.7.1 Chemical antioxidant activity
- 2.7.2 Taste activity
- 2.7.3 Taste modulating effect
- 2.7.4 Pharmacological activity
 - 2.7.4.1 Modulation effect on intracellular antioxidant system
 - 2.7.4.2 Modulation effect on immunoglobulin A (IgA) production in mouse lymphocytes
 - 2.7.4.3 Modulation effect on interleukin-6 (IL-6) production in mouse lymphocytes
- 2.7.5 Comparison of bioactivity of compounds **34** and **35**

3 Materials and methods

3.1 Chemicals and materials

3.2 In vitro antioxidant assays

- 3.2.1 ORAC (Oxygen radical absorbance capacity) assay
- 3.2.2 ABTS radical scavenging (ARS) assay

3.3 Investigation of processing conditions for processed AGE powder with high antioxidative activity

- 3.3.1 Preparation of powdered AGE containing four levels of water content and heat-processing
- 3.3.2 Preparation of powdered AGE derived from pH-controlled liquified AGE and heat-processing

- 3.3.3 Optimization of heating temperature and time for generation of high antioxidative activity in powdered AGE

3.4 Fractionation of processed AGE (pAGE)

- 3.4.1 Ultrafiltration of pAGE
- 3.4.2 MPLC separation of pAGE and evaluation of antioxidative activities
- 3.4.3 Isolation and structure elucidation of antioxidants obtained from MPLC fraction No.4
- 3.4.4 Isolation and structure elucidation of antioxidants obtained from MPLC fraction No.5
- 3.4.5 Isolation and structure elucidation of antioxidants obtained from MPLC fraction No.6
- 3.4.6 Isolation and structure elucidation of antioxidants obtained from MPLC fraction No.7

3.5 Model reactions for generation of sulfur-containing compounds, spiro-alkaloids and a new pyrrole derivative (27—35)

- 3.5.1 Preparation of reaction matrices for screening study
- 3.5.2 Extraction and isolation of target compounds
- 3.5.3 Purification and structure elucidation of compounds **27—35**
- 3.5.4 Synthesis, purification and structure elucidation of decarboxylates of compounds **34** and **35**
- 3.5.5 Model reactions using S-allyl-L-cysteine and S-allyl-D-cysteine
- 3.5.6 Identification of isolated compounds (**27—37**) in pAGE

3.6 Model reactions for proposal of generation pathways on isolated compounds 8, 15, 20, 21 and 26

3.7 Identification of known antioxidative compounds in pAGE

3.8 Quantitative analyses of identified compounds

- 3.8.1 Quantitative analysis of compounds **1—37** in processed and non-processed AGE powder
- 3.8.2 Quantitative analysis of compounds **38—41** and **45—55** in processed and non-processed AGE powder
 - 3.8.2.1 Quantitation of compounds **38—41** and **51—54**
 - 3.8.2.2 Quantitation of compounds **45—50** and **55**
- 3.8.3 Quantitative analysis of compounds **27—35** in garlic preparations
- 3.8.4 Quantitative analysis of compounds **1—35** in re-processed AGE powder

3.9 Evaluation of identified compounds on antioxidative and taste activity, taste modulating effect, and pharmacological activities

3.9.1 Evaluation of antioxidative activity

3.9.2 Evaluation of taste activity

3.9.2.1 Panel training

3.9.2.2 Bitter taste threshold

3.9.3 Evaluation of kokumi-enhancement in a model broth

3.9.4 Evaluation of pharmacological activity

3.9.4.1 Modulation effect on intracellular antioxidant system

3.9.4.2 Modulation effect on immunoglobulin A (IgA) production in mouse lymphocytes

3.9.4.3 Modulation effect on interleukin 6 (IL-6) production in mouse lymphocytes

3.10 Chromatographic methods

3.10.1 Gradient medium pressure liquid chromatography (MPLC)

3.10.2 Analytical high performance liquid chromatography (HPLC)

3.10.3 Semipreparative high performance liquid chromatography (semipreparative HPLC)

3.11 Spectroscopic methods

3.11.1 Nuclear magnetic resonance spectrometry (NMR)

3.11.2 Time of flight mass spectrometry (TOF-MS)

3.11.3 Tandem mass spectrometry (MS/MS)

3.11.4 Circular dichroism spectrometry (CD)

3.11.5 Specific optical rotation

4 Summary

5 Cited Literature

Abbreviations

ARS	ABTS radical scavenging
CD ₃ OD	deuterated methanol
CDCl ₃	deuterated chloroform
CE	collision energy
COSY	correlated spectroscopy
D ₂ O	deuterium oxide
DAD	diode array detector
dd	double of doublets
DMSO- <i>d</i> ₆	deuterated dimethylsulfoxide
ESI	electrospray ionization
GCLM	glutamate-cysteine ligase modifier subunit
HMBC	heteronuclear multiple bond coherence spectroscopy
HO-1	hemoxygenase-1
HPLC	high performance liquid chromatography
HSQC	heteronuclear single quantum coherence spectroscopy
m	multiplet
MeOH	methanol
MR	Maillard reaction
MRM	multiple reaction monitoring
MS/MS	tandem mass spectrometry
n.d.	not detected
ORAC	oxygen radical absorbance capacity
q	quartet
RNS	reactive nitrogen species
ROS	reactive oxygen species
RP	reversed phase
RT	room temperature
s	singlet
t	triplet
TMS	trimethylsilane
TOF	time of flight
UPLC	ultra performance liquid chromatography
UV/Vis	ultraviolet visible spectrometry

Symbols

J	coupling constant [Hz]
m/z	mass-to-charge ratio
σ	chemical shift [ppm]
λ	wavelength [nm]

1 Introduction

1.1 Reactive oxygen species (ROS) and antioxidants

Aerobic organisms utilize oxygen for energy metabolism to live. During oxidative phosphorylation, oxygen is however incompletely reduced to reactive oxygen species (ROS), e.g. hydrogen peroxide, superoxide anion radicals and hydroxyl radicals. According to a study (*Tahara et al., 2009*), ROS formation is less than 0.2% of oxygen consumption in most tissues. Such marginal ROS have important roles to operate cellular systems. For example, mitochondria are the powerhouses of the cells producing a considerable share of cellular ATP with consumption of oxygen, then mitochondrial ROS generated are essential for the elimination of bacteria by macrophages (*West et al., 2011*), the induction of differentiation of hematopoietic progenitors in fruit flies (*Owusu-Ansah et al., 2009*), and the control of insulin release in pancreatic β -cells (*Sakai et al., 2003*).

On the other hand, an excessively elevated ROS level induced by smoking, overeating, overdrinking, stressful daily life and aging could be one of triggers for cellular oxidation related disease such as diabetes, cancer and Parkinson's disease due to oxidation of cellular biological components, for instance lipids, proteins and DNA (*Szatrowski et al., 1991, Zhang et al., 1999, Anderson et al., 2009*). These studies indicate that lowering ROS level is necessary for health balancing redox state in cells.

The aerobic organisms originally have developed a very efficient defense network with several antioxidants including small molecules and enzymes against such oxidative stress, which enables to control cellular redox-balance instead of undesirable disorders in case of the normal ROS situation. *Niki (2010)* proposed that functions of the antioxidants in vivo would be classified into preventing antioxidants, scavenging antioxidants and repairing antioxidants, however the direct repairing effect on damaged cellular components by antioxidants is questionable because of no scientific evidences for it. Therefore, main roles of antioxidants would be the former two functions (**Figure 1**).

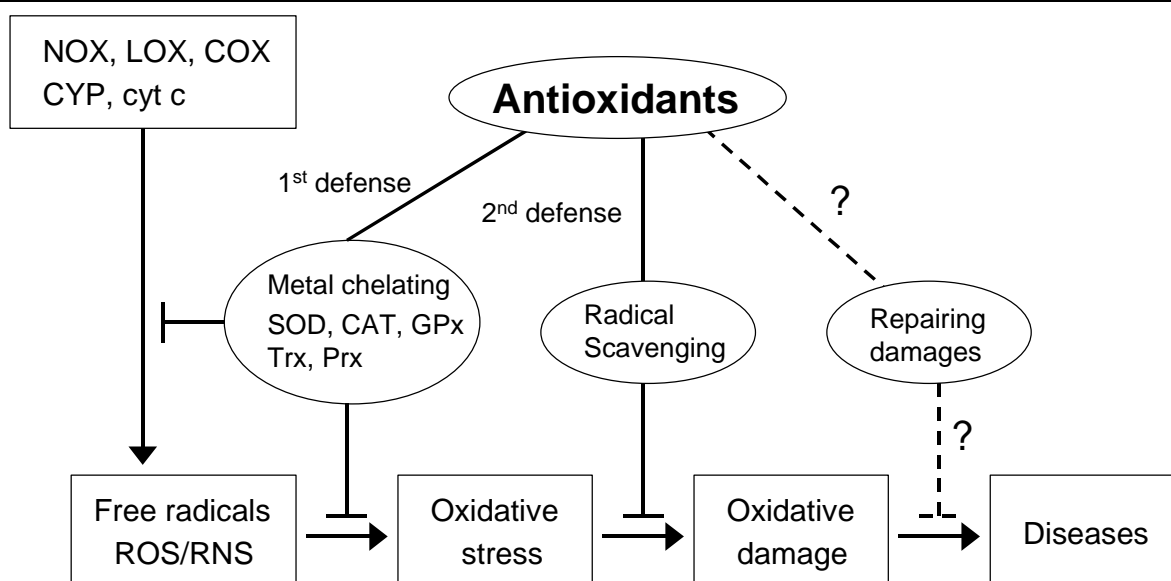


Figure 1. In vivo defense network against oxidative stress (taken from *Niki et al., 2010* with some modifications).

At the first line of defense, preventing antioxidants, for example superoxide dismutase (SOD), catalase (CAT), phospholipid-hydroperoxide glutathione peroxidase (GPx), thioredoxin (Trx) and peroxiredoxin (Prx), suppress the generation of free radicals by ROS generated by metabolism-related enzymes such as NADPH oxidase (NOX), lipoxygenase (LOX), cyclooxygenase (COX), cytochrome P450 (CYP), cytochrome c oxidase (cyt c). Additionally, antioxidative proteins like as transferrin, ferritin and lactoferrin can sequester oxidative metal ions (iron and copper) resulting in prevention of the formation of ROS.

Thereafter, the scavenging antioxidants remove the reactive species rapidly before they attack biologically essential molecules. Not only endogenous vitamins (A, C and E) in cells, but also exogenous antioxidants play an important role. Interestingly, vitamin A (β -carotene), C (ascorbic acid) and E (α -tocopherol) could act complementarily to generate greater antioxidant activity. *Niki (1995)* found a cooperative inhibition effect on LDL oxidation by using β -carotene and α -tocopherol. Ascorbic acid rapidly reduces α -tocopheroxy radicals to regenerate α -tocopherol, thus resulting in a synergistic antioxidant activity as well as suppression of a further oxidation by the α -tocopheroxy radicals (*Packer et al., 1979*).

In addition to the endogenous antioxidants, phenolic compounds and flavonoids, such as ferulic acid, resveratrol, quercetin and catechins are known as exogenous antioxidants. Recently, extraordinary strong antioxidants with biflavone-structure were discovered in *Garcinia buchananii* by Stark et al (2012, 2014) (**Figure 2**). In particular, manniflavanones (**Figure 2—E and—F**) exhibit strong antioxidant activity.

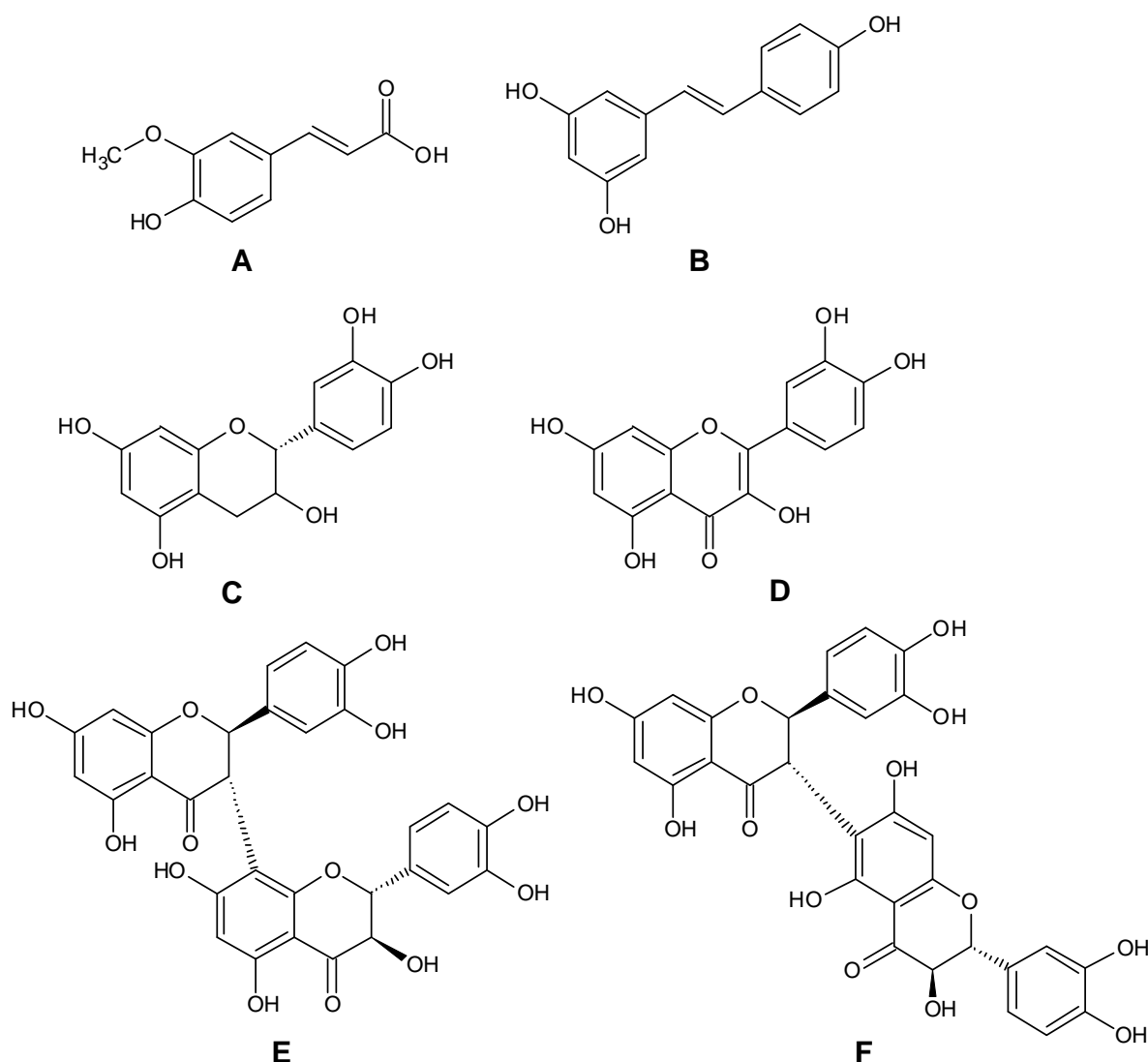


Figure 2. Chemical structure of known antioxidants, namely ferulic acid (**A**), resveratrol (**B**), (+)-catechin (**C**), quercetin (**D**), (2R,3S,2''R,3''R)-manniflavanon (**E**) and (2R,3S,2''R,3''R)-isomanniflavanon (**F**).

1.2 Maillard reaction and antioxidative products

The reaction between the carbonyl group of reducing carbohydrates and the amino group of free amino acids as well as the amino function of proteins is known as the initial step of the Maillard reaction (MR), which is observed during thermal processing and storage of food at ambient temperatures (*Labuza et al., 1981, Rystov et al., 2011*). MR is a type of non-enzymatic browning reaction and is also related to aroma and taste changing, and therefore it has been a central and major challenge in food industry for improving the appearance of food products.

The chemistry underlying MR is very complex, and a reaction pathway proposed by *Hodge et al. (1953)* is widely agreed as the primary cascade that progresses in three steps. First, carbonyl functions of sugars react with amino functions of amino acids, and conjugates called as Schiff bases are formed, then the conjugates are transformed into Amadori products through rearrangement. Subsequently, the Amadori products are degraded, followed by the production of reactive dicarbonyls, such as e.g. 1-deoxyglucosone, 3-deoxyglucosone and methylglyoxal, and, then, the highly reactive bicarbonyls successively reacted with other compounds in the reaction matrix. Finally, low molecular weight reaction products are polymerized into high molecular weight compounds. Thus, MR products are not limited to low molecular weight compounds having volatility, color and taste (*Hofmann et al, 1995 and 2005, Frank et al., 2000*), but also high molecular weight with dark brown color, namely melanoidins (*Lindenmeier et al., 2002*).

Figure 3 shows a generation pathway of α -dicarbonyl compounds upon MR using glucose. *Gobert et al. (2009)* verified the generation of 1-deoxyglucosone, 3-deoxyglucosone, glucosone, 1-deoxythreosone, 3-deoxythreosone, 1-deoxypentosone, 3-deoxypentosone, glyoxal and methylglyoxal in a MR mixture prepared using ^{13}C -labeled glucose and lysine by means of LC-MS/MS. According to a literature by *Voigt et al. (2009)*, 1-deoxyglucosone is an intermediary for the generation of threosone, 1-deoxythreosone and 3-deoxythreosone, and the formation of glyoxal, methylglyoxal, threosone 1-deoxypentosone and 3-deoxypentosone was also confirmed via a degradation study of glucosone in the same way. The glyoxal generation originated from

glucosone is supported by a study of *Hofmann et al. (1999)*. In addition to the methylglyoxal formation derived from glucosone, an alternative pathway from 1-deoxyglucosone, which is currently thought as the primary system, was found by *Yaylayan et al. (2000)*.

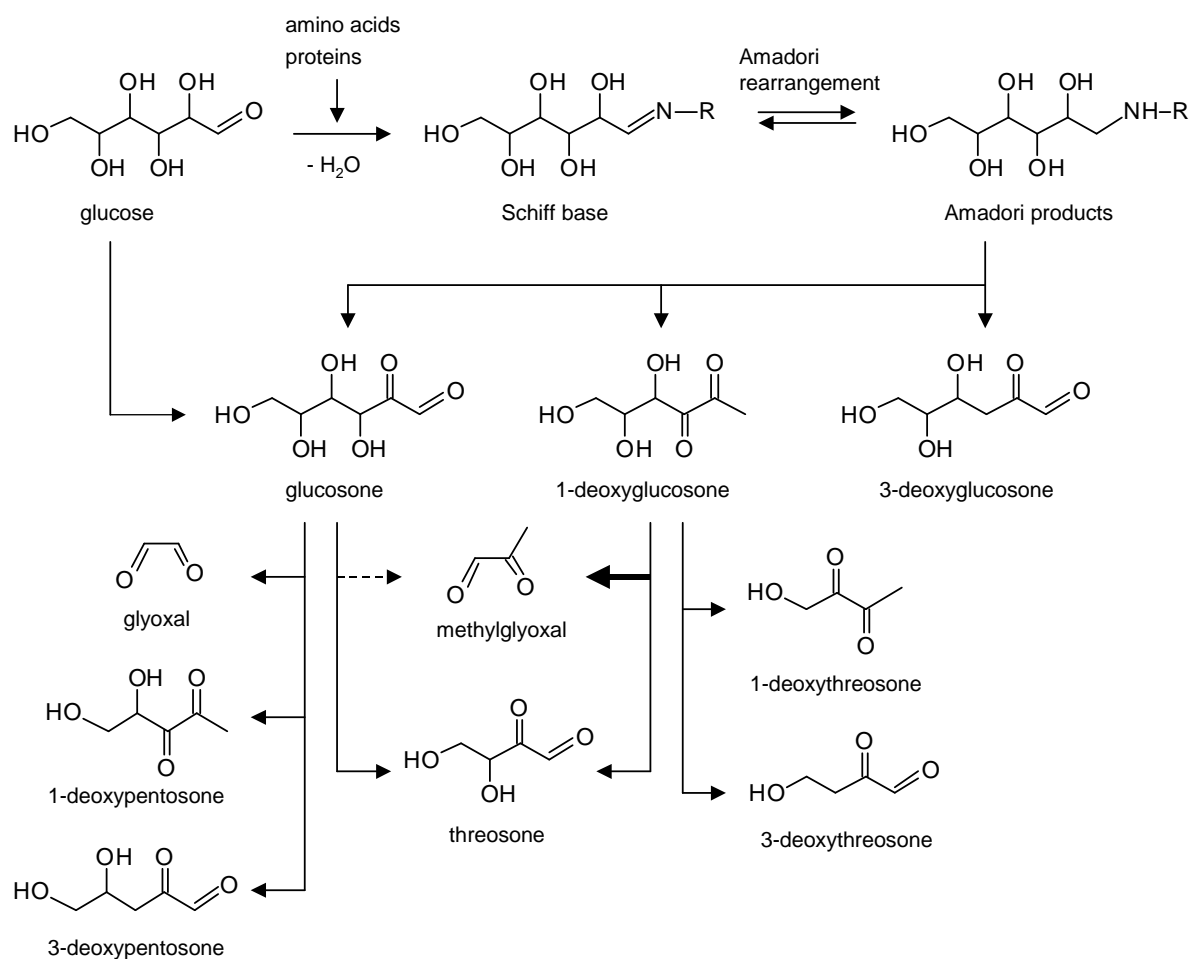


Figure 3. A possible reaction pathway for the generation of α -dicarbonyl compounds via Maillard reaction using glucose.

Additionally, it is found that MR mixtures possess antioxidative activity scavenging chemically stable radicals or oxidants, such as 2,2'-azino-bis(3-ethylbenzothiazoline-6-sulphonic acid) (ABTS), 2,2-diphenyl-1-picrylhydrazyl (DPPH), and 2,2'-azobis(2-amidinopropane) dihydrochloride (AAPH), and reducing power against metal ions (i.e. Fe^{3+} and Cu^{2+}) as well as anti-inflammation effect on Caco-2 cells, which is related to intracellular oxidation (Yoshimura *et al.*, 1997, Dittrich *et al.*, 2003, Chen *et al.*, 2008, 2011a, 2011b, 2012 and 2015). Studies on MR-derived antioxidants have been mainly done with model solutions using amino acids and sugars, and model powders containing sugars, amino acids and/or proteins, foods like milk, onion and garlic powder (Moreno *et al.*, 2003, Zulueta *et al.*, 2009). However, only few antioxidants were determined so far in their chemical structures (**Figure 4**). Thus, lots of scientific reports consisted of superficial phenomenology on generation of antioxidant activities in MR matrices, hence structure elucidation of such antioxidative MR products is a still undeveloped research topic (Lindenmeier *et al.*, 2002, Chen *et al.*, 2011c).

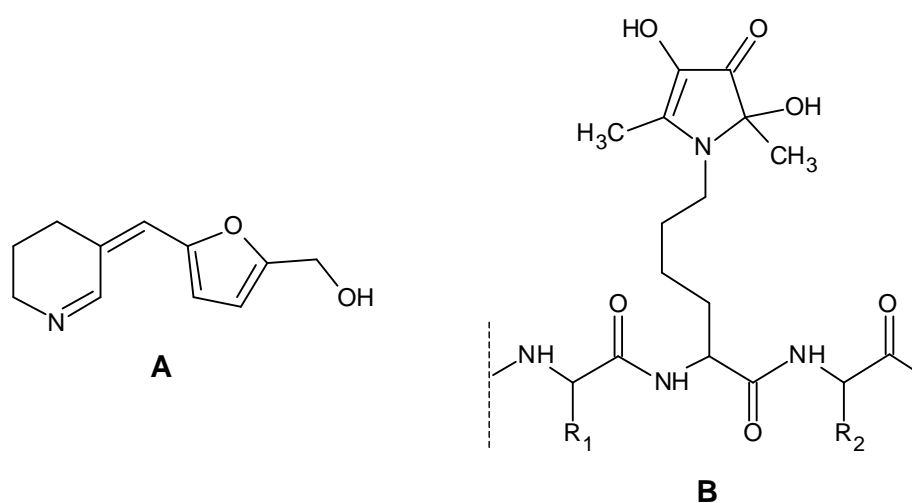


Figure 4. Chemical structures of [5-(5,6-dihydro-4H-pyridin-3-ylidene)methyl]furan-2-yl]methanol (A) and pronyl-L-lysine (B) as chemically and biologically antioxidative compounds isolated from MR mixtures.

1.3 Garlic

1.3.1 Botany and use of garlic

Garlic (*Allium sativum* L.) belongs to the genus *Allium* consisted of 600—750 species like as onion, shallot, leek and chive. Garlic has own flat leaves and bulbs, and these features enable to distinguish from other *Allium* members. Each bulb of garlic possesses several small cloves covered by a white or purplish skin for the purpose of self-protection. As garlic is often a sterile plant and does not produce true seeds, it is basically propagated asexually from underground cloves.

As sub-species of garlic, hardneck and softneck garlic are known (Volk *et al.*, 2004). Hardneck cultivars (*Allium sativum* var. *ophioscorodon*) produce scapes or flower stalks, and these cultivars have a single circle of 4 to 12 cloves around the woody stalk. Before flowering, hardneck garlic scapes are generally coiled, and normally nipped three weeks before the harvest time to accelerate the growth of the bulbs.

Softneck cultivars (*Allium sativum* var. *sativum*) produce a short scape. These cultivars have better tolerances for cold climates, and are generally more productive than hardneck cultivars, because much energy is concentrated on producing a bulb. Bulbs of hardneck garlic have 10 to 40 cloves in several layers around a soft central stem accompanying smaller cloves. As the softneck garlic has much longer shelf life than hardneck garlic, typically it can be stored for 6 to 8 months safely.

Since ancient times, garlic has been grown and consumed. For examples, ancient Egyptians had built pyramids having garlic to keep their strength and in health, and Roman soldiers had a bulb of garlic around their necks to gain strength. Currently, garlic is one of the most important vegetables throughout the world, with a total harvested area of 1.437.690 ha and an annual production of 24.255.303 tones of dry bulbs (FAO, 2013), and commonly used as a flavorful spice and a key ingredient in many dishes of various regions such as Asia, the Middle East, northern Africa, southern Europe, and parts of South and Central America, respectively. In addition to the daily use as spice, garlic is utilized for

health beneficial purposes, such as e.g. to reduce cardiovascular risk, to normalize blood pressure in some hypertensives, and to decrease levels of cholesterol (Fenwick *et al.*, 1985, Das *et al.*, 1995, Quidwai *et al.*, 2000).

1.3.2 Chemical composition of garlic

The nutritional constituents of garlic are approximately 59% water, 33% carbohydrates and 6% proteins (**Table 1**, *USDA National Nutrient data base, 2014*). Among the amino acids, L-arginine is predominant with the highest concentration with 615 mg/100 g (Souci Fachmann Kraut, 1991). In addition, organosulfur compounds are characteristic and important constituents in garlic, and generally garlic bulbs contain about 2.3% organosulfur compounds (Omar *et al.*, 2010)

Table 1. Nutrient value/100 g of garlic (*USDA National Nutrient data base, 2014*).

constituents		contents (g) per 100 g of edible portion
water		58.58
proteins		6.36
lipids (fat)		0.50
carbohydrates		33.06
carbohydrates	(fiber)	2.10
carbohydrates	(sugars)	1.00
minerals	calcium	0.18
	phosphorus	0.15
	potassium	0.40
vitamins	vitamin C	0.03

Among the organosulfur compounds (**Table 2**), the following six compounds are well known, and S-allyl-L-cysteine sulfoxide (alliin), γ -glutamyl-S-allyl-L-cysteine and γ -glutamyl-S-(*trans*-1-propenyl)-L-cysteine are found with highest abundance. Lancaster *et al.* (1989) found that S-alk(en)nyl-L-cysteine sulfoxides could be biosynthesized from γ -glutamyl-S-alk(en)nly-L-cysteines, thus indicating the γ -glutamyl species are important precursors in garlic chemistry.

Table 2. The composition of the major sulfur-containing constituents in garlic (*Koch et al., 1996*).

constituents	contents in garlic (mg/g)
S-alk(en)nyl-L-cysteine sulfoxides	
(+)-S-allyl-L-cysteine sulfoxide (alliin)	5.4—14.5
(+)-S-methyl-L-cysteine sulfoxide (methiin)	0.2—2.0
(+)-S-(trans-1-propenyl)-L-cysteine sulfoxide (isoalliin)	0.1—2.0
γ -glutamyl-S-alk(en)nyl-L-cysteines	
γ -glutamyl-S-allyl-L-cysteine	1.9—8.2
γ -glutamyl-S-methyl-L-cysteine	0.1—0.4
γ -glutamyl-S-(trans-1-propenyl)-L-cysteine	3.0—9.0
thiosulfinates	
allicin	2.5—5.0

A series of complex chemical transformation starts after the disruption of cell membranes generating volatile and non-volatile compounds. When garlic is crushed or cut, α,β -elimination of alliin occurs at the cytoplasm level through an enzymatic reaction catalyzed by alliinase which is located at the vacuole to give odorant allicin (**Figure 5**, *Bloem et al., 2010*).

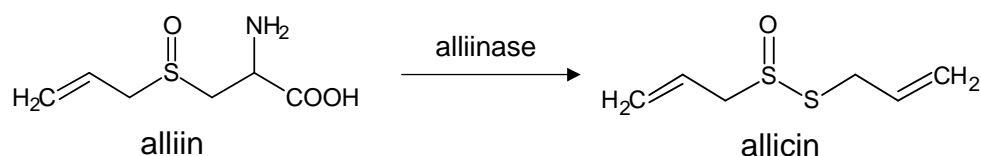
**Figure 5.** Alliinase-catalyzed generation of allicin from alliin.

Figure 6 shows an example of the generation of volatiles from allicin. Allicin gives 2-vinyl-4*H*-1,2-dithiin (**3'**) and 3-vinyl-4*H*-1,3-dithiin (**4'**) via the decomposition product thioacrolein (**1'**) (*Block et al., 1984 and 1986*). Reaction of another degradation product of allicin, 2-propenethiol (**5'**), with allicin generates diallyldisulfide (**6'**) and 2-propenesulfenic acid (**2'**) which readily condenses with itself regenerating allicin. Diallyltrisulfide (**11'**) is the major product of allicin degradation, and its generation is thought to start from reaction

of alliin with **2'** to give intermediates **7'** that produces the second intermediate **8'** and allyl alcohol (**9'**) upon hydrolysis. At last, reaction of 2-propene-1-sulfenothioic acid (**10'**), generated from **8'** via reductive cleavage, with alliin affords **11'**.

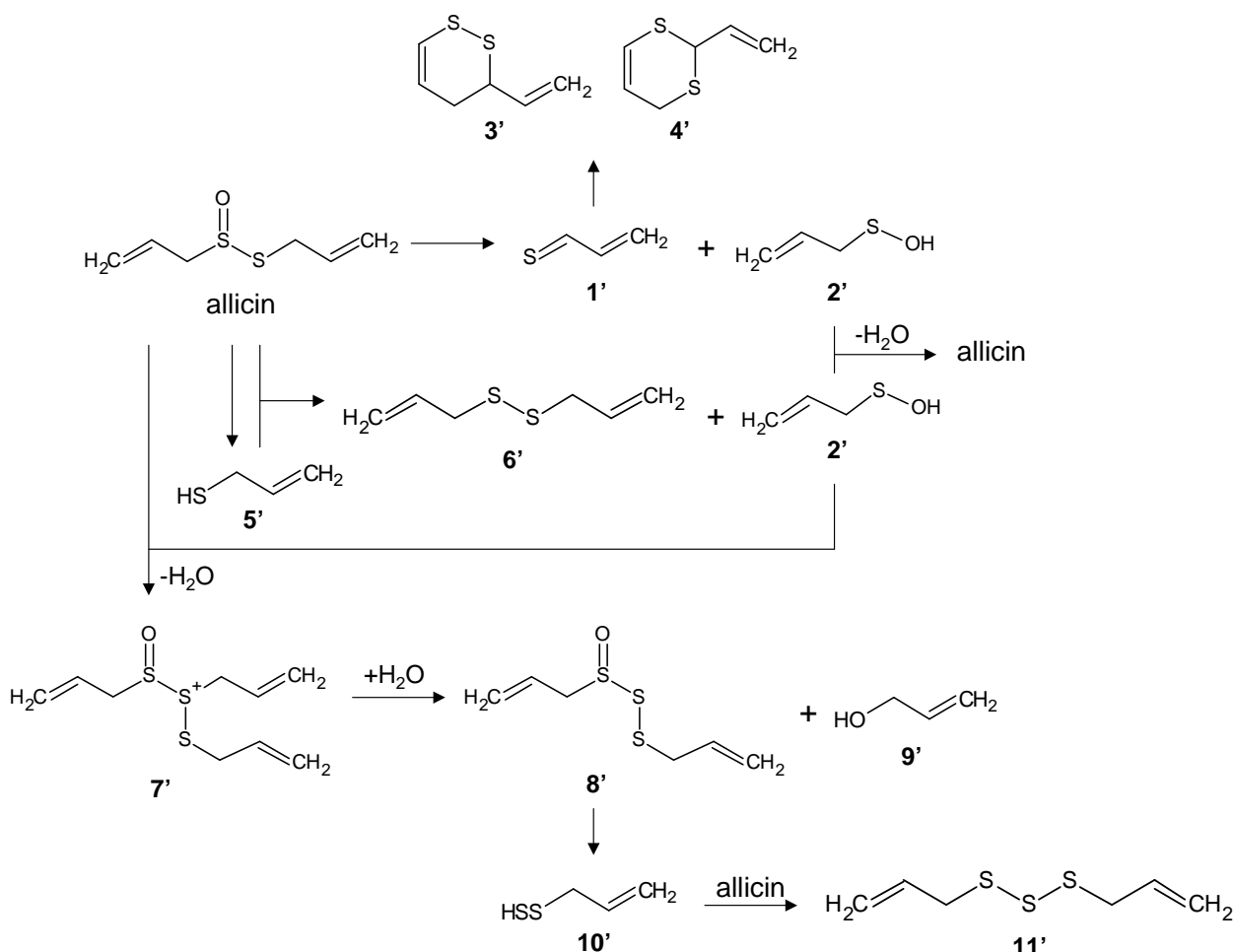


Figure 6. Generation of major volatiles from alliin.

In contrast to the volatiles, sulfur containing non-volatile compounds are enzymatically generated starting from γ -glutamyl-S-alk(en)yl-L-cysteine with γ -glutamyltranspeptidase which is widely distributed in organisms from bacteria to plants and mammals (*Tate et al., 1981*). γ -Glutamyl-S-allyl-L-cysteine and γ -glutamyl-S-(*trans*-1-propenyl)-L-cysteine are quantitatively predominant compounds in raw garlic (**Table 2**) and their corresponding hydrolysis products, S-allyl-L-cysteine and S-(*trans*-1-propenyl)-L-cysteine, could be detected in crushed garlic.

1.3.3 Taste and pharmacological activities of garlic constituents

As described before, garlic is used as a spice for daily dishes and therapeutic purposes, therefore its constituents have been investigated regarding taste and pharmacological activities so far. Allicin, allylsulfides and vinylthiols have strong garlic-like odor, being greatly responsible to pungency of crushed garlic, (*Bersuker et al., 1989, Edris et al., 2002*). *Ueda et al. (1990, 1994)* reported that alliin, glutathione, S-methyl-L-cysteine sulfoxide (methiin), γ -glutamyl-S-allyl-L-cysteine, S-1-propenyl-L-cysteine sulfoxide (isoalliin), and γ -glutamyl-S-1-propenyl-L-cysteine increased mouthfulness, thickness and long-lastingness of the taste in an umami solution, concluding the effects as kokumi-enhancement.

As pharmacological reports, antibacterial activities of allicin, apoptotic effect in HL-60 cells and inhibitory effects on the proliferation of human tumor cells by diallyldisulfide as well as antithrombotic and cholesterol lowering effects of vinylthiols are published (*Cavallite et al., 1944, Nishimura et al., 1971, Sendle et al. 1992, Sundaram et al., 1996a and 1996b, Kwon et al., 2002*). While *Higuchi et al. (2003)* revealed that diallyltrisulfide, 2-vinyl-4H-1,2-dithiin and 3-vinyl-4H-1,3-dithiin possess chemical antioxidant activity for inhibiting LDL oxidation, their activities were lower than that of ascorbic acid.

1.4 Garlic preparations

1.4.1 Non-thermally processed garlic preparations

While garlic is well known as one of the most beneficial foods for health, components of freshly crushed or sliced garlic are chemically unstable, and reactive products like allicin and diallyldisulfide have been reported to cause undesirable side effects, such as stomach irritation (*Nakagawa et al., 1980*) and allergic reactions (*Papageorgiou et al., 1983*). In order to gain the maximum biological benefits of garlic, various processing methods have been applied to garlic such as, e.g. garlic powder, garlic oil, garlic oil macerate, and aged garlic extract (AGE).

Table 3. Non-thermally produced garlic preparations and their composition. +++; >1.00 mg. ++; 0.20—1.00 mg. +; 0.05—0.20 mg. ±; 0.01—0.05 mg. N.D.; <0.01mg (values are amount in 1 g equivalent of raw garlic.).

constituents	garlic powder	garlic oil	garlic oil macerate	AGE
alliin	+++	N.D.	N.D.	±
alliinase	detected	N.D.	N.D.	N.D.
allicin	N.D.	N.D.	N.D.	N.D.
allyl sulfides	N.D.	+++	+++	+
γ-glutamyl-S-allyl-L-cysteine	+++	N.D.	++	++
S-allyl-L-cysteine	N.D.	N.D.	+++	+++
S-allylmercapto-cysteine	N.D.	N.D.	N.D.	+
inulin	+++	N.D.	+++	+++

Garlic powder, one of the most popular products, is obtained simply via dehydration of pulverized garlic clove (*Amagase et al., 2001*). Some products of the garlic powder contain alliin and its corresponding enzyme, namely alliinase, which can generate allicin via the addition of water. Garlic oil is generally produced by steam-distillation process (*Amagase et al., 2001*). The oil products mainly contain several kinds of volatile sulfides, which give a great contribution to the garlic odor and cause body odor after eating, and of course, this does not contain non-volatile compounds. Garlic oil macerate is manufactured through oil extraction of raw garlic, sliced or ground raw garlic. As the oil extraction can eliminate allicin generation, this product is believed to be good to avoid the

stomach injury derived from allicin.

Aged garlic extract (AGE), which is prepared by extracting sliced garlic with aqueous ethanol and maturing the extract for more than 10 months (*Ide et al., 1999a*) to define a highly safe garlic preparation (*Sumiyoshi et al., 1984 and Steiner et al., 1996*). In the aging period, allicin is decomposed into several sulfides, for example methyl sulfides, allyl sulfides and allyl methyl sulfides. Although these sulfides are detectable in AGE by means of GCMS (*Weinberg et al., 1993*), they are removed to a major extent by vacuum concentration during AGE manufacturing. In addition, the aging process affords sulfur-containing compounds, such as S-allyl-L-cysteine, S-1-propenyl-L-cysteine, S-methyl-L-cysteine and S-allylmercapto-L-cysteine (**Figure 7**), through some chemical and/or enzymatic reactions (*Alison et al., 2006*).

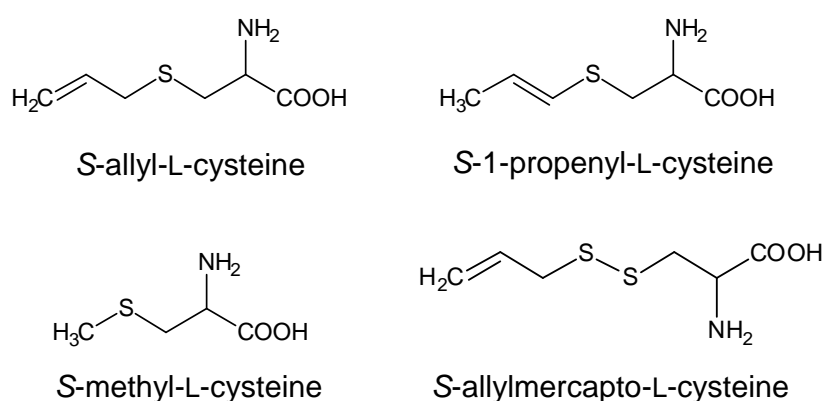


Figure 7. Chemical structures of non-volatile sulfur-containing compounds found in AGE.

Currently, S-allyl-L-cysteine is found to be the most abundant sulfur compound in AGE (2.1 mg/g-dry weight) (*Imai et al., 1994*), and its generation starts from γ -glutamyl-S-allyl-L-cysteine via γ -glutamyltranspeptidase (*Colín-González et al., 2012*). Studies on its biological activities have shown hepato-protective effects, an inhibitory activity against carcinogenesis, cholesterol lowering effect as well as antioxidant activity (*Sumiyoshi et al., 1990, Yeh et al., 2001 and Nakagawa et al., 1989*).

In addition to the organosulfur compounds, antioxidative Maillard reaction (MR) products (**Figure 8**) were isolated from AGE by means of activity-guided fractionation and chemical synthesis (*Ichikawa et al., 2002, Ryu et al., 2001*). The arginine derivative (**1'**) and these carbolins (**2'—5'**) have not been detectable in raw garlic, but have been shown to be generated by Maillard-type reaction between D-glucose and L-arginine and L-tryptophan, respectively.

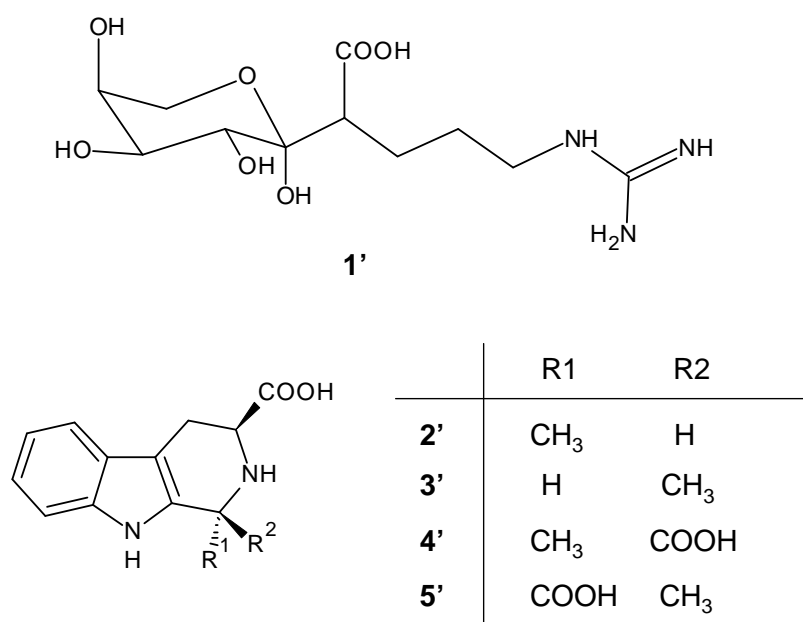


Figure 8. Chemical structures of *N*α-(1-deoxy-D-fructos-1-yl)-L-arginine (**1'**), (1*R*,3*S*)-1-methyl-1,2,3,4-tetrahydro-β-carboline-3-carboxylic acid (**2'**), (1*S*,3*S*)-1-methyl-1,2,3,4-tetrahydro-β-carboline-3-carboxylic acid (**3'**), (1*R*,3*S*)-1-methyl-1,2,3,4-tetrahydro-β-carboline-1,3-dicarboxylic acid (**4'**), and (1*S*,3*S*)-1-methyl-1,2,3,4-tetrahydro-β-carboline-1,3-dicarboxylic acid (**5'**) identified in AGE.

As amino acids and sulfur-containing compounds are present in concentrations of approx. 360 and 40.4 mmol/kg dry weight in AGE, respectively, and sugars (D-fructose; 650 mmol/kg dry weight, D-glucose; 100 mmol/kg dry weight) are also highly abundant (**Table 4**). A further progress of the Maillard reaction in AGE is expected to generate more antioxidative compounds.

Table 4. A list of concentrations of amino acids and sulfur-containing compounds in AGE (Wakunaga Pharmaceutical. Co. Ltd., personal communication).

concentrations (mmol/kg dry weight of AGE)			
amino acids		S-containing compounds	
Arginine	161.5	S-allyl-L-cysteine	26.1
Threonine	53.6	S-1-propenyl-L-cysteine	21.7
Glutamic acid	38.5	γ -glutamyl-S-allyl-L-cysteine	10.6
Alanine	21.3	S-methyl-L-cysteine	4.6
Aspartic acid	13.9	S-allylmercapto-L-cysteine	2.7
Glycine	11.1	S-methylmercapto-L-cysteine	0.8
Serine	9.3		
Lysine	8.6	Sum	40.4
Proline	8.3		
Valine	8.1		
Phenylalanine	7.3		
Tyrosine	6.0		
Leucine	5.7		
Isoleucine	3.4		
Methionine	3.1		
Cysteine	0.7		
Trptophane	0.6		
Sum	361.0		

1.4.2 Thermally processed garlic preparation

The most important, blackened garlic (**Figure 9**) is prepared by heating at approx. 70 °C with 75—95 % relative humidity for 30—40 days. The blackened garlic is already a popular product in East Asia, especially in Japan and Korea, and estimated market value reached 94 million US dollars in Korea (*imnews, 2011*). This preparation has attracted growing interest because of its higher antioxidative activity, an enriched S-allyl-L-cysteine content (approx. 100 µg/g dry weight), anti-tumor activity, anti-bacterial activity and lowering effect of blood lipid parameters as well as a lack of an unpleasant taste and odor of raw garlic and more sweet taste (*Sato et al., 2006, Sasaki et al., 2007, Wang et al., 2010, Bae et al., 2012, Kim et al., 2012, Jung et al. 2014*).



Figure 9. Picture of a blackened garlic (*Sato et al., 2006*).

Moreover, *Montano et al. (2004)* revealed that the heating for its preparation denatures alliinase, therefore, inhibiting transformation of alliin into allicin. And other investigations of the blackened garlic revealed changes of pH, browning intensity, chemical antioxidant activity, reducing power and S-allyl-L-cysteine concentration by processing (*Sato et al., 2006, Bae et al., 2014*). So far, only S-allyl-L-cysteine, S-methyl-L-cysteine, alliin and amino acids have been identified (*Sasaki et al., 2007, Jung et al., 2014*), as ingredients of blackened garlic, thus offering lots of opportunities for the discovery of unknown reaction products in heated garlic preparations.

1.5 Objectives

Antioxidants are potentially key molecules to maintain health reducing elevated ROS level in cells. Although thermally processed garlic preparations as well as AGE are known for their antioxidant activity, the corresponding antioxidative molecules have yet not been fully elucidated. As AGE contains sugars and amino acids abundantly, a further heat-processing for AGE could induce Maillard-type reactions elevating its antioxidant activity, thus offering opportunities to discover unknown antioxidants in AGE.

The objectives of this study were, therefore, to develop a processing method using heating for a new garlic preparation with high antioxidative activity and to locate key antioxidants in the preparation. In the first part of this study, optimal processing conditions have been determined for generation of high antioxidative activity using a simple heating. In order to achieve this, pH, heating temperature and heating time were examined in liquid and solid state of the AGE. Antioxidative activity of each preparation was evaluated by means of ABTS radical scavenging and ORAC assays.

In the second part, isolation and identification of antioxidants in processed AGE (pAGE) were conducted by means of three approaches: (I) activity-guided fractionation of pAGE using *in vitro* antioxidant assays, (II) a model reaction employing SAC and D-glucose to mimic a chemical reaction during processing and (III) identification of known antioxidant through LC-MS/MS. In the case of (II), after complete structure elucidation of the compounds, antioxidative activities of the identified compounds were evaluated. In addition, sensory experiments regarding bitterness and taste-modulating effect were performed for nine new structures, as well as bioassays for pharmacological effects.

Finally, the compounds identified in pAGE were quantified by means of LC-MS/MS analysis to conclude which compounds are characteristic in the pAGE, and then the key compounds in pAGE were further assessed in re-processed AGE powders changing pH and heating time, to reveal generation profiles for the compounds. Moreover, in order to clarify natural occurrences of the nine compounds elucidated from (II), quantitative analysis was carried out in raw garlic and garlic powder with/without roasting.

2 Results and discussion

2.1 Influence of thermal processing on the antioxidant activity of AGE

To study the potential to increase the antioxidant activity of AGE by further processing, experiments were performed in the following with liquid and powdered AGE, respectively, heat-treated under various conditions (pH, heating time, heating temperature). Since no single antioxidant assay alone is able to show comprehensive antioxidant capacity of a compound or a sample, *Prior et al.* (2005) recommended that at least two different antioxidant assays should be performed. Therefore two different antioxidant assays, the ABTS radical scavenging (ARS) assay and the oxygen radical absorbance capacity (ORAC) assay, were adopted in this study. The ARS assay is for assessment of the radical reduction capacity of an antioxidant through transferring one electron. On the other hand, the ORAC assay is used for determination of the radical-quenching capacity of an antioxidant by hydrogen donation.

2.1.1 Influence of heating time and temperature on antioxidant activity of AGE

In order to select preferred reaction condition promoting the generation of antioxidants in processed AGE, four batches of AGE powder containing 3.5, 5.4, 8.0 and 10.5% water were prepared from a liquid AGE (pH: 5.8, water content: 71.8%) through spray-drying. Then the powder and the liquid forms were heated at 80 °C in closed glass vials using a laboratory oven for 30 days to compare generation profiles of their ARS activities (**Figure 10**).

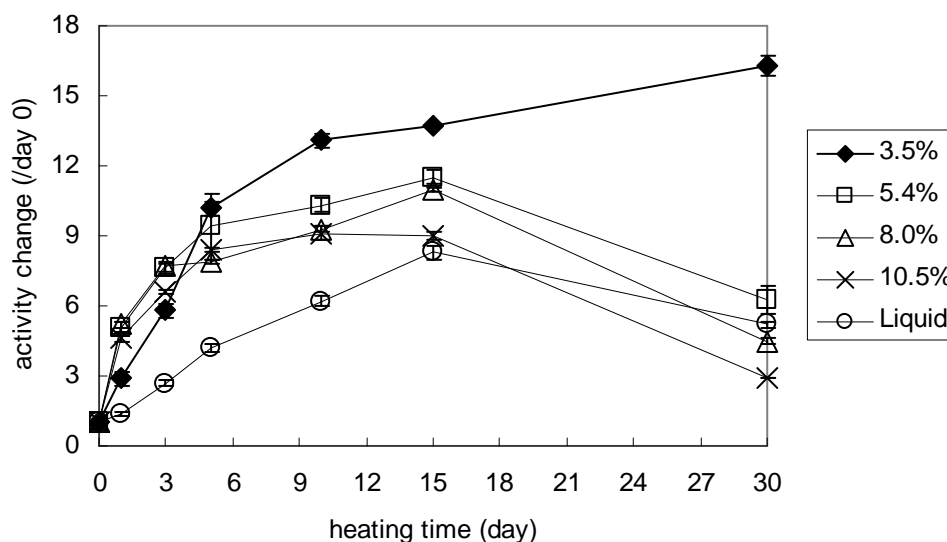


Figure 10. Changes of ARS activities of the liquid and of four powders of AGE with heating time at 80 °C. Data represent the ratios of the activities to each initial activity (average \pm S.D, n=3).

The ARS activities of liquid AGE and three different powder formulations, including 5.4, 8.0 and 10.5 % water, respectively, increased with reaction time and reached the maximum activity at day 15, showing a 8.3, 11.5, 11.0 and 9.0 fold increase compared to the initial activity. In comparison, powdered AGE containing 3.5 % water showed a continual increase of antioxidant activity till day 30, which resulted in the highest activity (16.3 fold, day 30) of all preparations.

In addition, the same experiments without liquid AGE were performed at 100 °C (**Figure 11**). Although changes of the ARS activity in all preparations at 100 °C were in line with the results obtained from the heating study at 80 °C, the changes were accelerated at 100 °C, because activities of each powder reached the maximum level already after five days. Both experiments indicated that the powdered AGE containing 3.5 % water is the best material to generate higher antioxidative activity, therefore this the powder was selected for further investigations.

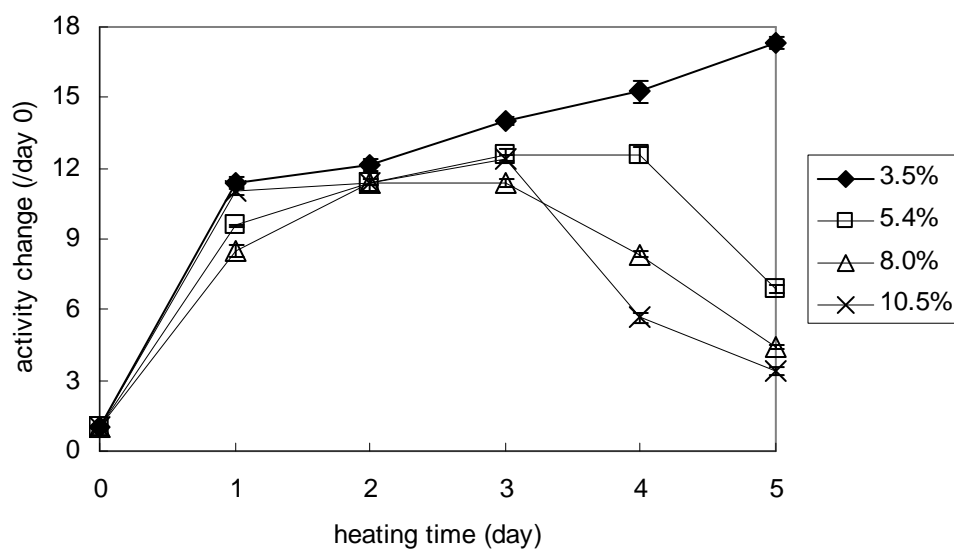


Figure 11. Change of ARS activities of four powdered formulations of AGE with heating time at 100 °C. Data represent the ratios of the activities to each initial activity (average \pm S.D, n=3).

2.1.2 Influence of pH on antioxidant activity of processed AGE

Three different AGE powders prepared from three batches of the liquid AGE of pH 4.0, 6.0 and 8.0 were heated in the same way as described above. Thereafter their ARS and ORAC activities were analyzed (**Figure 12—15**). In both assays, remarkable differences could not be observed at 80 and 100 °C, thus indicating that pH adjustment between pH 4.0 and 8.0 is not essential. Therefore, the optimal pH was chosen as 6.0 which is in close relation to that of the original AGE (pH 5.8).

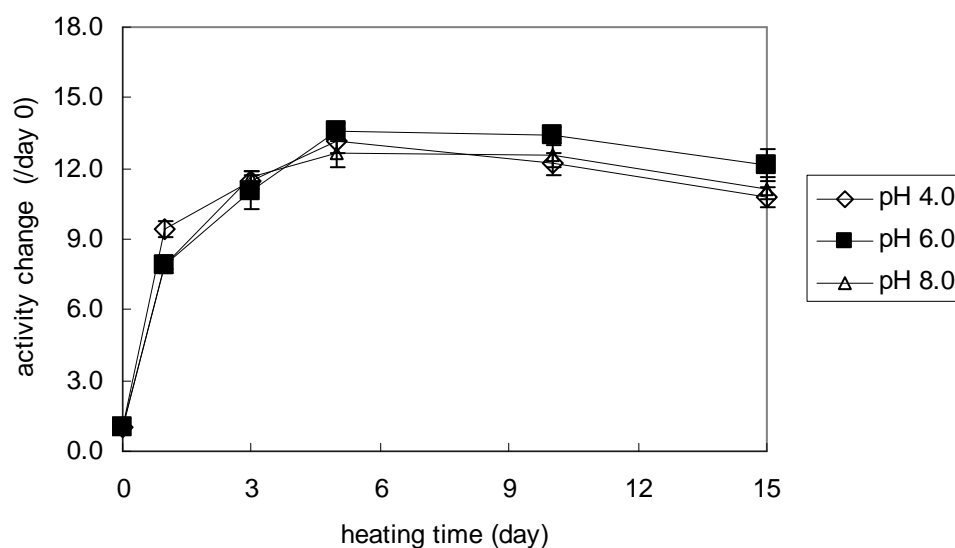


Figure 12. Influence of pH value on the ARS activity of powdered AGE heated at 80 °C. Data represent the ratios of the activities to each initial activity (average \pm S.D, n=3).

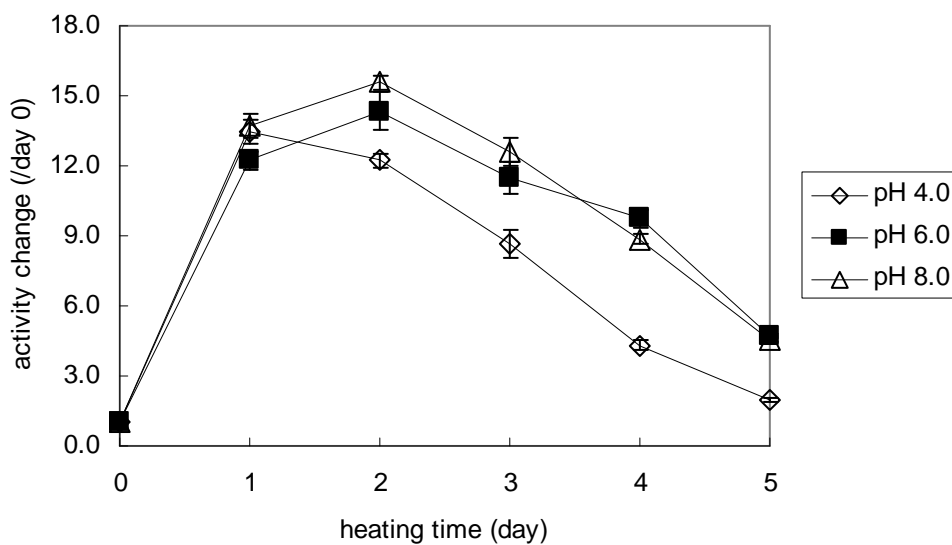


Figure 13. Influence of pH value on the ARS activity of powdered AGE heated at 100 °C. Data represent the ratios of the activities to each initial activity (average \pm S.D, n=3).

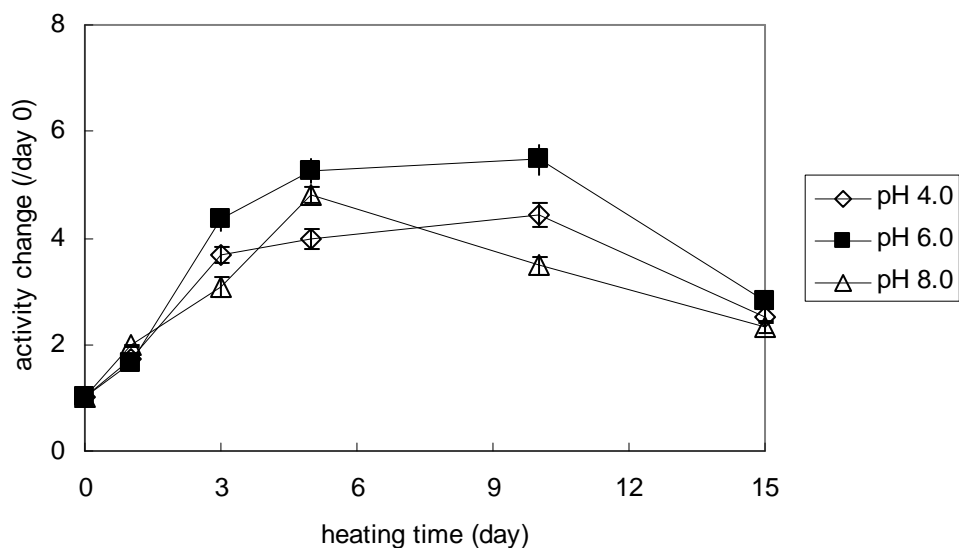


Figure 14. Influence of pH value on the ORAC activity of powdered AGE heated at 80 °C. Data represent the ratios of the activities to each initial activity (average \pm S.D, n=3).

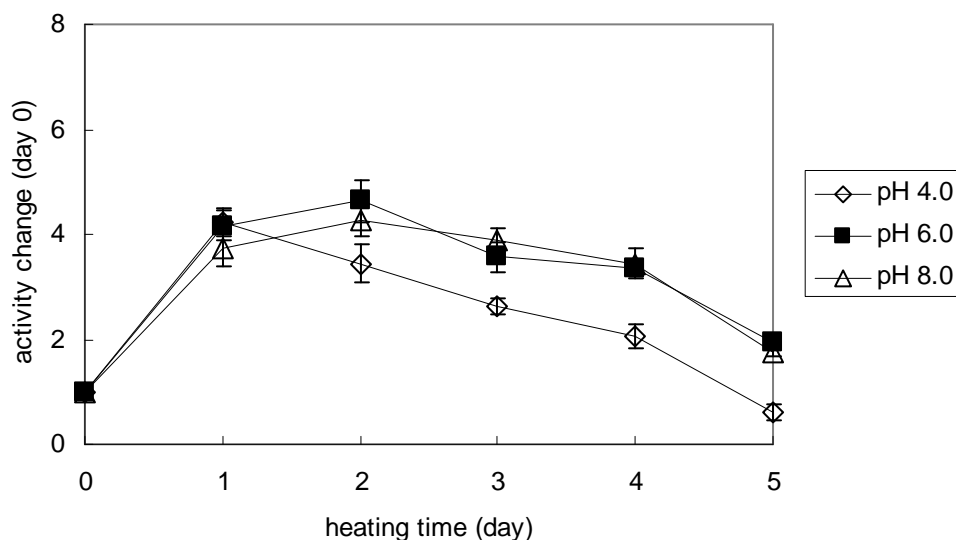


Figure 15. Influence of pH value on the ORAC activity of powdered AGE heated at 100 °C. Data represent the ratios of the activities to each initial activity (average \pm S.D, n=3).

2.1.3 Optimization of heating temperature and time for generation of increased antioxidative activity

In the previous study, the heating experiments were performed for 15—30 days at 80 °C and five days at 100 °C, however, the heated AGE powder of pH 6.0 already possessed elevated antioxidative activities after three and five days at 80 °C as well as after one and two days at 100 °C. Aimed at generating a processed AGE with high antioxidant activity in the shortest time possible, four batches of AGE powder at pH 6.0 were prepared again and heated for three and five days at 80 °C as well as one and two days at 100 °C. Consequently the antioxidative activities using ARS and ORAC assays were evaluated to determine the optimal heating temperature and time.

Figure 16 showed that ARS activity of the batch heated for 1 day at 100 °C was the highest, and all batches showed quite similar ORAC activity. In conclusion, thermal treatment of the AGE powder (pH6.0, 3.5% water) at 100 °C for one day could generate strongly increased antioxidative activity. This powder was used

for the following studies and is named as “processed AGE” (pAGE). To bridge the knowledge gap between chemical processing and antioxidative compounds generated, pAGE was used for activity-guided fractionation to isolate and identify the key antioxidants.

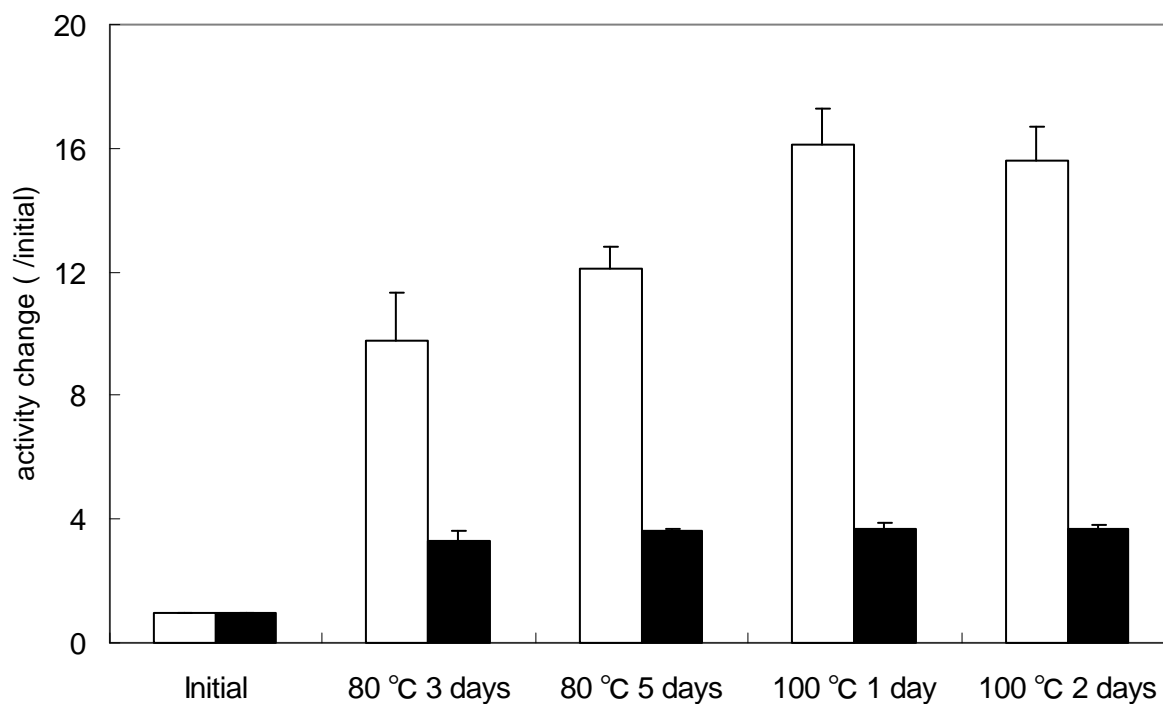


Figure 16. ARS (white) and ORAC (black) activities of four batches of processed AGE powder (pH 6.0). Data represent changing ratios of the activities to each initial activity (average \pm S.D, n=3)

2.2 Activity-guided fractionation of processed AGE and identification of antioxidants

2.2.1 Separation of processed AGE by means of ultrafiltration

To gain first insight into the molecular weight of the high antioxidants in processed AGE (pAGE), an aqueous solution of pAGE was separated by sequential ultrafiltration using membranes with a cut-off of 5 and 1 kDa, respectively, obtaining a low molecular weight fraction (<1 kDa), a middle molecular weight fraction (1—5 kDa), a high molecular weight fraction (>5 kDa). At the first step of the ultrafiltration using a 5 kDa cutoff membrane, 1.0 g of the pAGE was separated, and then the sum of yields of the residue and the filtrate exhibited about 1.0 g. The second separation with a 1 kDa membrane gave a total yield of 466 mg (97%) indicating very good recovery.

Thereafter, antioxidative activities of the three fractions, a recombined solution with each fraction using natural ratios, and the pAGE were evaluated employing ARS and ORAC assays (**Figure 17**). In both assays, the recombined solution showed same activities as the pAGE indicating that no significant losses took place during the ultrafiltration. Although the ARS activity of the 1—5 kD fraction was evaluated with the highest value, differences between the three fractions were marginal. In contrast, the low molecular weight fraction showed the highest contribution 55% in ORAC assay, and the activity exhibited a great difference compared to the others. Therefore, the low molecular weight fraction was further fractionated by means of chromatographic approaches.

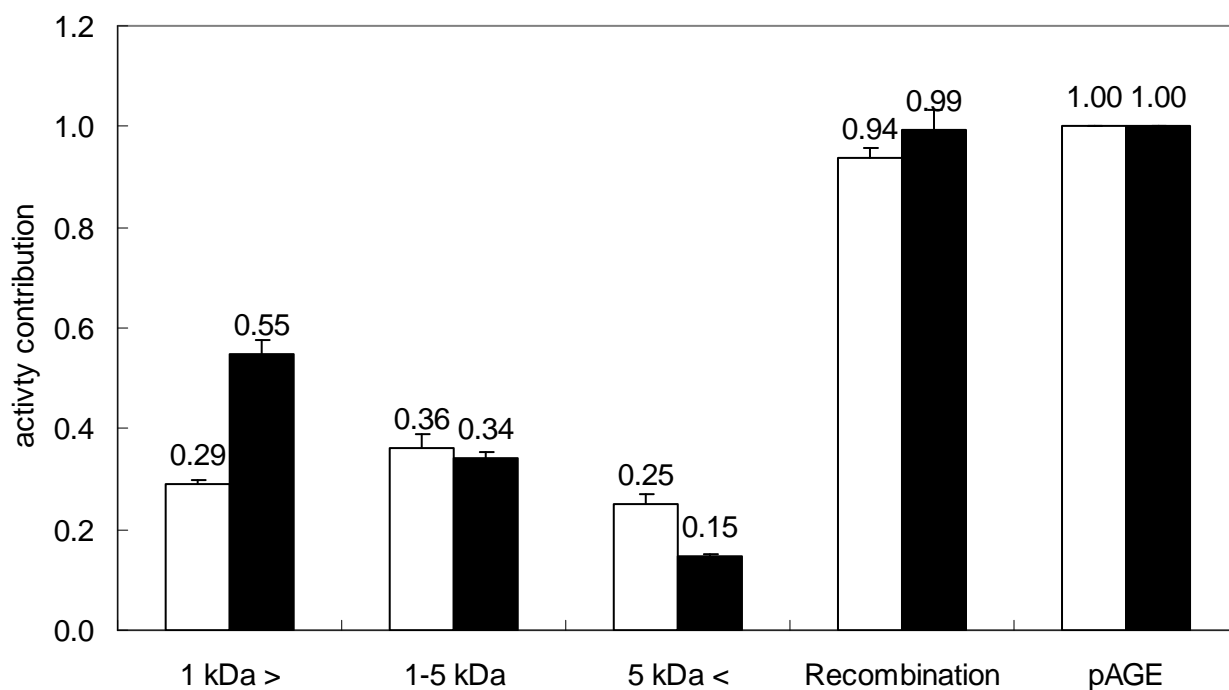


Figure 17. ARS (white) and ORAC (black) activities of three fractions, a recombined mixture and the pAGE. Data represent ratios of the activities to pAGE (average \pm S.D, n=3).

2.2.2 MPLC separation of low molecular weight fraction of pAGE

The low molecular weight fraction (<1 kDa) of the pAGE was separated by means of medium pressure liquid chromatography (MPLC) into 17 fractions and then antioxidant activity was evaluated using the ARS and ORAC assays (**Figure 18** and **19**). The sum of yields of the 17 fractions was 481.2 mg, and the recovered ratio of the weight exhibited 96.2%. Using ARS assay (**Figure 18**), fraction four showed the highest activity, followed by seven fractions (No.5—11) which also showed relatively high activities. The sum of activities of No.4—11 accounted for 89% of the whole activity of the low molecular weight fraction.

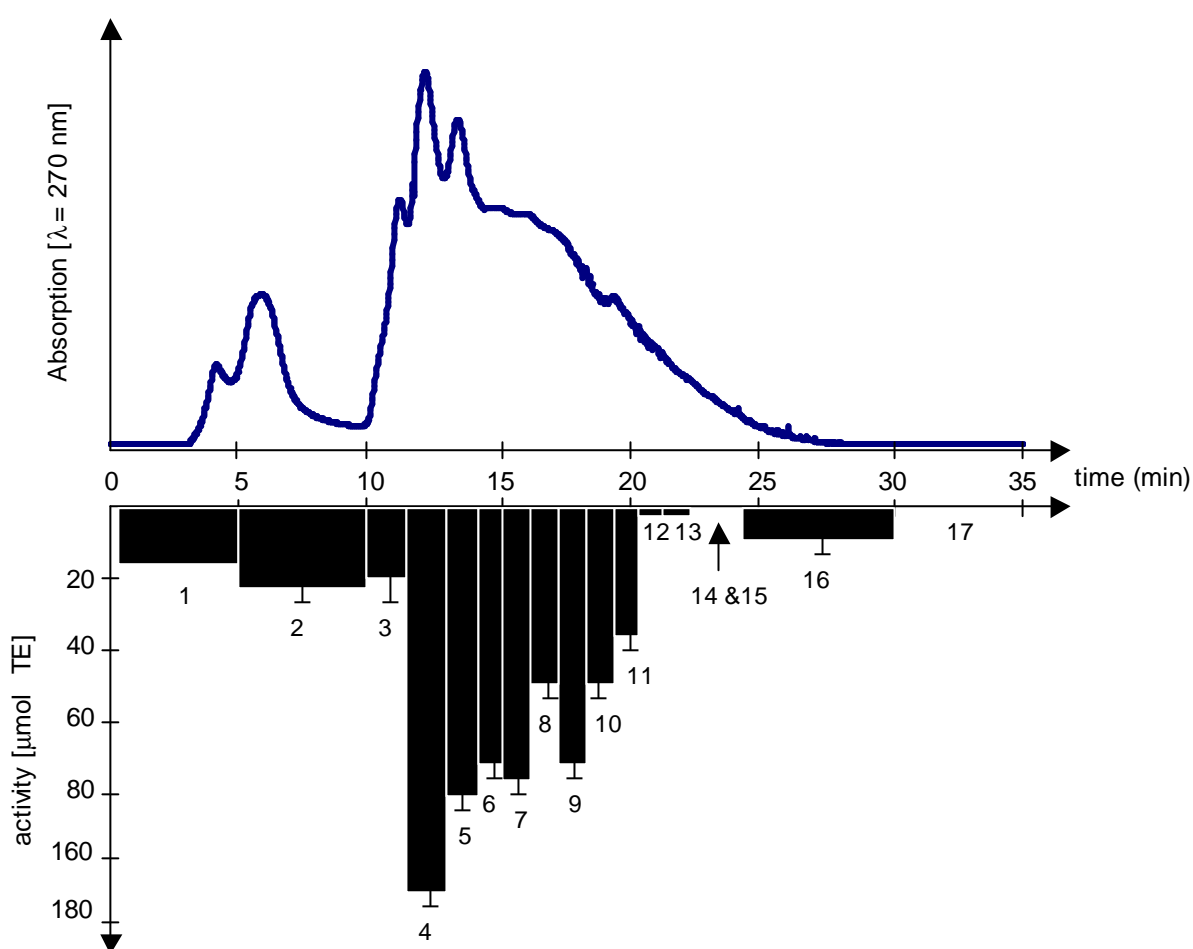


Figure 18. MPLC and ARS activities of fractions separated from the low molecular weight fraction of the pAGE. Data represent antioxidative activity of each fraction expressed as Trolox equivalents (TE) (average \pm S.D, $n=3$). The whole activity of the low molecular weight fraction was 644.9 [$\mu\text{mol TE}$], and the calculated sum of each fraction was 675.2 [$\mu\text{mol TE}$].

In addition, No.4 exhibited the highest ORAC activity, and seven fractions from No.5 to 11 as well as No.2 showed relatively high activities (**Figure 19**). The sum of the ORAC activities of the eight fractions (No.2, 5—11) accounted for 80% of the whole activity of the low molecular weight fraction. Considering both assays, eight fractions between No.4 and No.11, which possess higher activities in both assays, were considered for further investigation.

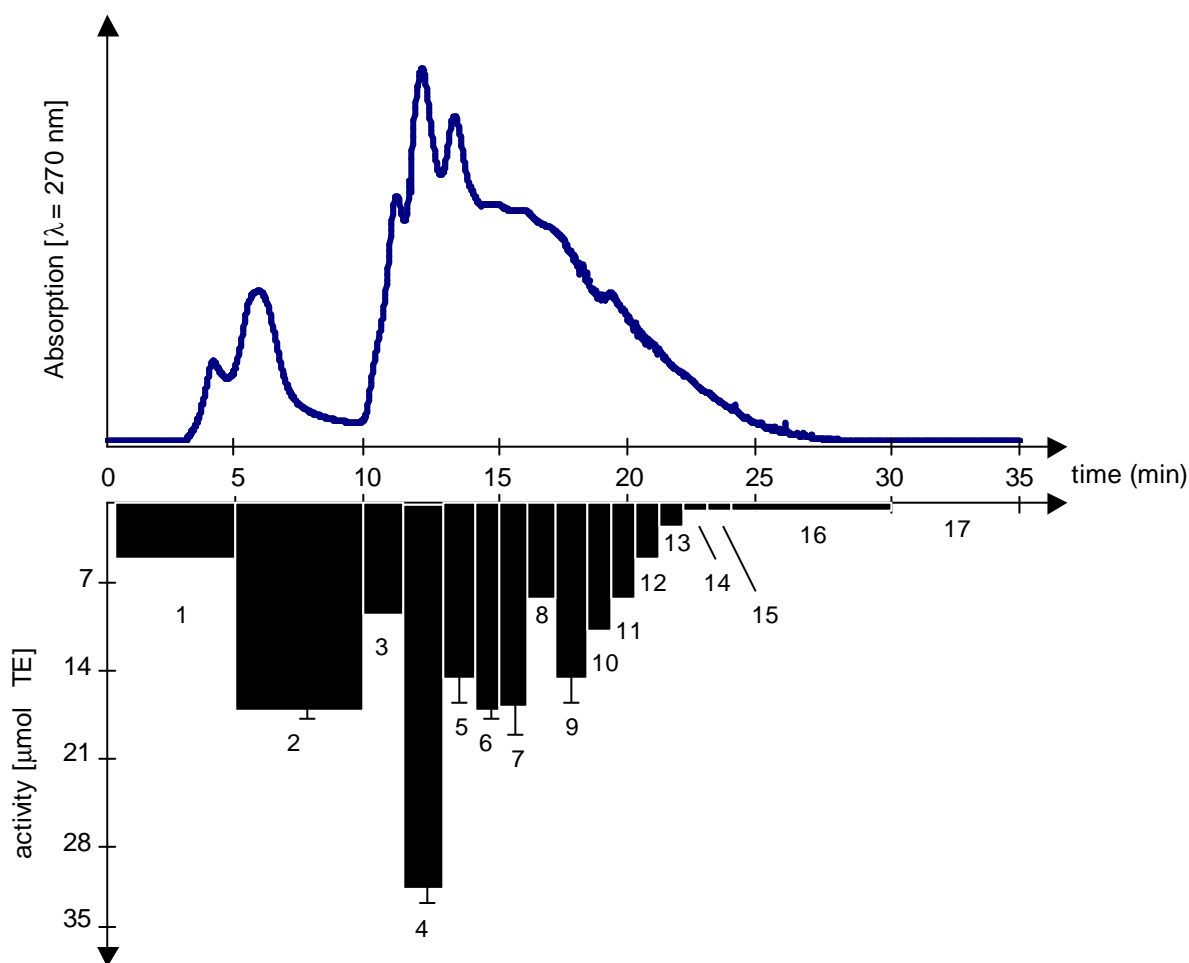


Figure 19. MPLC and ORAC activities of fractions separated from the low molecular weight fraction of the pAGE. Data represent antioxidative activity of each fraction expressed as Trolox equivalents (TE) (average \pm S.D, $n=3$). The whole activity of the low molecular weight fraction was 162.7 [$\mu\text{mol TE}$], and the calculated sum of each fraction was 161.8 [$\mu\text{mol TE}$].

2.2.3 Isolation and structure elucidation of antioxidants in MPLC fraction No.4

First, the MPLC fraction No.4, which showed the highest activities in ARS and ORAC assays, was investigated to isolate and identify antioxidants in the pAGE. An aliquot of the fraction No.4 was fractionated into 21 subfractions by means of semipreparative HPLC (**Figure 20—21**), and each subfraction was analyzed on antioxidative activities using ARS and ORAC assays.

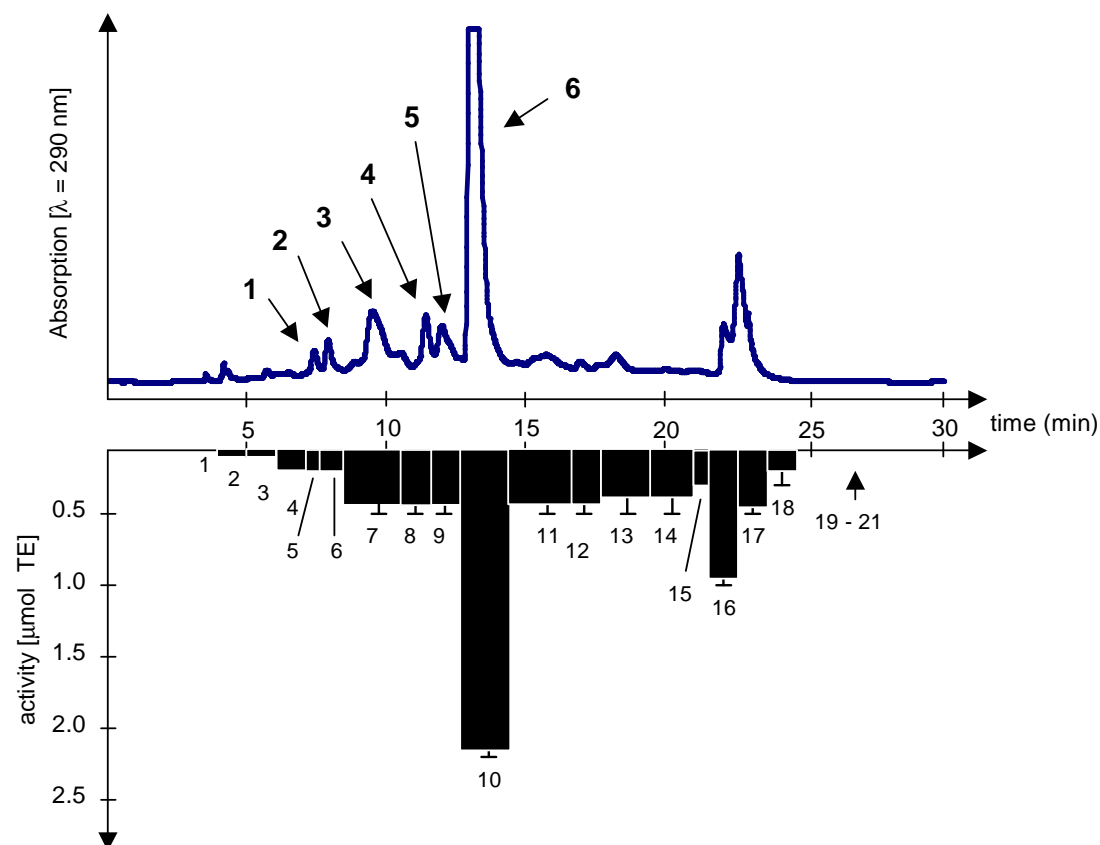


Figure 20. HPLC separation and ARS activities of subfractions from the MPLC fraction No.4. Data represent antioxidative activity expressed as Trolox equivalents (TE) (average \pm S.D, $n=3$). The whole activity of MPLC fraction No.4 was 7.55 [$\mu\text{mol TE}$], and the calculated sum of each fraction was 7.47 [$\mu\text{mol TE}$]. Numbering of compounds is given in bold.

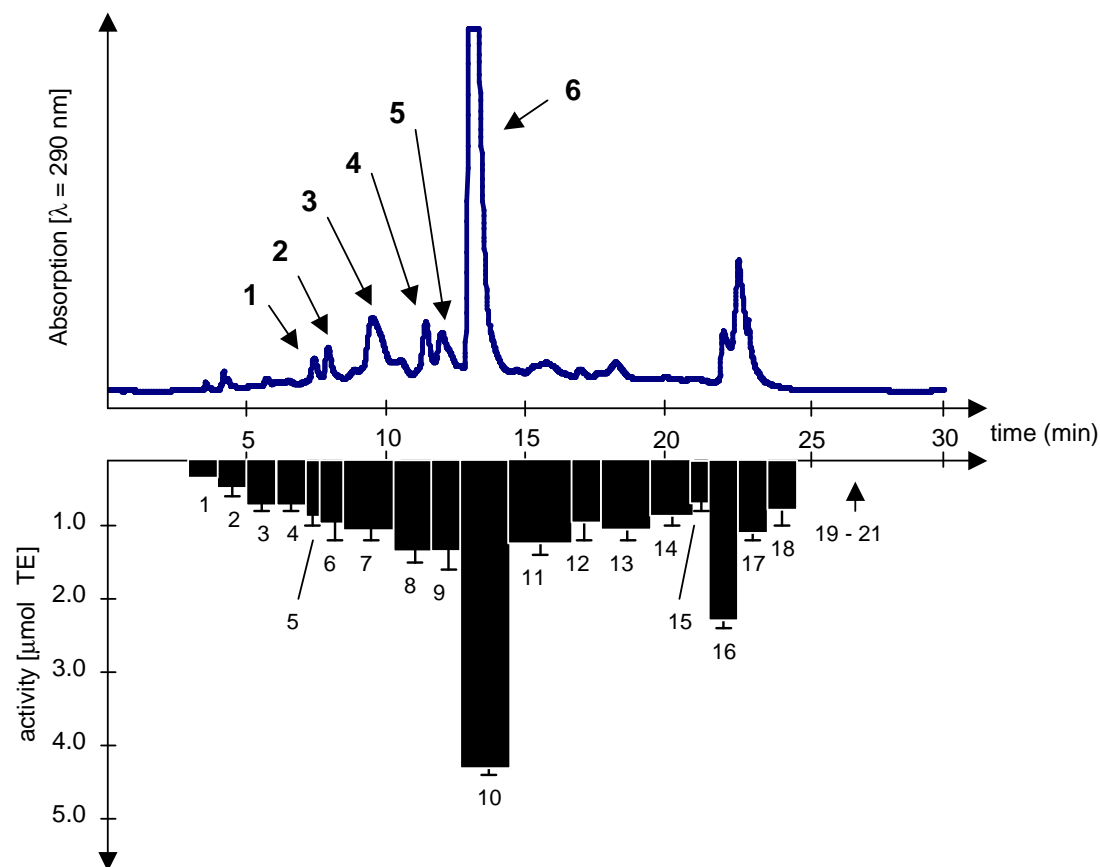


Figure 21. HPLC separation and ORAC activities of subfractions from MPLC fraction No.4. Data represent antioxidative activity expressed as Trolox equivalents (TE) (average \pm S.D, n=3). The whole activity of MPLC fraction No.4 was 21.67 [μ mol TE], and the calculated sum of each fraction was 20.74 [μ mol TE]. Numbering of compounds is given in bold.

ARS and ORAC activities of the whole MPLC fraction No.4 showed 7.6 and 21.7 [μ mol TE], respectively, and these values were in the same range as the calculated sums of each subfraction (7.5 and 20.7 [μ mol TE]), thus indicating that the HPLC separation and the antioxidative evaluation were successful.

In the HPLC, a main peak (No.4—10) and seven minor peaks (No.4—5, 6, 7, 8, 9, 16 and 17) were observed. No.4—10 possessed the highest activities in both assays, followed by the minors. While additional HPLC runs of the brown colored fractions No.4—16 and 17 using the same column with a slower gradient implied that the fractions (No.4—16 and 17) contain polymerized and complexed compounds because the peaks formed a hump peak in the

chromatography (data not shown). Hence, the main peak and the five minor peaks (No.4—5, 6, 7, 8 and 9) were focused on for structure elucidation in this fraction. After purification employing HPLC, compounds **1**—**6** were afforded from No.4—5, 6, 7, 8, 9 and 10, respectively, and their chemical structures were determined using 1D/2D-NMR and UPLC-ESI-TOF MS (**Figure 22**).

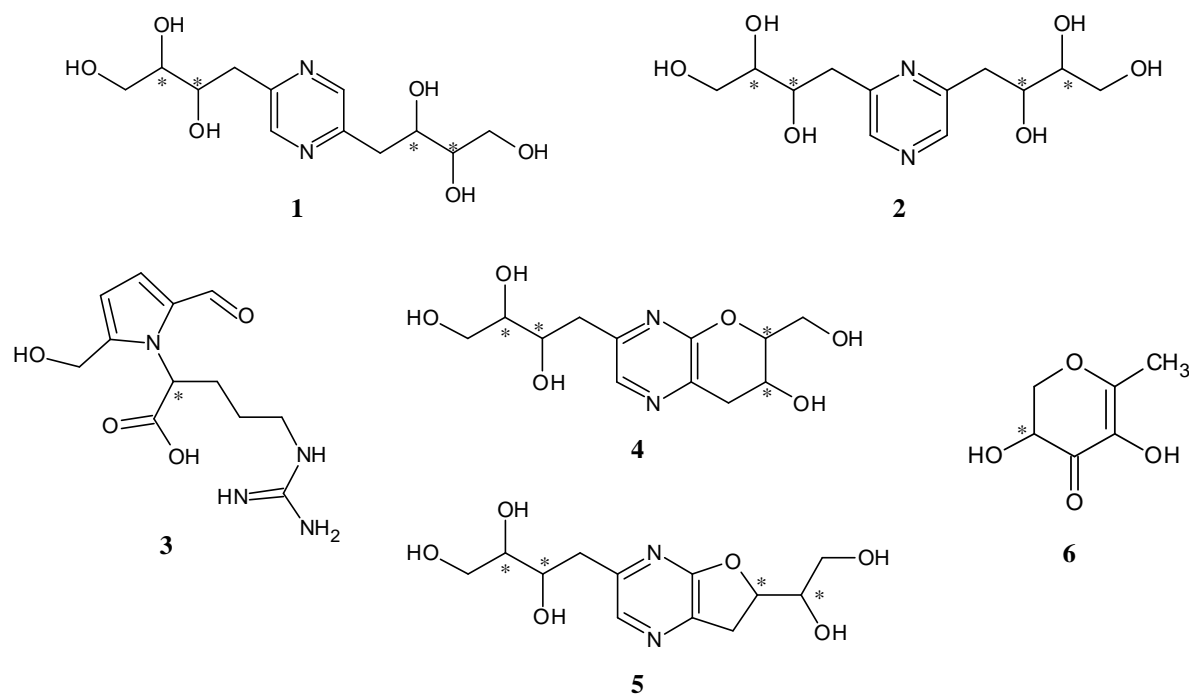


Figure 22. Chemical structures of isolated compounds **1**—**6** from MPLC fraction No.4.

Compounds **1**—**2** were obtained from No.4—5 and 6, respectively, as an amorphous brown powder. UPLC-ESI-TOF MS in the positive mode of both compounds showed a same pseudomolecular ion peak of m/z 289.1412 $[M+H]^+$, suggesting a molecular formula $C_{12}H_{20}N_2O_3$. In the ^{13}C NMR spectra of both compounds, obvious six signals were observed, as well as seven signals for proton in the 1H spectra, thus indicating that **1** and **2** are symmetrical compounds. The 1H spectrum of compound **1** showed four nonequivalent methylene protons at 2.89 [H-C(7a,11a)], 3.19 [H-C(7b,11b)], 3.63 [H-C(10a,14a)] and 3.78 ppm [H-C(10b,14b)] as well as two heteroatom-bearing methyne protons at 3.55 [H-C(9,13)], and 3.94 ppm [H-C(8,12)]. From the ^{13}C spectrum and heteronuclear HSQC correlations, two methylene carbons resonating at 39.26 [C(7,11)] and 64.57 ppm [C(10,14)] and two methyne carbons at 73.01 [C(8,12)] and 76.14 [C(9,13)] ppm were assigned. These assignments indicated two 1,2,3-butanetriol motifs, which was supported by heteronuclear COSY

connectivities of H-C(7)/H-C(8), H-C(8)/H-C(9), H-C(9)/H-C(10), H-C(11)/H-C(12), H-C(12)/H-C(13) and H-C(13)/H-C(14). In addition, a signal of an aromatic proton resonating at 8.48 ppm [H-C(3,6)] and two aromatic carbons at 145.62 [C(3,6)] and 154.14 ppm [C(2,5)] were observed in the ^1H and ^{13}C spectra. The heteronuclear HMBC spectrum showed cross peaks of H-C(3)→C(2,7) and H-C(6)→C(5,11) in high intensity as well as of H-C(3)→C(6) in low intensity (**Figure 23**). Taking all spectroscopic data into consideration, the chemical structure of **1** was determined as a symmetrical compound consisting of two 1,2,3-butanetriol motifs linked at C(2) and C(5) to the pyrazine ring, namely 1,2,3-Butanetriol, 4, 4'-(2,5-pyrazinediyl)bis-.

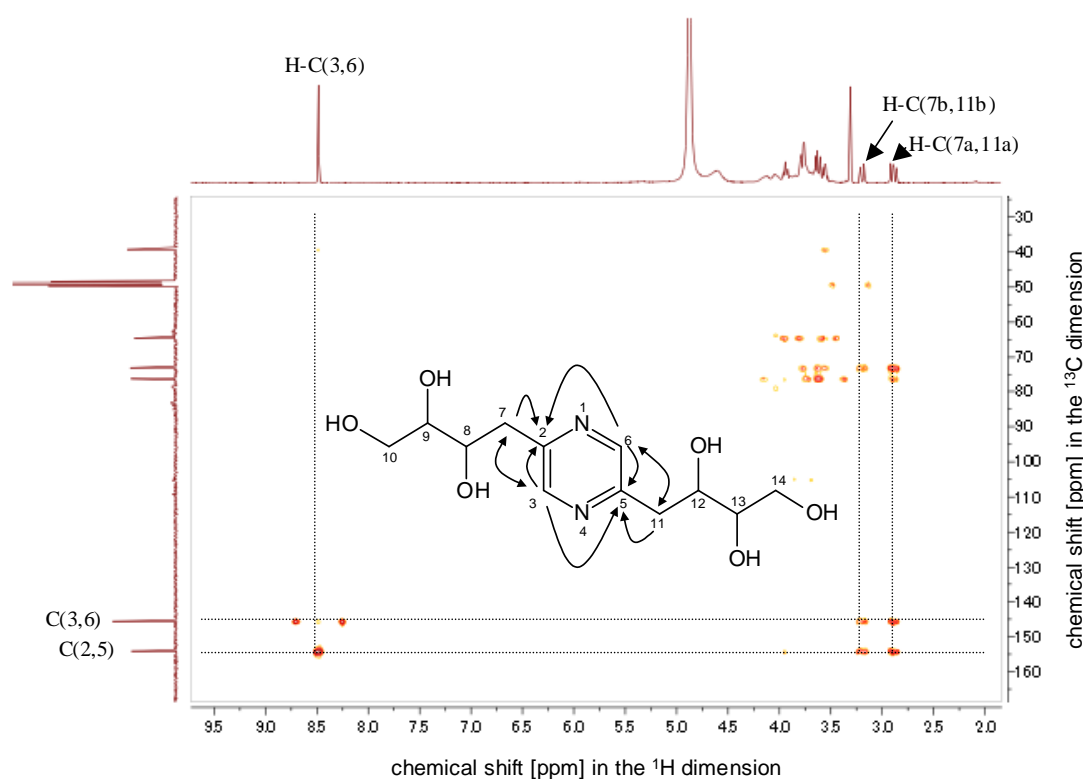


Figure 23. Excerpt of the HMBC spectrum (400 MHz, $\text{D}_2\text{O}/\text{MeOD}-d_4$, 9/1, v/v) and key correlations of compound **1**.

While compound **2** exhibited same ^1H , ^{13}C , COSY and HSQC spectra as compound **1**, one signal in the HMBC spectrum was different from that of **1**. The HMBC spectrum showed correlations of $\text{H-C}(3)\rightarrow\text{C}(2,5,7)$ and $\text{H-C}(5)\rightarrow\text{C}(3,6,11)$ in strong intensity (**Figure 24**), thus indicating that two 1,2,3-butanetriol motifs are connected to the pyrazine ring at C(2) and C(6). Therefore, the chemical structure of **2** was determined as 1,2,3-Butanetriol, 4, 4'-(2,6-pyrazinediyl)bis-. Although *Magaletta et al. (1996)* identified the structures of compounds **1** and **2** in roasted peanut by means of GCMS, the publication didn't show any NMR data.

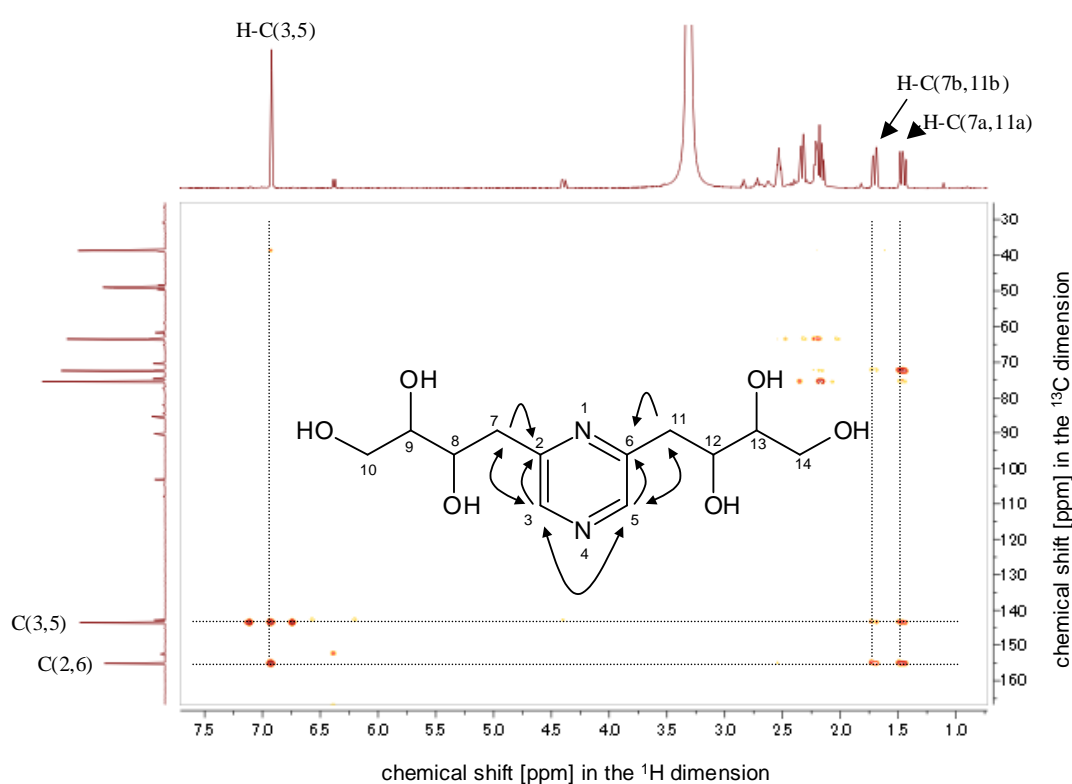


Figure 24. Excerpt of the HMBC spectrum (500 MHz, $\text{D}_2\text{O}/\text{MeOD-}d_4$, 9/1, v/v) and key correlations of compound **2**.

Compound **3** was obtained from No.4—7 as an amorphous powder. UPLC-TOF MS in the ESI⁺ mode showed a pseudomolecular ion peak of m/z 283.1403 [M+H]⁺, suggesting a molecular formula C₁₂H₁₈N₄O₄. In the ¹H spectrum, six nonequivalent aliphatic protons resonating at 1.01 [H-C(8a)], 1.42 [H-C(8b)], 1.86 [H-C(7a)], 2.43 [H-C(7b)], 2.95 [H-C(9a)] and 3.07 ppm [H-C(9b)], one methyne proton at 5.59 ppm [H-C(6)] and an amide proton at 9.11 ppm [H-N(10)] were observed. One methyne carbon at 60.30 ppm [C(6)], three methylene carbons at 26.24 [C(8)], 30.35 [C(7)] and 40.27 ppm [C(9)] and two quaternary carbons at 157.08 [C(11)] and 173.27 ppm [C(14)] were assigned from data of the HSQC and ¹³C NMR. In addition, the HMBC spectrum showed connectivities of H-C(7)→C(6,14), H-C(8)→C(6,7) and H-C(9)→C(7,8,11), resulting in the presence of an arginine motif. Besides, two olefinic protons resonating at 6.20 [H-C(4)] and 6.89 ppm [H-C(3)], two nonequivalent protons at 4.41 [H-C(12a)] and 4.47 ppm [H-C(12b)] and an aldehyde proton at 9.44 ppm [H-C(13)] were assigned as well as two quaternary carbons at 132.37 [C(5)] and 144.73 ppm [C(2)], two olefinic carbons at 109.91 [C(3)] and 122.78 ppm [C(4)] and an aldehyde carbon at 179.30 ppm [C(13)]. These assignment indicated the presence of a pyrrole ring with one hydroxymethyl and one aldehyde function, which was supported by the HMBC correlations of H-C(3)→C(2,4,5,12), H-C(12)→C(2,3), H-C(4)→C(2,3,5,13) and H-C(13)→C(5). A linkage between the arginine and the pyrrole motifs was found at C(6) via nitrogen of the pyrrole ring due to weak signals of H-C(3,4)→C(6) in the HMBC spectrum (**Figure 25**), therefore, the structure of **3** was determined as α -{(2-formyl-5-hydroxymethyl) pyrrol-1-yl}arginine, an arginine derivative of which the amino function is incorporated into the pyrrole system. To the best of our knowledge, this compound has not been reported before in the literature, but two analogs with glycine and alanine were isolated earlier (*Olsson et al. 1978.*, *Kim et al. 2014.*).

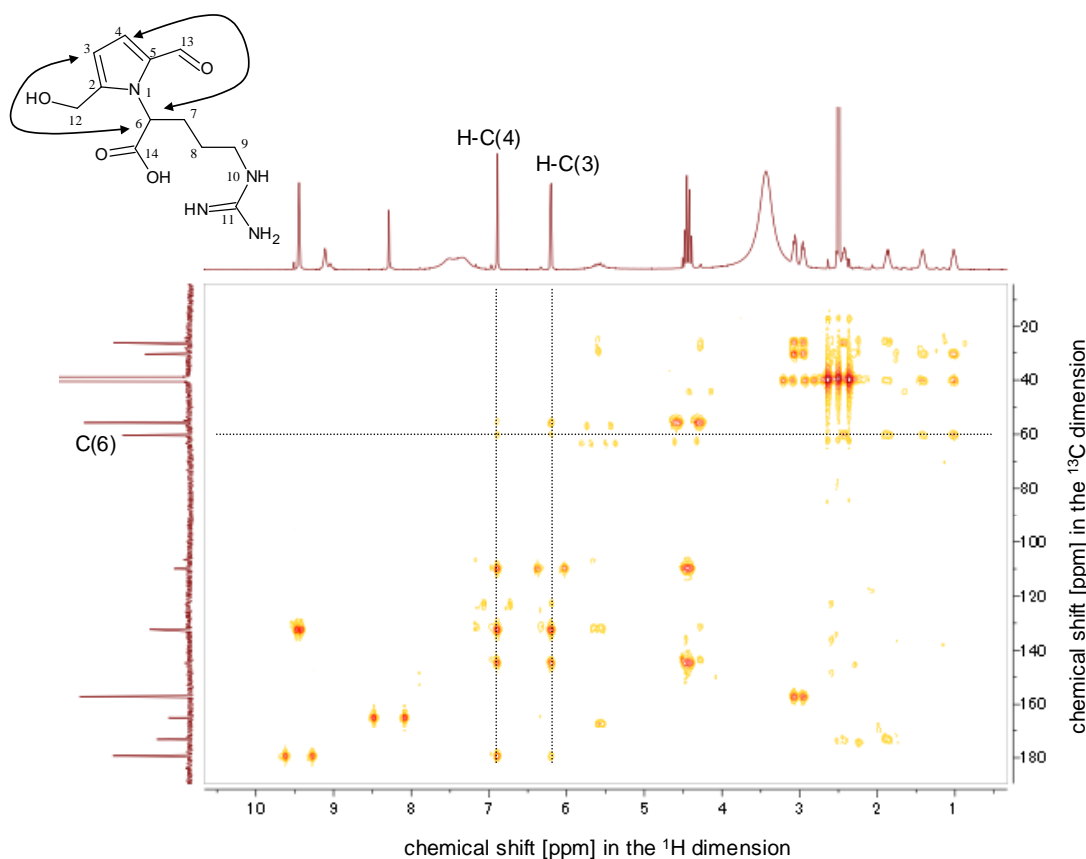


Figure 25. Excerpt of the HMBC spectrum (500 MHz, DMSO- d_6) and key correlations of compound **3**.

Compounds **4** and **5** were isolated from No.4—8 and —9, respectively, as an amorphous brown powder. UPLC-TOF MS in the ESI⁺ mode of both compounds revealed the same pseudomolecular ion peak of m/z 287.1252 [M+H]⁺, suggesting a molecular formula of C₁₂H₁₈N₂O₆ and implying isomers each other. The ¹³C and HSQC spectra of **4** showed similar data for **1** and **2**, such as two methylene carbons resonating at 38.03 [C(12)] and 63.25 ppm [C(15)], two methyne carbons at 74.90 [C(14)] and 71.23 ppm [C(13)], an aromatic quaternary carbon at 151.71 ppm [C(8)] and an aromatic methyne at 137.03 ppm [C(7)]. Additionally, two aromatic quaternary carbons at 135.39 [C(5)] and 155.84 ppm [C(10)] were also observed, and the carbons had HMBC connectivities of H-C(7)→C(5) in high intensity and of H-C(7)→C(10) in low intensity. These assignments indicated that compound **4** would have an asymmetrical alkylpyrazine structure. Furthermore, two methyne protons resonating at 4.12 [H-C(2)] and 4.07 ppm [H-C(3)] and two nonequivalent

methylene protons at 2.80 [H-C(4a)] and 3.08 ppm [H-C(4a)] exhibited HMBC cross peaks of H-C(2)→C(3,4,10), H-C(3)→C(5) and H-C(4)→C(2,3,5,10), which disclosed the presence of a tetrahydropyran motif linked to the pyrazine ring at C(10) and C(5) (**Figure 26**). Also, the COSY and HMBC spectra revealed a hydroxymethyl function connected at C(2) based on correlations of H-C(11)→C(2,3). Taking all spectroscopic data into account, the chemical structure of compound **4** was determined as 4-[7-hydroxy-6-(hydroxymethyl)-7,8-dihydro-6*H*-pyrano[2,3-*b*]pyrazine-3-yl]butane-1,2,3-triol.

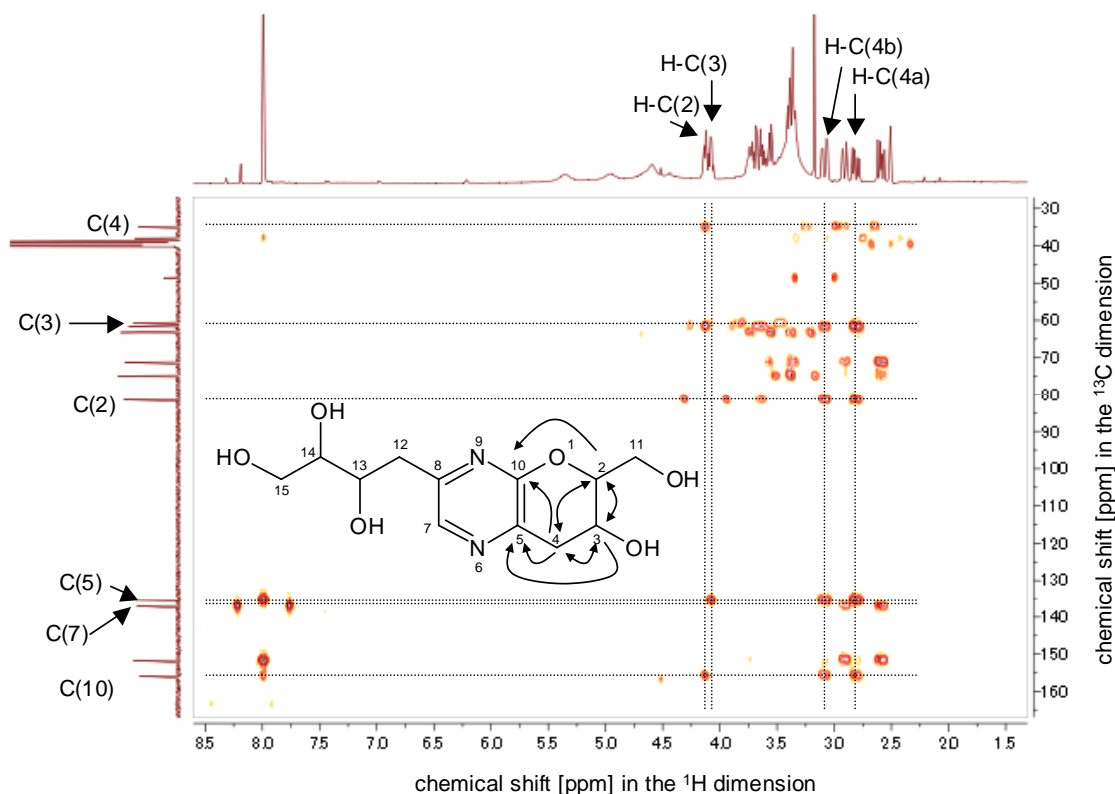


Figure 26. Excerpt of the HMBC spectrum (500 MHz, DMSO-*d*₆) and key correlations of compound **4**.

In contrast to NMR data of compound **4**, compound **5** showed different resonances for aromatic carbon at 143.23 [C(4)] and 161.86 ppm [C(9)], and the two carbons possessed HMBC connectivities to three aliphatic protons (H-C(2)→C(3,4,9), H-C(3)→C(2,4,9)). This difference indicated that **5** has a tetrahydrofuran motif bound to the pyrazine ring at C(9) and C(4) instead of the tetrahydropyran motif in **4**. Then, two aliphatic methylene protons resonating at 3.41 ppm [H-C(11)] and a heteroatom-bearing methyne at 3.83 ppm [H-C(10)]

showed correlations of $\text{H-C}(11) \rightarrow \text{C}(2,10)$ and $\text{H-C}(10) \rightarrow \text{C}(2,3,11)$ in the HMBC spectrum (**Figure 27**). These assignments indicated the presence of a dihydroxyethyl function connected to carbon C(2). Thus, the structure of **5** was determined as 4-[6-(1,2-dihydroxyethyl)-6,7-dihydrofuro[2,3-b]pyrazin-3-yl]-butane-1,2,3-triol. These two compounds have not been reported before in literature.

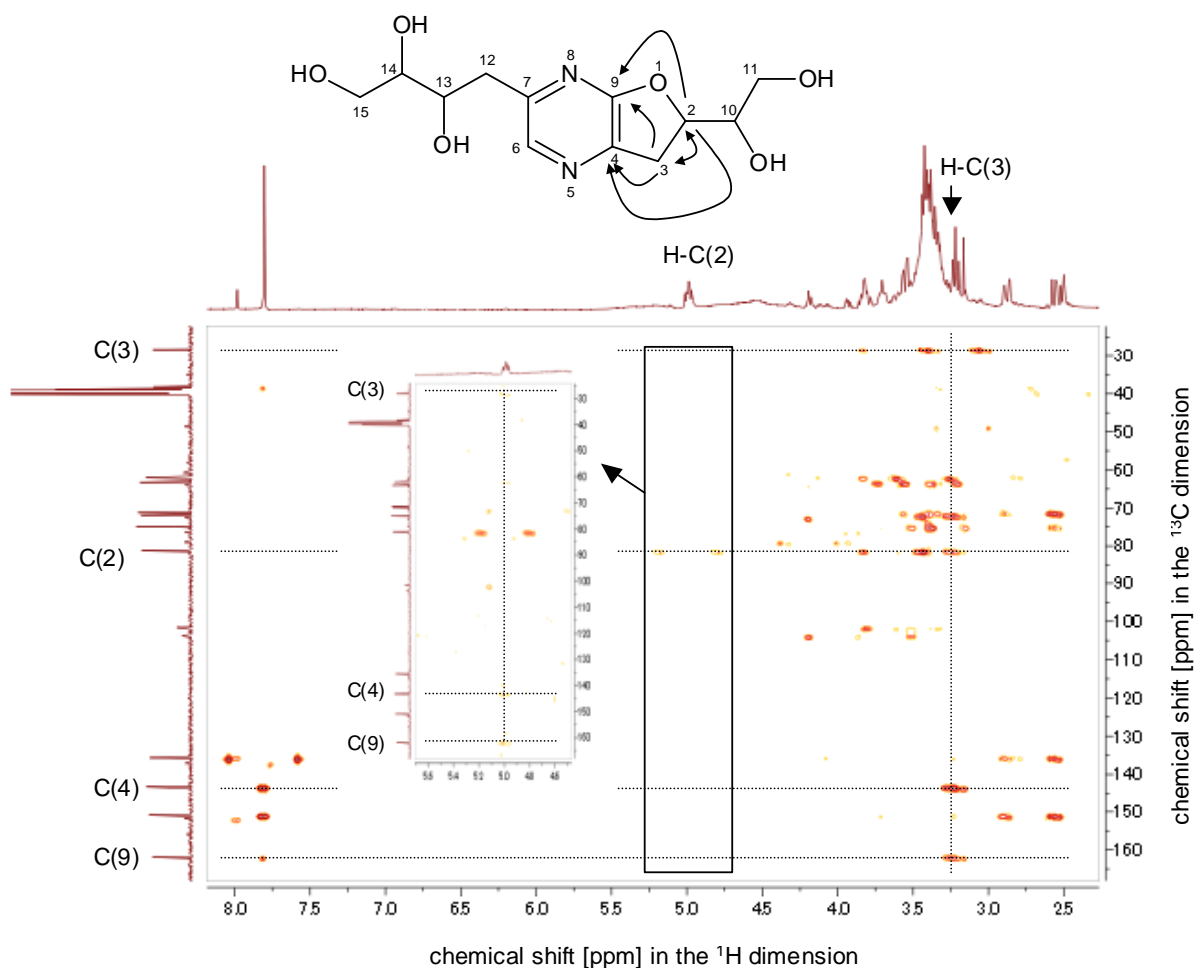


Figure 27. Excerpt of the HMBC spectrum (500 MHz, $\text{DMSO-}d_6$) and key correlations of compound **5**.

Compound **6** was obtained from No.4—10 as a brownish oil. UPLC-ESI-TOF MS in the positive mode exhibited a pseudomolecular ion peak of m/z 145.0495 $[M+H]^+$, suggesting a molecular formula $C_6H_8O_4$. The 1H and HSQC spectra revealed that two nonequivalent methylene protons resonating at 4.01 [H-C(2a)] and 4.24 ppm [H-C(2b)], a methyne proton at 4.02 ppm [H-C(3)] and a signal of one methyl function at 1.94 ppm [H-C(7)]. Also, a methyl carbon at 15.28 ppm [C(7)], a methylene carbon at 71.30 ppm [C(2)], a methyne carbon at 67.36 ppm [C(3)], two olefinic quaternary carbons at 131.28 [C(6)] and 157.67 ppm [C(5)] and one quaternary carbon at 187.32 ppm [C(4)] were assigned from data of the ^{13}C and HSQC spectra. In the HMBC spectrum, correlations of H-C(2) \rightarrow C(3,4,6), H-C(3) \rightarrow C(4), and H-C(7) \rightarrow C(5,6) were observed (**Figure 28**), thus the chemical structure of **6** was assigned as 2,3-dihydro-3,5-dihydroxy-6-methyl-4(H)-pyran-4-one. The 1H and ^{13}C NMR spectra of **6** are well in line with a literature (Hwang *et al.* 2013), and its reducing power for metal ions, DPPH and ABTS radical scavenging activities had been reported earlier (Hwang *et al.* 2013, Yu *et al.* 2013).

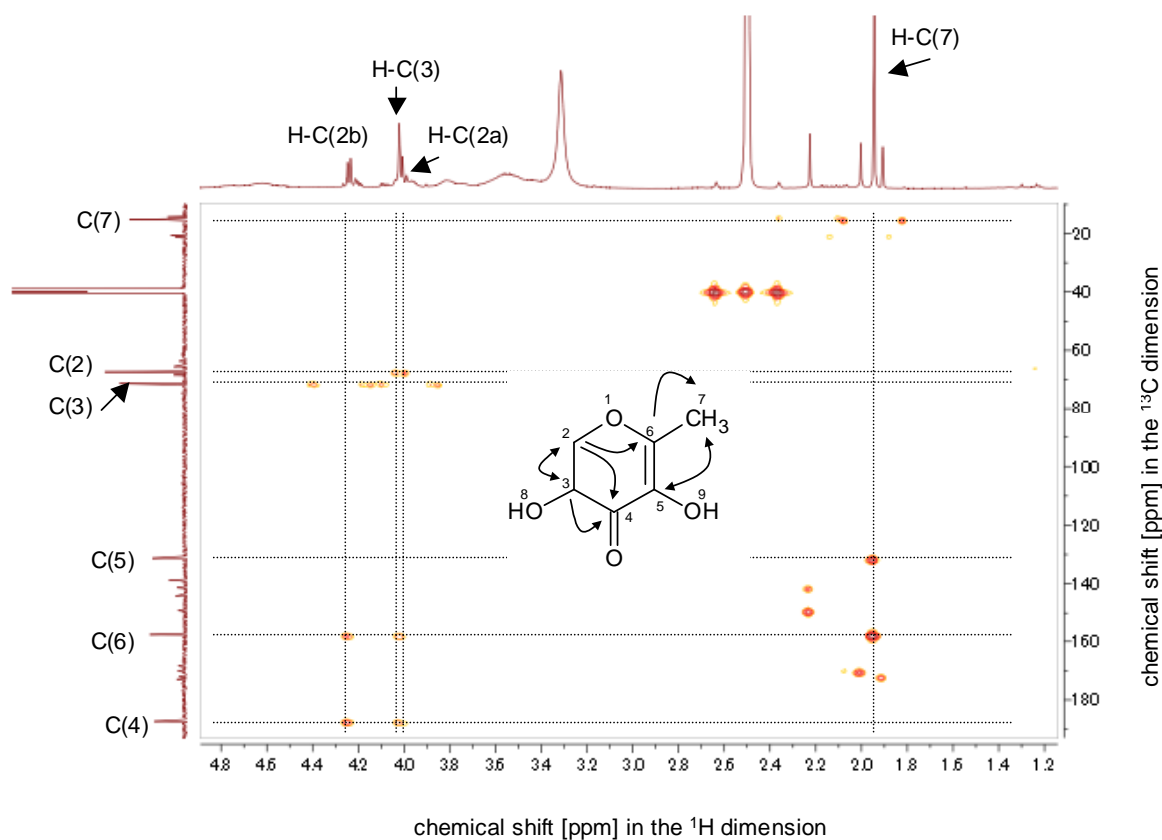


Figure 28. Excerpt of the HMBC spectrum (500 MHz, $DMSO-d_6$) and key correlations of compound **6**.

2.2.4 Isolation and structure elucidation of antioxidants in MPLC fraction No.5

Next, MPLC fraction No.5 was investigated to isolate and identify antioxidants. An aliquot of the fraction No.5 was separated into 25 subfractions by means of semipreparative HPLC (**Figure 29—30**), and each subfraction was analyzed for their antioxidative activity using the ARS and ORAC assay, respectively.

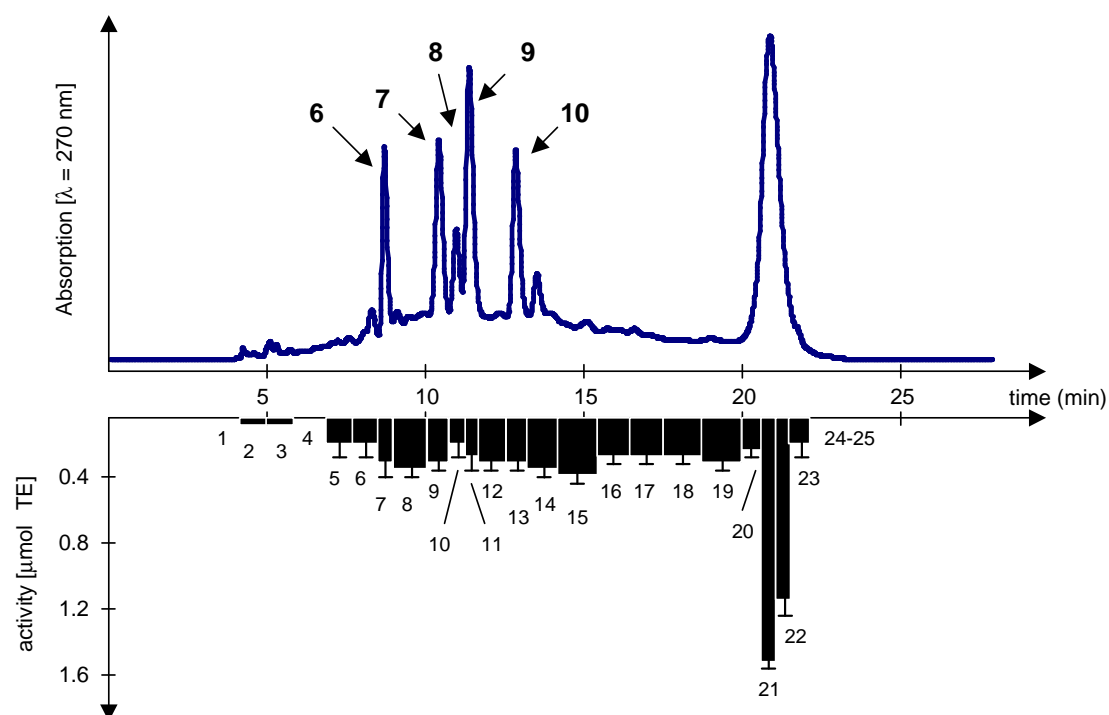


Figure 29. HPLC separation and ARS activities obtained from MPLC fraction No.5. Data represent antioxidative activity expressed as Trolox equivalents (TE) (average \pm S.D, $n=3$). The whole activity of MPLC fraction No.5 was 8.10 [$\mu\text{mol TE}$], and the calculated sum of each fraction was 7.88 [$\mu\text{mol TE}$]. Compound numbering is given in bold.

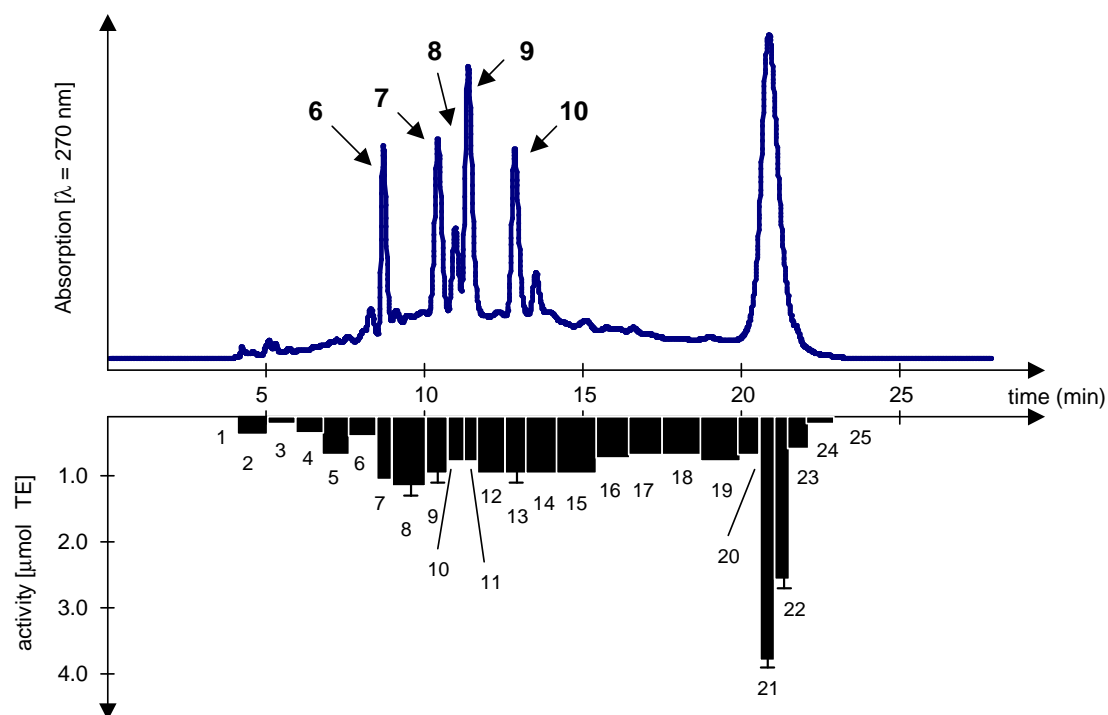


Figure 30. HPLC separation and ORAC activities obtained from MPLC fraction No.5. Data represent antioxidative activity expressed as Trolox equivalents (TE) (average \pm S.D, $n=3$). The whole activity of the MPLC fraction No.5 was 20.52 [$\mu\text{mol TE}$], and the calculated sum of each fraction was 20.56 [$\mu\text{mol TE}$]. Compound numbering is given in bold.

ARS and ORAC activities of the whole MPLC fraction No.5 showed 8.10 and 20.52 [$\mu\text{mol TE}$], respectively, and these values were comparable to the calculated sums of each subfraction (7.88 and 20.56 [$\mu\text{mol TE}$]). In the HPLC, six main peaks (No.5—7, 9, 10, 11, 13, 20, 21, 22, and 23) were observed. As antioxidative assays revealed that the five peaks (No.5—7, 9, 10, 11 and 13) show activities in both systems, the peaks were chosen for structure elucidation.

Although the predominant peak, which consisted of No.5—20, 21, 22, and 23 and eluted at 95% methanol in the chromatography, showed the highest activities in the assays, additional HPLC runs using the same column with a slower gradient implied that the fraction contained polymerized and complexed compounds because it eluted as a hump (data not shown). Further, the ^1H NMR spectrum showed no specific signals (**Figure 31**), thus suggesting the presence of polymeric material. Considering the above reasons, fractions of No.5—20, 21, 22, and 23 were not further investigated.

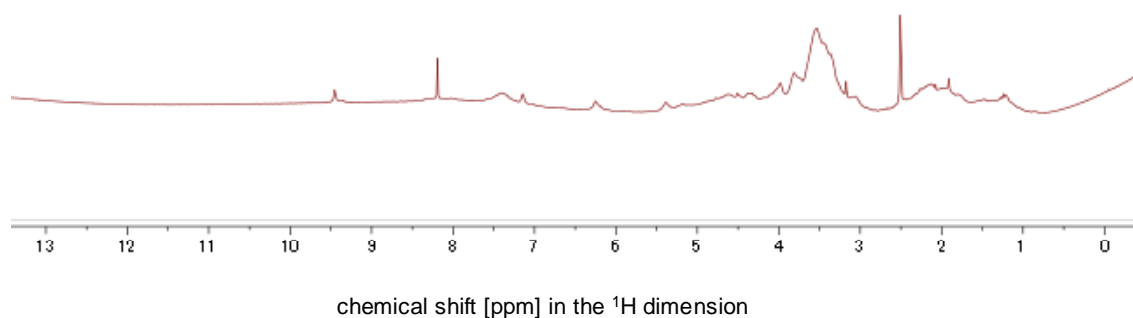


Figure 31. ^1H NMR spectrum (400 MHz, $\text{DMSO-}d_6$) of a mixture of the fraction No.5—20 to 5—23.

After purification by means of HPLC separation, compounds **6—10** were afforded from No.5—7, 9, 10, 11 and 13, respectively, and their chemical structures were established by means of 1D/2D-NMR and UPLC-ESI-TOF MS (**Figure 32**).

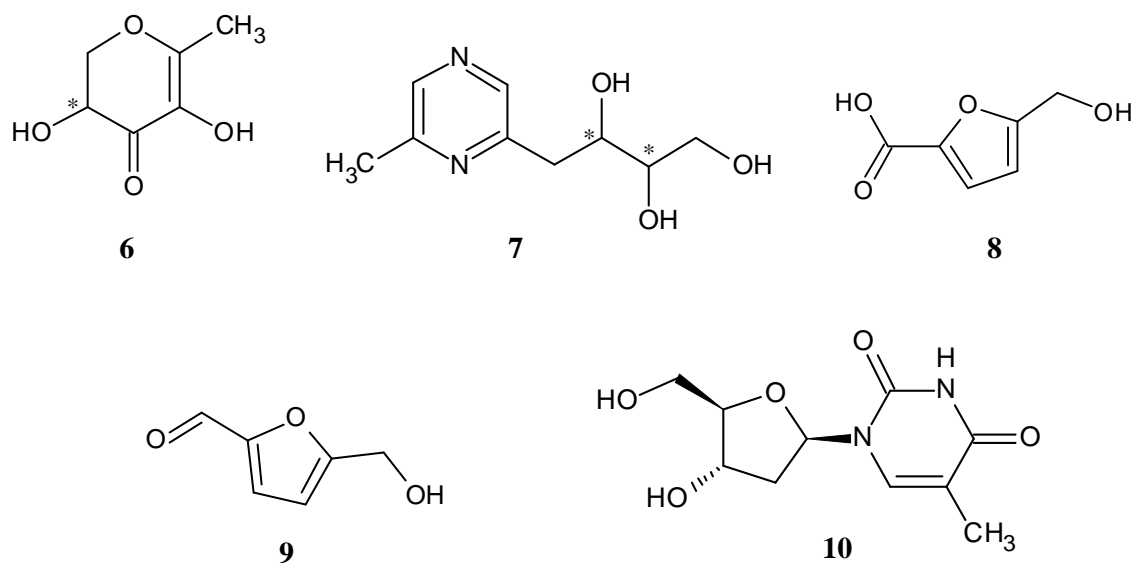


Figure 32. Chemical structures of isolated compounds **6**—**10** from MPLC fraction No.5.

NMR spectra and UPLC-TOF MS in the ESI⁺ mode of the fraction No.5—7 showed same data as described above for compound **6**.

Compound **7** was isolated from the fraction No.5—9 as a brown amorphous powder. UPLC-TOF MS in the ESI⁺ mode exhibited a pseudomolecular ion peak of m/z 199.1083 [M+H]⁺, suggesting a molecular formula C₉H₁₄N₂O₃. Similarity of the ¹³C and heteronuclear HSQC spectra between compounds **7** and **2** enabled to propose that **7** composed of an alkyipyrazine structure consisted of two methylene carbons resonating at 38.71 [C(7)] and 63.22 ppm [C(13)], two methyne carbons at 71.32 [C(8)] and 74.99 ppm [C(11)], two aromatic methyne carbons at 141.38 [C(5)] and 142.32 ppm [C(3)] and two aromatic quaternary carbons at 152.34 [C(6)] and 154.86 ppm [C(2)]. The HMBC correlations supported the structure showing cross peaks of H-C(3)→C(2,5,7), H-C(5)→C(3,6), H-C(7)→C(2,3,8,11), H-C(8)→C(2,11,13), H-C(11)→C(7,8,13) and H-C(13)→C(8,11), and then further signals on the COSY and HMBC connectivities of H-C(10)/H-C(5) and H-C(10)→C(5,6) clarified the presence of a methyl function at C(6) (**Figure 33**). All spectroscopic data led the identification of compound **7** as 1,2,3-butanetriol-4-(6-methyl-2-pyrazinyl).

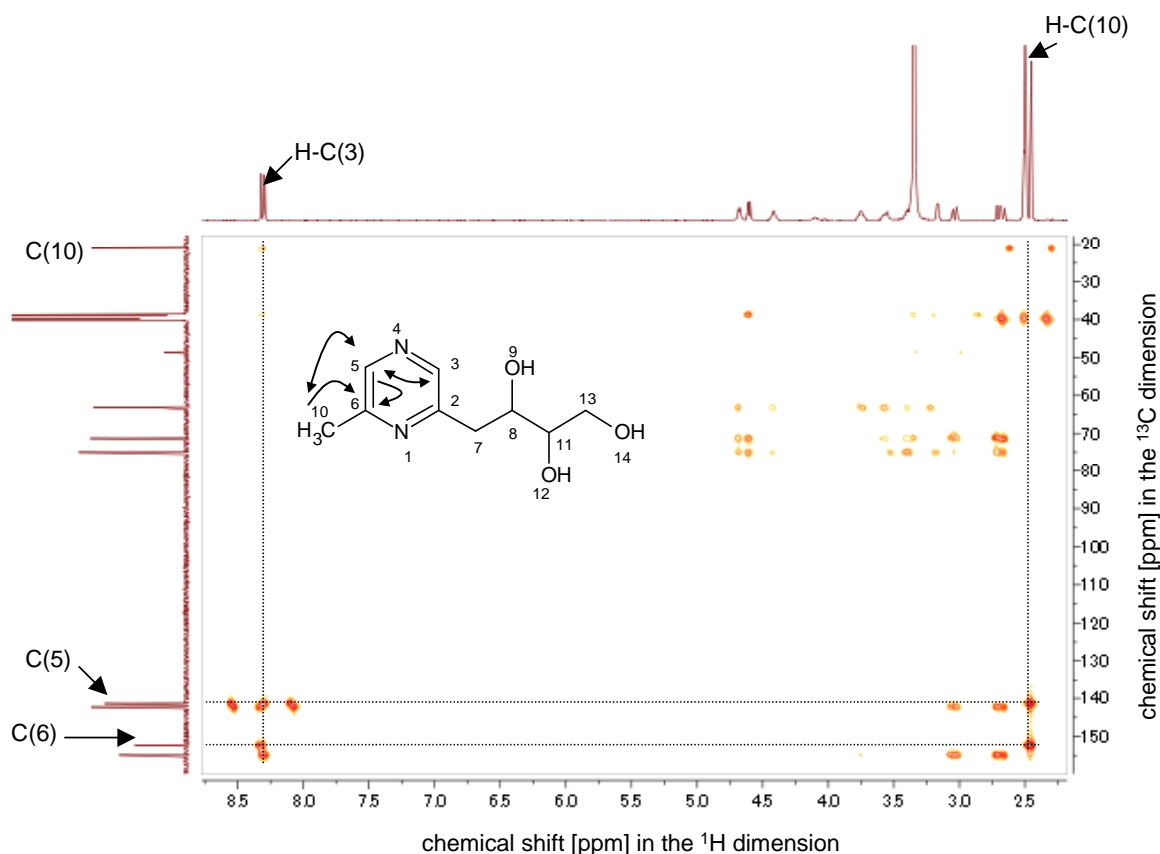


Figure 33. Excerpt of the HMBC spectrum (400 MHz, DMSO- d_6) and key correlations of compound **7**.

Compound **8** was obtained from fraction No.5—9 as a brown amorphous powder. The ^1H and ^{13}C spectra of **8** showed four and six signals, respectively. Two equivalent protons resonating at 4.44 ppm [H-C(6)], a hydroxyl function at 5.42 ppm [H-O(7)] and two olefinic methyne protons at 6.45 [H-C(3)] and 7.13 ppm [H-C(4)] were assigned based on the HSQC spectrum, as well as a methylene carbon at 55.79 ppm [C(6)], two olefinic methyne carbons at 108.90 [C(3)] and 118.41 ppm [C(4)] and two quaternary carbons at 159.34 [C(8)] and 159.61 ppm [C(2)]. In addition, the HMBC spectrum exhibited correlations of H-C(3) \rightarrow C(2,4,5,6), H-C(2) \rightarrow C(3,5,6) and H-C(6) \rightarrow C(2,3), which supported the proposed structure (**Figure 34**). UPLC-TOF MS in the ESI $^-$ mode showed a pseudomolecular ion peak of m/z 141.0192 [M-H] $^-$ which corresponded in the proposed structure. Also, its NMR data are well in line with literature (*Mitsukura et al. 2004*). Thus, the chemical structure of compound **8** was determined as 5-hydroxymethyl-2-furancarboxylic acid.

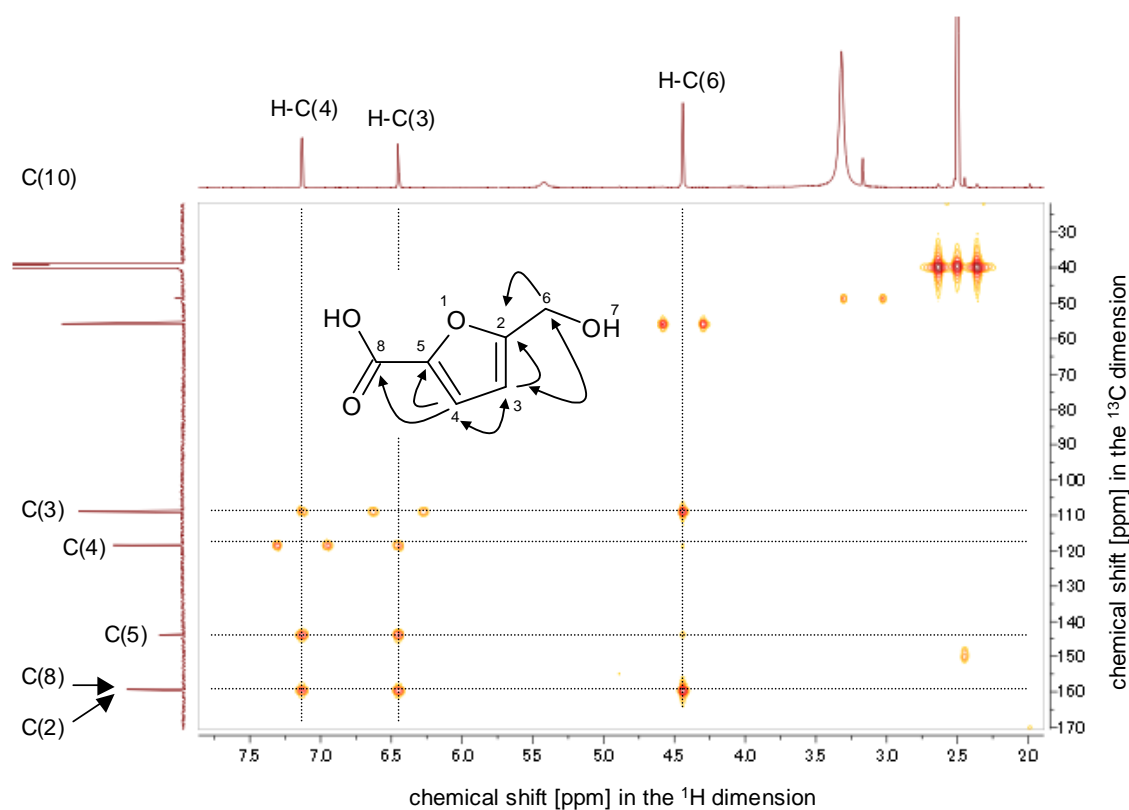


Figure 34. Excerpt of the HMBC spectrum (500 MHz, DMSO- d_6) and key correlations of compound **8**.

Compound **9** was obtained from fraction No.5—11 as an oily substance. UPLC-TOF MS in the ESI⁺ mode exhibited a pseudomolecular ion peak of m/z 127.0395 [M+H]⁺, suggesting a molecular formula C₆H₆O₃. The ¹H and ¹³C spectra of **9** were quite similar to the NMR data of **8**, as well as the corresponding coupling constant of $J=3.5$ Hz of the two olefinic protons (H-C(3) and H-C(4)), thus indicating to have the furan structure. Further, the ¹H and ¹³C spectra showed an obvious aldehyde signal of δ_H 9.54 and δ_C 178.00 that was differed from the signal in **8**, and the HMBC spectrum led its position to C(5) in the furan ring showing connectivities of H-C(8)→C(4,5) and H-C(4)→C(2,3,5,8). Therefore, the chemical structure was determined as 5-hydroxymethyl-2-furanaldehyde. The ¹H and ¹³C spectra of **9** are well in line with literature (Quiroz-Florentino *et al.*, 2008).

Compound **10** was isolated from fraction No.5—13 as a pale brown amorphous powder. UPLC-TOF MS in the ESI⁻ mode exhibited a pseudomolecular ion peak of m/z 241.0833 [M-H]⁻, suggesting a molecular formula C₁₀H₁₃N₂O₅. The ¹H spectrum showed three heteroatom-bearing protons resonating at 3.75 [H-C(5)], 4.23 [H-C(4)] and 6.16 ppm [H-C(5)] and four aliphatic methylene protons at 2.09 [2H, H-C(3)], 3.54 [H-C(13a)] and 3.59 ppm [H-C(13b)], and also two hydroxyl resonances at 5.02 [H-O(14)] and 5.23 ppm [H-C(12)]. The protons exhibited heteronuclear correlations, namely H-C(2)→C(4,5), H-C(3)→C(2,4,5), H-C(4)→C(5,13) and H-C(13)→C(4,5) in the HMBC spectrum as well as homonuclear connectivities of H-C(2)/H-C(3), H-C(3)/H-C(4), H-C(4)/H-C(5), and H-C(5)/H-C(13ab) in the COSY spectrum. The above assignments revealed a deoxy-sugar moiety for compound **10**. Besides, three aromatic carbon resonances at 109.40 [C(10)], 150.50 [C(7)] and 163.78 ppm [C(9)], a resonance for an olefinic methylene carbon at 136.15 ppm [C(11)] and a resonance for a methyl function at 12.29 ppm [C(15)] were observed in the ¹³C spectrum. Further, a signal of a nitrogen-binding proton at 11.27 ppm [H-N(8)] and an olefinic proton at 7.69 ppm [H-C(11)] were found in the ¹H spectrum. These assignments highlighted the thymine motif based on HMBC correlations of H-C(11)→C(7,9,10,15) and H-C(15)→C(9,10,11). Furthermore, the HMBC connectivities of H-C(2)→C(7,11) enabled to determine the linkage of C(2)-N(6) for both motifs (**Figure 35**), and the chemical structure was identified as thymidine. ¹H and ¹³C spectra were well in agreement with literature (Xiao *et al.* 2007).

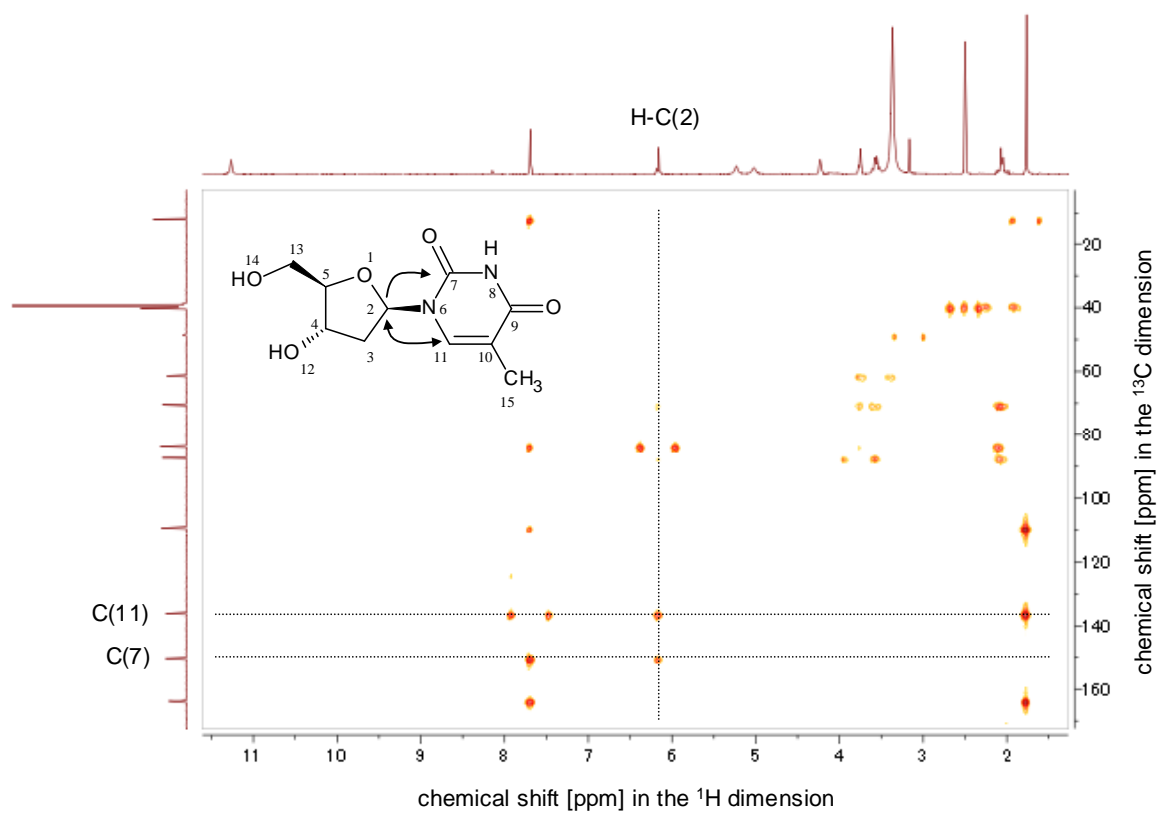


Figure 35. Excerpt of the HMBC spectrum (400 MHz, $\text{DMSO-}d_6$) and key correlations of compound **10**.

2.2.5 Isolation and structure elucidation of antioxidants in MPLC fraction No.6

Next, the MPLC fraction No.6 was investigated to isolate and identify antioxidants. An aliquot of the fraction No.6 was separated into 34 subfractions by means of semipreparative HPLC (**Figure 36—37**), and each subfraction was analyzed for antioxidative activities using ARS and ORAC assays.

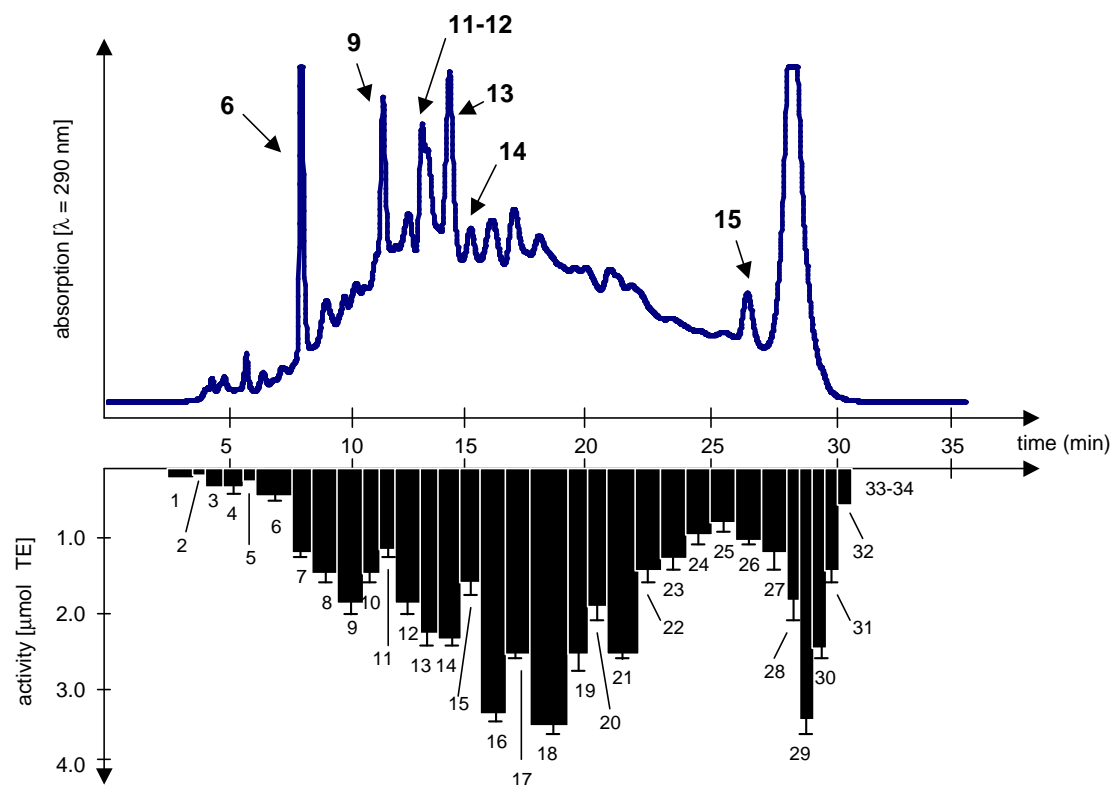


Figure 36. HPLC separation and ARS activities obtained from the MPLC fraction No.6. Data represent antioxidative activity expressed as Trolox equivalents (TE) (average \pm S.D, $n=3$). The whole activity of the MPLC fraction No.6 was 46.53 [$\mu\text{mol TE}$], and the calculated sum of each fraction was 48.75 [$\mu\text{mol TE}$]. Compound numbering is given in bold.

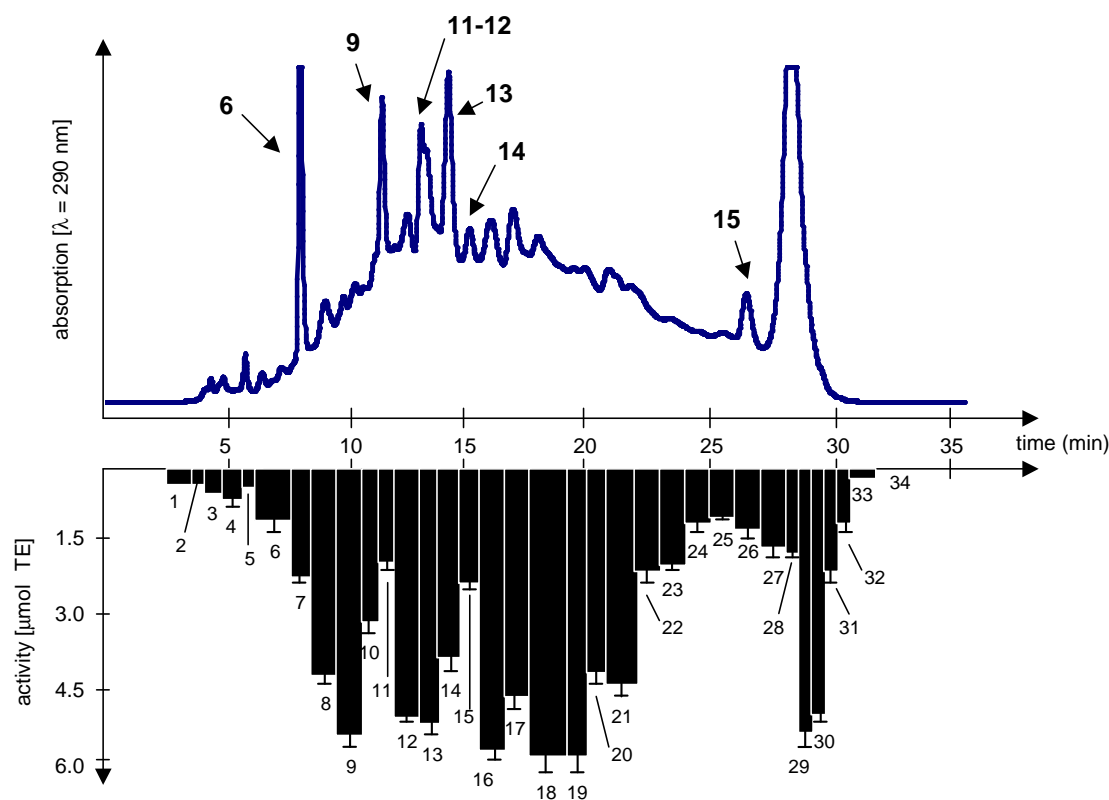


Figure 37. HPLC separation and ORAC activities obtained from the MPLC fraction No.6. Data represent antioxidative activity expressed as Trolox equivalents (TE) (average \pm S.D, $n=3$). The whole activity of the MPLC fraction No.6 was 90.82 [$\mu\text{mol TE}$], and the calculated sum of each subfraction was 91.26 [$\mu\text{mol TE}$]. Compound numbering is given in bold.

ARS and ORAC activities of the whole MPLC fraction No.6 showed 46.53 and 91.26 [$\mu\text{mol TE}$], respectively, and these activities were in the same range as the calculated sums of each subfraction (48.75 and 91,26 [$\mu\text{mol TE}$]). In the HPLC run, six main peaks (No.6—7, 11, 13, 14, 27, 28, 29, 30, and 31) and many tiny peaks were observed. Antioxidative assays revealed that the activities are distributed to all fractions and were independent of their peak intensities. Relatively higher antioxidative fractions, such as No.6—8, 9, 12, 16, 18, 19, 20 and 21, were purified to obtain antioxidants by means of further HPLC separations, however, yields of purified subfractions were too low to conduct structure determination. Finally, six fractions (No.6—7, 11, 13, 14, 15 and 26) that showed higher purities and yields were selected for structure determination. After purification of the six fractions employing HPLC separation, compounds **6**,

9, 11—15 were afforded from No.6—7, 11, 13, 14, 15 and 26, respectively, and their chemical structures were established by means of 1D/2D-NMR, UPLC-TOF MS and CD spectroscopy (**Figure 38**).

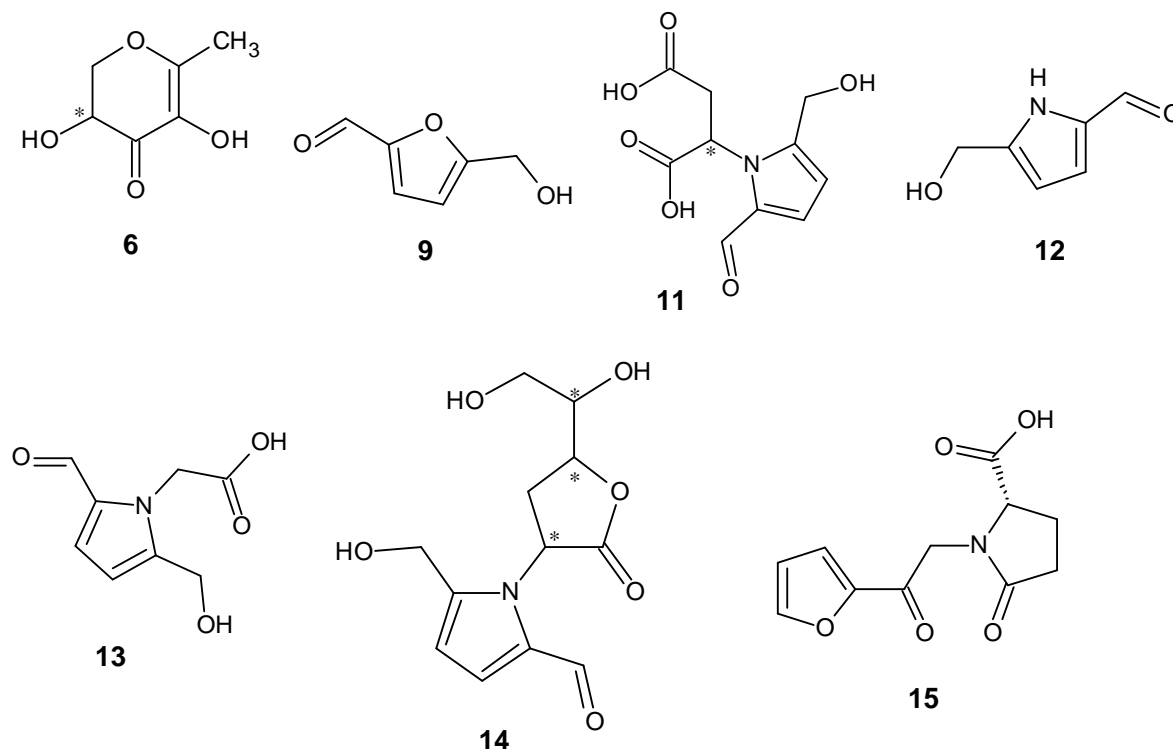


Figure 38. Chemical structures of isolated compounds **6, 9, 11—15** from the MPLC fraction No.6.

The ^1H spectra of fraction No.6—7 and 6—11 were identical to compounds **6** and **9**, respectively, therefore their structures were determined as 2,3-dihydro-3,5-dihydroxy-6-methyl-4(H)-pyran-4-one and 5-hydroxymethyl-2-furaldehyde isolated already from MPLC fraction No.5.

In the HPLC separation using a Polar-RP column (**Figure 36—37**), compound **11** and compound **12** were not baseline separated, and therefore, re-purified by another HPLC step yielding an amorphous pale brown and dark brown powder, respectively (**Figure 39**). **11** was an unstable compound and generated a breakdown compound due to intramolecular esterification during lyophilization, therefore pH of its solution obtained by the purification was adjusted to 7.0 using sodium hydroxide, and subsequently the solution was freeze-dried, which resulted in prevention of the degradation.

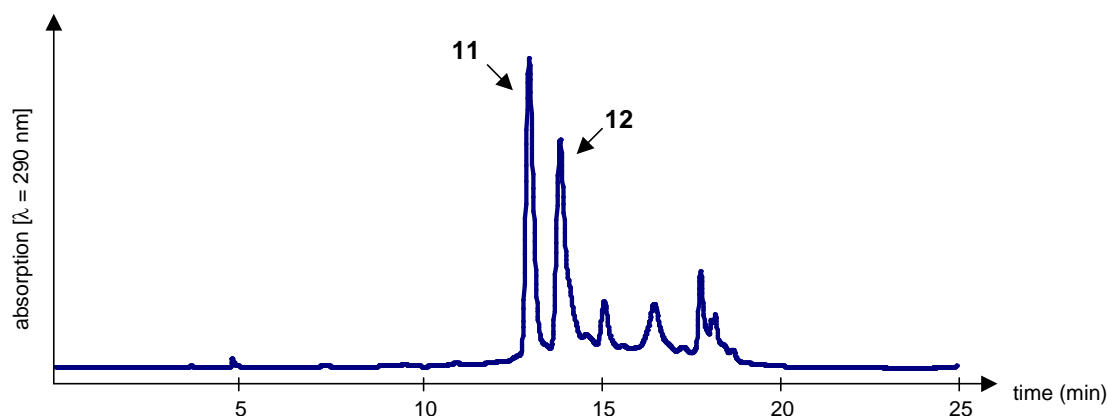


Figure 39. HPLC of the fraction No.6—13 for separation of compounds **11** and **12**.

UPLC-ESI-TOF MS in negative mode exhibited a pseudomolecular ion peak of m/z 240.0972 $[M-H]^-$, suggesting a molecular formula of $C_{10}H_{11}NO_6$. Considering similarity of some signals in the 1H and ^{13}C spectra for compound **11** to the NMR data of compound **3**, the presence of a pyrrole ring with a hydroxymethyl and an aldehyde functions was disclosed with resonances of two olefinic proton at 6.20 [H-C(3)] and 7.05 ppm [H-C(4)], of two equivalent aliphatic protons at 4.55 ppm [H-C(9)] and of an aldehyde proton at 9.33 ppm [H-C(10)] as well as of carbon signals at 55.26 [C(9)], 109.21[C(3)], 125.88[C(4)], 131.64 [C(5)], 144.58 [C(2)] and 178.41 ppm [C(10)]. Besides, δ_H of an aliphatic methyne proton at 5.48 ppm [H-C(6)] and two nonequivalent methylene at 2.81 [H-C(7a)] and 3.30 ppm [H-C(7b)] and δ_C of a methylene carbon at 37.13 ppm [C(7)], a methyne at 54.83 ppm [C(6)] and two quaternary at 170.17 [C(8)] and 172.02 ppm [C(11)] indicated the existence of an aspartic acid motif, based on the heteronuclear HMBC and homonuclear COSY correlations of H-C(7)→C(6,8,11) and H-C(7ab)/H-C(6) (**Figure 40**). The HMBC spectrum did not exhibit any signals for the linkage between the motifs, however it was clarified that the motifs were connected via a C(6)-N(1) linkage because any amino-proton signals were not observed in the 1H NMR spectrum using $DMSO-d_6$. Furthermore, six degrees of unsaturation, deduced from the proposed chemical structure due to two carbonyls, two olefines, one aldehyde and an aromatic ring, corresponded to the calculated elemental composition of $C_{10}H_{11}NO_6$ determined via mass spectrometry.

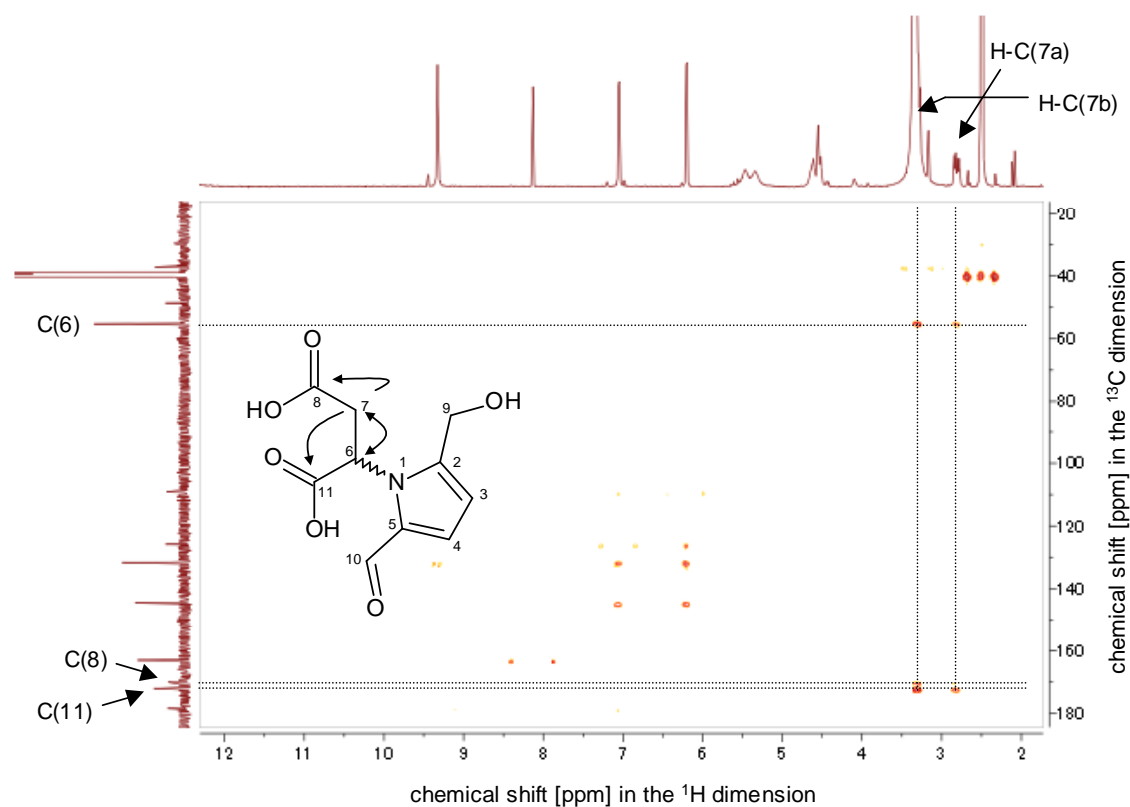


Figure 40. Excerpt of the HMBC spectrum (400 MHz, $D_2O/MeOD-d_4$, 9/1) and key correlations of compound **11**.

Taking all spectroscopic data into consideration, the chemical structure of **11** was determined as a derivative of aspartic acid, of which the amino function is incorporated into the pyrrole system line in compound **3**. To the best of our knowledge, this compound has not been reported in literature so far.

The 1H and ^{13}C spectra of compound **12** corresponded to the data for the pyrrole motifs in compounds **3** and **11**, and a broad signal of an amino proton resonating at 11.87 ppm [H-N(1)] was observable in the 1H NMR spectrum (**Figure 41**). In addition, UPLC-TOF MS in the ESI^+ mode exhibited a pseudomolecular ion peak of m/z 126.0554 $[M+H]^+$, suggesting a molecular formula of $C_6H_7NO_2$, therefore, the structure was identical as 5-hydroxymethyl-1*H*-pyrrole-2-carbaldehyde. Data of the 1H and ^{13}C spectra are well in agreement with the literature (*Sudhakar et al., 2011*).

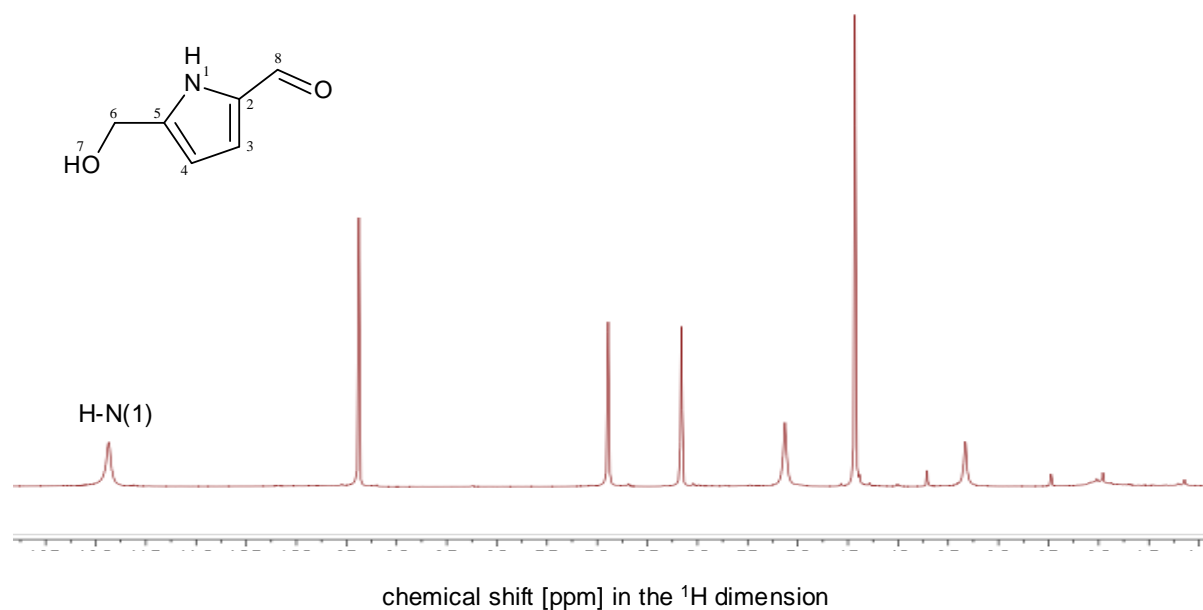


Figure 41. Excerpt of the ^1H NMR spectrum (500 MHz, $\text{DMSO}-d_6$) of compound **12**.

Compound **13** was isolated from the fraction No.6—14 as an amorphous brown powder. UPLC-TOF MS in the ESI^- mode exhibited a pseudomolecular ion peak of m/z 182.0452 $[\text{M}-\text{H}]^-$, suggesting a molecular formula $\text{C}_8\text{H}_9\text{NO}_4$. As the ^1H and ^{13}C spectra of **13** were totally similar to those of compound **11**, the chemical structure of **13** was predicted as a type of another amino acid with a pyrrole ring. The HSQC spectrum enabled to assign a quaternary carbon resonating at 169.69 ppm [C(7)], a methylene carbon at 46.80 ppm [C(6)] and two equivalent methylene protons at 5.06 ppm [H-C(6)], which led a glycine motif based on a HMBC correlation of $\text{H}-\text{C}(6) \rightarrow \text{C}(7)$. Then, a linkage of C(6)-N(1) between the glycine motif and the pyrrole ring was clarified by the HMBC correlations of $\text{H}-\text{C}(6) \rightarrow \text{C}(2,5)$ (**Figure 42**). Thus, the structure of **13** was established as α -{(2-formyl-5-hydroxymethyl)pyrrol-1-yl}glycine. The ^1H spectrum is well in agreement with the literature (*Olsson et al. 1978*).

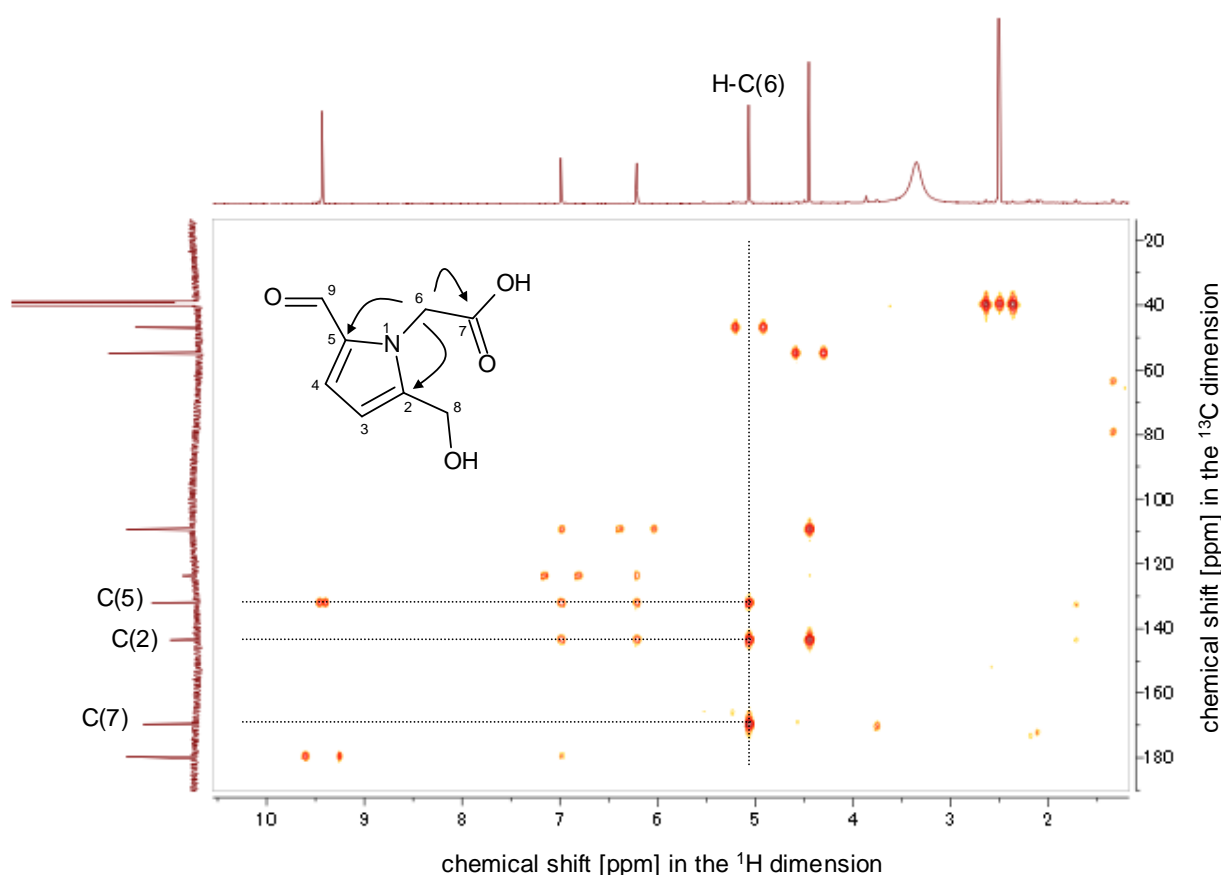


Figure 42. Excerpt of the HMBC spectrum (500 MHz, DMSO- d_6) and key correlations of compound **13**.

Compound **14** was obtained from the fraction No.6—15 as amorphous brown powder. UPLC-TOF MS in the ESI⁺ mode exhibited a pseudomolecular ion peak of m/z 270.0980 [M+H]⁺, suggesting a molecular formula of C₁₂H₁₆NO₆. The ¹H and ¹³C NMR data of **14** showed quite similar spectra to a pyrrole structure with an aldehyde and a hydroxymethyl functions in compounds **3**, **11**, **12** and **13**, which indicated the presence of the same pyrrole ring. In addition, two heteroatom-bearing methyne carbons at 54.36 [C(4)] and 78.10 ppm [C(2)], a methylene carbon at 27.92 ppm [C(3)] and a quaternary carbon at 172.86 ppm [C(5)] were assigned, and then the HMBC connectivities of H-C(2)→C(3,5), H-C(3)→C(2,4,5) and H-C(4)→C(3,5) revealed that the carbons formed a γ -butyrolactone motif. Further interpretation of the HMBC spectrum showed a C(4)-N(8) linkage between the pyrrole and γ -butyrolactone motifs due to signals of H-C(4)→C(9,12) (**Figure 43**).

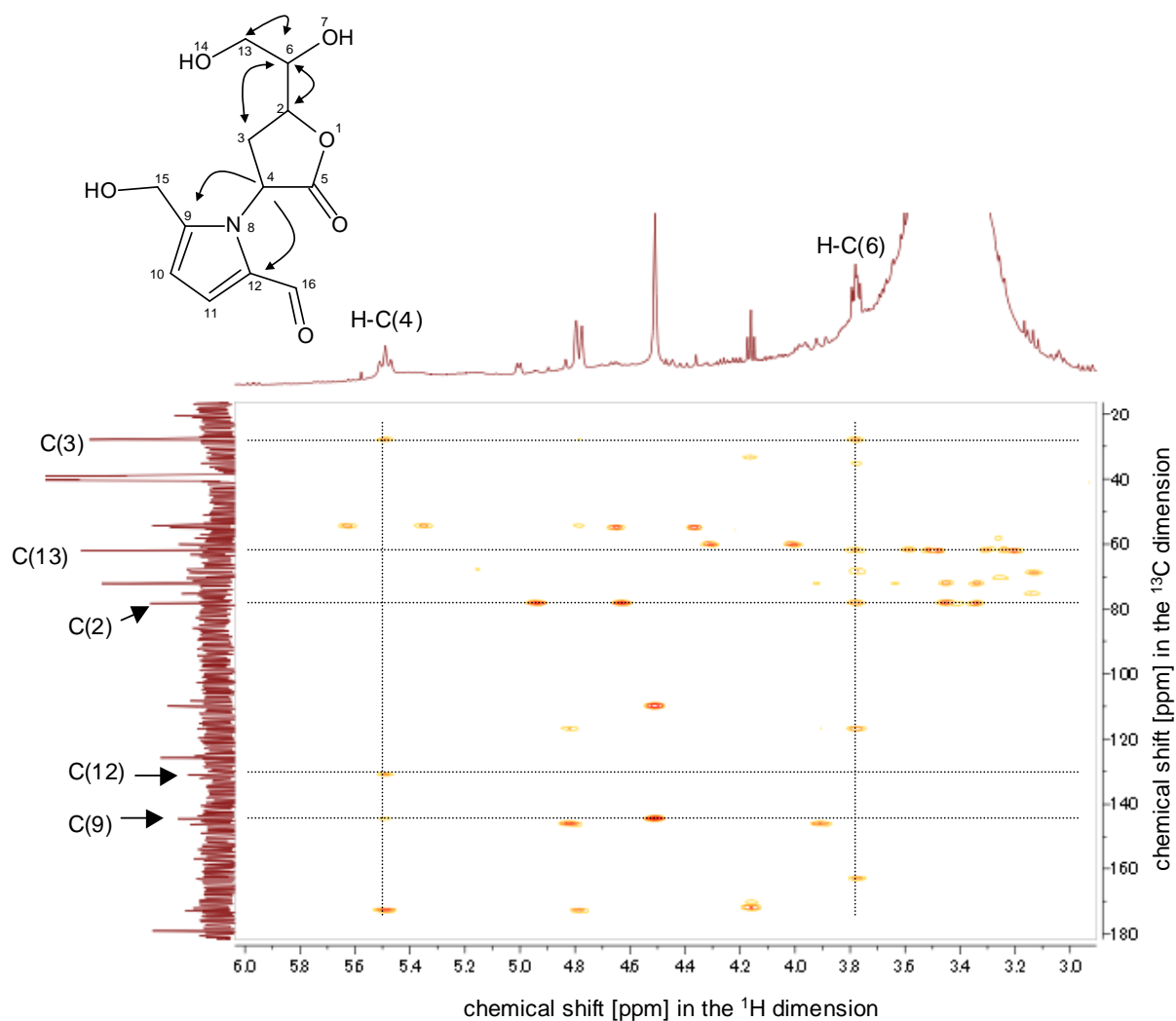


Figure 43. Excerpt of the HMBC spectrum (500 MHz, DMSO- d_6) and key correlations of compound **14**.

Moreover, a 1,2-ethyldiol motif consisted of carbon resonances at 61.84 [C(13)] and 72.01 ppm [C(6)] and proton resonances at 3.38 [2H, H-C(13)] and 3.78 ppm [H-C(6)] was identified based on the COSY correlation of H-C(6)/H-C(13), and its location was found to be on the γ -butyrolactone motif, making a C(2)-C(6) linkage, by the HMBC connectivities of H-C(6) \rightarrow C(2,3) and H-C(13) \rightarrow C(2,6) (**Figure 43**). Thus, the chemical structure of **14** was determined as 1-{5-(1,2-dihydroxyethyl)-2-oxotetrahydrofuran-3-yl}-5-(hydroxymethyl)-1*H*-pyrrole-2-carbaldehyde. To the best of our knowledge, this compound has not been reported before in literature.

Compound **15** was obtained from fraction No.6—26 as an amorphous brown powder. UPLC-TOF MS in the ESI⁻ mode showed a pseudomolecular ion peak of m/z 236.0559 [M-H]⁻, suggesting a molecular formula of C₁₁H₁₁NO₅. Three olefinic protons resonating as double doublet at 6.73 [H-C(3)], 7.56 [H-C(4)] and 8.02 ppm [H-C(2)] were observed in the ¹H spectrum. Their coupling constants (3.6 Hz) and chemical shifts of C(3) and C(4) were typical signals for a furan ring like in compounds **8** and **9**, and the COSY correlations of H-C(2)/H-C(3,4) enabled to identify a furan motif possessing the three protons. In addition, two quaternary carbons at 173.31 [C(13)] and 174.98 ppm [C(12)], two methylene carbons at 22.67 [C(10)] and 28.71 ppm [C(11)] and a methyne carbon at 59.55 ppm [C(9)] were assigned by the ¹³C and HSQC spectra, and the carbons showed HMBC cross peaks with corresponding protons of H-C(9)→C(10,11,13), H-C(10)→C(9,11,12,13) and H-C(11)→C(9,10,12), thus indicating the presence of a pyroglutamic acid motif. Also, two nonequivalent methylene protons resonating at 4.29 [H-C(7a)] and 4.86 ppm [H-C(7b)] showed HMBC connectivities to the carbons assigned above (C(5,9,12)) and a quaternary carbon (δ_c :182.83 ppm, C(6)) and these signals defined that the furan and pyroglutamic acid motifs were connected via an oxoethyl bridge (**Figure 44**).

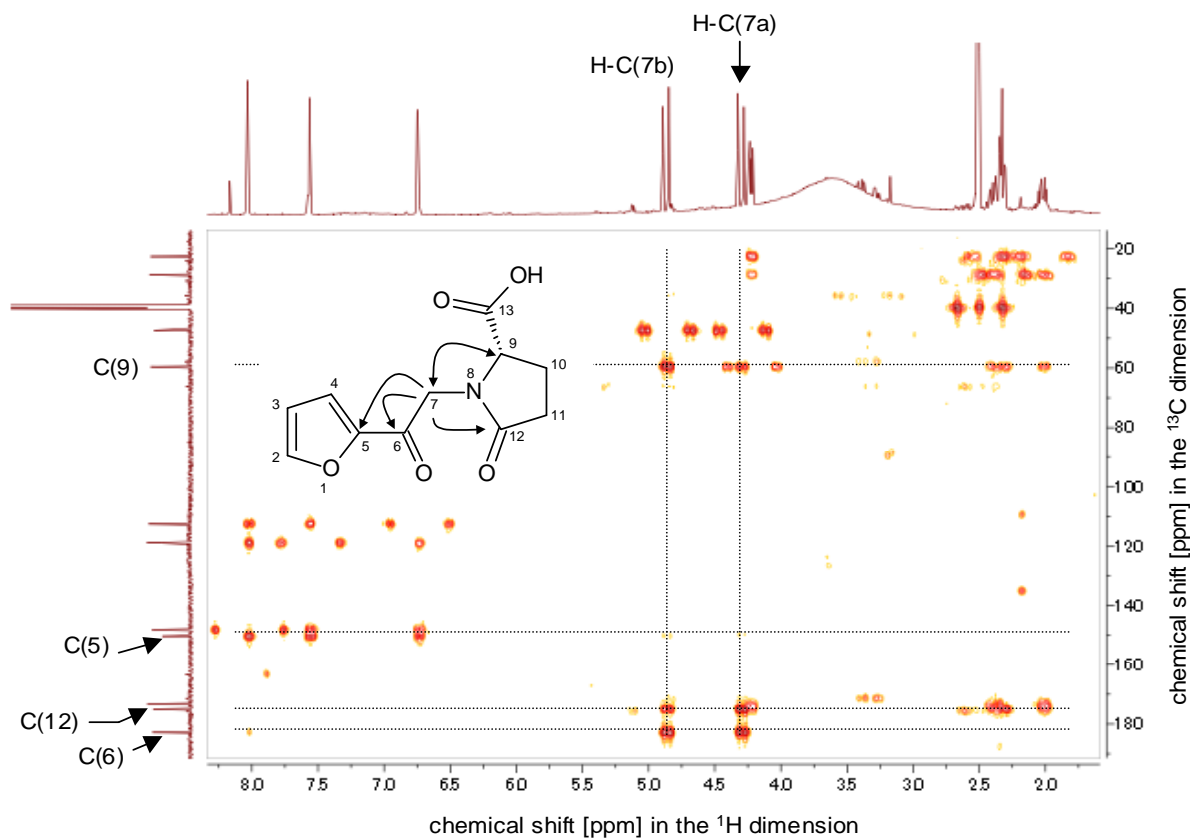


Figure 44. Excerpt of the HMBC spectrum (400 MHz, $\text{DMSO-}d_6$) and key correlations of compound **15**.

The CD spectrum of **15** showed a positive cotton effect at 206 nm and a negative cotton effect at 274 nm, and the CD as well as NMR data are well in agreement with literature (*Wang et al. 2013*). Therefore, the structure was unequivocally determined as (2*S*)-1-[2-(furan-2-yl)-2-oxoethyl]-5-oxopyrrolidine-2-carboxylic acid (**15**).

2.2.6 Isolation and structure elucidation of antioxidants in MPLC fraction No.7

The MPLC fraction No.7 was investigated to isolate and identified antioxidants. An aliquot of the fraction No.7 was separated into 36 subfractions by means of semipreparative HPLC (**Figure 45—46**), and each subfraction was analyzed on antioxidative activities using ARS and ORAC assays.

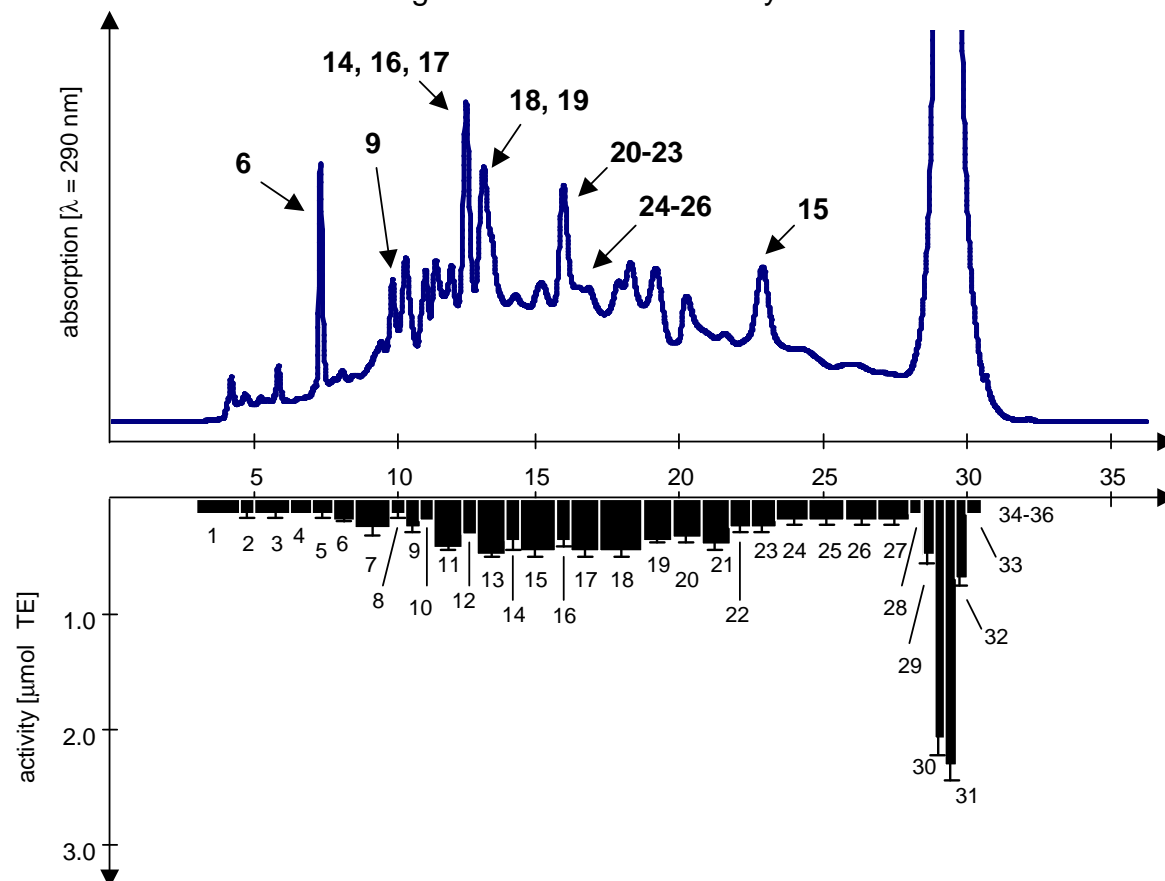


Figure 45. HPLC separation and ARS activities obtained from the MPLC fraction No.7. Data represent antioxidative activity expressed as Trolox equivalents (TE) (average \pm S.D, $n=3$). The whole activity of the MPLC fraction No.7 was 12.96 [$\mu\text{mol TE}$], and the calculated sum of each fraction was 12.33 [$\mu\text{mol TE}$]. Compound numbering is given in bold.

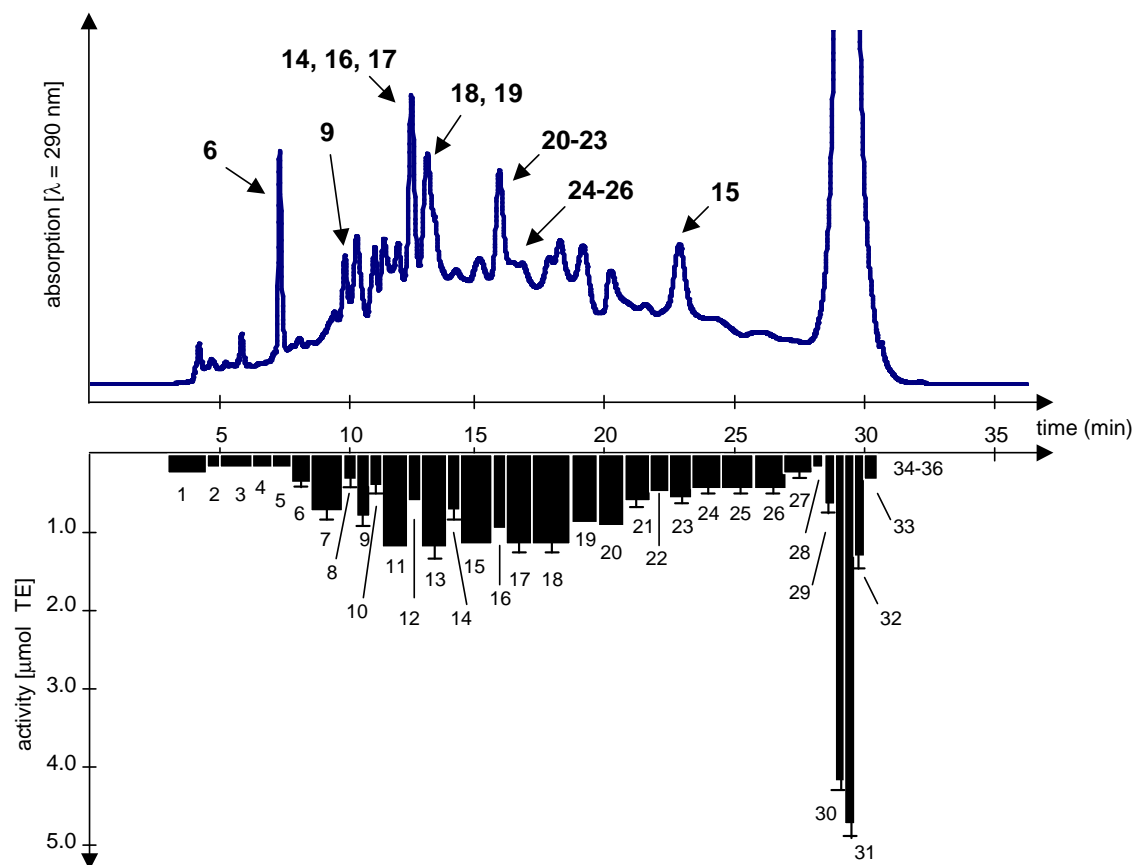


Figure 46. HPLC separation and ORAC activities obtained from the MPLC fraction No.7. Data represent antioxidative activity expressed as Trolox equivalents (TE) (average \pm S.D, $n=3$). The whole activity of the MPLC fraction No.7 was 28.04 [$\mu\text{mol TE}$], and the calculated sum of each fraction was 28.40 [$\mu\text{mol TE}$]. Compound numbering is given in bold.

ARS and ORAC activity of the whole MPLC fraction No.7 showed 12.96 and 28.04 [$\mu\text{mol TE}$], respectively, and these activities were comparable to the calculated sums of each subfraction (12.33 and 28.40 [$\mu\text{mol TE}$]). In the HPLC run, five main peaks (No.7—5, 12, 13, 16, 28, 29, 30, 31, 32 and 33) and many tiny peaks were observed. Both antioxidative assays disclosed that the activities distributed to all fractions, and this tendency was comparable to fraction No.6, which resulted in the same experimental strategy. As the ^1H NMR spectrum of the biggest peak consisted of No.7—28 to 7—33 showed no specific signals like in the former fractions (No.5 and 6), this peak was also expected as a complexed fraction (Data not shown). Relatively higher antioxidative fractions with higher UV absorbance, such as No.7—7, 9, 10, 11, 14, 15, 18, 19 and 20,

were purified by means of a further HPLC step, however, gained subfractions showed low yields and purities. In contrast, purification of seven fractions (No.7—5, 8, 12, 13, 16, 17 and 23) gave subfractions which had higher purities and yields. Taking the above experimental facts, the later subfractions were selected for structure elucidation using 1D/2D-NMR, UPLC-TOF MS and CD spectroscopy affording compounds **6**, **9**, **14**, **15** and **16—26** (Figure 47).

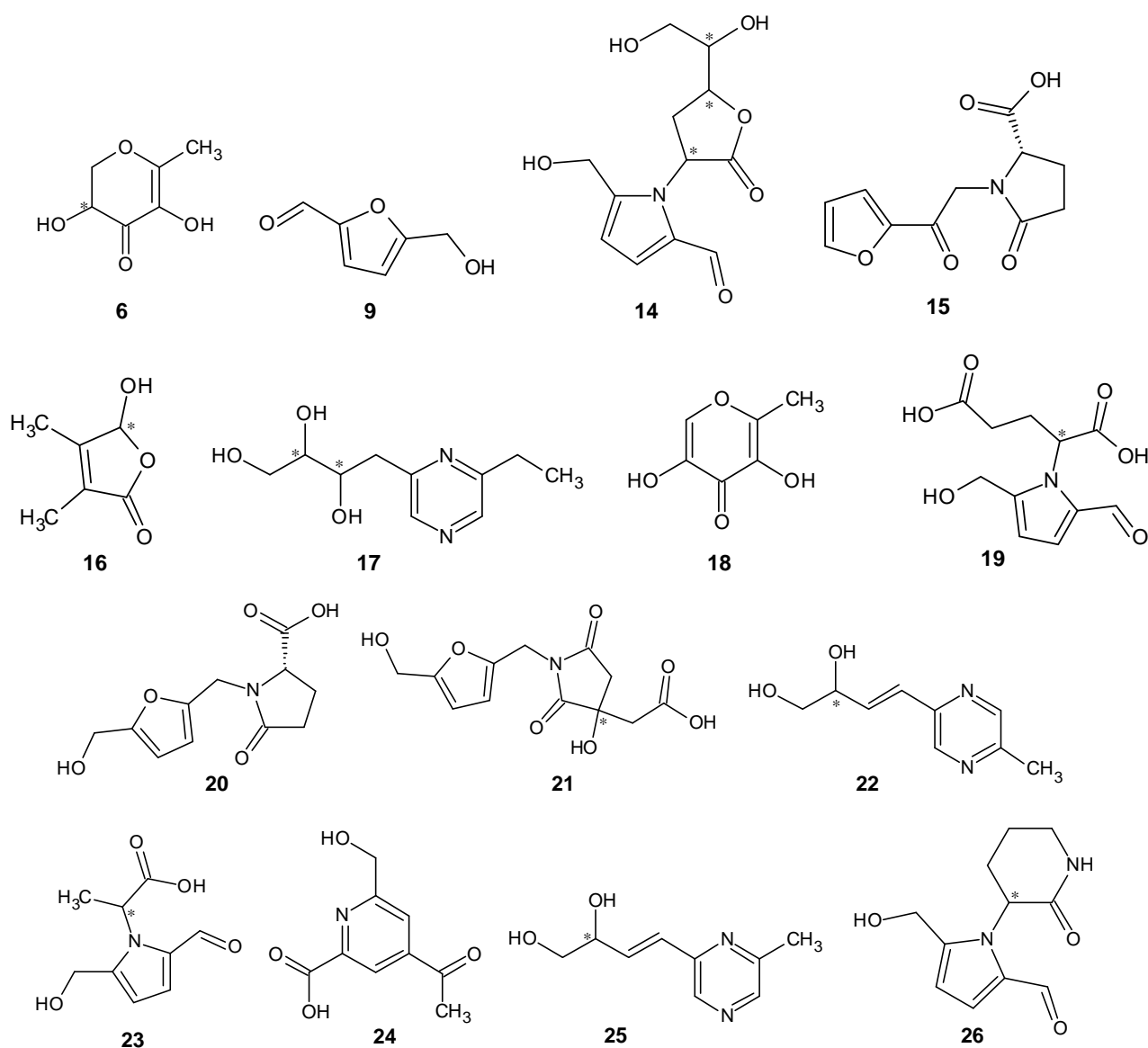


Figure 47. Chemical structures of isolated compounds **6**, **9**, **14—26** from the MPLC fraction No.7.

The ^1H NMR spectra of fraction No.7—5 and 7—8 were identical to compounds **6** and **9**, respectively, therefore their structures were determined as 2,3-dihydro-3,5-dihydroxy-6-methyl-4(*H*)-pyran-4-one and 5-hydroxymethyl-2-furaldehyde, respectively.

The fraction No.7—12 was purified by means of a further HPLC using a RP column (**Figure 48**), then newly separated three peaks were collected, concentrated and freeze-dried, which resulted in identification of compound **14**, **16** and **17**. The chemical structure of compound **14**, which was also identified in the former fraction No.6, was confirmed using NMR and MS data.

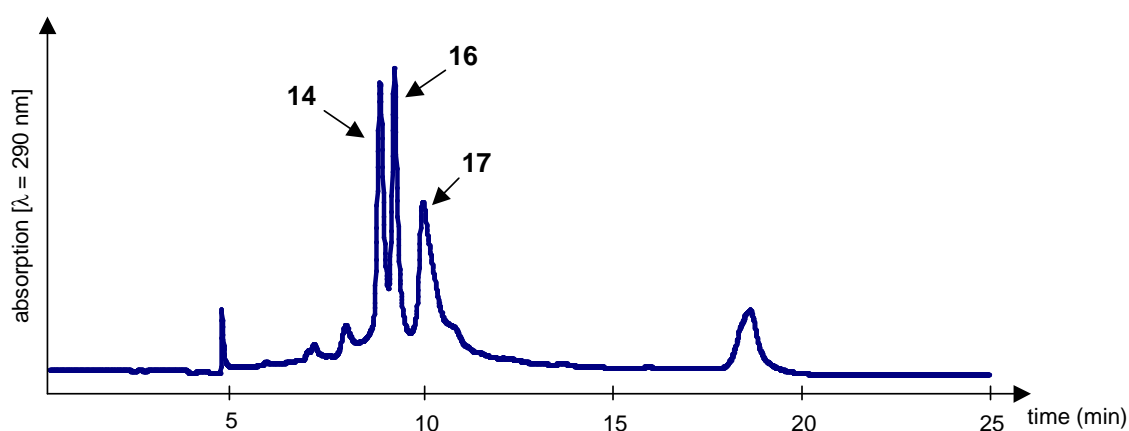


Figure 48. HPLC of the fraction No.7—12 for separation of compounds **14**, **16** and **17**.

Purification of the fraction No. 7—12 afforded compound **16** at 9.6 min (**Figure 48**). The ^1H NMR spectrum showed three signals, and they were assigned as six methyl protons resonating at 1.72 [3H, H-C(7)] and 1.91 ppm [3H, H-C(6)] and a heteroatom-bearing methyne proton at 5.85 ppm [H-C(2)]. Three quaternary carbons at 123.79 [C(3)], 157.06 [C(4)] and 171.85 ppm [C(5)] and one methyne carbon at 98.33 ppm [C(2)] were observed in the ^{13}C spectrum, then the four carbons were found to form an unsaturated γ -butyrolactone, which was supported by the heteronuclear HMBC correlations of H-C(2) \rightarrow C(3,5) (**Figure 49**). In addition, the HMBC connectivities of H-C(6) \rightarrow C(2,3,4) and H-C(7) \rightarrow C(3,4,5) clarified that the two methyl functions are located at C(3) and C(4). The presence of a hydroxyl function at C(2) was indicated by data of UPLC-TOF MS (ESI $^+$) which exhibited a pseudomolecular ion peak of m/z 129.0551 [M+H] $^+$ and suggested a molecular formula of $\text{C}_6\text{H}_9\text{O}_3$. The above

assignments enabled to propose the chemical structure of **16** as 5-hydroxy-3,4-dimethylfuran-2(5H)-one. Data of ^1H and ^{13}C NMR are well in agreement with literature (Surmont *et al.* 2010).

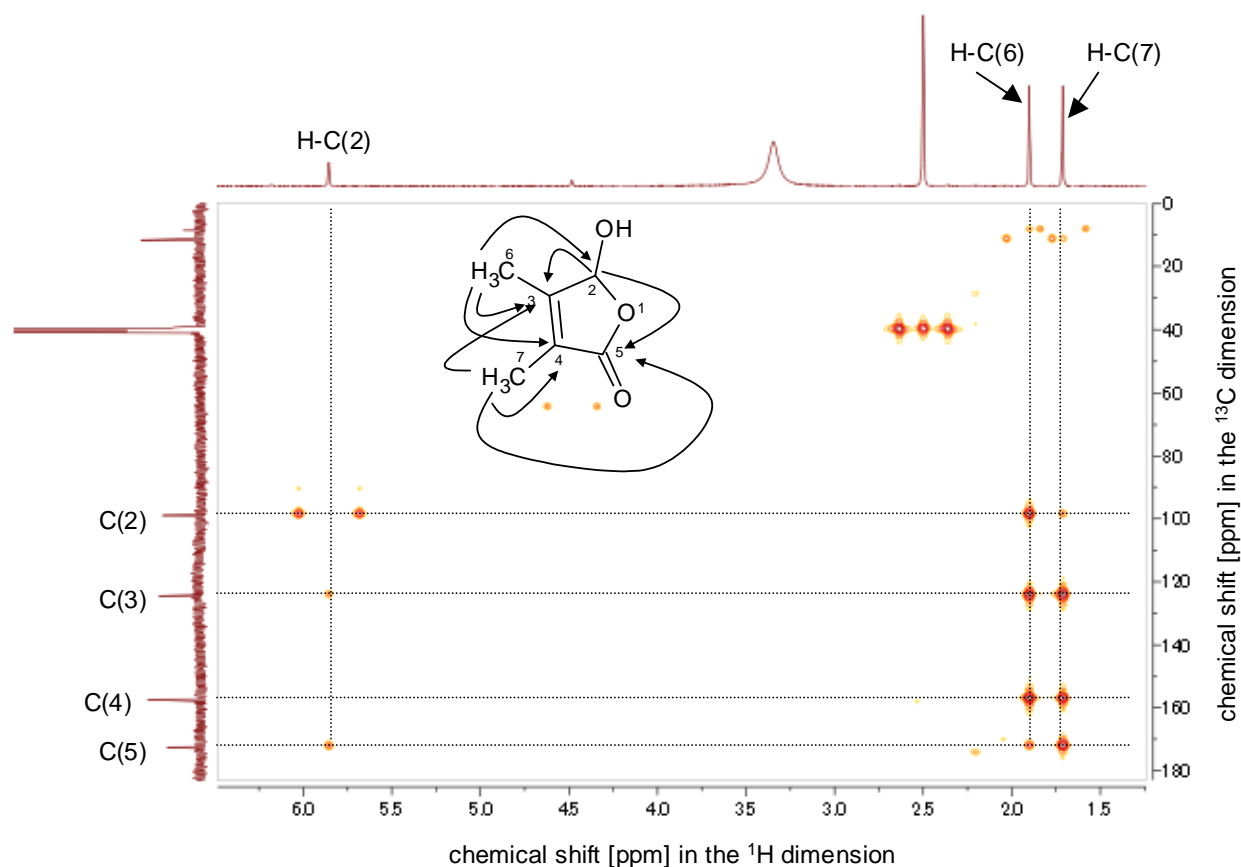


Figure 49. Excerpt of the HMBC spectrum (500 MHz, $\text{DMSO-}d_6$) and key correlations of compound **16**.

Compound **17** eluted at 10.6 min in the chromatogram (**Figure 48**) having an appearance of amorphous brown powder. UPLC-TOF MS in the ESI^+ mode showed a pseudomolecular ion peak of m/z 213.1242 $[\text{M}+\text{H}]^+$, suggesting a molecular formula of $\text{C}_{10}\text{H}_{16}\text{N}_2\text{O}_3$. Almost all NMR spectra looked quite similar to those of compound **7**, which implied that **17** would be an alkylpyrazine structure like as compounds **1,2** and **7**. Characteristic signals for this compound were δ_{C} 13.45 and 27.79 ppm which were bonded to three protons resonating at 1.23 ppm [3H, H-C(11)] and two protons at 2.75 ppm [2H, H-C(10)], respectively. Then formation of an ethyl group by the carbons was confirmed due to the homonuclear COSY correlations of H-C(11)/H-C(10). Besides, the position of

the ethyl function was disclosed to be at C(6) by the heteronuclear cross peaks of H-C(10)→C(5,6,11) and H-C(11)→C(6,10) (**Figure 50**). Thus, the chemical structure was determined as 1,2,3-butanetriol-4-(6-ethyl-2-pyrazinyl) (**17**), and there are no reports of comparable NMR data.

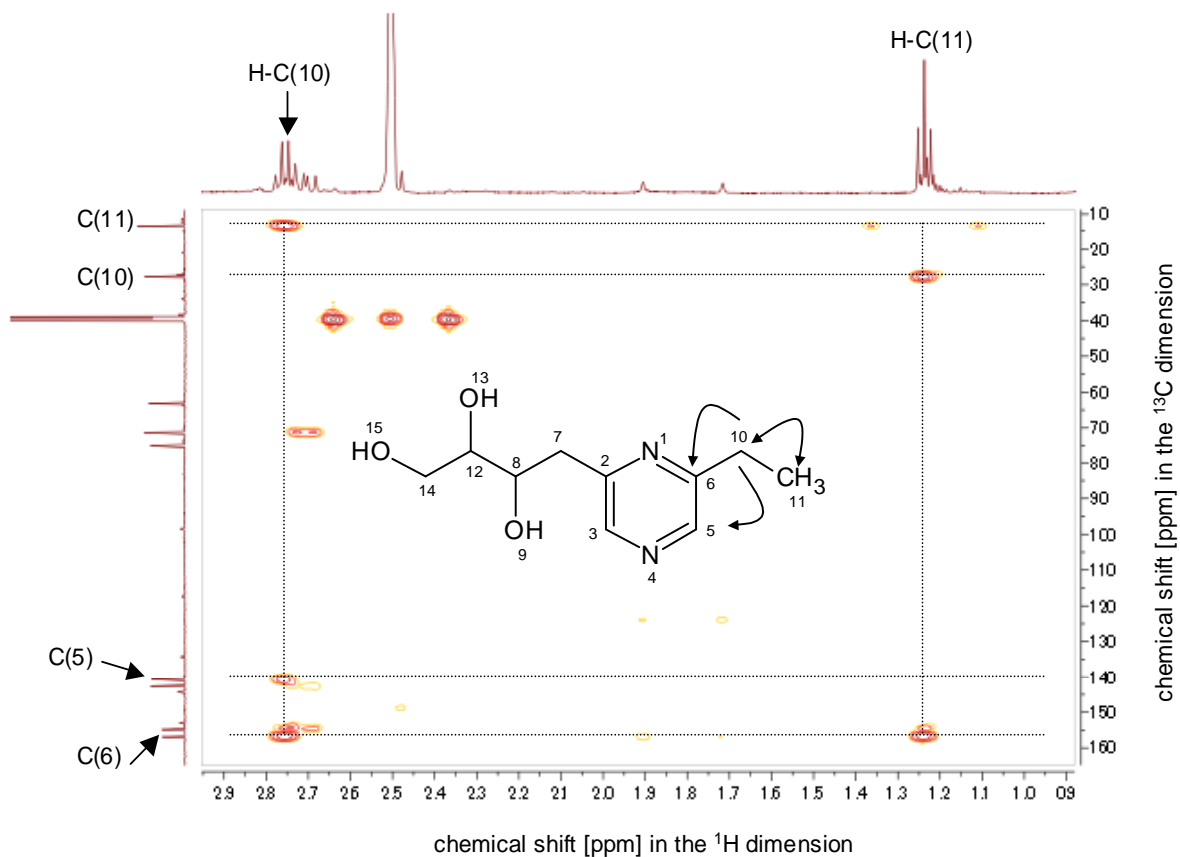


Figure 50. Excerpt of the HMBC spectrum (500 MHz, $\text{DMSO-}d_6$) and key correlations of compound **17**.

The fraction No.7—13 was purified by means of a further HPLC step using a RP column (**Figure 51**), then the two peaks which showed relatively bigger UV intensities in the chromatogram were collected, concentrated and freeze-dried, to afford compounds **18** and **19**.

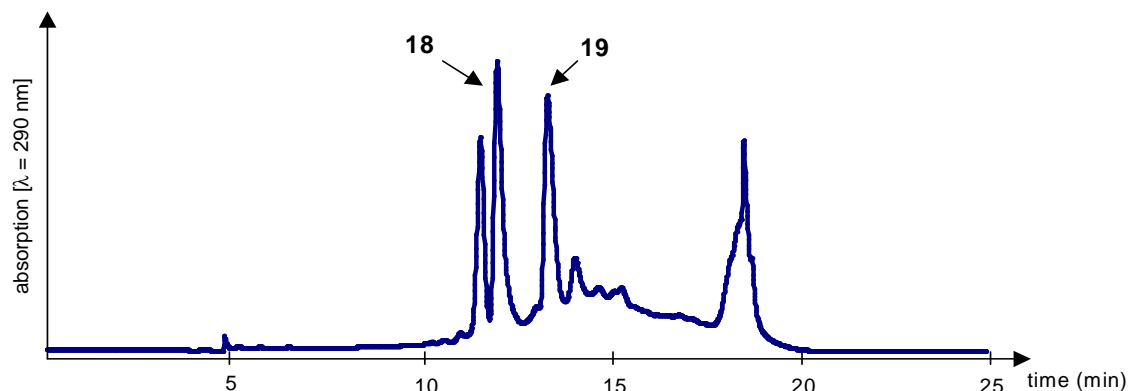


Figure 51. HPLC obtained from purification of the fraction No.7—13.

With an appearance of brown oil, compound **18** was isolated from the fraction No.7—13 through purification eluting at 12.2 min (**Figure 51**). In the ^{13}C NMR spectrum, four aromatic quaternary carbons resonating at 141.37 [C(5)], 144.24 [C(3)], 149.24 [C(6)] and 168.48 ppm [C(4)] and one aromatic methyne carbon at 138.96 ppm [C(2)] were observed. An aromatic methyne proton at 7.93 ppm [H-C(2)] and the above carbons showed HMBC correlations of H-C(2)→C(3,4,6), which indicated the presence of a 4-pyranone motif. Apart from the signals, a resonance (δ_{H} 2.22) derived from a methyl function, which was assigned by the HSCQ spectrum, exhibited HMBC connectivities of H-C(7)→C(5,6), and the emphasized signal of H-C(7)→C(6) led to its position in the 4-pyranone motif (**Figure 52**). Furthermore, UPLC-TOF MS in the ESI $^{+}$ mode exhibited a pseudomolecular ion peak of m/z 143.0344 [M+H] $^{+}$, suggesting a molecular formula of $\text{C}_6\text{H}_6\text{O}_4$ and proposing the occurrence of two hydroxyl functions. Therefore, the chemical structure was established as 5-hydroxymaltol, and the ^1H NMR is well in agreement with literature (*Kosuge et al. 1983*).

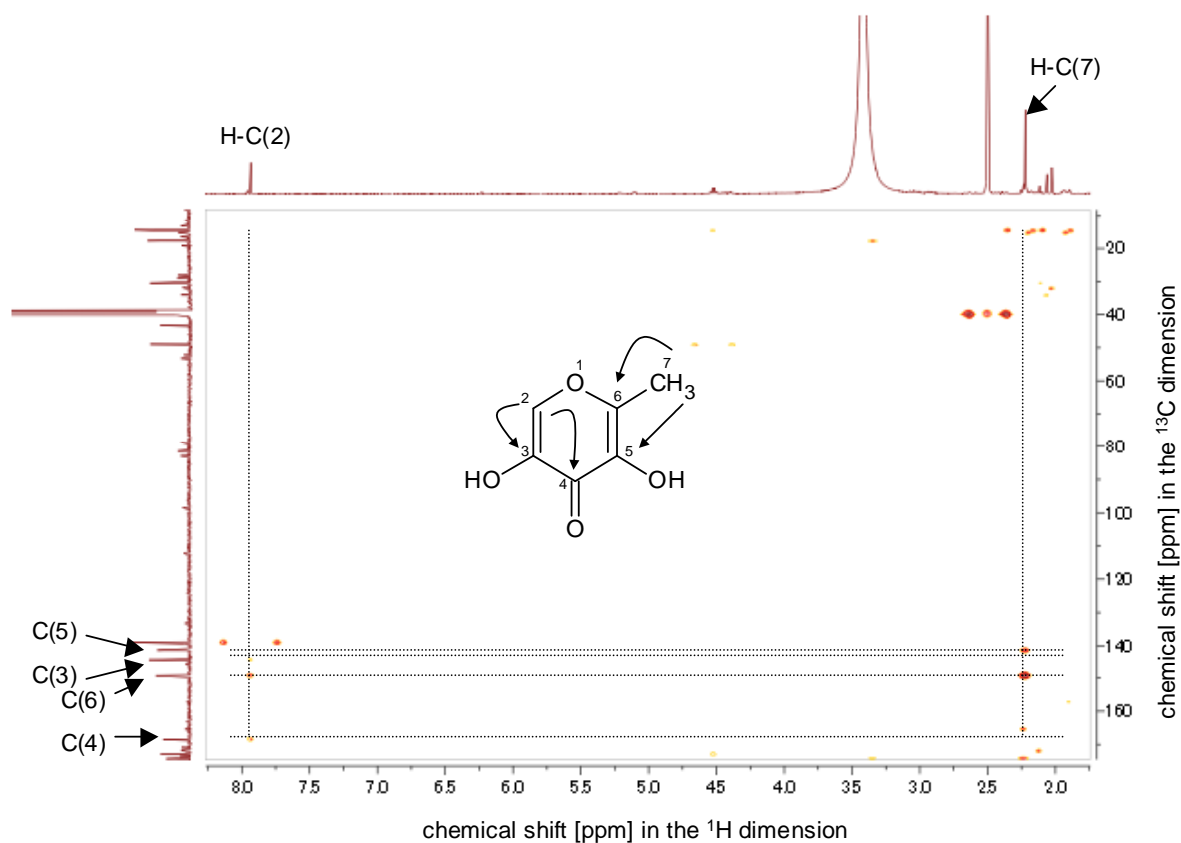


Figure 52. Excerpt of the HMBC spectrum (500 MHz, DMSO- d_6) and key correlations of compound **18**.

Purification of the fraction No.7—13 afforded compound **19** at 14.9 min (**Figure 51**). As this compound was also an instable compound like **11**, the pH of the purified solution was adjusted to 7.0 using sodium hydroxide, then the solution was freeze-dried for NMR analysis. The ^1H and ^{13}C NMR spectra of **19** were very similar to those of **11**, and this similarity implied **19** would be a pyrrole derivative of an amino acid. UPLC-TOF MS in the ESI $^-$ mode exhibited a pseudomolecular ion peak of m/z 254.0663 [M-H] $^-$, suggesting a molecular formula of $\text{C}_{11}\text{H}_{13}\text{NO}_6$. Differences of the molecular formulas between **11** and **19** were CH_2 , which proposed the structure of **19** as a pyrrole derivative of glutamic acid. In fact, four methylene protons resonating at 1.83 [H-C(8a)], 2.01 [H-C(8b)], 2.30 [H-C(7a)] and 2.54 ppm [H-C(7b)] showed COSY correlations of H-C(7ab)/H-C(8ab), thus clarifying methylene carbon C(7) and C(8) are direct neighbors. In addition, the protons showed HMBC cross peaks between two

quaternary and a methyne carbons (δ_C 61.38[C(6)], 178.00[C(12)], 182.76[C(9)]) of H-C(7) \rightarrow C(6,8,9,12) and H-C(8) \rightarrow C(6,7,9) (**Figure 53**). These observations enabled to determine the glutamic acid motif, thus establishing the chemical structure of **19** as α -{(2-formyl-5-hydroxymethyl)pyrrol-1-yl}glutamic acid, of which amino function is incorporated into the pyrrole system such as compound **3** and **11**. This compound has not been reported before in literature.

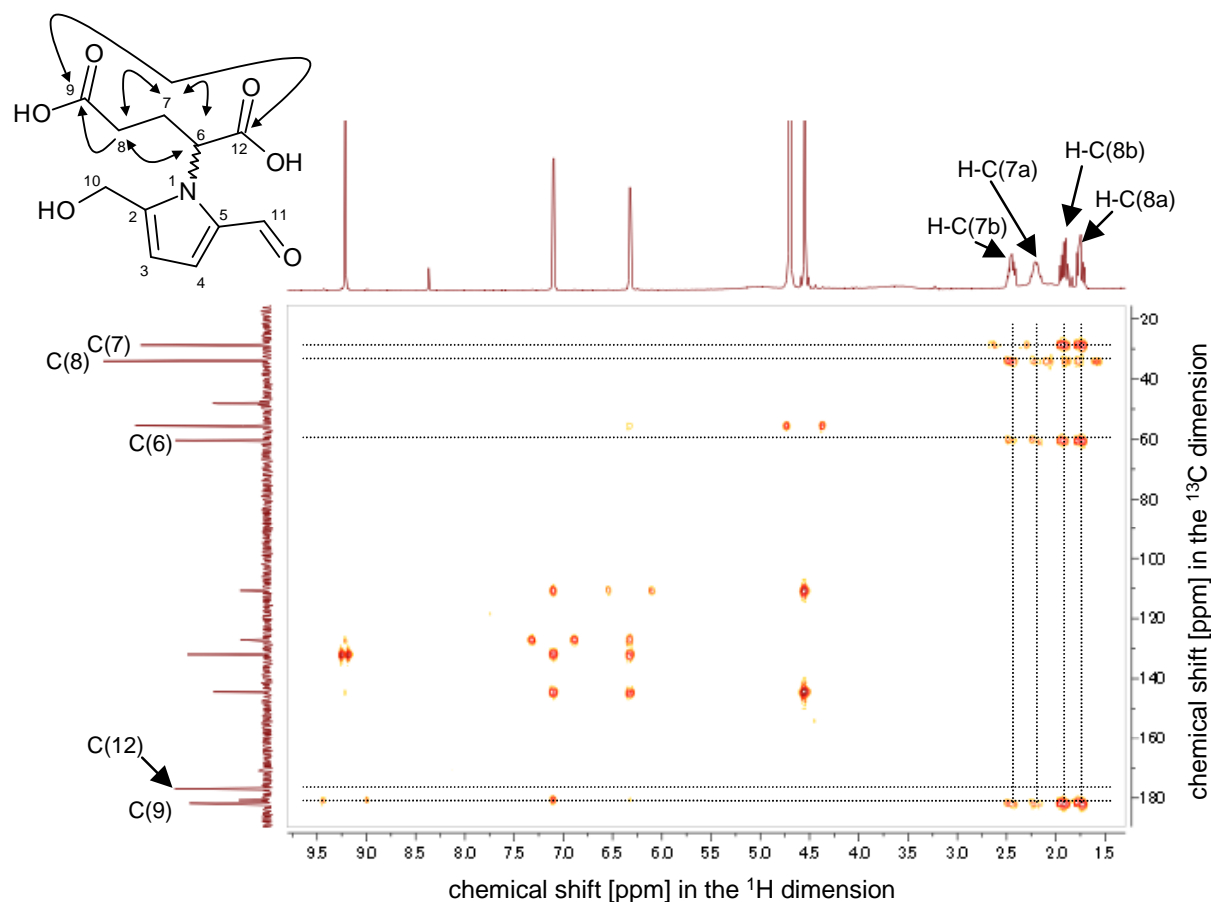


Figure 53. Excerpt of the HMBC spectrum (400 MHz, $\text{D}_2\text{O}/\text{MeOD-}d_4$, 9/1) and key correlations of compound **19**.

The fraction No.7—16 was purified by means of a further HPLC step using a RP column (**Figure 54**), and four peaks in the chromatogram were collected, concentrated and freeze-dried, affording compound **20—23**.

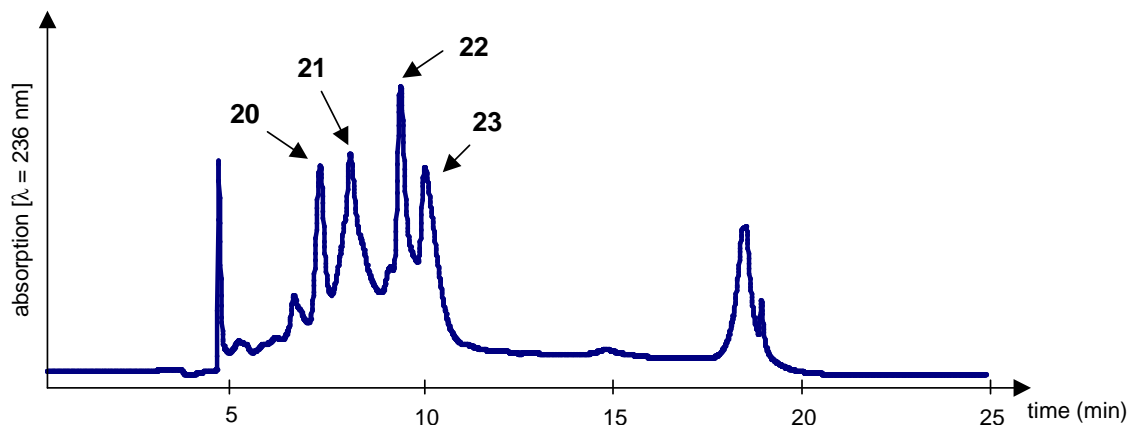


Figure 54. HPLC separation obtained from purification on the fraction No.7—16.

Compound **20**, which eluted at 7.3 min in the chromatogram (**Figure 54**), was isolated as amorphous brown powder. Some resonances of **20** (δ_{H} 1.93, 2.29, 2.30 and 3.97; δ_{C} 22.35, 28.98, 58.20, 173.20 and 174.12) were rather similar to the partial NMR spectra for a pyroglutamic acid motif of compound **15**. Two aromatic quaternary carbons at 148.72 [C(5)] and 155.48 ppm [C(2)] and two olefinic carbons at 107.61 [C(3)] and 109.31 ppm [C(4)] were assigned based on the ^{13}C and HSQC spectra, and two protons for the olefins resonating at 6.20 [H-C(3)] and 6.21 ppm [H-C(4)] showed a coupling signal in the COSY spectrum. Their coupling constants of 3.2 Hz are typical values for a furan ring such as detected in compounds **8** and **9**, which, here also led to a furan motif. Besides, two equivalent methylene protons at 4.33 ppm [2H, H-C(6)] showed HMBC signals of H-C(6) \rightarrow C(2,3), and two nonequivalent protons at 3.95 [H-C(8a)] and 4.77 ppm [H-C(8b)] exhibited HMBC cross peaks of H-C(8) \rightarrow C(4,5,10,13) (**Figure 55**). These HMBC connectivities disclosed that a hydroxyl function is located at C(2) and the pyroglutamic acid as well as the furan motifs were bound at N(9) and C(5) via a methylene bridge [C(8)]. Thus, the 2D backbone and relative structure of **20** was established, and a pseudomolecular ion peak of m/z 238.0715 [M-H] $^{-}$ confirmed the elemental composition.

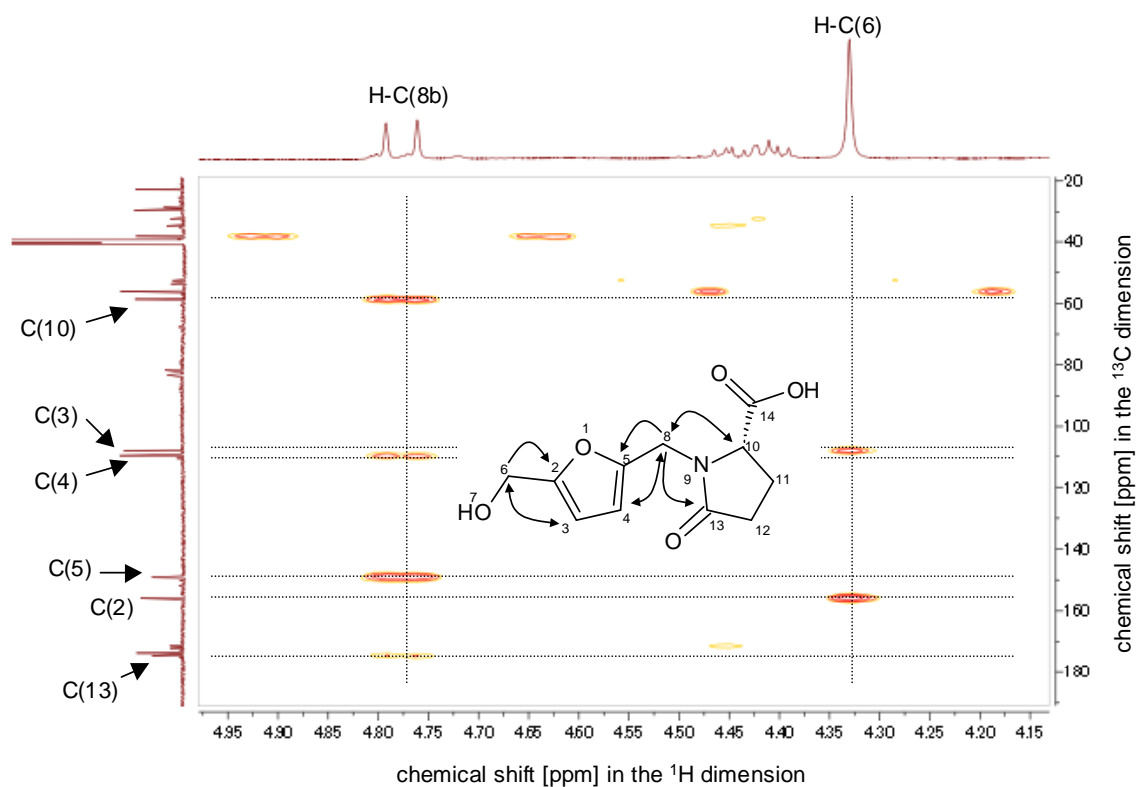


Figure 55. Excerpt of the HMBC spectrum (500 MHz, $\text{DMSO-}d_6$) and key correlations of compound **20**.

The CD spectrum of compound **20** showed a positive cotton effect at 221 nm (**Figure 56**). Comparison of the spectrum to that of compound **15**, a similar glutamic acid derivative, indicated that cotton effects around 220 nm are detectable based on UV absorption of amide groups neighboring chiral centers in the both compounds. This understanding enabled to deduce the stereochemistry of **20** as (*S*)-1-((5-hydroxymethyl)furan-2-yl)methyl)-5-oxopyrrolidine-2-carboxylic acid based on the similarity of cotton effects around 220 nm for both compounds.

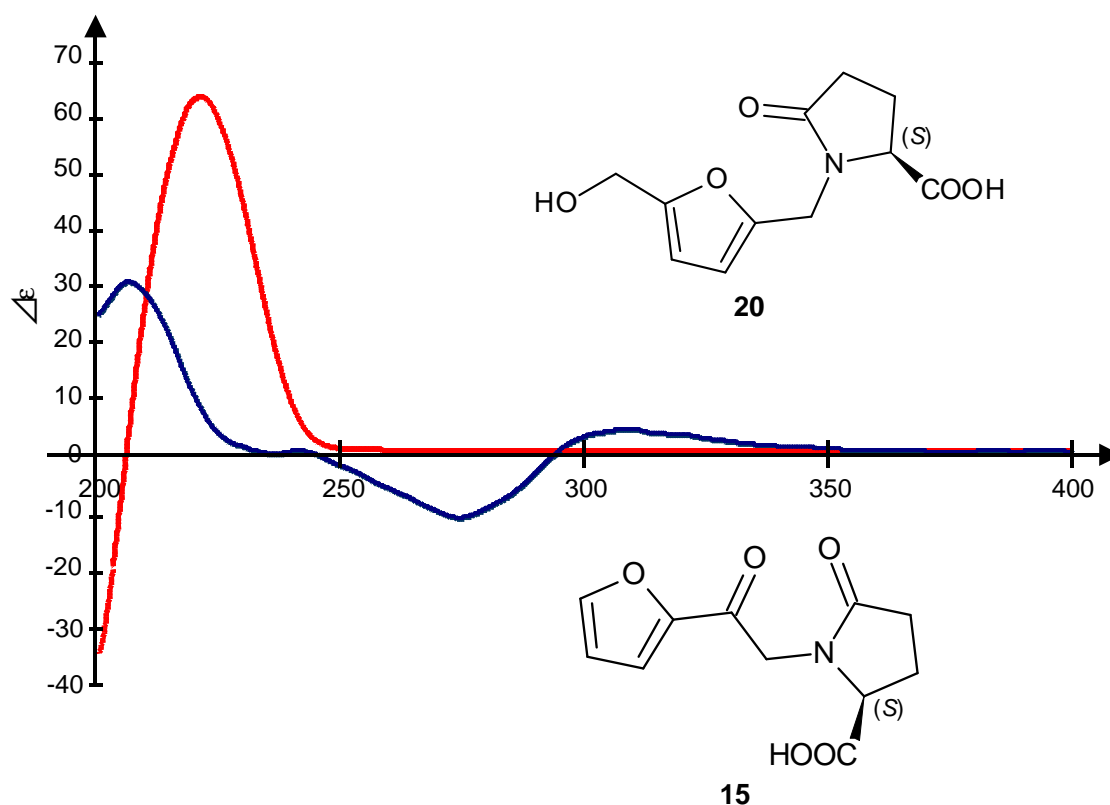


Figure 56. CD spectra of compound **15** (blue) and **20** (red)

Purification of the fraction No.7—16 afforded compound **21** at 8.1 min (**Figure 54**) and it was isolated as an amorphous brown powder. Some of the ^1H and ^{13}C NMR data of **21** (δ_{H} 4.32, 6.18 and 6.20; δ_{C} 55.59, 107.79, 108.33, 148.01 and 154.08) were identical to compound **20** for the hydroxymethylfuran moiety. Three quaternary carbons resonating 71.70 [C(11)], 174.41 [C(13)] and 177.85 ppm [C(10)] and a methylene carbon at 42.01 ppm [C(12)] were assigned by the HSQC spectrum, and the HMBC correlations of H-C(11)→C(10,11,13) indicated the presence of a 2,5-dioxopyrrolidine motif consisted of the carbon C(10,11,12,13) and a nitrogen (**Figure 57**). In addition, two methylene protons at 2.81 [H-C(14a)] and 2.90 ppm [H-C(14b)] showed HMBC cross peaks with a quaternary carbon at 171.46 ppm [C(15)] and the three above mentioned carbons [C(10), C(11) and C(12)] of the 2,5-dioxopyrrolidine motif, consequently these connectivities clarified that an ethyl carboxylic acid is bounded at C(11). A methylene bridge for a linkage between both motifs was confirmed by further HMBC signals of H-C(8)→C(4,5,10,13), and the presence of a hydroxyl function at the chiral center C(11) was proposed based on the elemental composition of $\text{C}_{12}\text{H}_{13}\text{NO}_7$. These assignments enabled to determine the structure of **21** as

3-hydroxy-1*H*-[5-(hydroxymethyl)furan-2-yl)methyl]-2,5-dioxo-3-pyrrolidine-acetic acid. To the best of our knowledge, such a citric acid derivative has not yet been reported in literature.

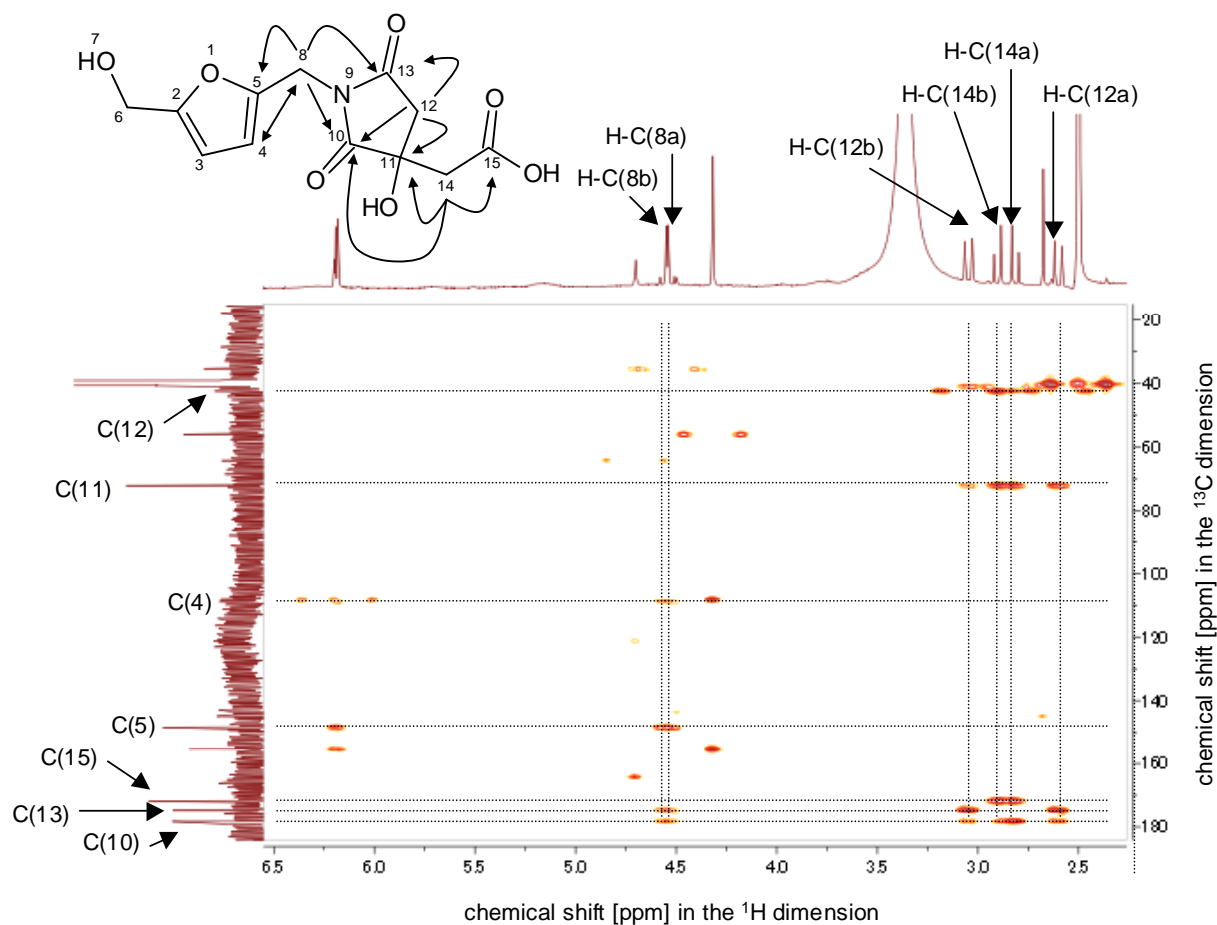


Figure 57. Excerpt of the HMBC spectrum (400 MHz, DMSO- d_6) and key correlations of compound **21**.

Compound **22** was isolated as an amorphous powder from the fraction No7—16 through purification, of which elution was 9.4 min in purification (**Figure 56**). UPLC-TOF MS analysis in the ESI⁺ mode showed a pseudomolecular ion peak of m/z 181.0979 [M+H]⁺, suggesting a molecular formula of C₉H₁₂N₂O₂. Some of the ¹H and ¹³C NMR data of **22** (δ_H 2.55, 8.45 and 8.53; δ_C 20.86, 141.86, 143.77, 147.62, 151.62) were well in agreement with partial data of **7** for the methylpyrazine motif. Then, the two aromatic methyne protons showed the HMBC correlation of H-C(3,6)→C(2), which confirmed the position of the methyl function at C(5). Two olefinic carbons resonating at 125.32 [C(7)] and 137.22 ppm [C(8)], a methyne carbon at 71.8 ppm [C(9)] and a methylene carbon at

65.72 ppm [C(11)] were observed in the ^{13}C spectrum, and COSY and HMBC correlations of H-C(11)/H-C(9), H-C(9)/H-C(8), H-C(8)/H-C(7) and H-C(3) \rightarrow C(7) clarified the presence of an unsaturated alkyl chains consisted of the carbons which bound at C(2) (**Figure 58**). Besides, coupling constants between the olefinic protons H-C(7) and H-C(8) exhibited 15.9 Hz, thus indicating the *trans* arrangement. These assignments led to the structure of **22** as (*E*)-4-(5-methylpyrazin-2-yl)but-3-ene-7,2-diol. This compound has yet not been reported in literature.

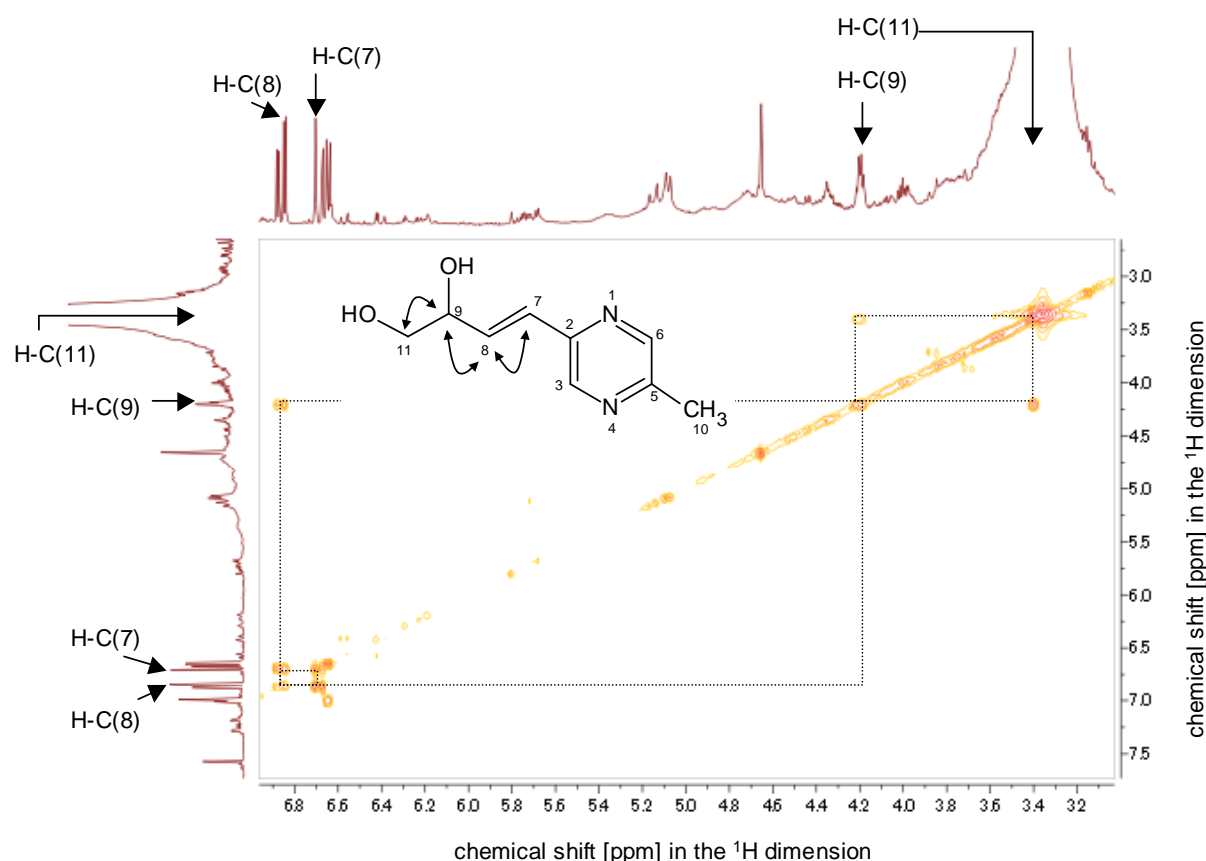


Figure 58. Excerpt of the COSY spectrum (500 MHz, $\text{DMSO-}d_6$) and key correlations of compound **22**.

With an appearance of an amorphous brown powder, compound **23** was given at 10.1 min by purification of the fraction No.7—16 (**Figure 54**). This compound was also an instable compound like compounds **11** and **19**, therefore the pH was adjusted to 7.0 using sodium hydroxide after the purification, followed by freeze-drying. UPLC-TOF MS in the ESI^- mode showed a pseudomolecular ion peak of m/z 196.0613 $[\text{M-H}]^-$, suggesting a molecular formula of $\text{C}_9\text{H}_{11}\text{NO}_4$. As

the following resonances (δ_{H} 4.64, 4.69, 6.38, 7.15, 9.30; δ_{C} 56.23, 111.75, 127.67, 132.55, 144.21, 181.62) were well in agreement with partial data of compounds **11** and **19**, these observations indicated the presence of a pyrrole ring with hydroxymethyl and aldehyde functions. Additionally, a methyne carbon resonating at 57.32 ppm [C(6)] and a quaternary carbon at 178.74 ppm [C(10)] were assigned, then a proton resonance at 1.51 ppm [H-C(7)] for a methyl function showed HMBC signals between these carbons (**Figure 59**), thus leading to the alanine motif. A linkage for the both motifs was confirmed by a long-range-coupling signal of H-C(4) \rightarrow C(6) in the HMBC spectrum (**Figure 59**). The above assignments enabled to establish the structure as α -{(2-formyl-5-hydroxymethyl)pyrrol-1-yl}alanine. This compound was found in fruits of *Morus alba* by Kim *et al.*, 2014, but spectroscopic data of the compound is not available in their literature.

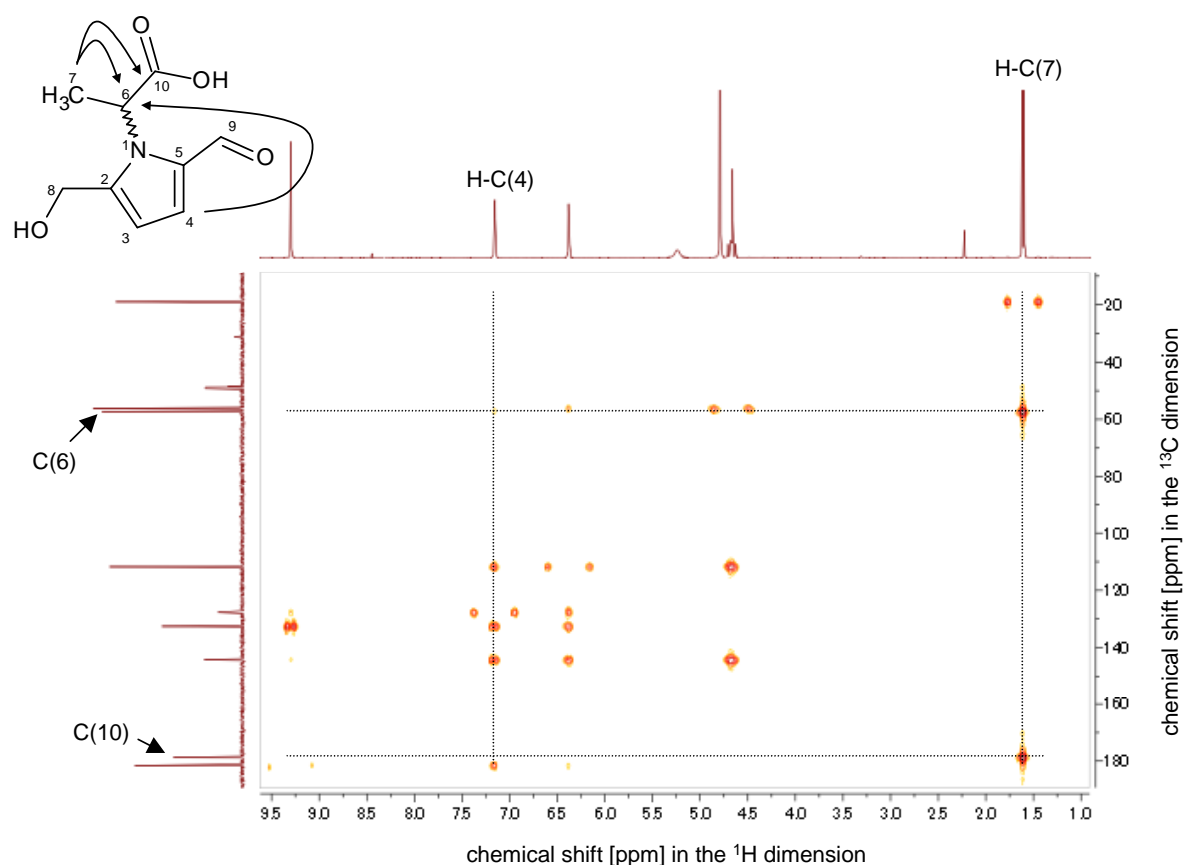


Figure 59. Excerpt of the HMBC spectrum (400 MHz, $\text{D}_2\text{O}/\text{MeOD-}d_4$, 9/1) and key correlations of compound **23**.

The fraction No.7—17 was purified by means of a further HPLC using a RP column (**Figure 60**), and three peaks in the chromatogram were collected, concentrated and freeze-dried, to afford compound **24—26**.

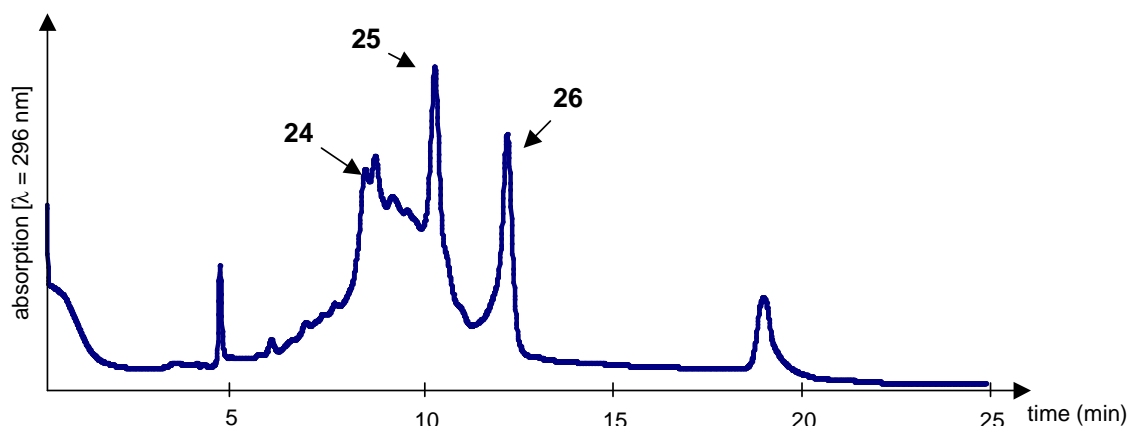


Figure 60. HPLC separation of fraction No.7—17.

Compound **24** eluted at 9.0 min in the chromatogram (**Figure 60**) and was obtained as brown oil. UPLC-TOF MS in the ESI⁻ mode showed a pseudomolecular ion peak of m/z 194.0457 [M-H]⁻, suggesting a molecular formula of C₉H₉NO₄. In the ¹H NMR spectrum, four signals were observed, and they were assigned as three methyl protons resonating at 2.68 ppm [3H, H-C(10)], two methylene protons at 4.71 ppm [2H, H-C(7)] and two aromatic methyne protons at 8.07 [H-C(3)] and 8.25 ppm [H-C(5)]. Two aromatic methyne carbons at 120.33 [C(5)] and 120.75 ppm [C(3)] and two aromatic quaternary carbons at 148.90 [C(6)] and 163.72 ppm [C(2)] showed HMBC connectivities of H-C(3)→C(2,4,5) and H-C(5)→C(3,6), thus indicating these carbons form the pyridine ring. In addition, HMBC signals of H-C(7)→C(2,3) and H-C(10)→C(4,8) confirmed presences and positions of hydroxymethyl and acetyl functions at C(2) and C(4) of a pyridine ring, respectively (**Figure 61**). A carboxylic function linked at C(6) was determined based on the calculated elemental composition and the HMBC correlation between the quaternary carbon resonance at 165.79 ppm [C(9)] and the proton resonance for H-C(5) (**Figure 61**). Therefore, the chemical structure was established as 4-acetyl-6-(hydroxymethyl)picolinic acid (**24**).

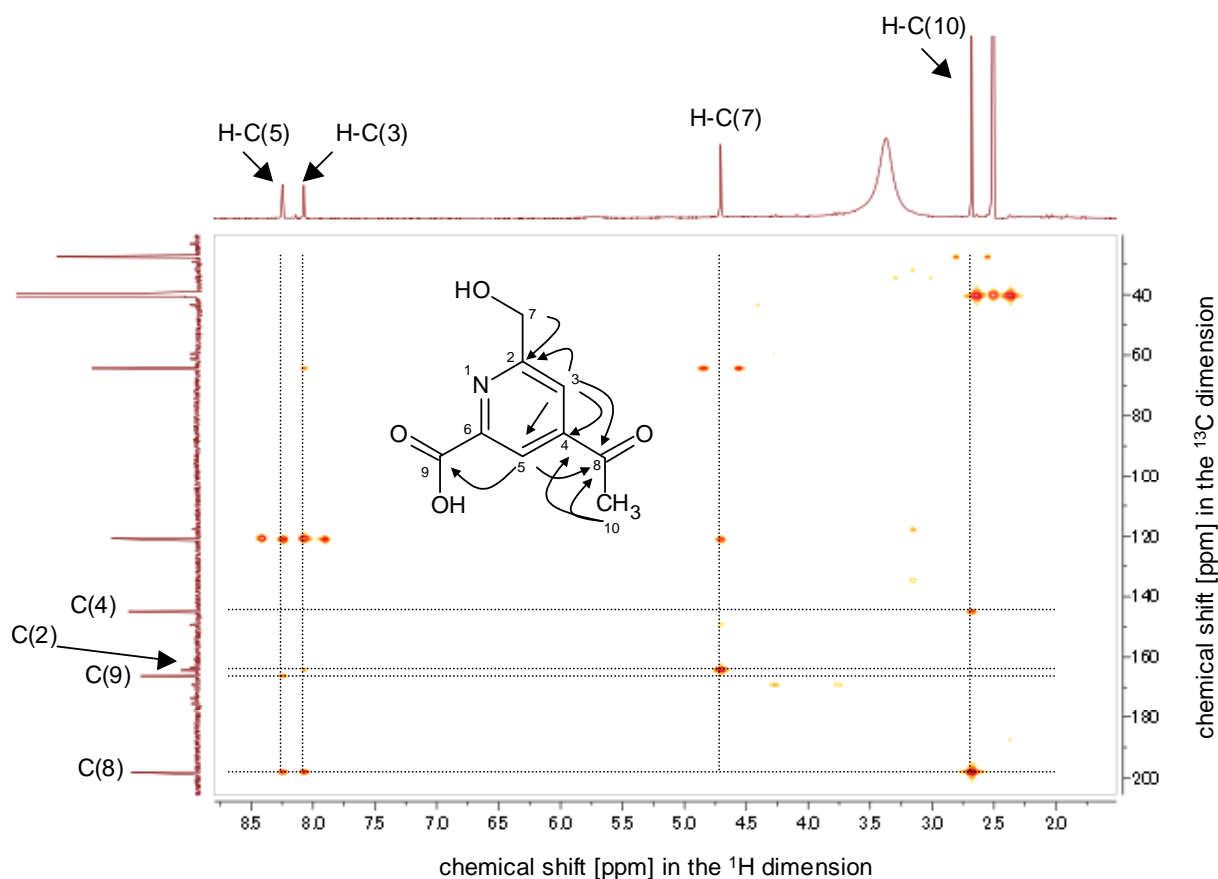


Figure 61. Excerpt of the HMBC spectrum (500 MHz, DMSO- d_6) and key correlations of compound **24**.

Rechromatography of the fraction No. 7—17 afforded compound **25** at 10.6 min (**Figure 60**). All of the ^1H and ^{13}C NMR spectra were in the same range as those of compound **22**, as well as UPLC-TOF MS (ESI $^+$) of m/z 181.0982 [M+H] $^+$. In contrast to **22**, the HMBC spectrum revealed that only one aromatic methyne proton resonating at 6.92 ppm [H-C(3)] exhibited a cross peak to the aromatic quaternary carbon at 149.26 ppm [C(2)] (**Figure 62**). This difference indicated that the methyl function is located at carbon C(6), thus leading the chemical structure of **25** as (*E*)-4-(6-methylpyrazin-2-yl)but-3-ene-1,2-diol, a constitution isomer of **22**. This compound is has not yet been reported in literature.

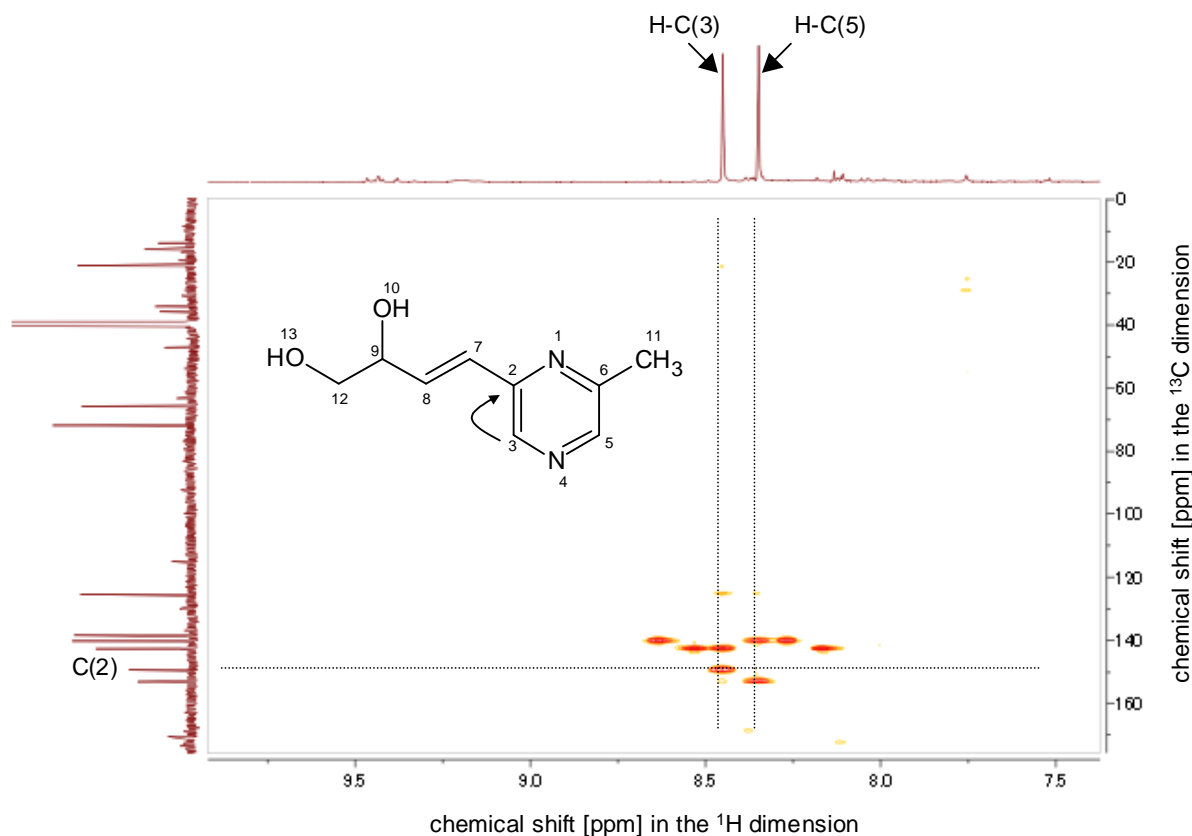


Figure 62. Excerpt of the HMBC spectrum (500 MHz, DMSO- d_6) and key correlations of compound **25**.

Compound **26** was obtained by repurification of the fraction No. 7—17 (**Figure 60**). The following resonances for proton and carbon (δ_{H} 4.50, 6.19, 7.00, 9.30; δ_{C} 55.54, 109.49, 125.39, 132.09, 144.46, 178.51) were well in agreement with a pyrrole motif carrying a hydroxymethyl and aldehyde function in compounds **3**, **11**, **13**, **14**, **19** and **23**. Besides, a methyne carbon resonating at 56.63 ppm [C(6)], three methylene carbons at 22.70 [C(8)], 29.45 [C(7)], 41.70 ppm [C(9)] and a quaternary carbon at 168.39 ppm [C(11)] were assigned by the HSQC spectrum. Additionally, a δ -lactam motif was identified by a resonance for an amide proton at 7.50 ppm and the COSY and HMBC connectivities of H-N(10)/H-C(9), H-C(6)/H-C(7), H-C(7)/H-C(8) and H-C(8)/H-C(9) (**Figure 63**) as well as H-C(6) \rightarrow C(7,11) and H-C(7) \rightarrow C(6,8,9). Furthermore, a linkage between the motifs was confirmed by HMBC correlations of H-C(6) \rightarrow C(2,5), then the structure was proposed as cordyrrole A (**26**). High-resolution mass spectrometry of this compound with a m/z 243.0903 [$M+\text{Na}$] $^+$ confirmed its

elemental composition as $C_{11}H_{14}N_2O_3$ corresponding to the proposed structure. Its NMR data are well in agreement with literature (Kim et al. 2014).

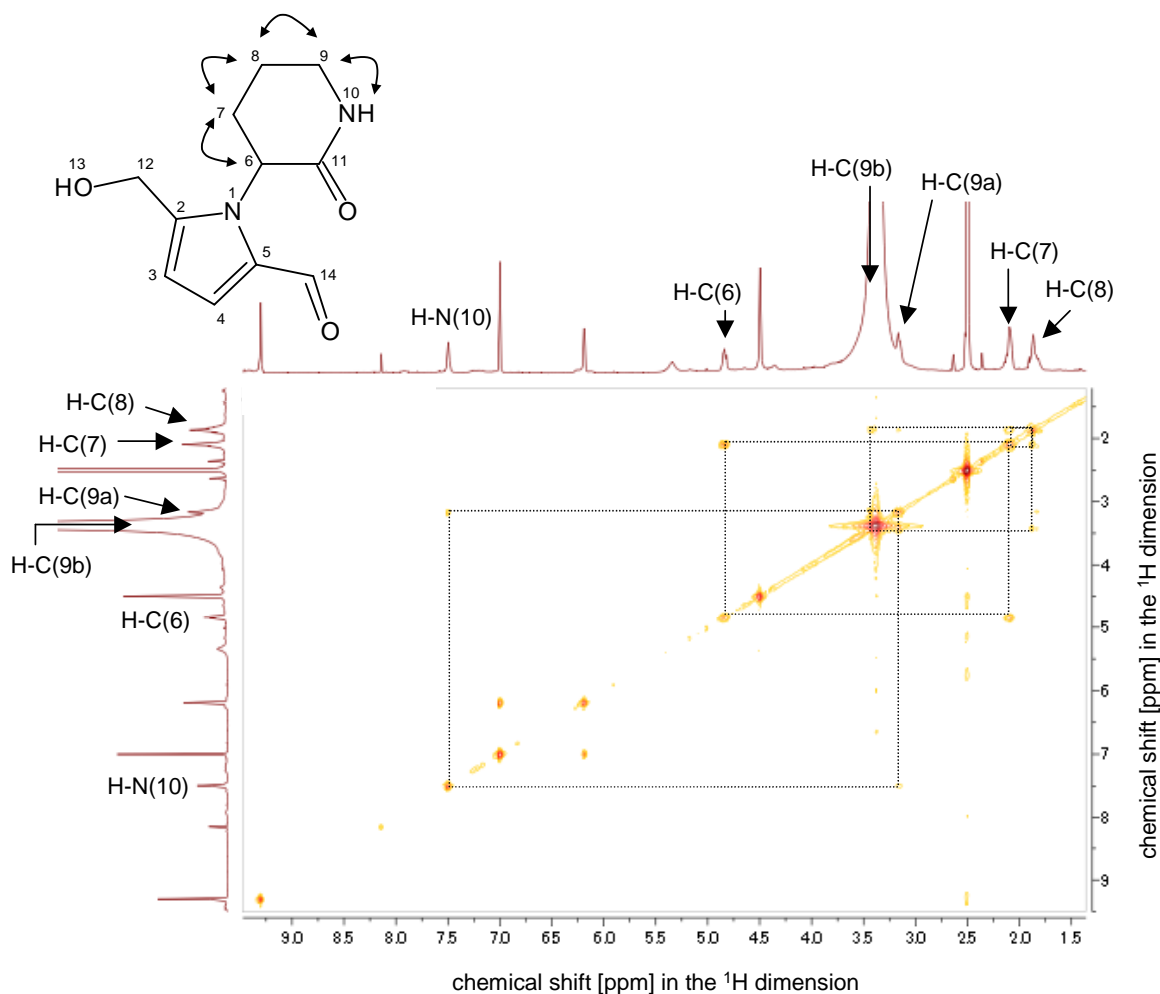


Figure 63. Excerpt of the COSY spectrum (500 MHz, $DMSO-d_6$) and key correlations of compound **26**.

In total, 26 compounds have been isolated and identified in pAGE using activity-guided fractionation. As the compounds seem to be amino acid derivatives, pyrazines or compounds consisted of six carbons, the identified compounds were assumed to be generated via Maillard type reactions, which will be discussed in a later chapter (chapter 3.6). Also, the compounds were quantified in pAGE (chapter.3.8.1), and antioxidative activities of all compounds were evaluated using ARS and ORAC assays (chapter 3.9.1).

2.3 Generation, isolation and identification of sulfur-containing compounds, spiro-alkaloids and a pyrrole derivative in model systems

The high concentrations of hexoses and S-allyl-L-cysteine (SAC) in AGE suggested that sulfur-containing Maillard-type products would be generated from SAC and sugars in powdered AGE via heat processing. Therefore, a model system using SAC and D-Glucose was developed, and reaction products were isolated and identified by means of 1D/2D NMR, UPLC-TOF MS and chiroptical analyses. Subsequently, the identified products were quantified in the pAGE by means of LC-MS/MS as well as evaluated on antioxidative activity using ARS and ORAC assays.

2.3.1 Development of a model reaction between S-allyl-L-cysteine and D-glucose

SAC in solution is a relatively stable compound, and a heating experiment (100 °C, 24 hours) using a liquid mixture of SAC and D-glucose in phosphate buffer (pH 6.0) resulted in only 10% decrease of SAC (data not shown). In comparison, a binary amorphous mixture prepared by freeze-drying generated lots of reaction products under the same heating conditions as mentioned above (**Figure 64**). Therefore the amorphous reaction system was used for further experiments. In order to target reaction products derived from SAC and D-glucose, three amorphous matrices were prepared using the binary mixtures, only SAC or D-glucose, and thermally processed. Comparison of HPLC separation of the three samples heated revealed the target products would elute at 23.8, 24.9, 30.5, 34.0, 37.2 and 38.4 min in the chromatogram (**Figure 64**, highlighted by arrows).

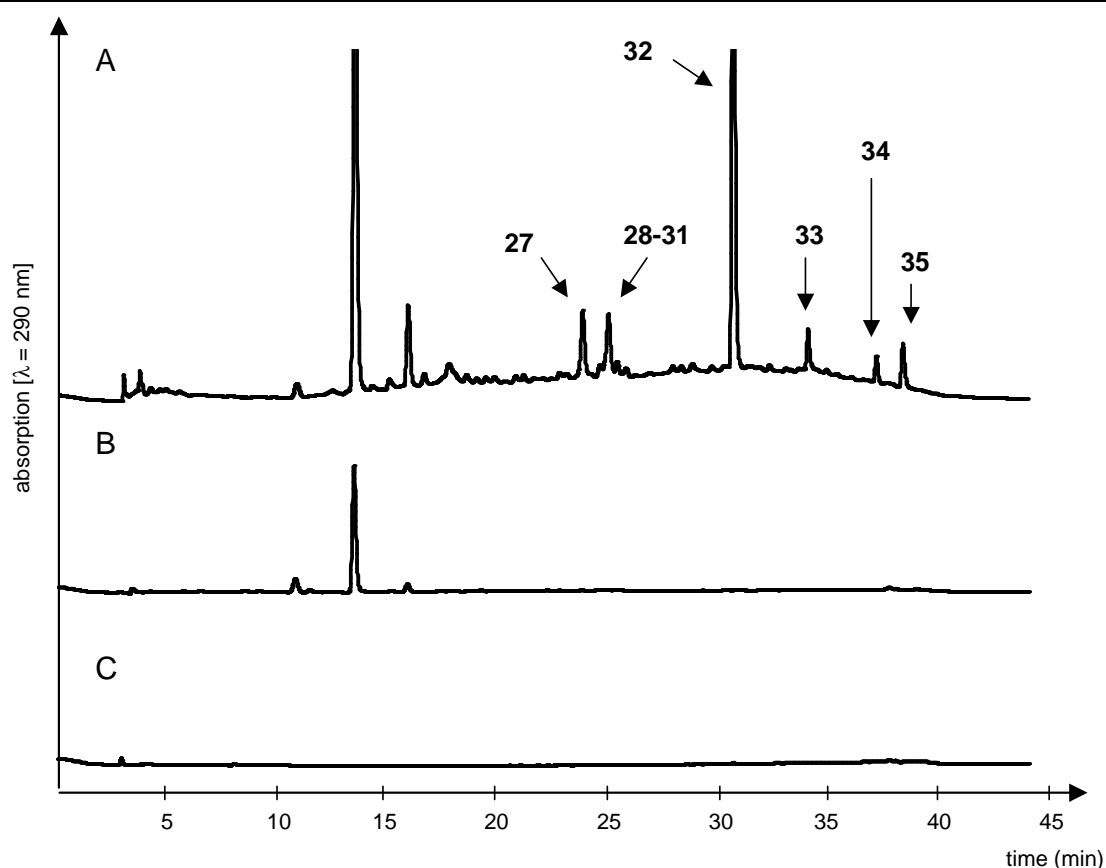


Figure 64. HPLC separation of (A) a mixture of SAC and D-glucose, (B) D-glucose and (C) SAC which were heated at 100 °C for 1 hour in amorphous state.

2.3.2 Isolation and structure determination of sulfur-containing compounds, spiro-alkaloids and a pyrrole derivative (27—35)

The heated binary mixture which was prepared in large scale was extracted with ethyl acetate to separate the reaction products from more polar components. Iterative separations from the organic layer by means of preparative and semipreparative HPLC enabled to obtain nine purified reaction products, namely **27** (25.7 mg), **28** (9.2 mg), **29** (23.9 mg), **30** (8.9 mg), **31** (10.8 mg), **32** (1206 mg, as Na salt), **33** (178.8 mg), **34** (13.0 mg) and **35** (29.9 mg), respectively (**Figure 65**). Chemical structures of the compounds were established using 1D/2D NMR spectroscopy and UPLC-TOFMS. In order to determine the absolute configuration, specific optical rotation for **27—30** and CD spectra for **31—35** were measured, and the optical data were compared to literatures.

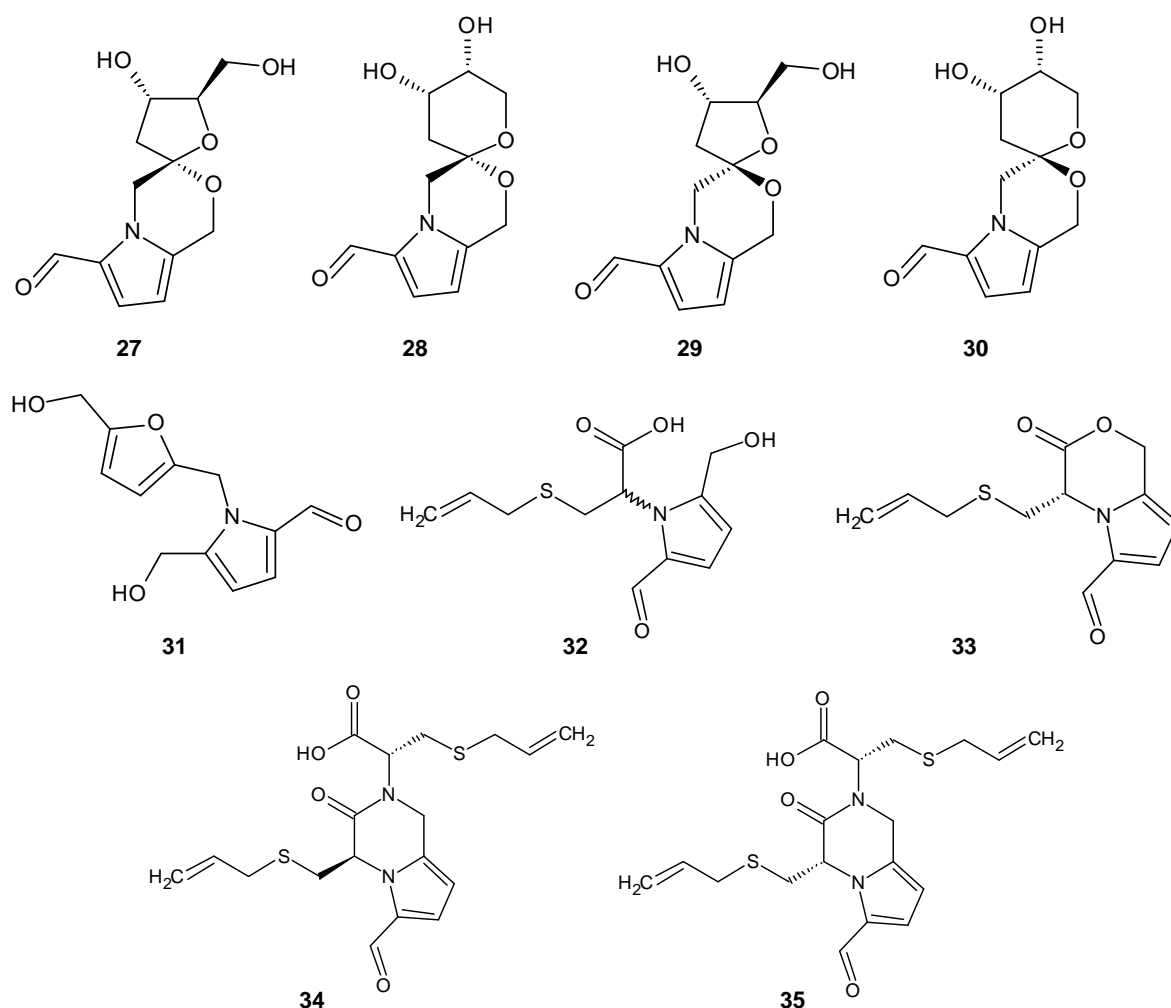


Figure 65. Compounds **27**–**35** isolated and identified in a model system of D-glucose and SAC.

Compound **27** was isolated being a pale brown colored powder. UPLC-TOF MS of **27** exhibited a m/z 254.1030 $[M+H]^+$, suggesting a molecular formula of $C_{12}H_{15}NO_5$. The 1H and ^{13}C spectra of **27** showed typical signals (δ_H 6.08, 7.03, 9.42; δ_C 104.79, 123.75, 130.64, 135.04, 178.95) for the pyrrole moiety with an aldehyde function like for compounds **3**, **11**, **13**, **14**, **19**, **23** and **26**. In addition, six nonequivalent heteroatom-bearing methylene protons at 4.44 [H-C(10b)], 4.17 [H-C(10a)], 3.54 [H-C(15b)], 3.44 [H-C(15a)], 2.30 [H-C(4b)] and 1.97 ppm [H-C(4a)], two equivalent methylene protons at 4.85 ppm [H-C(7)], an oxymethyne at 4.26 ppm [H-C(3)] and a heteroatom-bearing methyne at 3.88 ppm were also observed in the 1H NMR spectrum. Considering the following homonuclear COSY couplings of H-C(2)/H-C(3), H-C(3)/H-C(4), H-C(15)/H-C(2) and heteronuclear HMBC correlations of H-C(7) \rightarrow C(5,8), H-C(10) \rightarrow C(5,8),

H-C(2)→C(3), H-C(4)→C(2,3,5), a morpholine moiety consisted of one quaternary carbon at 102.38 ppm [C(5)] and two heteroatom-bearing methylene carbons at 57.16 [C(7)] and 50.75 ppm [C(10)] was proposed as well as a deoxysugar moiety possessing resonances at 102.38 [C(5)], 87.54 [C(2)], 69.89 [C(3)], 61.08 [C(15)] and 44.51 ppm [C(4)]. Bindings between the three moieties were clarified by means of further interpretation of HMBC connectivities of H-C(4)→C(5,10), H-C(7)→C(5,8,11), H-C(10)→C(4,8,13) (**Figure 66**), thus leading to the relative structure of **27** as a type of acortatarin A. This proposal was further confirmed by comparing NMR data measured in methanol- d_4 with those recently reported in the literature for acortatarin A, an antioxidative spiroalkaloid isolated from *Acorus tatarinowii* (Tong *et al.* 2010).

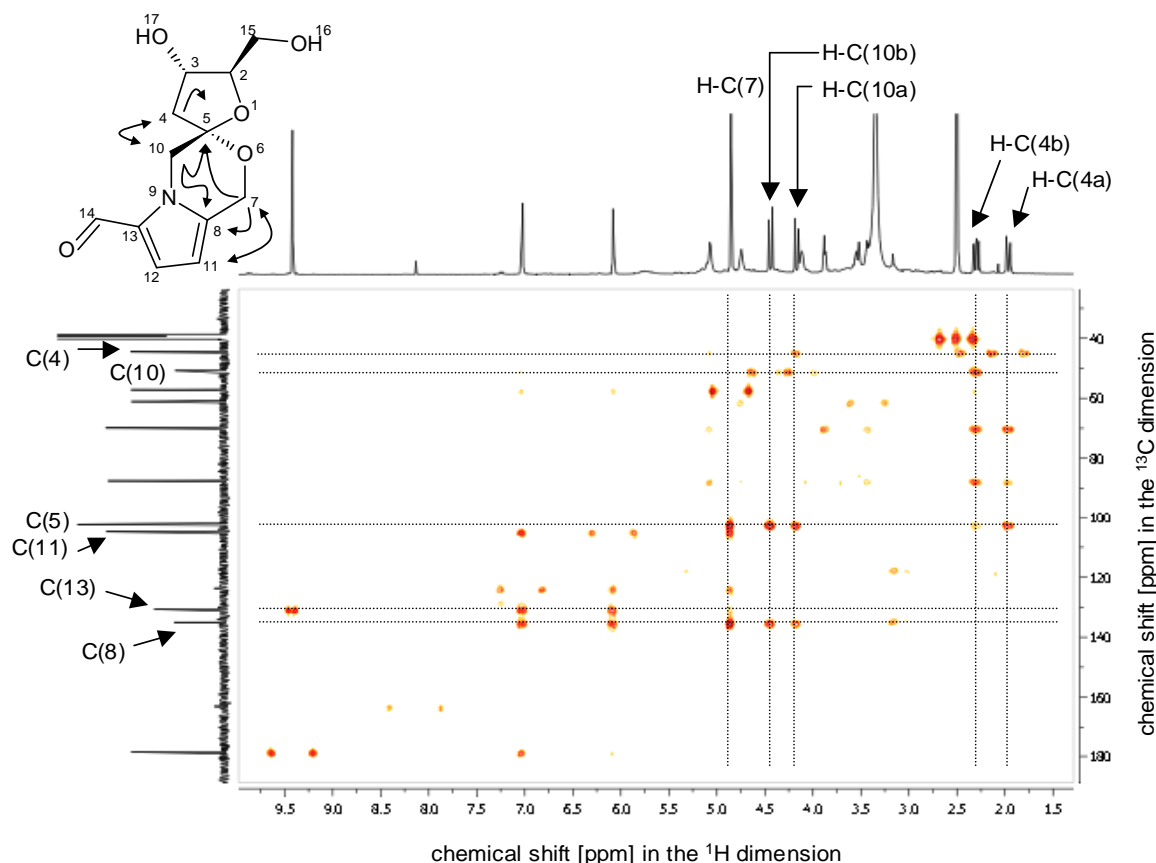


Figure 66. Excerpt of the HMBC spectrum (400 MHz, DMSO- d_6) and key correlations of compound **27**.

The absolute configuration of **27** was determined by measurements of specific optical rotation. The value ($[\alpha]^{24}_D +296$ (MeOH)) of **27** was very similar to that of acortatarin A ($[\alpha]^{22}_D +255$ (MeOH)), and consequently, the structure was unequivocally identified as acortatarin A (Li *et al.*, 2015).

Although compounds **28**—**31** were collected as one chromatographic peak, namely fraction B, in the first separation, each compound was well separated by means of a further semipreparative HPLC step. Using the same analytical strategy as described for compound **27**, the chemical structures of **28**, **29** and **30** were established.

Compound **29** showed extremely similar MS and 1D/2D NMR spectra to those of **27**. In contrast, a specific optical rotation value of $[\alpha]^{21}_D - 138.9$ (MeOH) recorded for **29** was not well in agreement with that of acortatarin A ($[\alpha]^{22}_D + 255$ (MeOH)) but with that reported in the literature for *epi*-acortatarin A ($[\alpha]^{19}_D - 111$ (MeOH)) (*Borrero et al. 2012*). The ^1H NMR spectrum additionally measured in CD_3OD also matched that of *epi*-acortatarin A (*Borrero et al. 2012*), thus leading to the identification of **29** as *epi*-acortatarin A.

While compounds **28** and **30** showed almost identical MS and NMR data to each other as well as to those of **27** and **29**, one chemical shift of quaternary carbon C(6) in **28** and **30** exhibited 93.4 and 94.9 ppm, respectively, which differed from the data of a quaternary carbon for **27** (102.4 ppm) and **29** (102.4 ppm). Although spiro-carbon atom C(5) in compounds **27** and **29** showed a HMBC correlation to two methylene protons for H-C(4) in the deoxysugar moiety, the quaternary carbons C(6) in **28** and **30** exhibited HMBC connectivities to two pairs of methylene protons for H-C(5) and H-C(2) (**Figure 67**). These differences clearly indicated that the deoxysugar moieties of **28** and **30** consisted of six heteroatoms, hence the relative structures of **28** and **30** were identified as pollenopyrroside A and xylapyrroside A, respectively, of which ^1H spectra matched to literature data (*Li et al. 2015, Guo et al. 2010*). The optical rotation values recorded for **28** ($[\alpha]^{22}_D + 123$ (MeOH)) and **30** ($[\alpha]^{23}_D - 156$ (MeOH)) were in line to pollenopyrroside A ($[\alpha]^{20}_D + 126$ (MeOH)) and xylapyrroside A ($[\alpha]^{22}_D - 189$ (MeOH)), respectively. This investigation undoubtedly confirmed the structure of **28** and **30** as pollenopyrroside A and xylapyrroside A, respectively (*Li et al. 2015, Guo et al. 2010*). To the best of our knowledge, this is the first time that the generation of such spiroalkaloids (**27**—**30**) is reported via a Millard-type reaction.

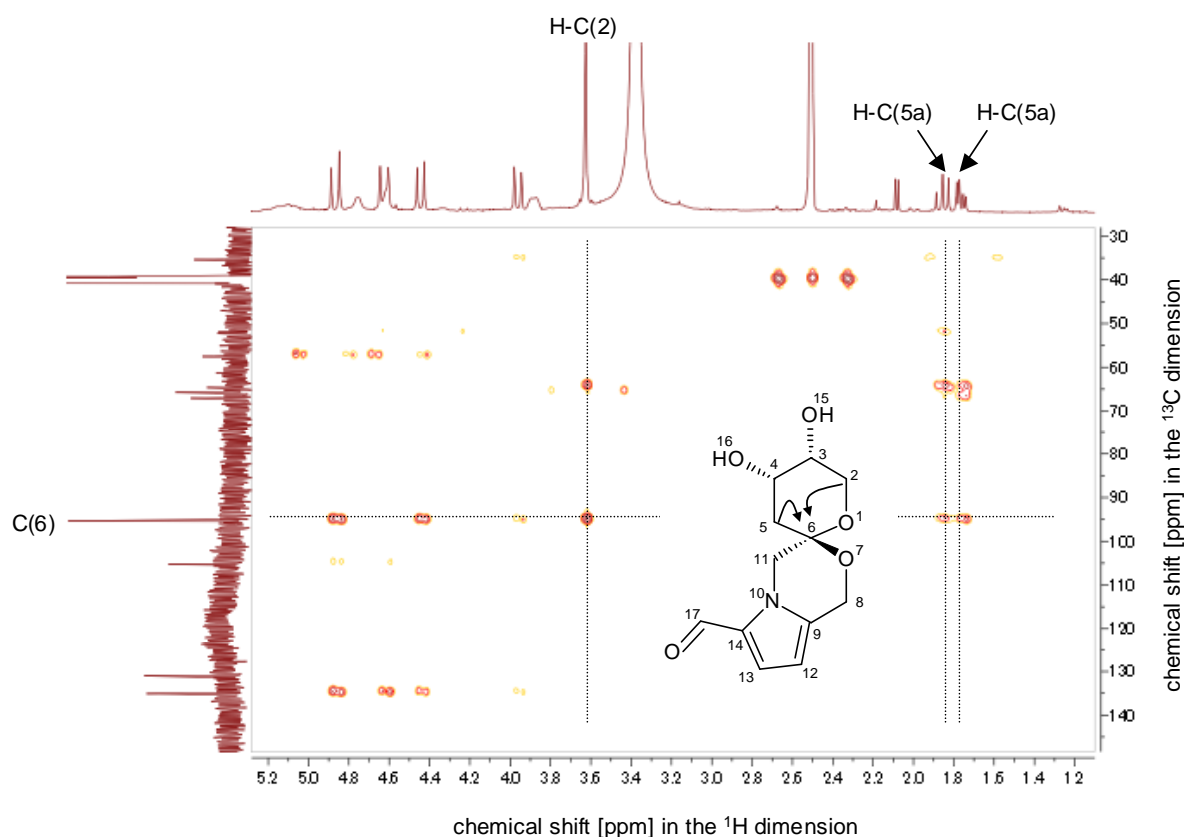


Figure 67. Excerpt of the HMBC spectrum (500 MHz, $\text{DMSO-}d_6$) and key correlations of compound **30**.

Compound **31** was obtained as a brown colored oil. UPLC-TOF MS of **31** showed a m/z 258.0739 $[\text{M}+\text{Na}]^+$, suggesting a molecular formula of $\text{C}_{12}\text{H}_{13}\text{NO}_4$. The ^1H and ^{13}C NMR spectra exhibited typical signals for a pyrrole motif with an aldehyde and a hydroxymethyl functions (δ_{H} 4.61, 6.23, 6.98, 9.50; δ_{C} 55.00, 109.57, 124.08, 131.52, 143.69, 179.47) and a furan motif with a hydroxymethyl function (δ_{H} 4.30, 6.14, 6.17; δ_{C} 55.60, 107.65, 108.34, 150.16, 155.23) like in previously identified compounds (**3**, **8**, **9**, **11**, **12**, **13**, **14**, **19**, **20**, **21**, **23** and **26**). Also, coupling constants of olefinic protons in the pyrrole and the furan motifs showed 4.0 and 3.1 Hz, respectively, that matched with those of the pyrrole and furan moieties in the compounds identified above, thus confirming the presence of the both motifs. In addition, two equivalent methylene protons resonating at 5.58 ppm [H-C(8)] showed HMBC correlations of H-C(8) \rightarrow C(4,5,10,13) indicating a linkage for the motifs (**Figure 68**), hence the structure was determined as 5-hydroxymethyl-1-[(5-hydroxymethyl-2-furanyl)methyl]-1*H*-pyrrole-2-carbaldehyde (**31**). This compound has not been reported so far.

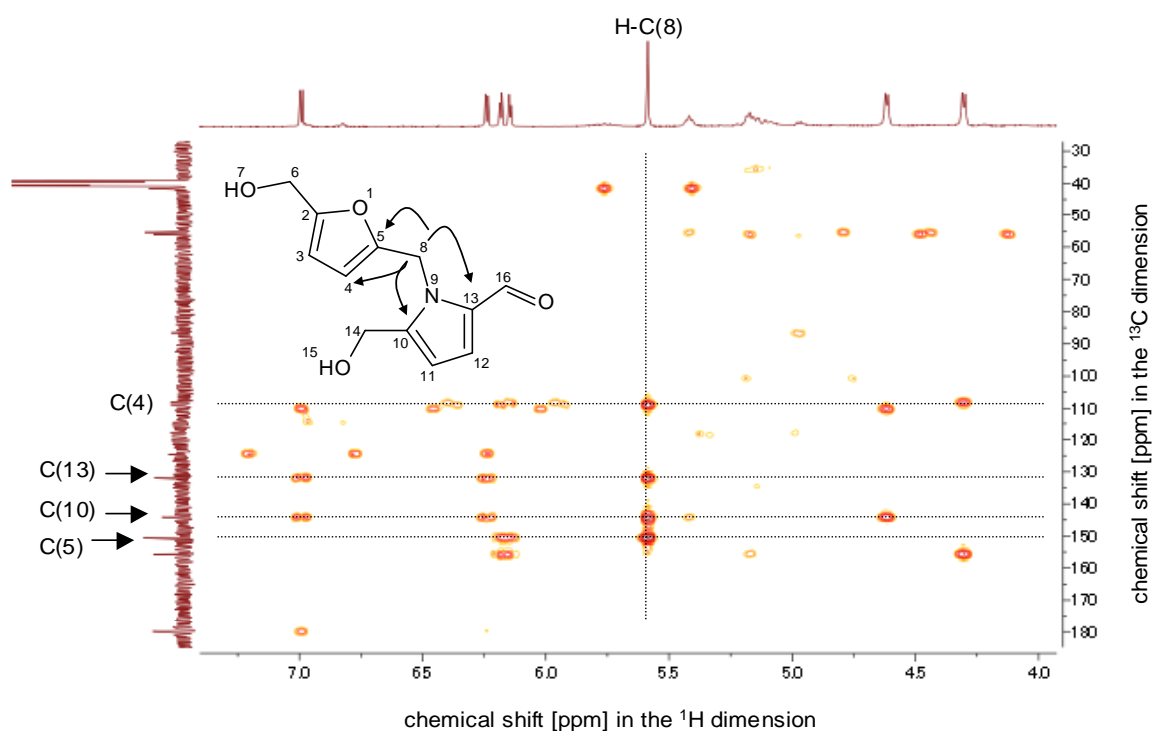


Figure 68. Excerpt of the HMBC spectrum (500 MHz, DMSO- d_6) and key correlations of compound **31**.

As compound **32** was also instable as found for compounds **11**, **19** and **23**, pyrrole derivatives of amino acids, pH adjustment of the purified solution containing **32** was done, followed by freeze-drying. Thereafter, an aliquot of **32** was analyzed by means of UPLC-TOF MS (ESI⁻) to reveal a pseudomolecular ion peak of m/z 268.0642 [M-H]⁻, thus suggesting a molecular formula of C₁₂H₁₅NO₄S. A pyrrole motif with an aldehyde and a hydroxymethyl functions was identified based on typical signals in the ¹H and ¹³C NMR spectra (δ_H 4.99, 6.19, 6.88, 9.30; δ_C 55.74, 110.18, 123.40, 132.77, 144.49, 179.23) like as **11**, **19** and **23**. Besides, four nonequivalent methylene protons at 2.76 [H-C(8a)], 2.92 [H-C(8b)], 2.92 [H-C(7a)] and 3.37 ppm [H-C(7b)], one olefinic methyne proton at 5.63 ppm [H-C(9)] and two nonequivalent olefinic methylene protons at 4.38 [H-C(10a)] and 4.43 ppm [H-C(10b)] were observed. These chemical shift values indicated the presence of a SAC moiety, and the assignment was achieved by the COSY of H-C(9)/H-C(8,10), HSQC and HMBC correlations of H-C(7)→C(6,8,13), H-C(8)→C(7,9,10), H-C(9)→C(8,10) and H-C(10)→C(8,9) (**Figure 69**). Furthermore, the HMBC spectrum confirmed the chemical structure of **32** as 3-(allylthio)-2-(2-formyl-5-hydroxymethyl-1*H*-pyrrol-1-yl)-propanoic acid,

of which amino group is incorporated into the pyrrole system. To the best of our knowledge, this compound has not been reported before in literature. CD spectroscopy of **32** exhibited no specific cotton effects, thus indicating this compound would be a racemate.

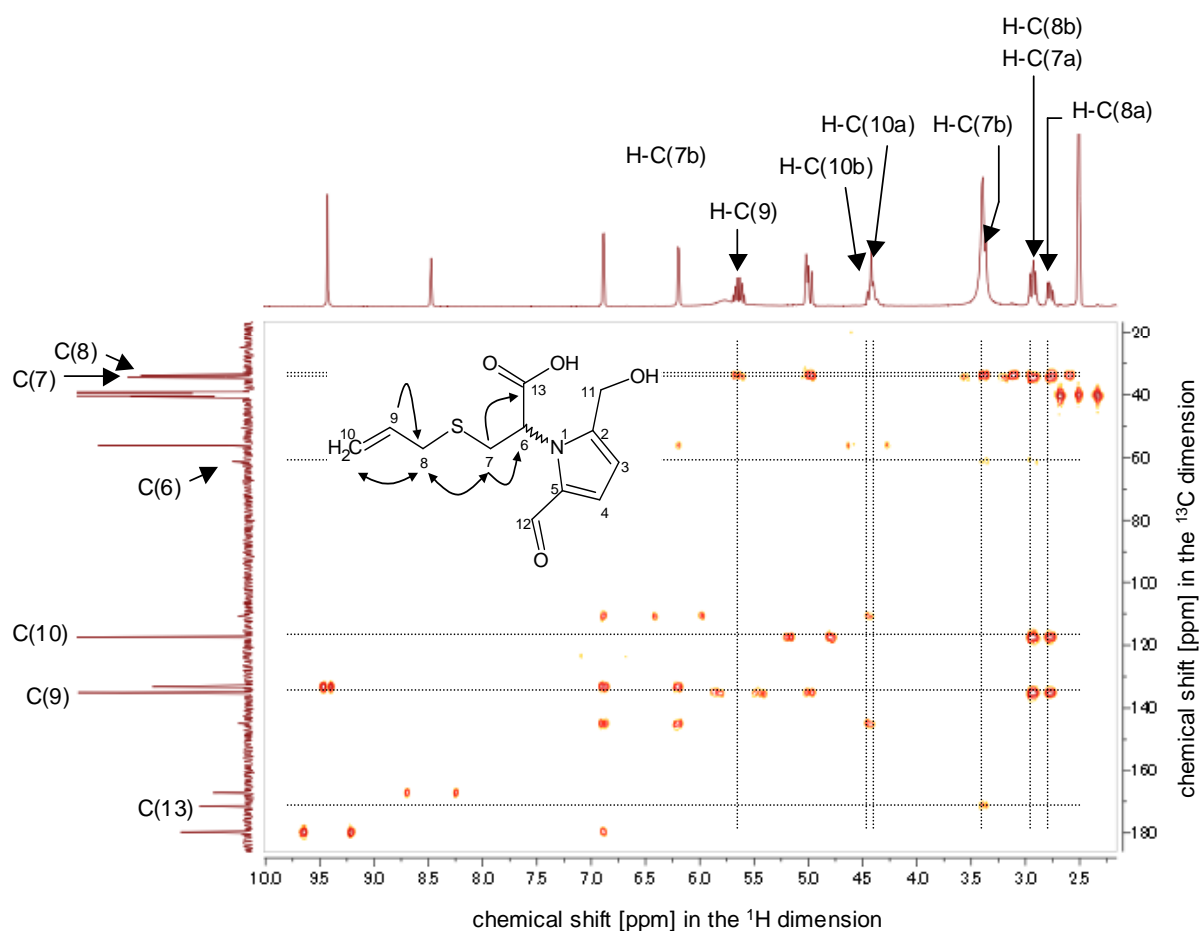


Figure 69. Excerpt of the HMBC spectrum (400 MHz, DMSO- d_6) and key correlations of compound **32**.

Compound **33** was isolated as a brownish oil. While NMR data (1D and 2D) of **33** were rather similar to those of **32**, remarkable differences of the ^1H NMR spectrum in compound **33** were that a methyne proton at the chiral center H-C(5) resonating at 5.59 ppm, and two nonequivalent methylene protons of H-C(2) resonating at 5.59 and 5.77 ppm. Then, the HMBC spectrum exhibited a cross peak between the nonequivalent methylene protons H-C(2) and the quaternary carbon C(6) (**Figure 70**), which was not detected in **32**. Considering the differences, the relative structure of **7** was determined as 4-(allylthiomethyl)-3,4-dihydro-3-oxo-1*H*-pyrrolo[2,1-*c*][1,4]oxazine-6-carbaldehyde, the corres-

ponding lactone of **32**. In addition, pseudomolecular ions of m/z 252.0697 $[M+H]^+$ and 274.2748 $[M+Na]^+$, detected by UPLC-TOF MS, confirmed the elemental composition of $C_{12}H_4NO_3S$ for **33**.

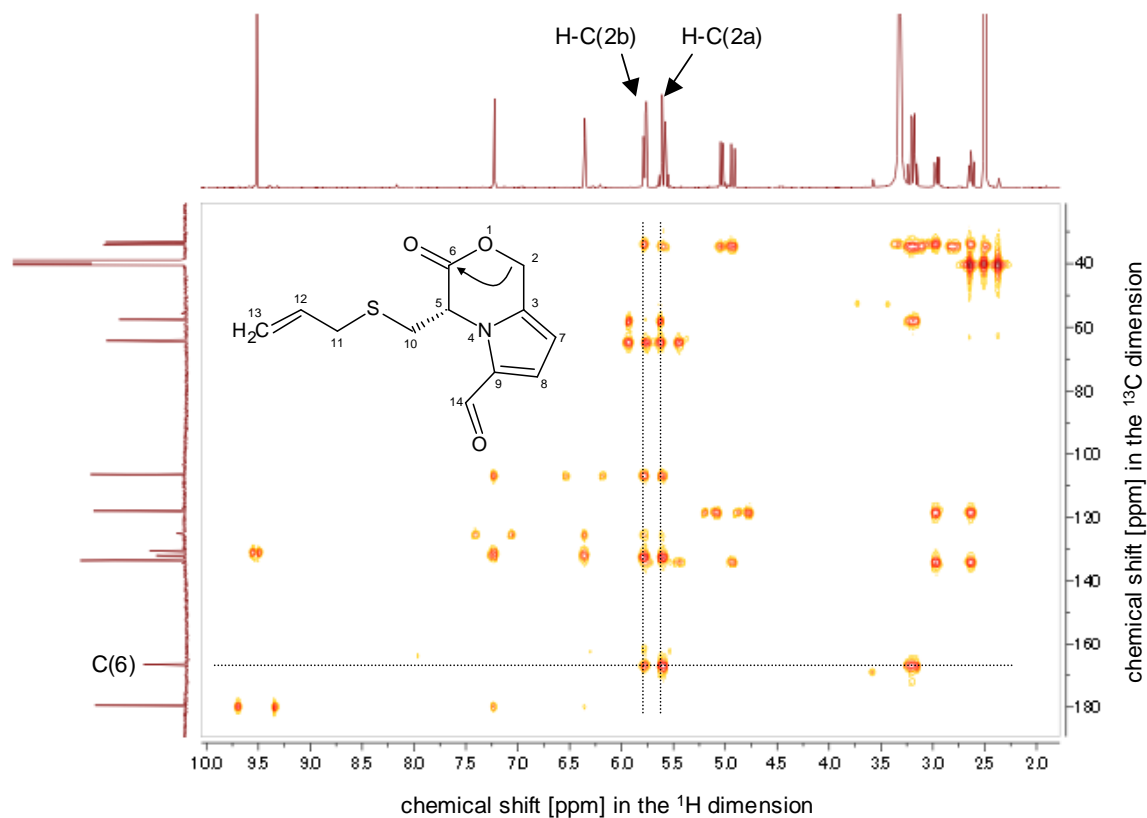


Figure 70. Excerpt of the HMBC spectrum (500 MHz, $DMSO-d_6$) and key correlations of compound **33**.

The absolute configuration of **33** was determined by means of CD spectroscopy. The CD spectrum of **33** showed a positive cotton effect at 295 nm, and this was well in line with literature data of structurally related *S*-configured derivatives (Wang *et al.* 2014), therefore, the stereochemistry of the chiral center C(5) could be deduced as *S*-configuration.

UPLC-TOF MS and NMR spectroscopic analysis of compounds **34** and **35** revealed rather similar data and indicated diastereomers with an empirical formula of $C_{18}H_{22}N_2O_4S_2$. In the 1H and ^{13}C NMR spectra, the following signals (δ_H 2.59, 2.88, 3.08, 4.93, 5.01, 5.54, 5.55, 6.29, 7.20, 9.47; δ_C 34.08, 34.23, 58.26, 106.47, 117.78, 125.42, 129.87, 133.89, 134.69, 165.95, 178.95) were well in agreement with partial data of compound **33**, whereas the methylene carbon C(2) showed a lower chemical shift value [41.76 ppm] than that of the corresponding carbon in **33** [64.23 ppm]. Two methylene protons of H-C(2) resonating at 4.69 and 4.93 ppm were also different from the corresponding methylene protons in **33** (5.59 and 5.77 ppm), thus indicating a hetero-lactone structure of the target compounds related to the lactone ring in **32**. Besides, further interpretation of the NMR spectra enabled to disclose the presence of another SAC-motif with typical signals for an aliphatic methyne proton at 4.93 ppm [H-C(10)], four aliphatic methylene protons at 2.96 [H-C(11)], 3.07 [H-C(11)] and 3.12 ppm [2H, H-C(12)], an olefinic methyne at 5.71 ppm [H-C(13)] and two olefinic protons at 5.10 ppm [2H, H-C(14)] and carbon resonances at 28.38 [C(11)], 33.50 [C(12)], 56.57 [C(10)], 117.41 [C(14)], 134.25 [C(13)] and 170.08 ppm [C(20)]. By means of the HMBC correlations, an aliphatic methyne proton [H-C(10)] of the SAC motif showed cross peaks of H-C(10) \rightarrow C(2,6), and this confirmed the SAC motif to be connected via the nitrogen atom being a part of a 2-ketopiperazine system (**Figure 71**). Hence, the relative structure of diastereomers **34** and **35** were identified as 3-(allylthio)-2-{4-(allylthiomethyl)-6-formyl-3-oxo-3,4-dihydropyrrolo[1,2-a]pyrazin-2(1*H*)-yl}-propanoic acid.

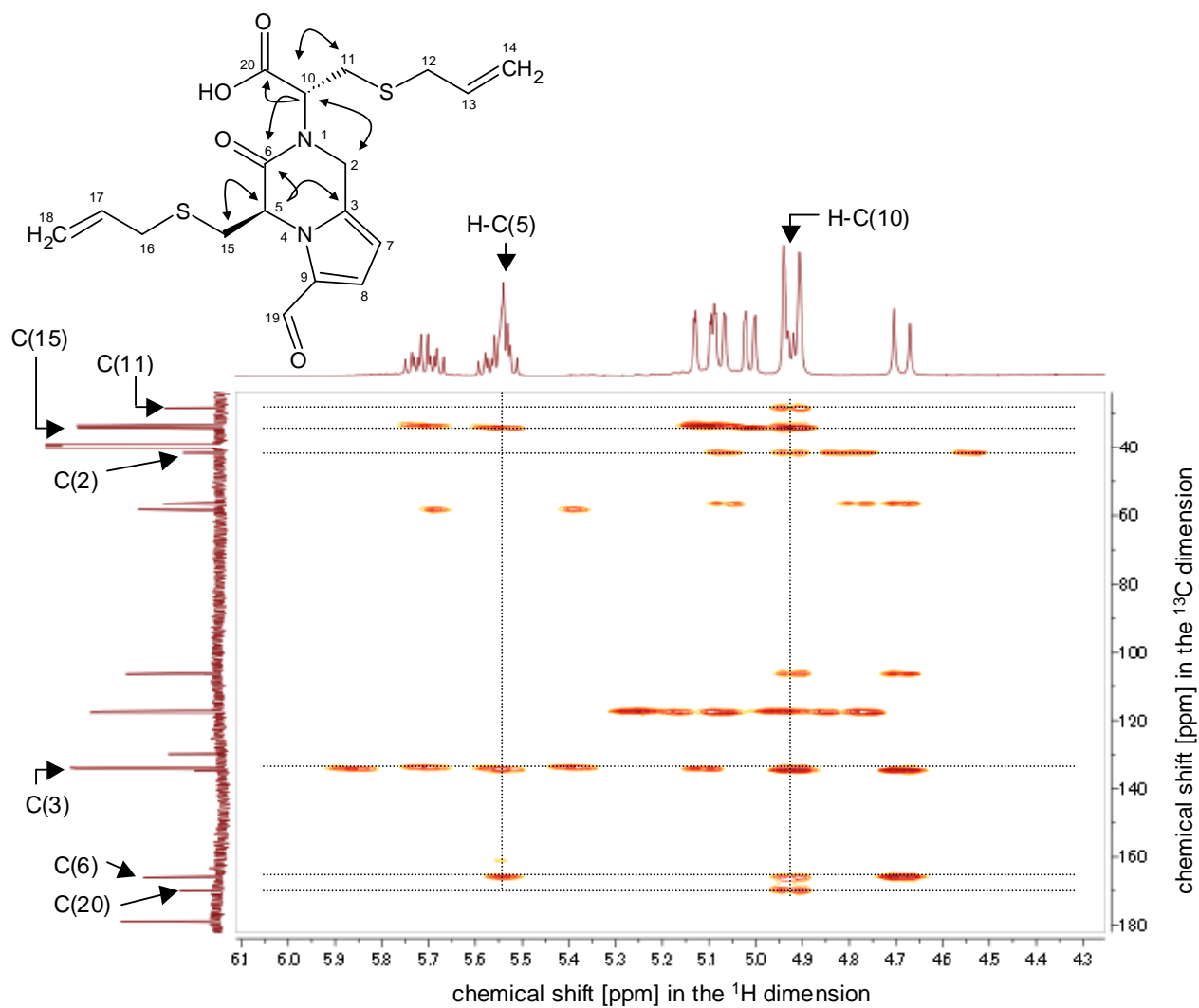


Figure 71. Excerpt of the HMBC spectrum (500 MHz, DMSO-*d*₆) and key correlations of compound **34**.

In order to determine the absolute configuration of **34** and **35**, two structurally related compounds **36** and **37** (**Figure 73**), differing from **34** and **35** by lacking the carboxyl group, were prepared by reacting SAC and purified compound **33** (**Figure 72**). After separation and purification of a chiral mixture of **36** and **37**, their structure determination was conducted as a racemate using NMR spectroscopy and UPLC-TOF MS. The high resolution mass spectrometry of the racemic mixture confirmed a m/z 351.1201 $[M+Na]^+$, which suggested an elemental composition of $C_{17}H_{23}N_2O_2S_2$ corresponding in the target structures. The 1H and ^{13}C NMR spectra of the racemate exhibited extremely similar signals recorded for **34** and **35**, and the 1H NMR data showed only one different signal of two methylene protons at 3.58 and 3.66 ppm $[H-C(10)]$ due to a lack of the carboxyl group. Then, the ^{13}C NMR spectrum didn't exhibit one quaternary carbon resonance derived from a carboxyl acid, thus meaning the total carbon signals of the racemate are less than that of **34** and **35** by one carbon. Therefore, the relative structure of the racemate was confirmed as a decarboxylated form of **34** and **35**.

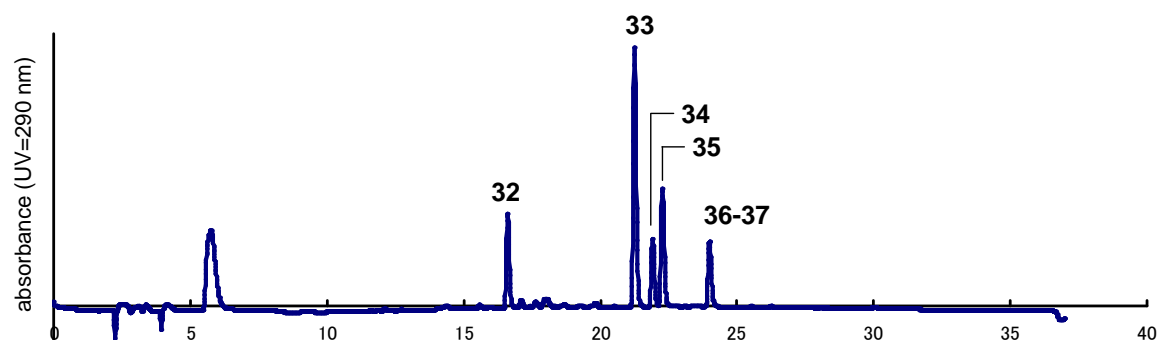


Figure 72. HPLC of the reaction matrix which was prepared using SAC and purified compound **33** and heated 100 °C for 50 min.

Subsequently, enantiopure **36** and **37**, obtained by means of chiral HPLC, were analyzed on CD spectroscopy to determine their absolute configurations comparing the CD spectrum recorded for **33** that shows a positive cotton effect at 295 nm (**Figure 73**). As the CD spectrum recorded for **36** exhibited a positive cotton effect at 296 nm, the stereochemistry of **36** was deduced *S*-configuration, and the mirror image spectra for compounds **36** and **37** led the stereochemistry of **37** as *R*-configuration.

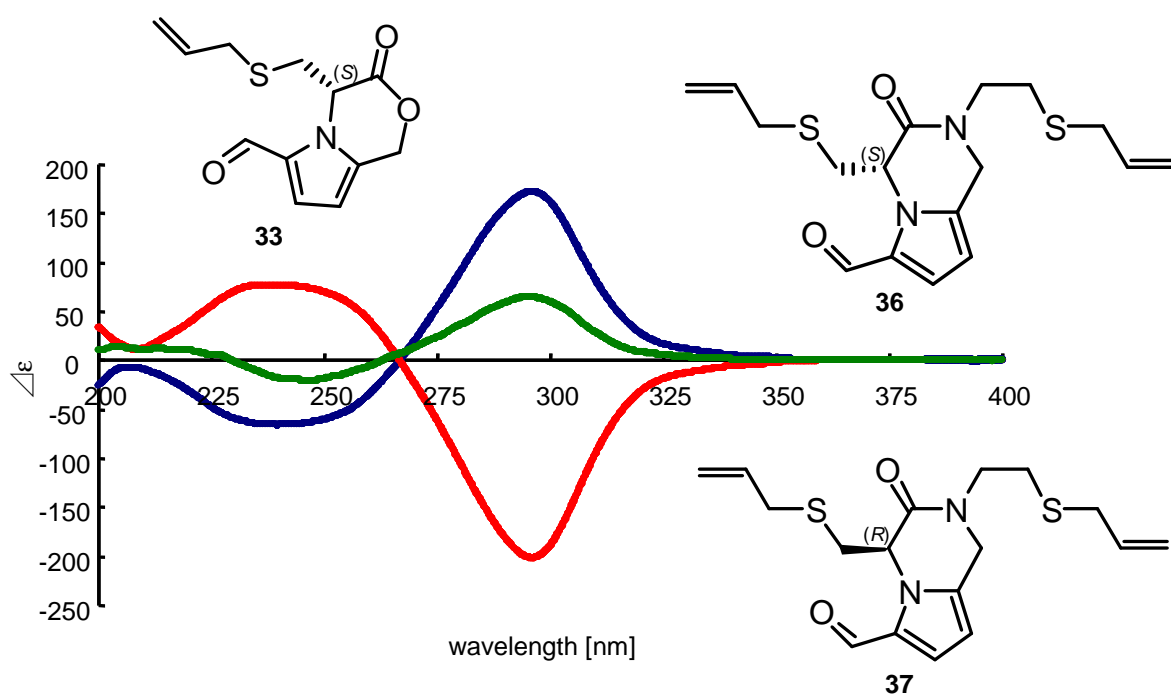


Figure 73. CD spectra of compounds **33** (green), **36** (blue) and **37** (red), and deduced absolute configurations.

Adopting the clarified structures **36** and **37**, absolute configurations of **34** and **35** were determined through comparison of CD spectra between **34**, **35**, **36** and **37** (Figure 74). The CD spectrum of **34** was well in line with that of the compound **37**, and that of **35** matched the spectrum obtained for **36**, thus indicating the stereochemistry at C(5) in the compound **34** to be *R*- and in the compound **35** to be *S*-configured, respectively. As the CD spectra of **34** and **35** were not mirror images, both compounds were deduced to be diastereomers with the same configuration at the remaining chiral carbon C(10).

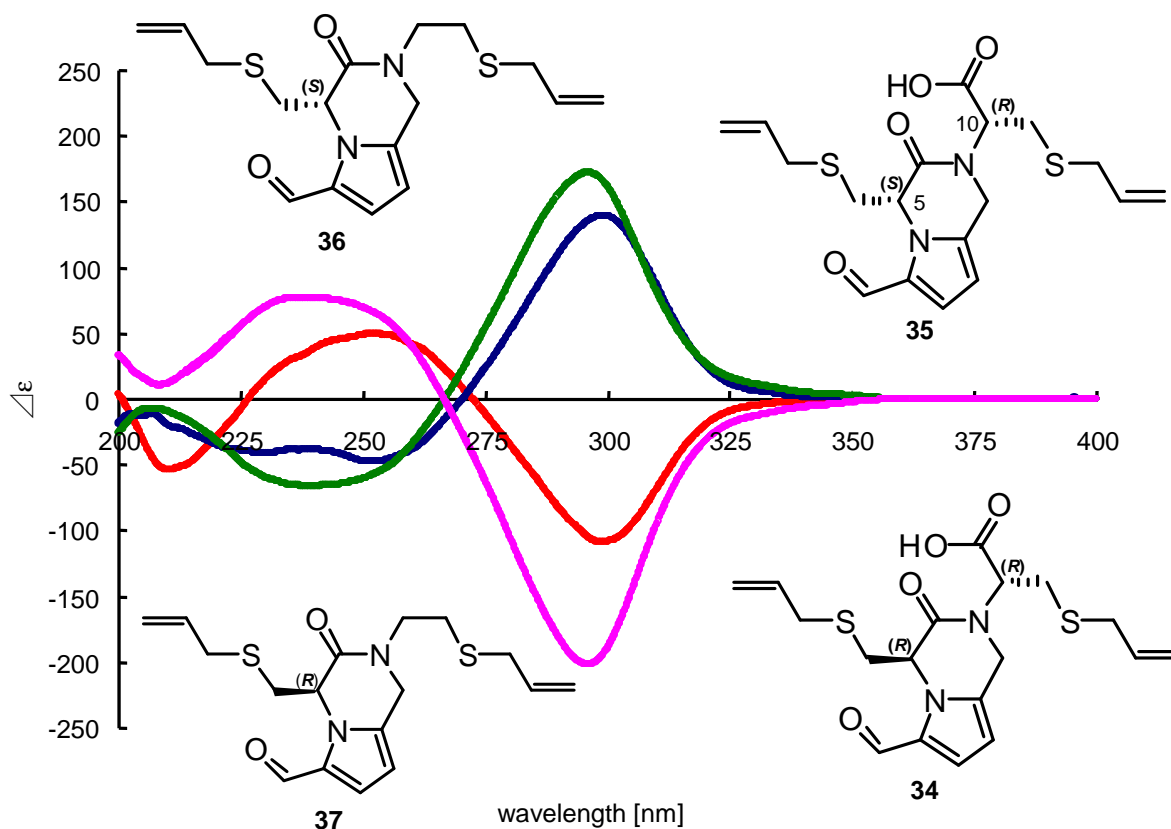


Figure 74. CD spectra of compounds **34** (red), **35** (blue), **36** (green) and **37** (purple), and deduced absolute configurations.

The stereochemistry of the chiral center C(10) was assigned by means of further model reactions with *S*-allyl-*L*-cysteine and *S*-allyl-*D*-cysteine, respectively. As described at the experimental part, next to **34** and **35** also compounds **36** and **37** were generated upon the reaction of compound **33** with *S*-allyl-*L*-cysteine, thus indicating that the formation of the ketopiperazine ring in **34**–**37** would start by nucleophilic attack with the amino function of *S*-allyl-*L*-cysteine to the carboxyl function of **33**. As *S*-allyl-*L*-cysteine acts as a nucleophile in the reaction, the original *R*-configuration of *S*-allyl-*L*-cysteine will be maintained in the *S*-allyl-*L*-cysteine moiety for **34** and **35**. Interestingly, as *S*-allyl-*L*-cysteine was more reactive than *S*-allyl-*D*-cysteine for production of the sulfur compounds **32**–**35** (Figure 75), the *R*-configured *S*-allylcysteine moiety would be predominant in case of co-existence of *S*-allyl-*L*-cysteine and -*D*-cysteine in the reaction system in **34** and **35**. These experimental data and their interpretation enabled to deduce the stereochemistry of the chiral carbon C(10) as *R*-configuration.

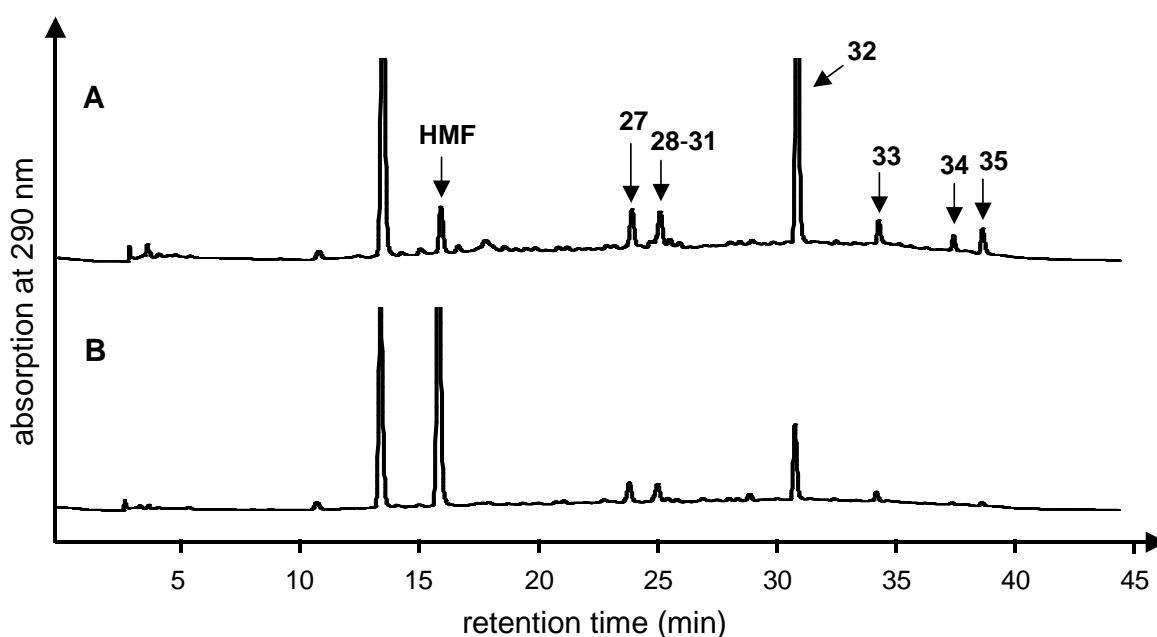


Figure 75. HPLC separation of heated mixtures using (A) *S*-allyl-*L*-cysteine and *D*-glucose and (B) *S*-allyl-*D*-cysteine and *D*-glucose.

2.3.3 Identification of the isolated compounds 27—37 in pAGE

The occurrence of the identified compounds **27—37** in the pAGE was investigated using UPLC-ESI-MS/MS. As compounds **27—30** are diastereomer, an optimized common MS/MS parameter of m/z 254.2 \rightarrow 206.1 was used for detection of the compounds. Four peaks were shown in the chromatogram for the pAGE analysis (**Figure 76—A**). Retention times of each peak were confirmed with reference compounds as co-chromatography (**Figure 76**), therefore the existence of the compounds **27—30** was undoubtedly proven in pAGE.

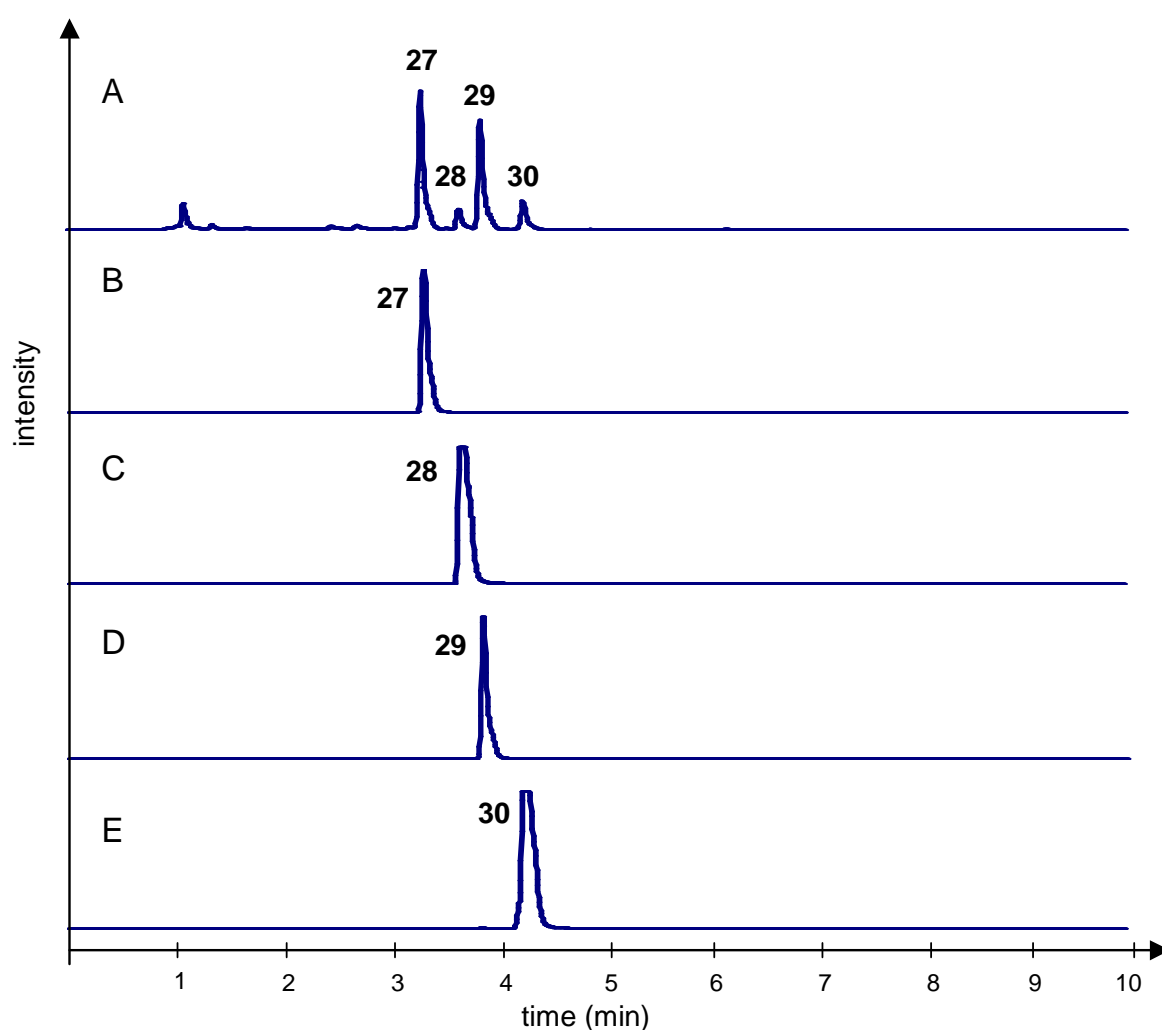


Figure 76. LC-MS/MS chromatograms of (A) pAGE, (B) compound **27**, (C) compound **28**, (D) compound **29** and (E) compound **30** monitoring m/z 254.2 \rightarrow 206.1. Signal intensities are normalized.

Three mass transitions of the sodium adduct of compound **31** were tuned to get the optimal detection regarding sensitivity as well as selectivity in pAGE. Analysis of compound **31** using the mass transition m/z 258.3 \rightarrow 200.1 revealed the presence of **31** in pAGE (**Figure 77—B**).

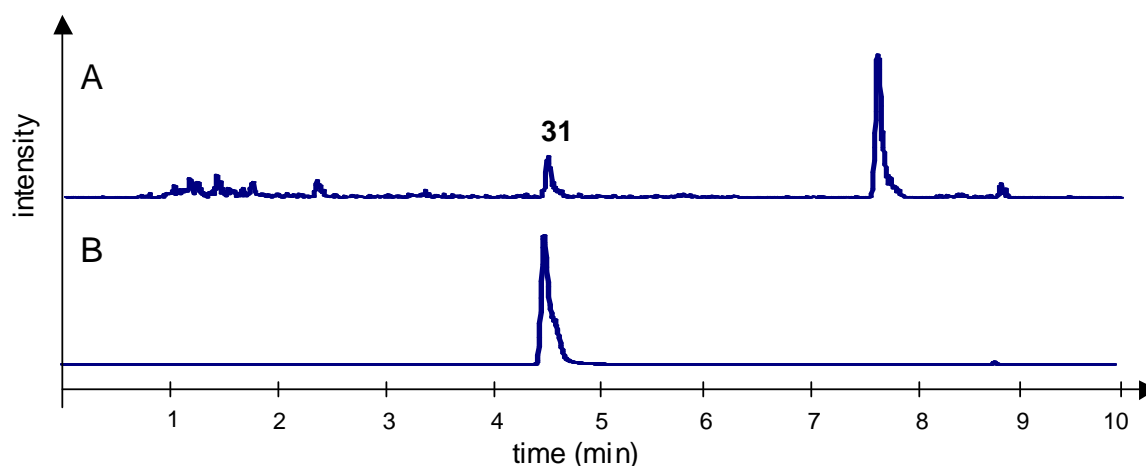


Figure 77. LC-MS/MS chromatograms of (A) pAGE, (B) compound **31**, monitoring m/z 258.3 \rightarrow 200.1. Signal intensities are normalized.

Using the same analytical strategy (retention time check and cochromatography), the presence of sulfur-containing compounds **32—35** as well as **36** and/or **37** was defined in pAGE (**Figure 78**). In conclusion, all compounds (**27—37**) isolated from the model system were identified in pAGE, hence, they were evaluated on antioxidative activities like other identified compounds and quantified (chapter 3.8.1 and 3.9.1).

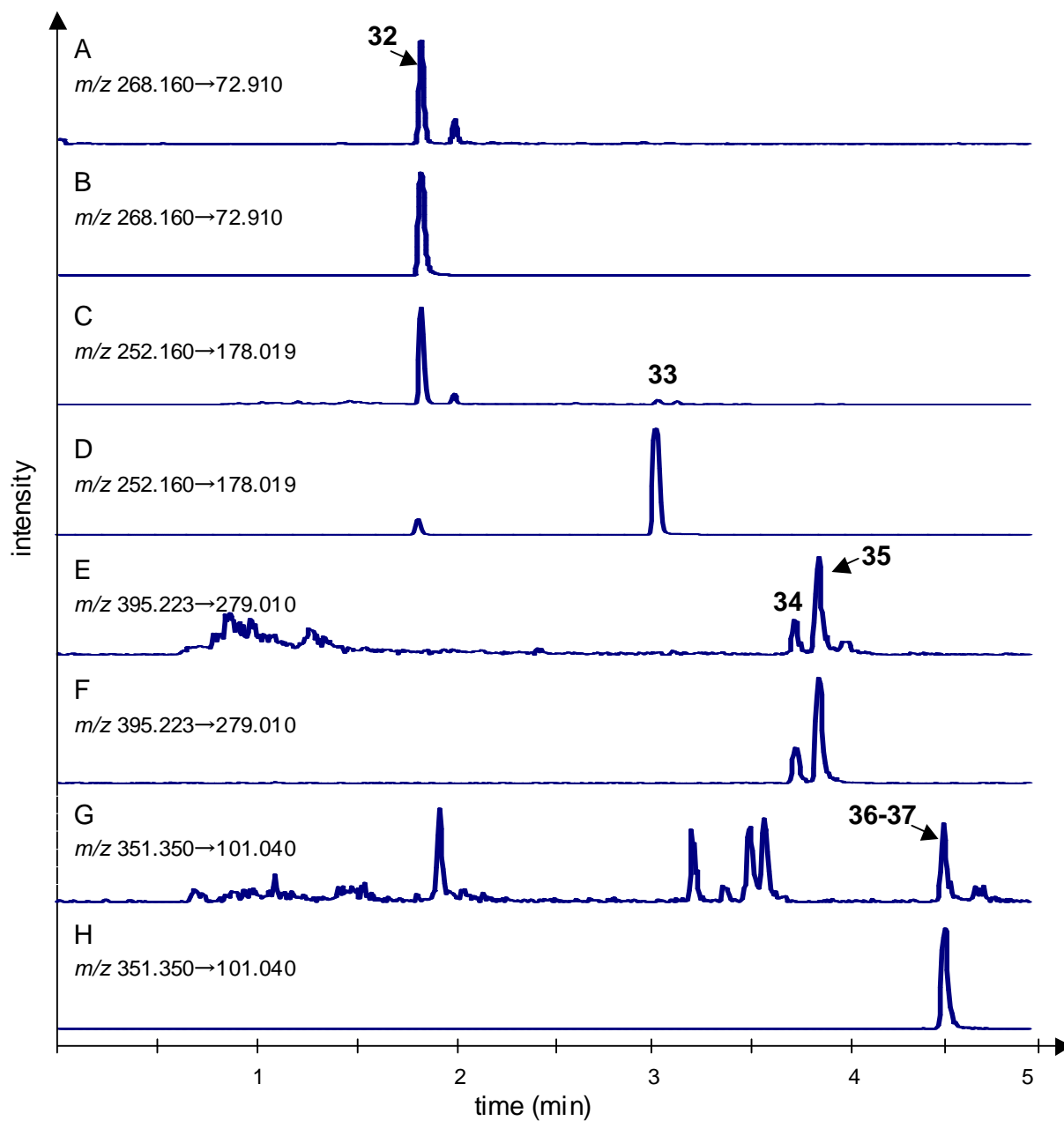


Figure 78. LC-MS/MS chromatograms of (A, C, E G) pAGE, (B) compound **32**, (D) compound **33**, (F) a mixture of **34** and **35**, (H) a racemate of **36** and **37**. Signal intensities are normalized.

2.4 Proposed reaction pathways governing the formation of isolated compounds 1—37

As the powdered AGE abundantly contains sugars and amino acids, it was assumed that Maillard-type reactions would greatly contribute to generation of numerous antioxidants in the pAGE. So far, literature showed that 2,3-dihydro-3,5-dihydroxy-6-methyl-4(*H*)-pyran-4-one (**6**) and 5-hydroxymethyl-2-furaldehyde (**9**) can be produced from 1-deoxyhexosone and 3-deoxyhexosone, respectively (Voigt *et al.* 2010, Jadhav *et al.* 2011). 5-Hydroxymaltol (**18**) is a similar compound to **6**, and Kim *et al.* (1996) proposed that **6** generates **18** via oxidation using model reactions with carbon-labeled compound **6**. As thymidine (**10**) is a pyrimidine deoxynucleoside, it must be extracted and transferred from cell nuclei of raw garlic to the AGE under manufacturing, instead of its generation by the heat processing for the processed AGE. Besides, some of the proposed reaction pathways were underlined using model reactions with reasonable compounds (2-keto-D-glucose, citric acid, L-glutamic acid, L-ornithine) and detection by means of LC-MS/MS.

2.4.1 Formation of pyrazine derivatives 1, 2, 4, 5, 7, 17, 22 and 25

Considering the 1,2,3-butanetriol moiety attached to the pyrazine ring in compounds **1**, **2**, **4** and **5**, the following cascade could be proposed starting at 3-deoxyhexosone (**1**) generated from sugars in course of the Maillard reaction (**Figure 79**). Reaction of **1** with amino acids leads to 1-amino-1-deoxyfructose (**2**) and 2-amino-deoxyfructose (**3**), and then homo-molecular condensation of **2** as well as hetero-molecular condensation of **2** and **3**, followed by oxidation, yields compounds **1** and **2**. While **3** also generates a symmetric intermediate (**4**) via homo-molecular condensation, the intermediate can be cyclized by nucleophilic attack of the hydroxyl functions to the dihydro-pyrazine ring to give hetero-five and six membered rings (**Figure 79, flow: a, b**). Finally, further oxidation produces compounds **4** and **5**.

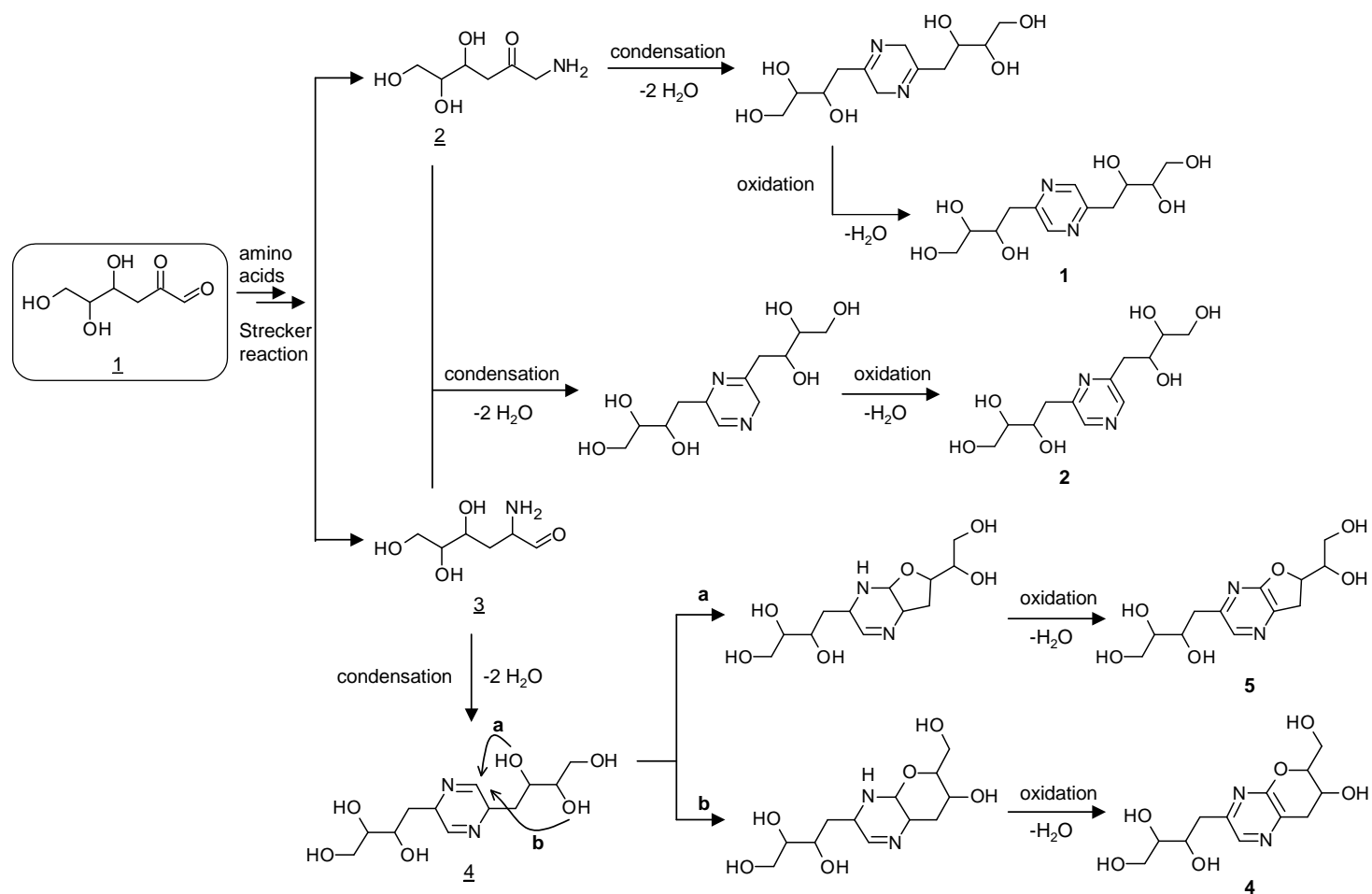


Figure 79. A proposed reaction pathway for generation of pyrazine derivatives (compounds **1**, **2**, **4** and **5**).

In contrast to compounds **1**, **2**, **4** and **5**, compound **17** exhibits not only 1,2,3-butanetriol but also an ethyl group, and this difference enabled to propose a pathway starting from 2-oxobutanal (**5**) (**Figure 80**). *Hofmann et al. (1998)* disclosed that 2-oxobutanal is generated from glycolaldehyde and acetaldehyde via an Aldol-type reaction in course of the Maillard reaction, therefore **5** should be existed in pAGE. 2-Aminobutanal (**6**) is an intermediate generated from **5** upon Strecker reaction using amino acids and this reacts with 1-amino-1-deoxyfructose (**2**) to form compound **17** upon condensation followed by oxidation (**Figure 80**).

As compounds **7**, **22** and **25** have a methyl group linked to the pyrazine ring, methylglyoxal (**7**) would be a potential precursor involved in the formation. 2-Aminopropanal (**8**) and 1-amino-2-propanone (**9**) produced from **7** via Strecker reaction with amino acids lead to 1,2,3-butanetriol-4-(6-methyl-2-pyrazinyl) (**7**) and its diastereomer, respectively, by a reaction with **2** upon condensation and oxidation. Compounds **22** and **25** are, subsequently, generated from the alkylpyrazines via dehydration at the 1,2,3-butanetriol group (**Figure 80**).

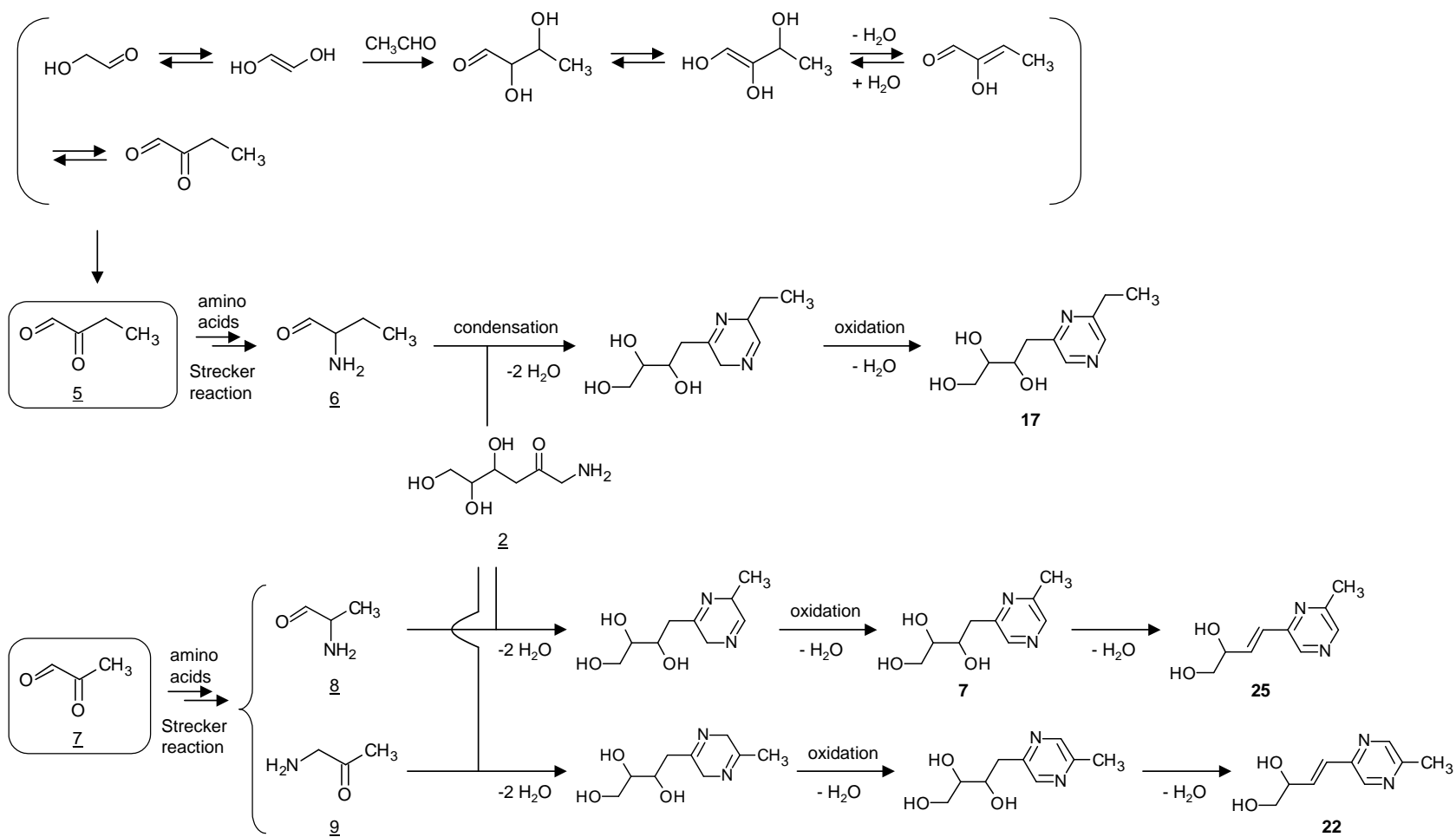


Figure 80. A proposed reaction pathway for generation of pyrazine derivatives (compounds **7**, **17**, **22** and **25**).

2.4.2 Formation of amino acid pyrrole derivatives **3**, **11**, **13**, **19**, **23**, **26** and **32—37**

The presence of a 5-hydroxymethyl-pyrrole-2-carbaldehyde moiety in the compounds **3**, **11**, **13**, **19**, **23**, **26**, **32** — **37** enabled to determine 3-deoxyhexosone (**1**) as a key substance for the formation pathway (**Figure 81**). Reaction of 3,4-dideoxyosone (**10**), generated from **1** upon water elimination and tautomerization, with amino acids (arginine, aspartic acid, glycine, glutamic acid, alanine and SAC) affords compounds **3**, **11**, **13**, **19**, **23**, **32** via intramolecular cyclization followed by dehydration.

In particular, compound **32**, isolated and identified in the model system using SAC and D-glucose, leads to further derivatives as follows. **32** generates its corresponding lactone (**33**) upon intramolecular esterification. As described before (**Figure 75**), SAC and compound **33** are reaction intermediates for the generation of **34—37**, and this enabled to propose the following reaction pathway (**Figure 81**). Reaction of the lactone (**33**) with another SAC forms the dipeptide-type intermediate (**11**) that reacts upon dehydration at the 5-hydroxymethylpyrrole moiety, followed by another ring closure via the peptide nitrogen atom to give rise to the compounds **34** and **35**. Finally, decarboxylation of compounds **34** and **35** yield compounds **36** and **37**.

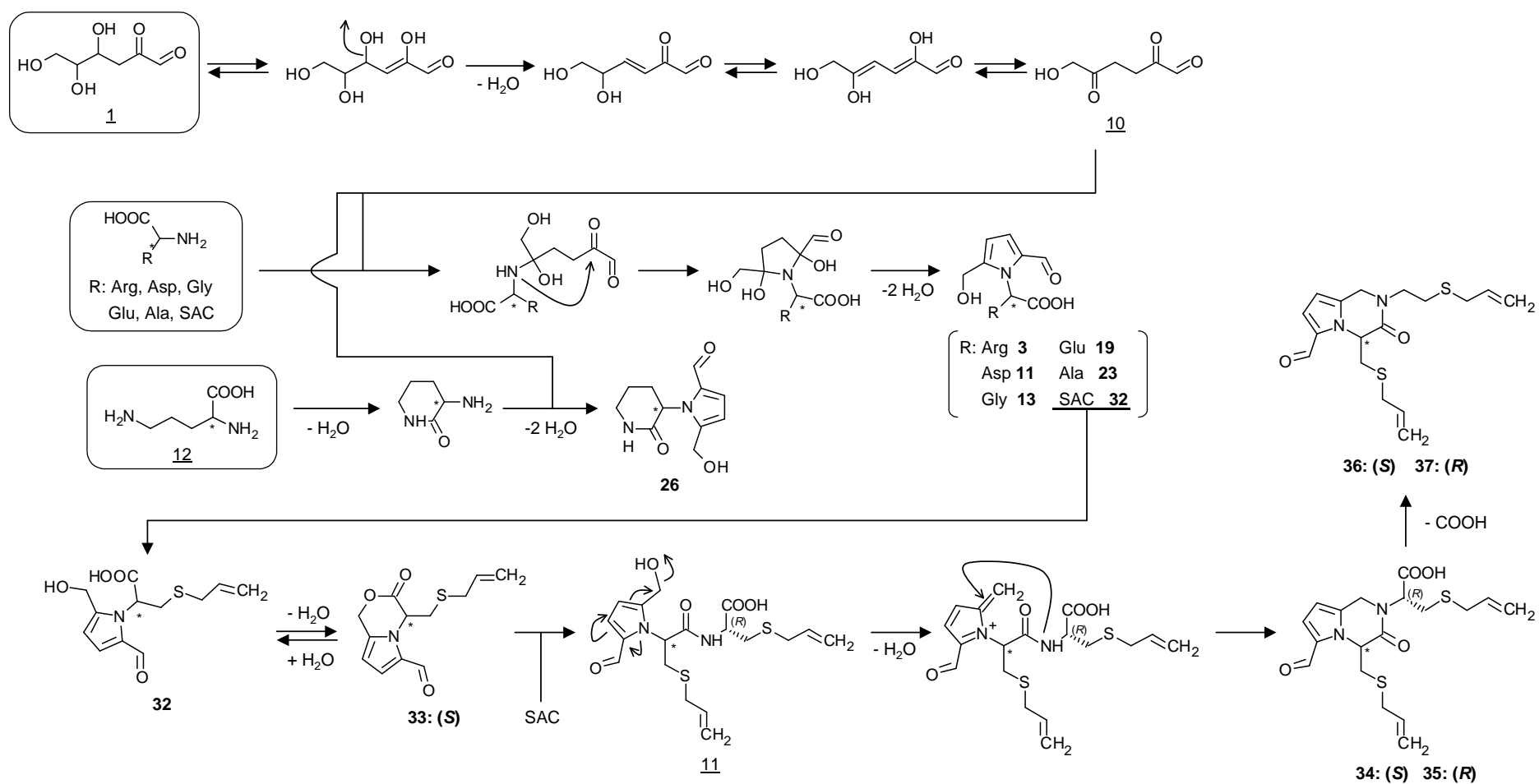


Figure 81. A proposed reaction pathway for generation of amino acid pyrrole derivatives (compounds 3, 11, 13, 19, 23, 26, 32—37).

A look of the δ -lactam structure in compound **26** allowed to assume L-ornithine (**12**) as an initial substance for the generation pathway, therefore a model reaction using L-ornithine and D-glucose was carried out to proof the concept. LC-MS/MS analysis on the model reaction matrix showed the presence of **26** (**Figure 82**), thus proposing the following reaction pathway for the generation of **26** (**Figure 81**). When **12** gives the cyclized form via intramolecular dehydration, the primary amine of the cyclized intermediate reacts with carboxyl functions of 3,4-dideoxyosone (**10**) like shown above forming the pyrrole system upon dehydration.

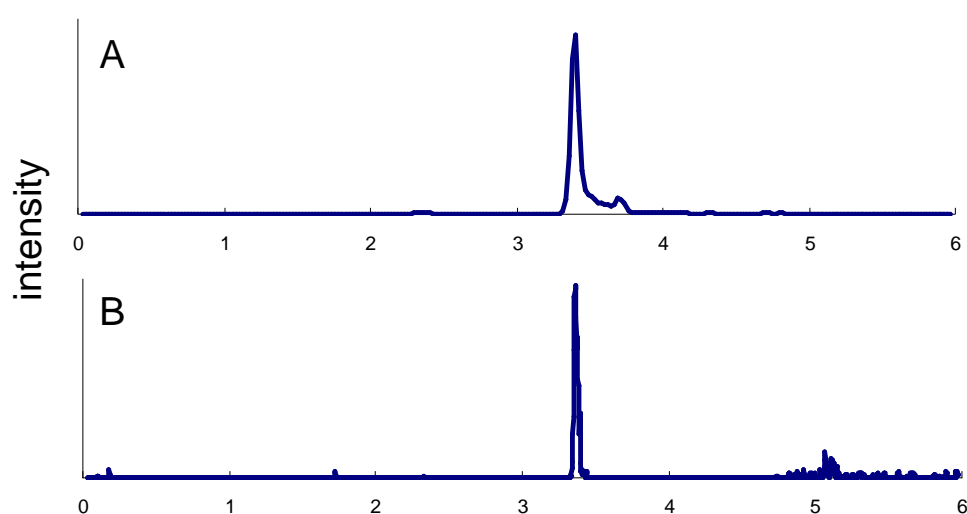


Figure 82. LC-ESI-MS/MS chromatograms of the model reaction between (A) L-ornithine and D-glucose which was performed in amorphous state at 100 °C for 2 hours and (B) compound **26** monitoring the mass transition m/z 221.0 \rightarrow 191.1.

2.4.3 Formation of a citric acid derivative, spiro-alkaloids and a pyrrole derivative (compounds **21** and **27—31**)

Taking into consideration the functional groups of a 5-hydroxymethyl-furan-2-aminomethyl as well as a tricarbonyl groups in compound **21**, it was assumed that 1-amino-1-deoxyfructose (**2**) derived from 3-deoxyhexosone (**1**) and citric acid would be reaction partners for the generation of **21**, hence a demonstration using citric acid, D-glucose and glycine was carried out. LC-MS/MS analysis of the reaction matrix revealed that **21** can be generated in the model matrix (**Figure 83**), thus leading to the formation pathway displayed in **Figure 84**.

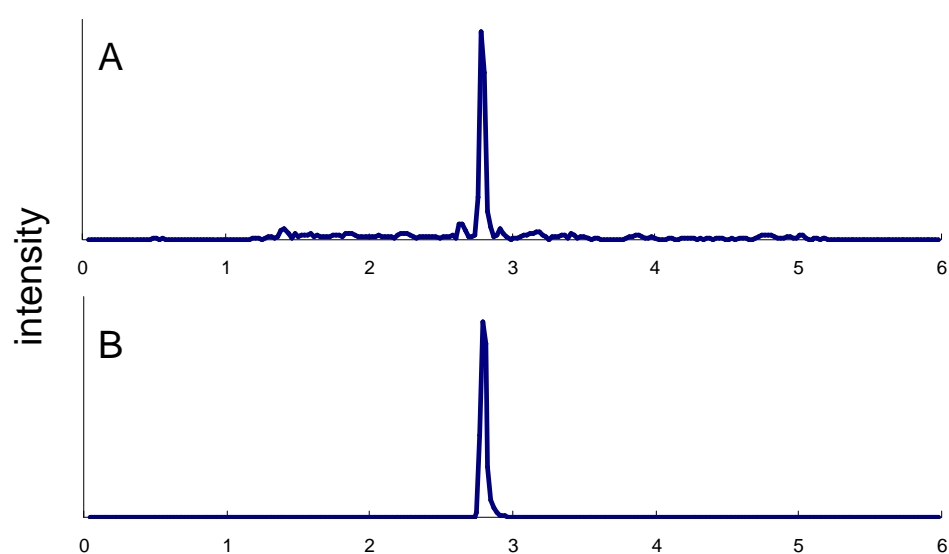


Figure 83. LC-MS/MS chromatograms of the model reaction between (A) citric acid, glycine and D-glucose which was performed in amorphous state at 100 °C for 18 hours and (B) compound **21** monitoring the mass transition of m/z 282.0 \rightarrow 220.0.

Reaction of **2** with citric acid generates via water elimination an amide-conjugate, followed by a further dehydration between the carboxylic acid group of the citric acid moiety and the amide nitrogen, yielding in the cyclized intermediate (**13**). Finally, **21** is formed from **13** upon dehydration.

While compounds **27—31** have not been earlier reported as Maillard reaction products, here, the experimental facts allowed to propose a new Maillard-type reaction cascade starting from 1-amino-1-deoxyfructose (**2**) and 3,4-dideoxyosone (**10**) based on moieties of deoxysugar, 5-hydroxymethyl-

2-aminomethylfuran, and 2-pyrrolaldehyde groups. Reaction of 2 with 10 gives rise to *N*-(1-amino-1-deoxyfructosyl)-5-hydroxymethylpyrrole-2-carbaldehyde (14). This key intermediate can be either cyclized via nucleophilic attack of the hydroxyl group of the 5-hydroxymethylpyrrole-2-carbaldehyde moiety giving the common intermediate (16) for the target furanosides (**27**, **29**) and pyranosides (**28**, **30**) (**Figure 84, flow chart: d→e, f**), or via reaction of the hydroxyl group at position 5 of 14 with the carbonyl function to afford via the intermediate 15 compound **31** (**Figure 84, flow chart: c**).

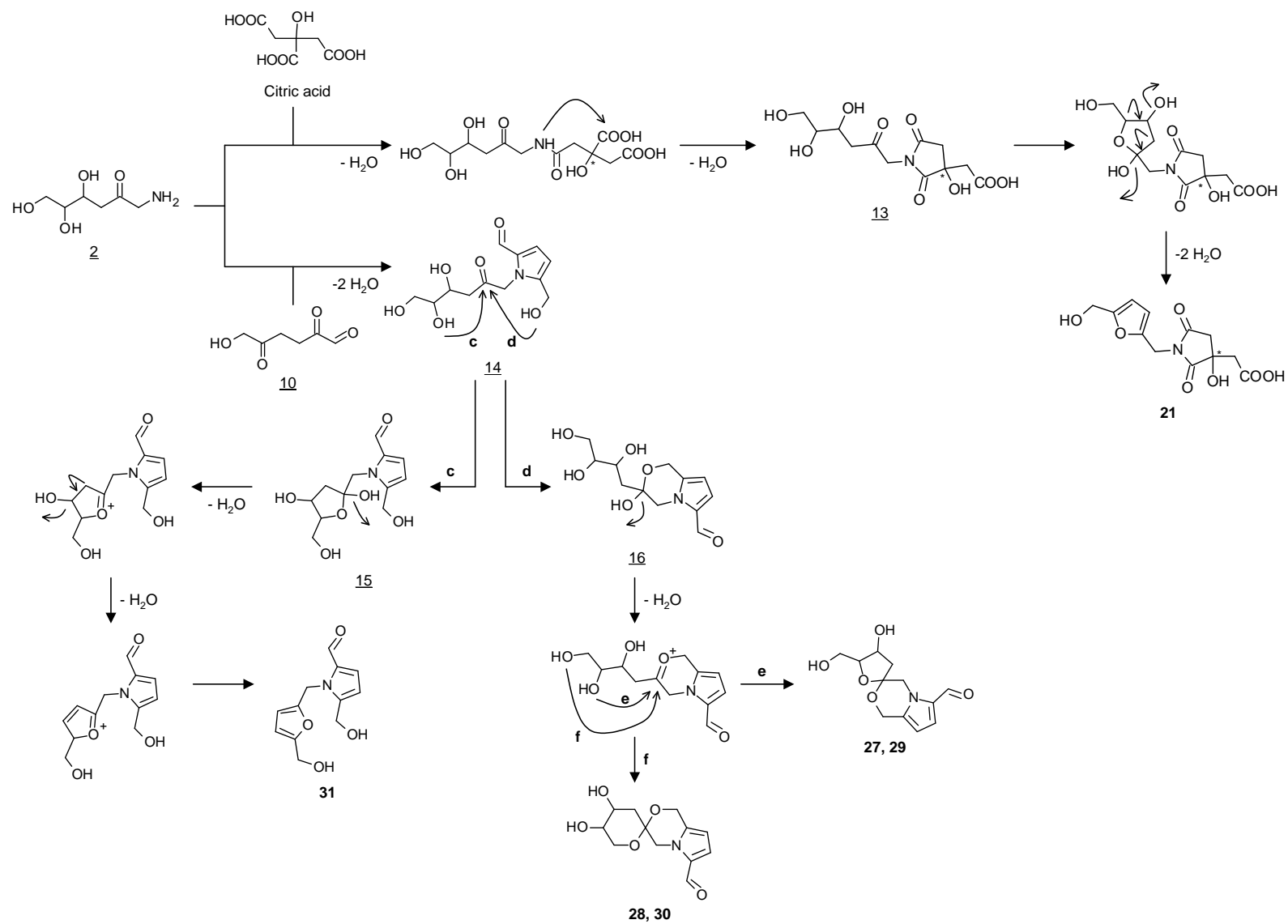


Figure 84. A proposed reaction pathway for generation of spiro-alkaloids and a pyrrole derivative (compounds **21** and **27–31**).

2.4.4 Formation of compounds **8**, **12** and **14**

Considering the existence of the lactone moiety of compound **14** and the carboxylic acid group of compound **8**, 2-keto-D-glucose (**17**) and/or 3,4-dideoxyosone (**10**) derived from 3-deoxyhexosone were assumed as reaction substrates for the generation of compounds **8**, **12** and **14**. LC-MS/MS analysis of the model reaction matrix using 2-keto-D-glucose (**17**) confirmed that compound **8** can be generated from **17** (**Figure 85**), and this allows to propose the following formation pathway (**Figure 86**). **17** gives 2-keto-3-deoxygluconic acid (**19**) via water elimination, water addition and tautomerization, and it is subsequently cyclized by means of the nucleophilic attack of the hydroxyl group to the carbonyl function at position C(2) to afford compound **8** upon dehydration.

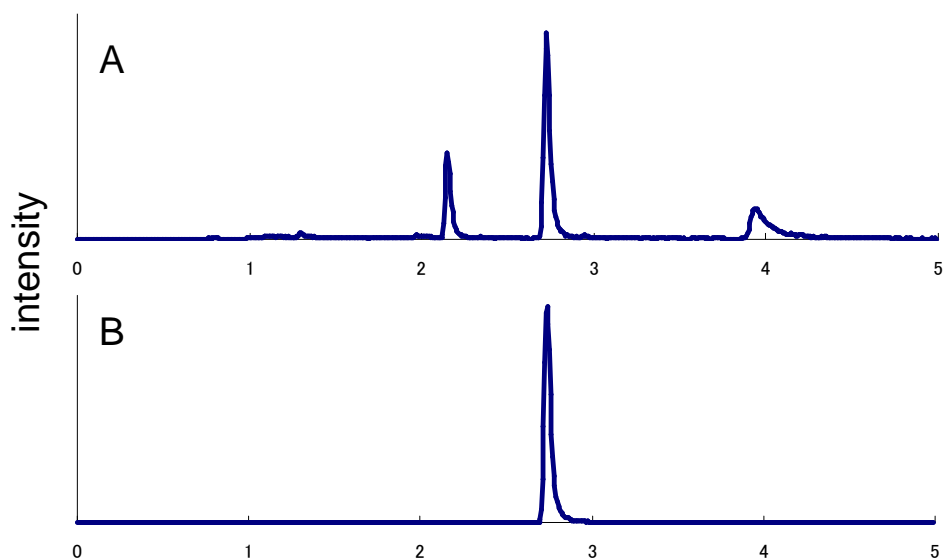


Figure 85. LC-MS/MS chromatograms of the model reaction between (A) 2-keto-D-glucose and (B) compound **8** which was performed in amorphous state at 100 °C for 1 hour monitoring the mass transition of m/z 143.1 \rightarrow 78.9.

Continuous reactions from **17** upon water addition, tautomerization and dehydration generate 4,5,6-trihydroxy-2-oxohexanoic acid (**18**) that gives 2-amino-4,5,6-trihydroxyhexanoic acid via Strecker reaction with amino acids. Intramolecular dehydration organized by the hydroxyl group at position C(4) of the amino intermediate and the carbonyl function results in cyclization of the

amino intermediate, then reaction of the cyclized intermediate with 10 leads to compound **14** upon water elimination (**Figure 86**).

Alternatively, the pathway for compound **12** is proposed starting from 17. 3,6-dihydroxy-2,5-dioxohexanal (20) is a key intermediate generated from 17 via tautomerization. Strecker reaction of the intermediate with amino acids forms 2-amino-3,6-dihydroxy-5-oxohexanal that is cyclized by nucleophilic attack by the amino group to the carbonyl function at position C(5) giving rise to compound **12** via water elimination (**Figure 86**).

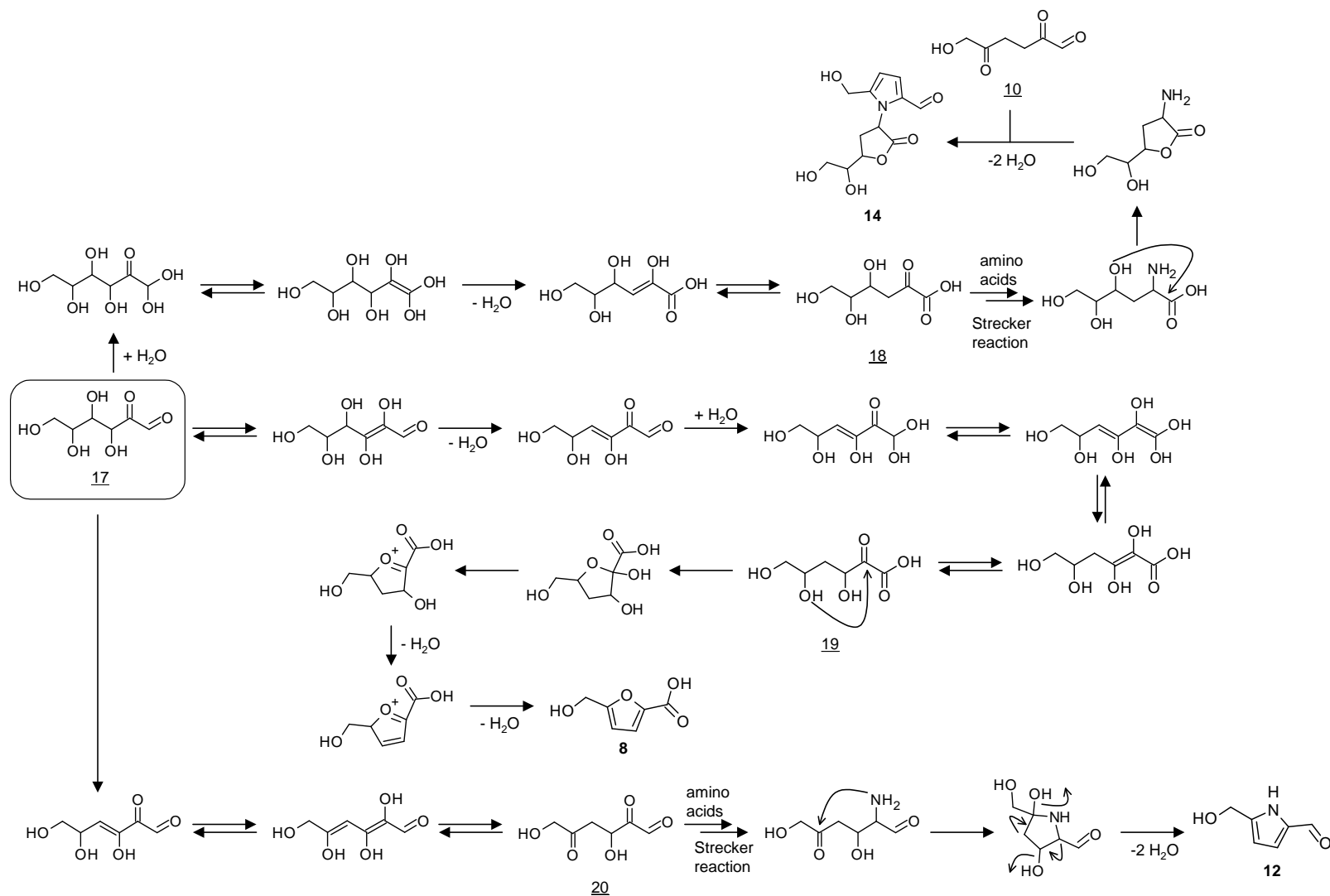


Figure 86. A proposed reaction pathway for generation of compounds 8, 12 and 14.

2.4.5 Formation of glutamic acid derivatives **15** and **20**

Focusing on pyroglutamic acid and furan moieties in the compound **15**, L-glutamic acid and 2-keto-D-glucose (**17**) are adopted as reaction substances. Therefore the proof of principle was carried out using the two mentioned compounds. LC-MS/MS analysis of the model reaction matrix showed the presence of **15** in the model system (**Figure 87**), and this enabled to propose the following generation pathway (**Figure 88**).

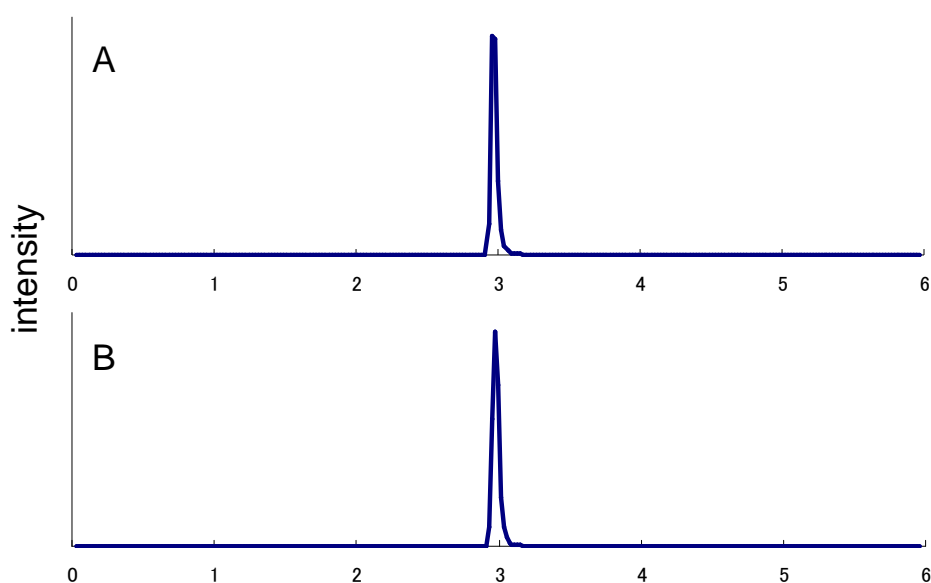


Figure 87. LC-MS/MS chromatograms of the model reaction between (A) 2-keto-D-glucose and L-glutamic acid which was performed in amorphous state at 100 °C for 1 hour and (B) compound **15** monitoring the mass transition of m/z 236.1 \rightarrow 66.7.

Reaction of L-glutamic acid with **17** upon water elimination yields a conjugate that affords via further intramolecular dehydration between the secondary amine and the carboxylic acid group a cyclic intermediate (**22**). Tautomerization, followed by water elimination on **22** results via the intermediate (**23**) in compound **15** (**Figure 88**).

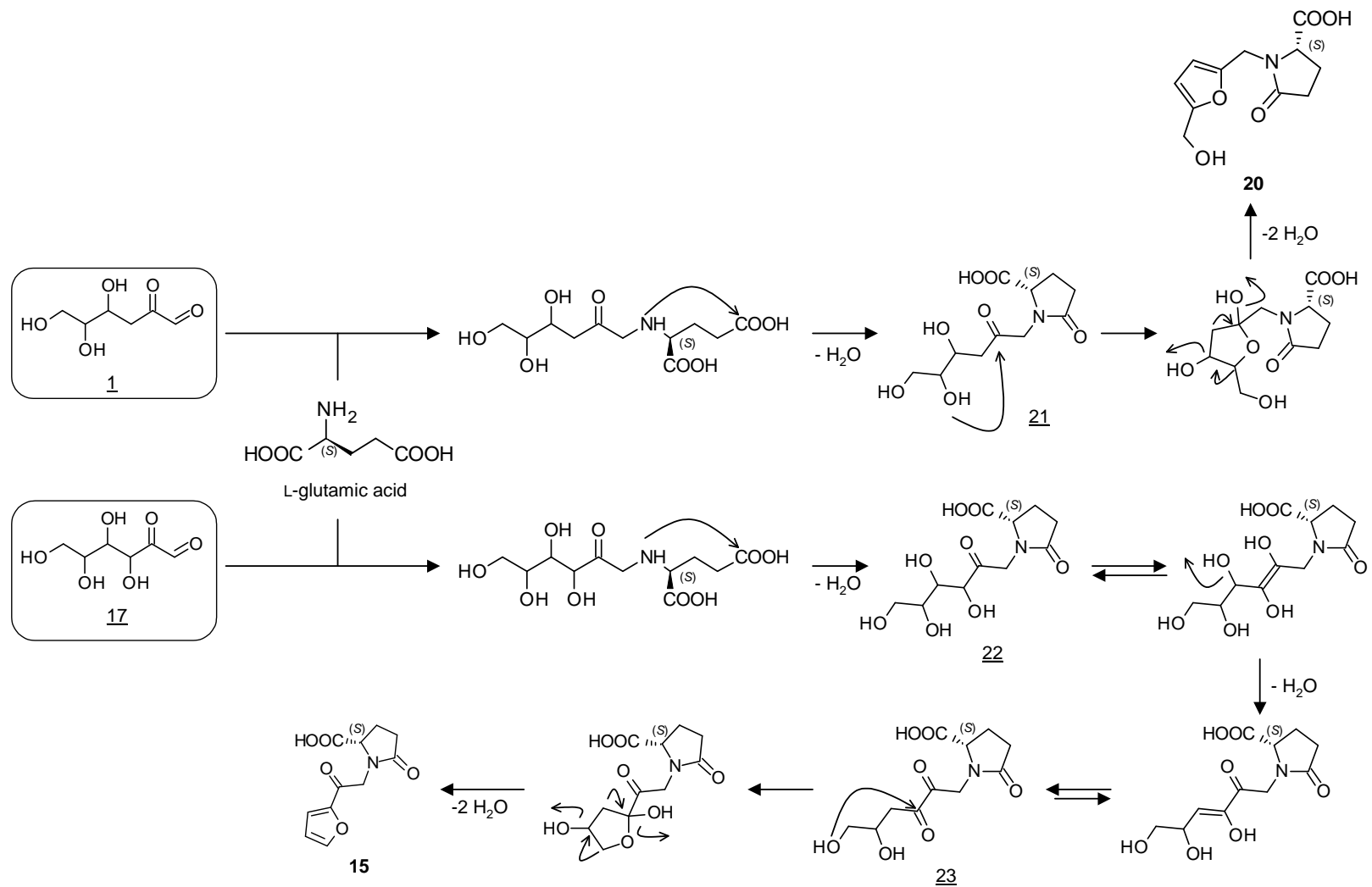


Figure 88. A proposed reaction pathway for generation of compounds **15** and **20**.

In contrast to compound **15**, generation of compound **20** is proposed starting from L-glutamic acid and 3-deoxyhexosone (**1**), because its generation was not observed in the model system using L-glutamic acid and 2-keto-D-glucose, but observed in another model using L-glutamic acid and D-glucose (**Figure 89**). This pathway is quite similar to that for **15**. Reaction of **1** with L-glutamic acid forms a pyrogulutamic acid type intermediate (**21**) via intramolecular cyclization of an amino-conjugate, then dissociation of two water molecules from (**21**) should complete hydroxymethylfuran system for compound **20**.

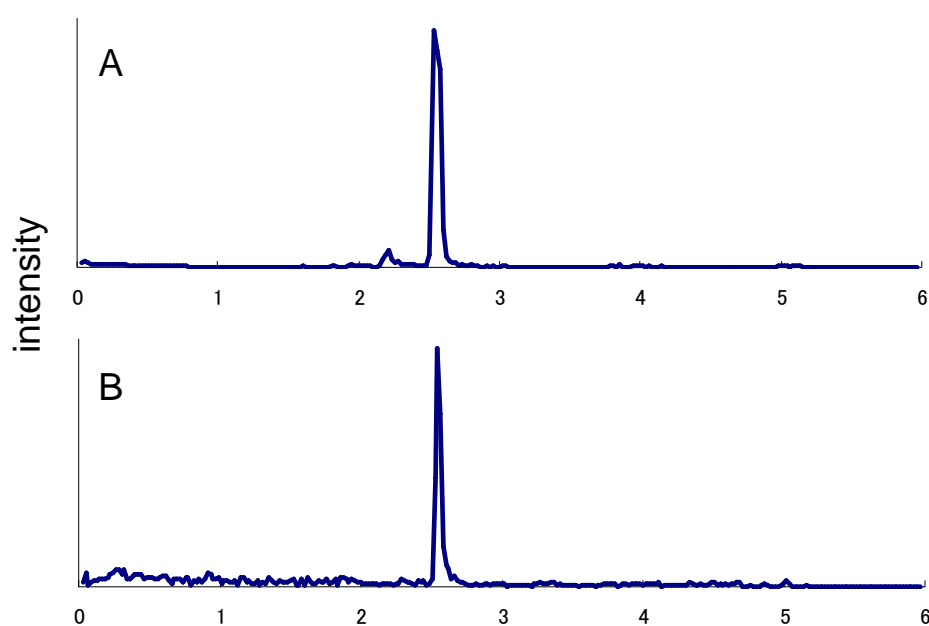


Figure 89. LC-MS/MS chromatograms of the model reaction between (A) D-glucose and L-glutamic acid which was performed in amorphous state at 100 °C for 1 hour and (B) compound **20** monitoring the mass transition of m/z 238.0 \rightarrow 164.1.

2.4.6 Formation of the pyridine derivative 24

As described before, compounds **6** and **18** were proposed to be generated from 1-deoxyhexosone (**24**) in literature (Voigt *et al.*, 2010, Jadhav *et al.*, 2011, Kim *et al.*, 1996). Focusing on the acetyl group in the compound **24**, the generation pathway is proposed starting from reaction of **24** with pyruvic acid (**26**) (Figure 90).

24 gives 6-hydroxy-2,3,5-hexanetrione (**25**) via water elimination followed by tautomerization, then aldol condensation reaction of **25** with **26**, followed by Strecker reaction with amino acids, yields an intermediate (**27**). Thereafter, intramolecular-nucleophilic attack by the amino group in **27** to the carbonyl, followed by oxidation, would give rise to the formation of the pyridine system of compound **24** (Figure 90).

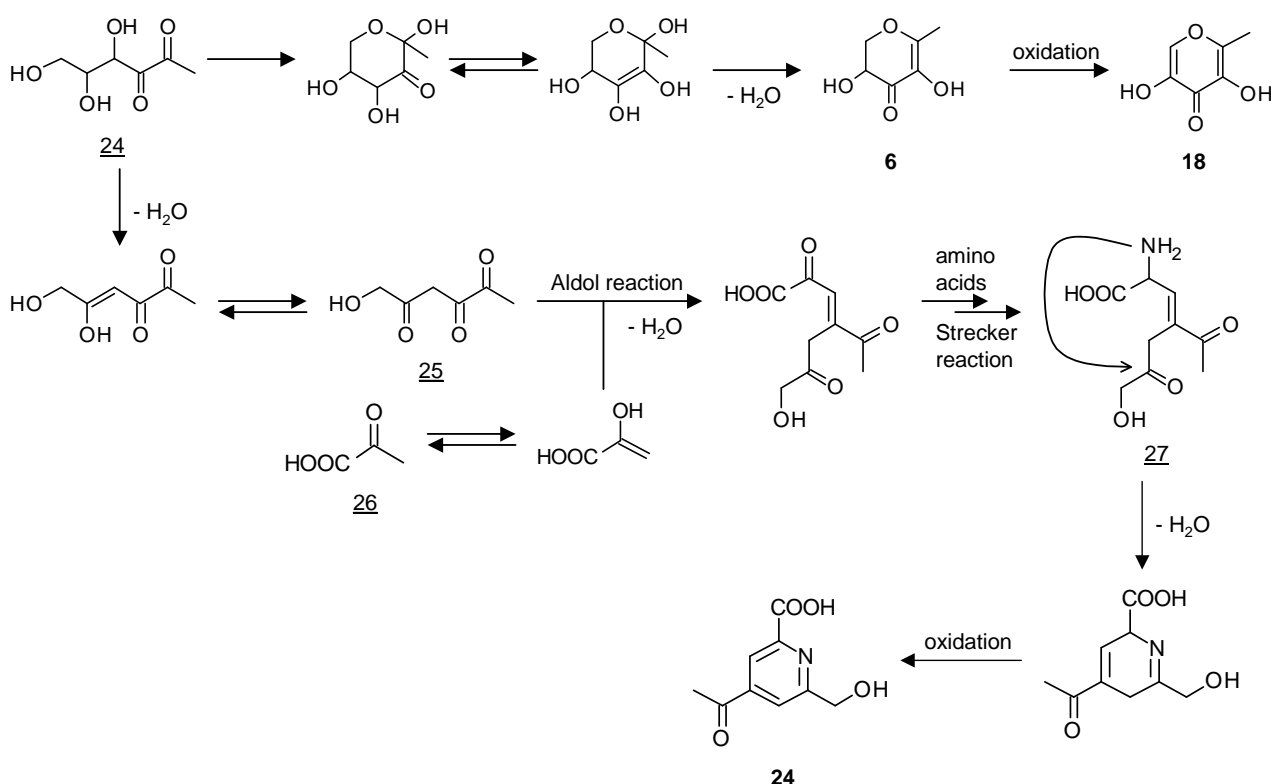


Figure 90. A proposed reaction pathway for generation of compounds **6**, **18** and **24**. The pathway for **6** and **18** is related to the literature (Kim *et al.* 1996).

2.5 Identification of known compounds in pAGE by means of LC-MS/MS

In order to identify already known antioxidants from the original AGE potentially in pAGE, LC-MS/MS parameters for 21 compounds (**Table 5, Figure 91**), were determined. Then, pAGE was analyzed for the compounds. In-depth comparison between chromatographic peaks observed in the pAGE and those of reference compounds as well as chromatography enabled to identify 15 antioxidants (compounds **38—41** and **45—53, Figure 91**) in pAGE, hence the 15 compounds were further quantified in the pAGE.

Table 5. A list of investigated compounds and results on their existences in pAGE.

compounds	occurrence
<i>N</i> α-(1-deoxy-D-fructos-1-yl)-S-allyl-L-cysteine (38)	+
<i>N</i> α-(1-deoxy-D-fructos-1-yl)-γ-glutamyl-S-allyl-L-cysteine (39)	+
<i>N</i> α-(1-deoxy-D-fructos-1-yl)-L-phenylalanine (40)	+
<i>N</i> α-(1-deoxy-D-fructos-1-yl)-L-tyrosine (41)	+
<i>N</i> α-(1-deoxy-D-fructos-1-yl)-L-tryptophan (42)	-
<i>trans</i> -1-[(1 <i>R</i> ,2 <i>R</i> ,3 <i>S</i> ,4 <i>S</i>)-1,2,3,4,5-pentahydroxypent-1-yl]-1,2,3,4-tetrahydro-β-carboline-3-carboxylic acid (43)	-
<i>cis</i> -1-[(1 <i>R</i> ,2 <i>R</i> ,3 <i>S</i> ,4 <i>S</i>)-1,2,3,4,5-pentahydroxypent-1-yl]-1,2,3,4-tetrahydro-β-carboline-3-carboxylic acid (44)	-
1-methyl-1,2,3,4-tetrahydro-β-carboline (45)	+
<i>N-trans</i> -feruloyltyramine (46)	+
<i>N-trans</i> -feruloylphenetyramine (47)	+
<i>N-trans</i> -coumaroyltyramine (48)	+
<i>N-trans</i> -coumaroylphenetyramine (49)	+
<i>N-trans</i> -cinnamoylphenetyramine (50)	+
ethyl ferulate (51)	+
ethyl <i>p</i> -coumarate (52)	+
ethyl vanilate (53)	+
ethyl <i>p</i> -hydroxybenzoate (54)	+
(-)-(2 <i>R</i> ,3 <i>S</i>)-dihydrodehydrodiconiferyl alcohol (55)	+
(+)-(2 <i>S</i> ,3 <i>R</i>)-dehydrodiconiferyl alcohol (56)	-
<i>erythro</i> -guaiacylglycerol-β-O-4'-conifery ether (57)	-
<i>threo</i> -guaiacylglycerol-β-O-4'-conifery ether (58)	-

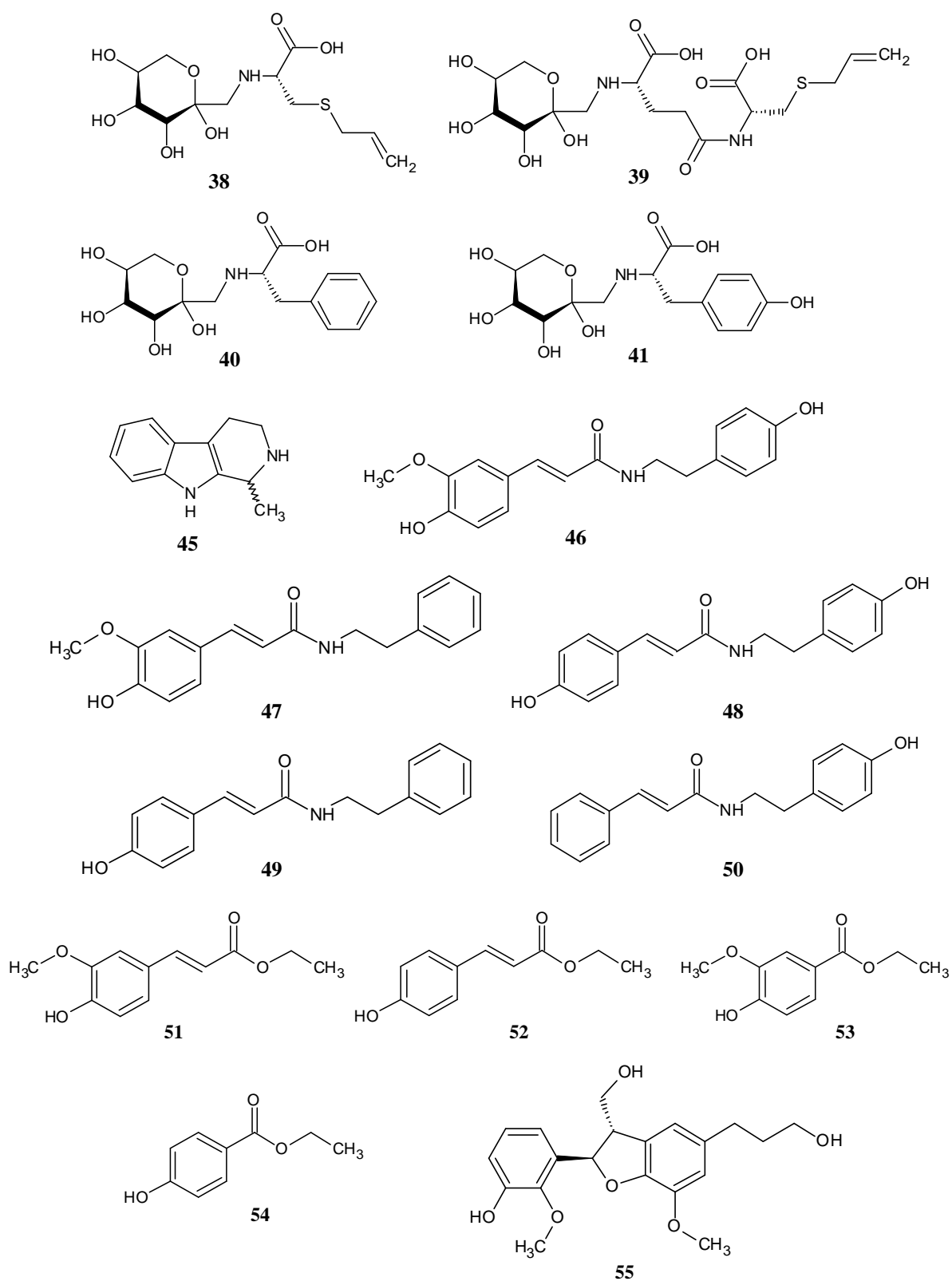


Figure 91. Chemical structures of identified compounds 38–41 and 45–55 in the pAGE.

2.6 Quantitative analysis of the identified compounds

All the identified compounds (**1—41**, **45—55**) were quantified in the pAGE and the non-processed AGE powders. In addition, compounds **27—35**, isolated and identified from the model system using D-glucose and SAC, were quantified in garlic preparations using raw garlic and garlic powder for the purpose of investigation of their existences in natural resources. In order to gain first insight into the generation profiles of compounds **1—37**, processed products, AGE powders of which pH values were adjusted to 4.0, 5.8, and 8.0 were heated at 100 °C for 0.5, 1.5, 3, 6, 9, 12, 18 and 24 hours, respectively.

2.6.1 Quantitative analysis of compounds **1—36**, **38—41** and **45—55** identified in processed and non-processed AGE powder

For compounds **1—36**, **45—55** and **55** quantitative methods were developed using MS/MS analysis in the MRM mode, and the quantitation was carried out using external standard methods. Compounds **38—41** and **51—54** were quantified using an in house developed stable isotope dilution assay (SIDA).

Using the purified compounds **1—36**, mass transitions for detection of the compounds were tuned, and optimal parameters for each compound were selected considering their own selectivity and sensitivity. Proper dilutions of the 36 compounds ranging from 4 ng/mL to 4 µg/mL were prepared and analyzed for calibration curves. Good linearity ($R^2=0.99—0.999$) of the calibration curves enabled to determine concentrations of the compounds in the processed and non-processed AGE powder (Table **6—7**).

UPLC-MS/MS analysis on dilutions of the pAGE revealed that compound **6** showed the highest concentration of 36090 µg/kg that was much higher than those of others. Next to **6**, compounds **26**, **9**, **5**, **1**, **10**, **2**, **4**, **7**, **3** and **8** exhibited relatively higher concentrations, and they were 7905, 2472, 1971, 1604, 1287, 1195, 983, 810, 702 and 654 µg/kg, respectively. As compound **6** could be generated via caramelization with sugars and Maillard type reactions with amino acids and sugars, it showed the highest value. While the concentration of L-ornithine in the AGE is still unknown, second highest concentration of compound **26** implied that L-ornithine might be a predominant constituent in

AGE or it might be produced via another pathway using L-arginine, the most abundant amino acid in AGE (**Table 4**). Concentrations of the others ranged from 0.01 to 605 $\mu\text{g}/\text{kg}$, and in particular sulfur-containing compounds **33—36** as well as the tetrahydro- β -carboline (**45**), *N*-phenylpropenoic acid amides (**46—50**), ethyl esters (**51—54**) and dilignol (**55**) showed quite lower concentrations. In the non-processed AGE powder, compound **39** showed the highest value of 1564 $\mu\text{g}/\text{kg}$, followed by **10** (1309 $\mu\text{g}/\text{kg}$), **38** (897 $\mu\text{g}/\text{kg}$), **40** (462 $\mu\text{g}/\text{kg}$), **41** (289 $\mu\text{g}/\text{kg}$) and **16** (201 $\mu\text{g}/\text{kg}$). Taking differences of the data between the processed and non-processed AGE powders into consideration, compounds **1—36** with the exception of **10** were defined to be characteristic products in the processed AGE due to increase in the concentrations by heating, and especially compound **6**, 1-deoxyhexosone derivative, and compound **26**, L-ornithine derivative, are remarkable occurrences in the processed AGE. **10** showed similar concentration in both samples, thus indicating it derives from the AGE instead of its generation by the processing. In contrast, compounds **38—41** and **45—55** were never generated upon the processing, and *N*-*trans*-feruloyltylamine (**46**), ethyl ferulate (**51**) and (-)-(2*R*,3*S*)-dihydrodehydrodiconiferyl alcohol (**55**) were found to be greatly degraded through the heat processing.

Table 6. Quantitative data for compounds **1—26** in the processed and non-processed AGE powder. All data represent mean \pm S.D by three independent preparations.

n.d.: not detected

compounds	concentration [$\mu\text{mol/kg}$ powder] in	
	processed AGE	AGE
1	1604 \pm 125	6 \pm 0.9
2	1195 \pm 12	2 \pm 0.1
3	702 \pm 33	30 \pm 4
4	983 \pm 114	23 \pm 1.5
5	1971 \pm 64	23 \pm 4
6	36090 \pm 2890	n.d.
7	810 \pm 13	15 \pm 1
8	654 \pm 38	n.d.
9	2472 \pm 110	7 \pm 0.1
10	1287 \pm 177	1309 \pm 126
11	114 \pm 8	6 \pm 1
12	31.3 \pm 3	2.1 \pm 0.1
13	20 \pm 2	2 \pm 0.1
14	233 \pm 21	5 \pm 0.1
15	506 \pm 38	n.d.
16	362 \pm 27	201 \pm 9
17	183 \pm 1	5 \pm 0.3
18	12 \pm 1	0.5 \pm 0.1
19	80 \pm 8	48 \pm 3
20	135 \pm 8	n.d.
21	261 \pm 28	n.d.
22	102 \pm 9	0.1 \pm 0.04
23	266 \pm 29	4 \pm 0.1
24	41 \pm 6	n.d.
25	529 \pm 40	1 \pm 0.1
26	7905 \pm 750	n.d.

Table 7. Quantitative data for compounds **27—55** in the processed and non-processed AGE powder. All data represent mean \pm S.D by three independent preparations.

n.d.: not detected

compounds	concentration [$\mu\text{mol/kg}$ powder] in	
	processed AGE	AGE
27	199 \pm 4	n.d.
28	29 \pm 1	n.d.
29	142 \pm 3	n.d.
30	89 \pm 1	n.d.
31	154 \pm 6	n.d.
32	17.6 \pm 1	n.d.
33	0.86 \pm 0.09	n.d.
34	0.39 \pm 0.05	n.d.
35	0.40 \pm 0.02	n.d.
36 (37)	0.19 \pm 0.02	n.d.
38	12 \pm 0.2	897 \pm 32
39	133 \pm 7	1564 \pm 23
40	125 \pm 7	462 \pm 12
41	15 \pm 1	289 \pm 9
45	0.38 \pm 0.050	0.27 \pm 0.02
46	0.01 \pm 0.001	0.09 \pm 0.01
47	0.04 \pm 0.003	0.02 \pm 0.003
48	2 \pm 0.06	2 \pm 0.14
49	0.06 \pm 0.004	0.06 \pm 0.004
50	0.19 \pm 0.01	0.14 \pm 0.01
51	0.01 \pm 0.001	2 \pm 0.14
52	0.53 \pm 0.02	0.78 \pm 0.04
53	2 \pm 0.23	3 \pm 0.26
54	4 \pm 0.45	3 \pm 0.15
55	5 \pm 0.47	24 \pm 1

2.6.2 Quantitation of compounds 27—35 in garlic preparations

To imitate a kitchen-type preparation of garlic, freshly cut garlic slices and commercial garlic powder were pan-fried at 250 °C for 8 min or 3 min, and subsequently extracted with water/acetonitrile and analyzed by means of UPLC-ESI-MS/MS. As the control, non-treated fresh garlic and garlic powder were analyzed in the same way. While the intact garlic samples were essentially free of any of the compounds, compounds **27—35** could be identified in the pan-fried garlic powder, and compounds **27—32**, but not **33—35**, were detected in the pan-fried garlic slices.

Quantitative analysis revealed rather low amounts of 6.8—91.6 and 2.1—12.5 nmol/kg for non-sulfur containing compounds **27—31** in the roasted garlic slices and the roasted garlic powder, respectively (**Table 8**). In contrast, the sulfur-containing compounds **32—35** were detected in high concentrations in roasted garlic powder, and **32** showed the highest concentration of 793.7 $\mu\text{mol/kg}$, followed by its lactone **33** (51.4 $\mu\text{mol/kg}$), and the diastereomers **34** (5.9 $\mu\text{mol/kg}$) and **35** (2.8 $\mu\text{mol/kg}$), respectively. These data suggest that a heating condition of low water content might be a critical step for the generation of the sulfur-containing compounds **32—35**.

Table 8. Quantitative data for compounds **27—35** in garlic preparations. All data represent mean \pm S.D by three independent preparations. n.d.: not detected

compounds	contents [$\mu\text{mol/kg} \pm \text{S.D}$] in			
	garlic powder		raw garlic	
	intact	roasted	intact	roasted
27	n.d.	0.013 \pm 0.0007	n.d.	0.092 \pm 0.0028
28	n.d.	0.003 \pm 0.0002	n.d.	0.009 \pm 0.0008
29	n.d.	0.008 \pm 0.0004	n.d.	0.025 \pm 0.0017
30	n.d.	0.005 \pm 0.0008	n.d.	0.007 \pm 0.0004
31	n.d.	0.002 \pm 0.0005	n.d.	0.040 \pm 0.0015
32	n.d.	793.7 \pm 22.5	n.d.	0.21 \pm 0.0400
33	n.d.	51.4 \pm 8.1	n.d.	n.d
34	n.d.	5.9 \pm 0.9	n.d.	n.d
35	n.d.	2.8 \pm 0.2	n.d.	n.d

2.6.3 Influence of processing conditions on the generation of thermally produced compounds 1—35 in pAGE

In order to investigate influence of processing conditions on the generation of thermally produced compounds 1—35, three formulations of powdered AGE (pH 4.0, 6.0 and 8.0) were individually heated at 100 °C for 24 hours, then their concentrations were monitored at several points sampled by means of UPLC-ESI-MS/MS. For an overview and a better understanding of the whole data obtained, the results are expressed as a heatmap (**Figure 92**). The major compound **6** in pAGE reached its maximum concentrations at every pH level after three hours (159.6 at pH 4.0, 67.5 at pH 6.0, and 112.1 mmol/kg at pH 8.0) and this was found to be a predominant antioxidant among the evaluated compounds. **26**, the secondary major antioxidant in pAGE, needed more heating time for its maximum concentration than **6** of which times were nine hours for pH 4.0 processing (11.2 mmol/kg), six hours for pH 6.0 processing (11.1 mmol/kg) and twelve hours for pH 8.0 processing (12.1 mmol/kg), respectively. Thymidine (**10**), pyrimidine deoxynucleoside, is known as a stable compound, and only this compound showed stable tendency in the heatmap, thus indicating antioxidants 1—36 except **10** were unequivocally thermally generated compounds. The generation of hydroxymethylfurfural (**9**) was remarkably affected by pH values. Thermal processing of AGE at pH 4.0 maximized its concentration of 16.7 mmol/kg after 24 hours, being approx. 7 fold higher than maximum values at pH 6.0 (2.5 mmol/kg) and pH 8.0 (2.3 mmol/kg), respectively. From overall interpretation, antioxidants **3, 6, 8, 9, 11—15, 18, 21—23** and **33, 4, 5, 16, 17, 24, 25, 32, 34, 35** and **36**, and **1, 2, 19, 20** and **26** were preferentially generated by thermal processing at pH 4.0, 6.0, 8.0, respectively, thus indicating that pyrazine derivatives containing shorter alkylchains (**7** and **17**), furans (**8** and **9**), 5-hydroxymaltol (**18**), cyclized glutamic acid derivatives (**15** and **20**), and spiro-alkaloids (**27—30**) need longer heating time of over 12 hours to reach their maximum concentrations.

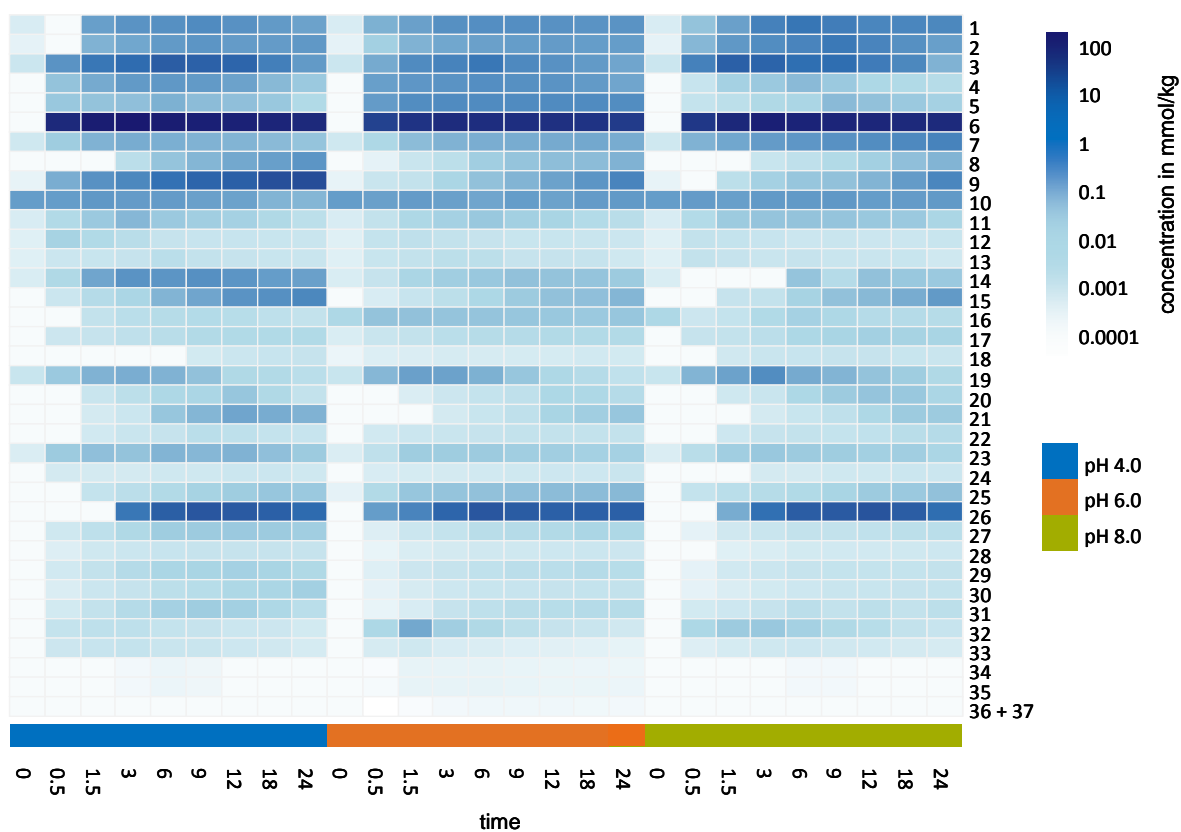


Figure 92. Heatmap diagram of quantitative analysis on compounds 1—37 in processed AGE powders (pH4.0, 6.0 and 8.0, 100 °C, 24 hours). The horizontal axis represents heating hours. The sampling was carried out seven times in 24 hours.

2.7 Antioxidant, taste, and pharmacological activities of the identified compounds

All isolated and identified compounds from the pAGE (1—37) were evaluated in their chemical antioxidant activity using ARS and ORAC assays, as well as compounds 38—41 and 45—55 (Figure 93) which were provided from the chair of food chemistry and molecular sensory science. In addition, compounds 27—35, isolated from the model system using D-glucose and SAC and obtained in higher yields, were assessed on taste and pharmacological activity. Furthermore, compound 32 with the highest yield in the model system was evaluated on taste-modulating effect using a savory tasting model broth.

2.7.1 Chemical antioxidant activity

As described before, the pAGE has been separated by means of the activity-guided fractionation with ARS and ORAC assays, and in summary 26 compounds (1—26) were isolated and identified. In order to clarify chemical antioxidant activity of the compounds, they were evaluated using both assays. Additionally, further 26 compounds (27—41 and 45—55), identified in the pAGE employing model reactions and from a compound library at chair, were also evaluated.

In the ARS assay (Table 9), *N-trans*-coumaroyltyramine (48) showed the highest activity (1.83 $\mu\text{mol TE}/\mu\text{mol}$), followed by *N-trans*-feruloyltyramine (0.96 $\mu\text{mol TE}/\mu\text{mol}$, 46), *N-trans*-cinnamoylphenetyramine (0.90 $\mu\text{mol TE}/\mu\text{mol}$, 50), ethyl ferulate (0.86 $\mu\text{mol TE}/\mu\text{mol}$, 51), 5-hydroxymaltol (0.49 $\mu\text{mol TE}/\mu\text{mol}$, 18), *N* α -(1-deoxy-D-fructos-1-yl)-L-tyrosine (0.44 $\mu\text{mol TE}/\mu\text{mol}$, 41) and ethyl *p*-coumarate (0.40 $\mu\text{mol TE}/\mu\text{mol}$, 52). These activities were relatively high compared to the others ranging from 0.01 to 0.26 $\mu\text{mol TE}/\mu\text{mol}$, however, it was concluded that they are not remarkable activities due to comparison to activities of typical antioxidants, such as ascorbic acid (1.24 $\mu\text{mol TE}/\mu\text{mol}$) and quercetin (3.85 $\mu\text{mol TE}/\mu\text{mol}$).

Table 9. ARS and ORAC activities of the compounds **1—37**.All data represent mean \pm S.D by three independent assays.

compounds	ARS assay [$\mu\text{mol}/\mu\text{mol}$]	ORAC assay [$\mu\text{mo}/\mu\text{mol}$]
1	0.01 \pm 0.001	0.01 \pm 0.001
2	0.02 \pm 0.001	0.06 \pm 0.004
3	0.13 \pm 0.019	0.10 \pm 0.002
4	0.02 \pm 0.002	0.02 \pm 0.003
5	0.01 \pm 0.001	0.02 \pm 0.002
6	0.12 \pm 0.008	0.16 \pm 0.003
7	0.01 \pm 0.001	0.01 \pm 0.001
8	0.03 \pm 0.007	0.11 \pm 0.001
9	0.01 \pm 0.002	0.01 \pm 0.001
10	0.13 \pm 0.008	0.03 \pm 0.001
11	0.01 \pm 0.002	0.05 \pm 0.007
12	0.02 \pm 0.009	0.08 \pm 0.002
13	0.00 \pm 0.000	0.05 \pm 0.003
14	0.05 \pm 0.005	0.10 \pm 0.005
15	0.04 \pm 0.002	0.09 \pm 0.002
16	0.14 \pm 0.007	0.41 \pm 0.010
17	0.01 \pm 0.001	0.11 \pm 0.006
18	0.49 \pm 0.018	3.50 \pm 0.150
19	0.06 \pm 0.003	0.13 \pm 0.010
20	0.03 \pm 0.003	0.35 \pm 0.007
21	0.02 \pm 0.001	0.33 \pm 0.004
22	0.04 \pm 0.002	0.11 \pm 0.001
23	0.01 \pm 0.001	0.05 \pm 0.001
24	0.01 \pm 0.000	0.02 \pm 0.001
25	0.01 \pm 0.001	0.03 \pm 0.010
26	0.01 \pm 0.000	0.01 \pm 0.001
27	0.03 \pm 0.007	0.10 \pm 0.004
28	0.02 \pm 0.002	0.09 \pm 0.020
29	0.05 \pm 0.001	0.13 \pm 0.001
30	0.04 \pm 0.002	0.21 \pm 0.030
31	0.08 \pm 0.002	0.40 \pm 0.007
32	0.18 \pm 0.020	0.73 \pm 0.035
33	0.03 \pm 0.004	0.49 \pm 0.012
34	0.04 \pm 0.002	0.72 \pm 0.010
35	0.05 \pm 0.003	0.52 \pm 0.060
36 (37)	0.01 \pm 0.002	0.52 \pm 0.006
ascorbic acid	1.24 \pm 0.013	0.78 \pm 0.046
quercetin	3.85 \pm 0.050	6.45 \pm 0.029

Table 9 continued.

compounds	ARS assay [$\mu\text{mol}/\mu\text{mol}$]	ORAC assay [$\mu\text{mol}/\mu\text{mol}$]
38	0.03 \pm 0.002	0.31 \pm 0.010
39	0.06 \pm 0.003	0.39 \pm 0.010
40	0.03 \pm 0.002	0.01 \pm 0.002
41	0.44 \pm 0.050	0.98 \pm 0.010
45	0.08 \pm 0.003	1.74 \pm 0.040
46	0.96 \pm 0.050	5.62 \pm 0.650
47	0.20 \pm 0.001	4.19 \pm 0.390
48	1.83 \pm 0.070	6.31 \pm 0.740
49	0.23 \pm 0.030	3.19 \pm 0.140
50	0.90 \pm 0.030	1.10 \pm 0.100
51	0.86 \pm 0.090	1.86 \pm 0.040
52	0.40 \pm 0.010	3.25 \pm 0.150
53	0.15 \pm 0.005	4.32 \pm 0.120
54	0.01 \pm 0.001	1.12 \pm 0.070
55	0.26 \pm 0.020	2.60 \pm 0.200
ascorbic acid	1.24 \pm 0.013	0.78 \pm 0.046
quercetin	3.85 \pm 0.050	6.45 \pm 0.029

The presence of a double bond or phenolic moiety in the seven compounds (**18**, **41**, **46**, **48** and **50**–**52**) would account for their higher ARS activity. In the ARS assay, analytes react with ABTS radicals, therefore, the activity can be calculated from decolorization of the radicals' blue-green color. Generally, olefins are one of possible reaction targets for radicals, and phenol moieties are also due to their proton donor property known as responsible functions for radical-scavenging and forming stable phenoxyradicals (Yehye *et al.*, 2015).

In the ORAC assay (Table 9), *N-trans*-coumaroyltyramine (**48**) showed the highest activity (6.31 $\mu\text{mol TE}/\mu\text{mol}$), followed by *N-trans*-feruloyltyramine (5.62 $\mu\text{mol TE}/\mu\text{mol}$, **46**), ethyl vanillate (4.32 $\mu\text{mol TE}/\mu\text{mol}$, **53**) *N-trans*-feruloylphenetyramine (4.19 $\mu\text{mol TE}/\mu\text{mol}$, **47**), 5-hydroxymaltol (3.50 $\mu\text{mol TE}/\mu\text{mol}$, **18**), ethyl *p*-coumarate (3.25 $\mu\text{mol TE}/\mu\text{mol}$, **52**), *N-trans*-coumaroylphenetyramine (3.19 $\mu\text{mol TE}/\mu\text{mol}$, **49**), and (-)-(2*R*,3*S*)-dihydrodehydrodiconiferyl alcohol (2.60 $\mu\text{mol TE}/\mu\text{mol}$, **55**). These activities were higher than for ascorbic acid, but not for quercetin. The other compounds (**1**–**17**, **19**–**41**,

45, **51** and **52**) show activities of 0.01—1.74 $\mu\text{mol TE}/\mu\text{mol}$ and therefore comparably low.

As ORAC activity means a chemical property of compounds donating hydrogen to reduced compounds. Phenolic functions in the compounds **46**—**49**, **52**, **53** and **55** are able to fulfill this task. Interestingly, 5-hydroxymaltol (**18**) exhibited by a factor of 22 higher ORAC activity (3.50 $\mu\text{mol TE}/\mu\text{mol}$) than structurally similar compound **6** (0.16 $\mu\text{mol TE}/\mu\text{mol}$). This would be explainable by electron delocalization effect in the whole structure of **18** after releasing the hydrogen (**Figure 93**). The effect could lead due to two olefins and one keton to a more stable anion in compound **18** than the anionic form of **6**, which should be a better hydrogen donor.

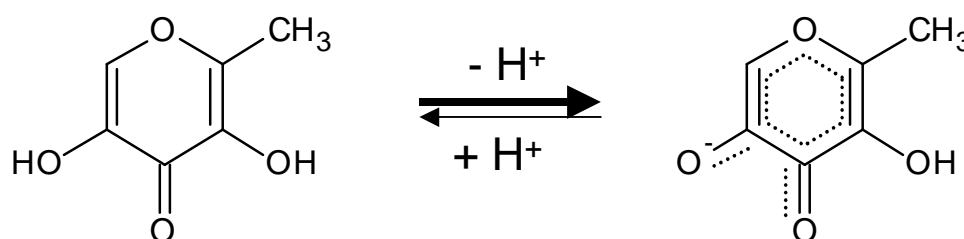


Figure 93. A proposed mechanism for higher ORAC activity of compound **18** than **6**. The dotted line represents an electron location.

2.7.2 Taste activity

Sensory analysis of the purified compounds **27**—**35** revealed an intrinsic bitter taste for all compounds with the exception of **32** and **33**, that did not show any taste activity on their own until the highest tested concentration of 1000 and 500 $\mu\text{mol}/\text{kg}$ (**Table 10**). The bitter taste threshold concentrations of the seven compounds (**27**—**31**, **34** and **35**) ranged from 0.5 (**35**) to 785 $\mu\text{mol}/\text{kg}$ (**31**). The diastereomers **27** (300 $\mu\text{mol}/\text{kg}$) and **29** (370 $\mu\text{mol}/\text{kg}$) as well as **28** (471 $\mu\text{mol}/\text{kg}$) and **30** (263 $\mu\text{mol}/\text{kg}$) exhibited similar threshold values for bitterness, however the threshold of the (*S,R*)-configured **35** was 40 fold below to the threshold found for its (*R,R*)-configured diastereomer **34**, thus indicating the absolute configuration of the ketopiperazine moiety in **34** and **35** to play an important role in their taste activity. Taking the quantitative data (**Table 8**) of the compounds in garlic preparations into consideration, the taste activity value

(concentration/threshold) calculated from compound **35** in the roasted garlic powder is 5.6, thus indicating **35** might give a contribution for bitter taste of roasted garlic powder.

Table 10. Taste properties and threshold concentrations of compounds **27—35**.

compounds	sensory properties	threshold conc [$\mu\text{mol/kg}$]
27	bitter	300
28	bitter	370
29	bitter	471
30	bitter	263
31	bitter	785
32	tasteless	> 1000
33	tasteless	> 500
34	bitter	20
35	bitter	0.5

2.7.3 Taste modulating effect

As compound **32** is the main product in the model system, it was obtained in higher yields to evaluate taste modulating effects using a savory tasting model broth. While compound **32** did not show any intrinsic taste in water, a model solution containing **32** in a concentration of 500 $\mu\text{mol/kg}$ showed a strong mouthfulness enhancing activity and increased complexity and long-lastingness of the savory sensation, thus concluding compound **32** possesses kokumi activity (Ueda *et al.*, 1990). In the model broth, a threshold concentration of 186 $\mu\text{mol/kg}$ was determined for the kokumi effect that is rather below the threshold data found for the kokumi effect of alliin (283 $\mu\text{mol/kg}$) and glutathione (326 $\mu\text{mol/kg}$) (Ueda *et al.*, 1990). In addition, the calculated activity value in roasted garlic powder is approx. 4.3, thus indicating the kokumi effect of **32** could account for taste modulation effect of roasted garlic.

2.7.4 Pharmacological activity

2.7.4.1 Modulation effect on intracellular antioxidant system

In order to investigate a modulation effect of compounds **27**—**35** on an intracellular antioxidant system, the compounds were added to human umbilical endothelial cells, then gene expression of HO-1 and GCLM encoding antioxidant enzymes in cells was evaluated. While compounds **27**—**33** did not affect gene expressions, compounds **34** and **35** prepared in 100 μM significantly accelerated both gene expressions (**Figure 94**). Interestingly, **34** showed by the fold change of 1.8 in GCLM and of 6.1 in OH-1 higher activity than that of **35**, thus indicating compound **34** could induce higher antioxidative state in cells. Besides, SAC also did not enhance the gene expressions, hence these observations enabled to conclude absolute configuration of the 2-ketopiperazine moiety in compound **34** has an important role for the activity.

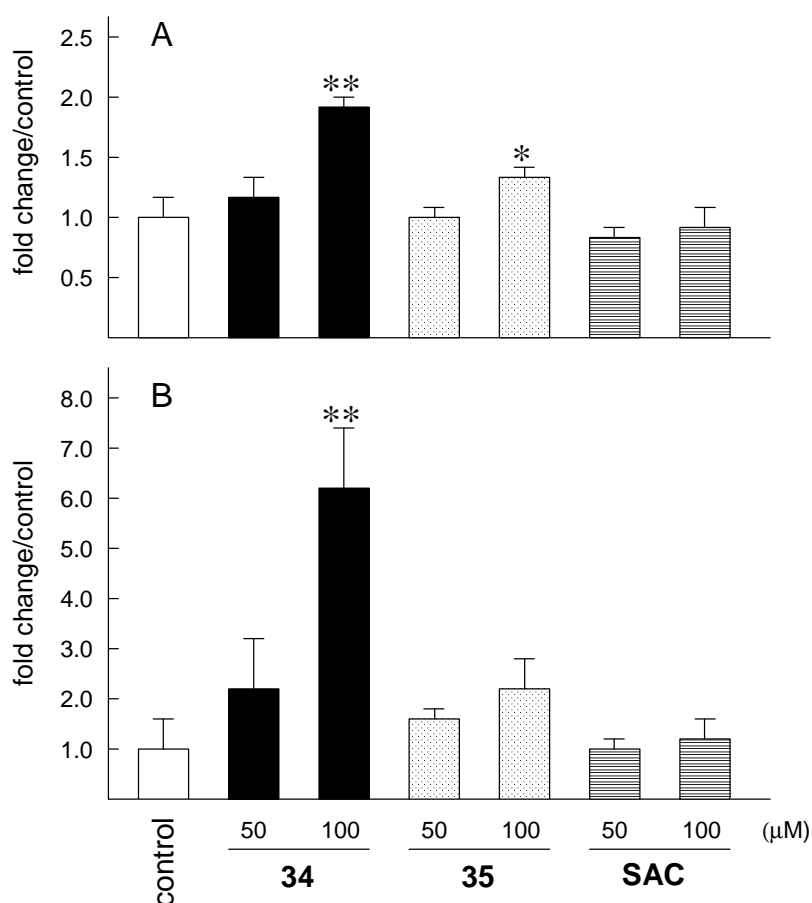


Figure 94. Gene expressions of GCLM (A) and OH-1 (B) in human umbilical endothelial cells stimulated by compounds **34** and **35**, and SAC. Data represent mean \pm S.D (n=3). * P < 0.05, ** P < 0.01 vs control (Tukey's test). Measurements were done in collaboration with Wakunaga Pharmaceutical Co. Ltd.

2.7.4.2 Modulation effect on immunoglobulin A (IgA) production in mouse lymphocytes

Lymphocytes have an important role to keep the balance of the immune system in mammals producing immunoglobulins. In order to investigate a modulation effect of compounds **27**—**35** on immunoglobulin A (IgA) production in mouse lymphocytes, the mouse lymphocytes were cultured with the compounds individually, and subsequently the culture mediums were quantified for IgA concentrations. While compounds **27**—**33**, **35** and SAC did not affect the IgA production, compound **34** significantly accelerated the IgA production of the lymphocytes by a factor of 1.5 versus the control (**Figure 95**). The data implied that **34** could up-regulate the immune system against invaders via lymphocytes. The stereochemistry of the 2-ketopiperazine moiety in compound **34** seems to have an important role for the activity.

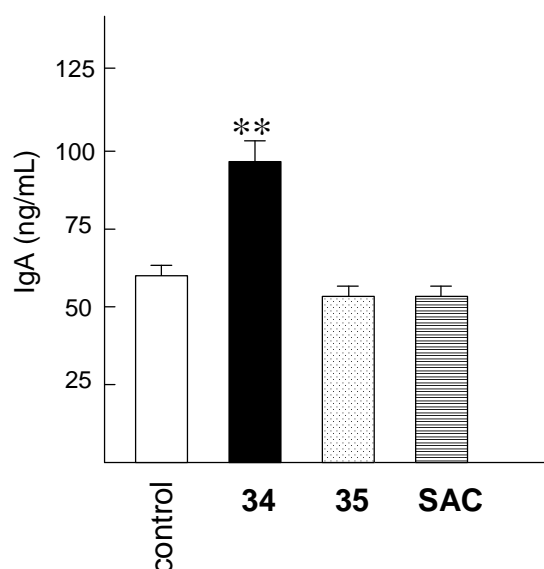


Figure 95. IgA concentrations in the culture mediums for mouse lymphocytes stimulated by compounds **34** and **35**, and SAC. Data represent mean \pm S.D (n=3). ** P < 0.05 vs control (Bonferroni's test). Measurements were done in collaboration with Wakunaga Pharmaceutical Co. Ltd.

2.7.4.3 Modulation effect on interleukin-6 (IL-6) production in mouse lymphocytes

The IL-6 is a kind of inflammatory cytokines produced by lymphocytes and it regulates immune systems in mammals to reduce inflammatory level caused by infections, diseases and injuries. In order to investigate a modulation effect of compounds **27**–**35** on IL-6 production in mouse lymphocytes, the mouse lymphocytes were cultured with the compounds individually, and subsequently the culture mediums were quantified for the IL-6 concentrations. In this study, lipopolysaccharides were used to induce an inflammatory response of the lymphocytes. While compounds **27**–**33**, **35** and SAC did not affect the IL-6 production of the lymphocytes, compounds **34** significantly suppressed the IL-6 production by a factor of 0.6 versus the control (**Figure 96A**). In addition, this effect could happen dose-dependently in the range of the concentration from 6.7 to 60 μM (**Figure 96B**). These data indicate that compound **34** exhibit anti-inflammatory effect and that the steric configuration of the 2-ketopiperazine moiety in compound **34** seems to play an important role for the activity.

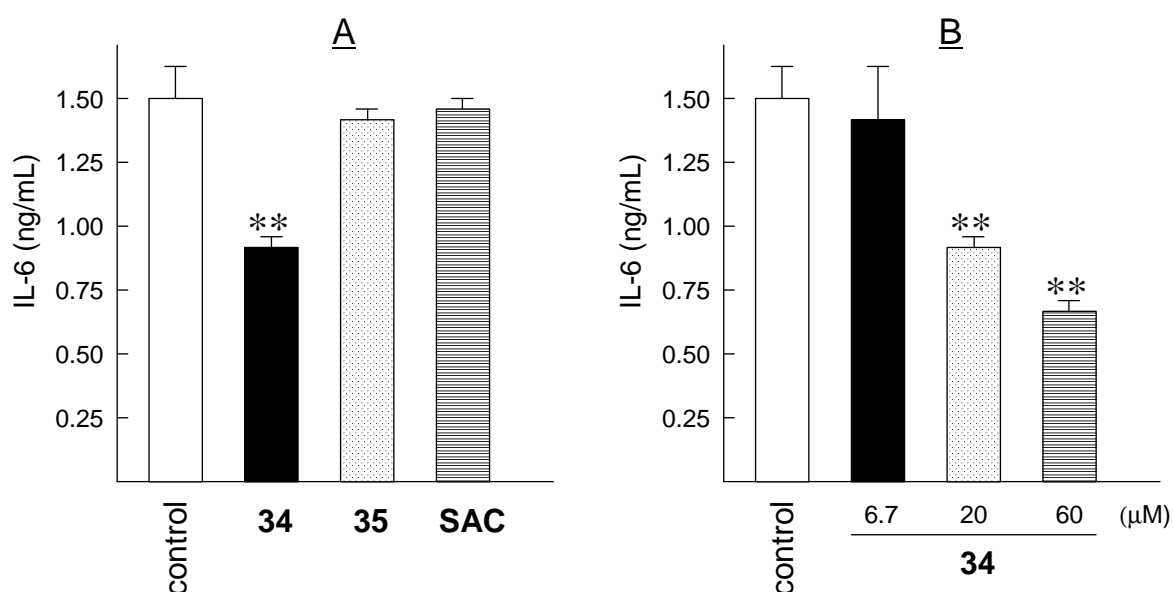
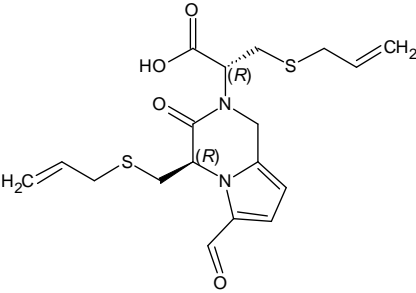
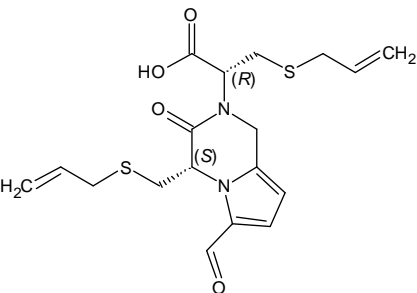


Figure 96. (A) IL-6 concentrations in the culture mediums for mouse lymphocytes stimulated by compounds **34** and **35**, and SAC (20 μM) with lipopolysaccharides. (B) Dose-dependent changes of IL-6 production in the lymphocytes stimulated by the compound **34** with lipopolysaccharides. Data represent mean \pm S.D (n=3). ** $P < 0.05$ vs control (Bonferroni's test). Measurements were done in collaboration with Wakunaga Pharmaceutical Co. Ltd.

2.7.5 Comparison of bioactivity of compounds 34 and 35

In summary, compounds **27** and **29** are diastereomers as well as **28** and **30**, and their threshold concentrations for bitterness were in the same range. Also, the four compounds did not cause any effects in the three cell-based assays. In contrast, diastereomers **34** and **35** showed unique differences in taste and pharmacological activities, and the following SAR, which is organized by differences of the absolute configuration on the 2-ketopiperazine moiety of compounds **34** and **35**, is indicated in **Table 11**. Such effects organized by the difference of stereochemistry of the ketopiperazine system have never been reported in literature so far.

Table 11. Differential display for activities on compounds **34** and **35**

	compound 34	compound 35
structure		
bitterness (threshold conc.)	less bitter (20 μ M)	more bitter (0.5 μ M)
gene expression (HO-1 and GCLM)	strong enhancement (antioxidative effect)	weak enhancement
IgA production	enhancement (immuno-modulating effect)	no effect
IL-6 production	suppression (anti-inflammation effect)	no effect

A series of experiments achieved to identify 52 antioxidants in pAGE. While the isolated compounds **1—37** showed chemically weak or moderate antioxidant activities, the cell-based assay revealed at least that compound **34** upregulates cellular antioxidant activity. The use of chemical antioxidant assays as well as biological assays is unequivocally important to elucidate antioxidants in resources without missing biologically beneficial compounds.

3. Materials and methods

3.1 Chemicals and materials

The following chemicals were obtained commercially:

2-Keto-D-glucose, Sigma-Aldrich, Germany

2,2'-Azino-bis(3-ethylbenzothiazoline-6-sulfonic acid) diammonium salt, Sigma-Aldrich, Germany

2,2'-Azobis(2-methyl-propionamidine)dihydrochloride, Sigma-Aldrich, Germany

Citric acid monohydrate, Sigma-Aldrich, Germany

5-Hydroxymethyl-2-furancarboxylic acid, Sigma-Aldrich, Germany

6-Hydroxy-2,5,7,8-tetramethylchromane-2-carboxylic acid, Sigma-Aldrich, Germany

D-(+)-glucose, Sigma-Aldrich, Germany

D-(-)-fructose, VWR, Germany

Ethyl-3,3-dihydroxy cinnamate, ABCR, Germany

Ethyl-4-hydroxy-3-methoxy cinnamate, Alfa aesar, Germany

Ethyl-4-hydroxybenzoate, Fluka, Germany

Ethyl vanillate, Alfa aesar, Germany

Fluorescein sodium salt, Sigma-Aldrich, Germany

Potassium dihydrogen phosphate, Merck, Germany)

Potassium phosphate dibasic, Sigma-Aldrich, Germany

L-Ornithine hydrochloride, Sigma-Aldrich, Germany

L-Arginine, Fluka, Germany

L-Alanine, Sigma-Aldrich, Germany

L-Glycine, Sigma-Aldrich, Germany

L-Glutamic acid, Sigma-Aldrich, Germany

S-allyl-D-cysteine, Akos GmbH, Germany

S-allyl-L-cysteine, TCI Europe, Germany

Sodium chloride, Sigma-Aldrich, Germany

Sodium hydroxide solution, Sigma-Aldrich, Germany

Thymidine, Sigma-Aldrich, Germany

Materials and methods

The following compounds were provided from the chair of food chemistry and molecular sensory science.

(-)-(2*R*,3*S*)-dihydrodehydrodiconiferyl alcohol

(+)-(2*S*,3*R*)-dehydrodiconiferyl alcohol

cis-1-[(1*R*,2*R*,3*S*,4*S*)-1,2,3,4,5-Pentahydroxypent-1-yl]-1,2,3,4-tetrahydro- β -carboline-3-carboxylic acid

erythro-Guaiacylglycerol- β -O-4'-conifery ether

1-Methyl-1,2,3,4-tetrahydro- β -carboline

N α -(1-Deoxy-D-fructos-1-yl)-*S*-allyl-L-cysteine

N α -(1-Deoxy-D-fructos-1-yl)- γ -glutamyl-*S*-allyl-L-cysteine

N α -(1-Deoxy-D-fructos-1-yl)-L-phenylalanine

N α -(1-Deoxy-D-fructos-1-yl)-L-tyrosine

N α -(1-Deoxy-D-fructos-1-yl)-L-tryptophan

N-trans-Coumaroyltyramine

N-trans-Coumaroylphenetyramine

N-trans-Cinnamoylphenetyramine

N-trans-Feruloyltyramine

N-trans-Feruloylphenetyramine

threo-Guaiacylglycerol- β -O-4'-conifery ether

trans-1-[(1*R*,2*R*,3*S*,4*S*)-1,2,3,4,5-Pentahydroxypent-1-yl]-1,2,3,4-tetrahydro- β -carboline-3-carboxylic acid

Deionized water was purified through Milli-Q Gradient A10 system (Millipore, Schwalbach, Germany). Solvents used were of HPLC-grade (Merck, Darmstadt, Germany). Deuterated solvents for NMR experiments were obtained from Euriso-Top (Saarbrücken, Germany).

The following materials were employed properly.

0.45 μ m membrane filters, Sartorius AG, Germany

3.2 *In vitro* antioxidant assays

3.2.1 ORAC (Oxygen radical absorbance capacity) assay

ORAC activity of separated fractions and identified compounds was measured as described by *Ou et al. (2001)* with some modifications. Trolox (6-hydroxy-2,5,7,8-tetramethylchroman-2-carboxylic acid) and FL (Fluorescein sodium salt) were used as a standard and a fluorescent probe, respectively. Free radicals were produced by AAPH (2,2'-azobis(2-methyl-propionamide)-dihydrochloride) to oxidize FL. Trolox (2 mM) was dissolved in ethanol, then it was diluted for standard curves using phosphate buffer (10 mM, pH 7.4) as follows; 200, 100, 50, 25 and 12.5 μM . FL solution (10 mM) was prepared in ethanol, and it was diluted into 10 nM using the phosphate buffer. The tested samples were dissolved in the phosphate buffer, and also they were appropriately diluted with the phosphate buffer. Each Trolox dilution or sample solution (25 μL) and FL solution (150 μL) were mixed in a 96-well black microplate (VWR, Germany). The microplate was incubated at 37 °C for 30 min. Thereafter, its fluorescence was measured every 90 second at the excitation of 485 nm and the emission of 520 nm using FLUOstar OPTIMA plate reader (BMG VABTECH, Offenburg, Germany). After 3 cycles, AAPH solution (25 μL , 240 mM) was added in each well quickly, and then the measurement was resumed and continued up to 90 min (60 cycles in total). This assay was performed in triplicate and the ORAC activities were calculated employing the method of *Cao et al. (1993)*. Briefly, a standard curve was obtained from the area under the fluorescence versus time curve (AUC) for Trolox dilutions minus the AUC for blank. The AUC for the sample minus the AUC for the blank was calculated and compared to the standard curve. The ORAC activities were expressed as the Trolox equivalents ($[\mu\text{mol TE}/\mu\text{mol}]$ for compounds and $[\mu\text{mol TE}]$ for separated fractions).

3.2.2 ABTS radical scavenging (ARS) assay

ARS assay was performed according to a literature protocol (*Floegel et al., 2011*) with some modifications. ABTS (2,2'-azino-bis(3-ethylbenzothiazoline-6-sulfonic acid) diammonium salt) solution (2.5 mM) was prepared in phosphate buffer saline (PBS, 10 mM, pH 7.4), and AAPH (1 mM) was added in the solution. The mixture was heated in a water bath at 68 °C for 40 min, which resulted in change of the color of the solution into blue-green due to ABTS radicals

generated. The blue-green ABTS radical solution was cooled to room temperature and filtrated through a 0.45 μm membrane filter. The filtrate was subsequently diluted using the PBS until the absorbance of the solution reached 0.325 ± 0.01 at 730 nm. Then, Trolox dilutions (1000, 500, 250, 125 and 62.5 μM) or the tested samples, 4 μL each, were mixed with the diluted ABTS radical solution (196 μL) in a 96-well clear microplate (VWR, Germany), as well as a control solution using the PBS (4 μL). Additionally, the tested sample solution of 4 μL and the PBS of 196 μL were also prepared in the microplate as blank solutions. Thereafter, the microplate was incubated at 37 $^{\circ}\text{C}$ for 10 min, and the absorbance of each well was measured at 730 nm employing FLUOstar OPTIMA in triplicate. Finally, activities were calculated as reported by *Re et al.* (1999). Briefly, the percentage inhibitions of Trolox and tested samples were given through the equations;

$$\text{Trolox inhibition \%} = \{1 - (A_{\text{Trolox}} - A_{\text{PBS}})/A_{\text{control}}\} \times 100$$

$$\text{sample inhibition \%} = \{1 - (A_{\text{sample}} - A_{\text{blank}})/A_{\text{control}}\} \times 100$$

Where A_{Trolox} , A_{PBS} , A_{control} , A_{sample} , A_{blank} are the absorbance of the Trolox, the PBS, the control, the tested sample and the blank of the samples, respectively. The inhibition values of the samples are conversed into Trolox equivalents, which is expressed as [$\mu\text{mol TE}/\mu\text{mol}$] for compounds and [$\mu\text{mol TE}$] for fractions, by a liner regression obtained from Trolox inhibition rates versus its concentrations.

3.3 Investigation of processing conditions for processed AGE powder with high antioxidative activity

Liquid AGE and all powder formulations of AGE were provided from Wakunaga pharmaceutical. Co. Ltd.

3.3.1 Preparation of powdered AGE containing four levels of water content and heat-processing

Briefly, ethanol was removed from liquid AGE (pH 5.8) using an evaporator, and it was powderized using a spray-drying machine, which resulted in powdered AGE with 3.5% (w/w) water content. Then, three batches of the powdered AGE were put in chambers, which were controlled in the following conditions; temperature: 25 $^{\circ}\text{C}$, humidity: 60%, until their water content reached 5.4, 8.0 and 10.5%, respectively. Each water content was confirmed by means of an infrared

moisture meter (FD-720, KETT ELECTRIC LABORATORY, Japan). Liquid AGE and the four batches of powdered AGE were put into glass vials with caps, and they were heated in a laboratory oven at 80 and 100 °C. Samplings were performed on day 1, 3, 5, 10, 15 and 30 at 80 °C and day 1, 2, 3, 4 and 5 at 100 °C after starting the heating. Subsequently, aliquots (100 mg) of each heated material were weighed, dissolved and filled up to 10 mL with water. Each solution was filtrated using 0.45 µm syringe filters prior to measurements of ARS activity (cf. chapter 3.2.2).

3.3.2 Preparation of powdered AGE derived from pH-controlled liquid AGE and heat-processing

Three batches of pH-controlled liquid AGE, of which pH values are 4.0, 6.0 and 8.0, were prepared from the original liquid AGE (pH 5.8) without ethanol using citric acid and sodium hydroxide, then each batch was subjected to the spray-drying machine for powderization. Thereafter, water contents of the three batches of the powderized AGE were confirmed as approx. 3.5%, respectively, by using the infrared moisture meter. The three batches of the powdered AGE were put into glass vials with caps, and they were heated in the laboratory oven at 80 and 100 °C. Samplings were performed on day 1, 3, 5, 10, 15 and 30 at 80 °C and the day 1, 2, 3, 4 and 5 at 100 °C after starting the heating. Subsequently, aliquots (100 mg) of each heated material were weighed, dissolved and filled up to 10 mL with water. Each solution was filtrated using 0.45 µm syringe filters prior to measurements of ORAC and ARS activity (cf. chapters 3.2.1 and 3.2.2).

3.3.3 Optimization of heating temperature and time for generation of high antioxidative activity in powdered AGE

The powdered AGE with conditions of pH 6.0 and 3.5% water content was put into glass vials with caps, and the vials were heated in a laboratory oven at 80 °C for 5 days and at 100 °C for 2 days. Samplings were done on day 3 for 80 °C and day 1 for 100 °C after starting the heating. Subsequently, aliquots (100 mg) of each heated material were weighed, dissolved and filled up to 10 mL with water. Each solution was filtrated using 0.45 µm syringe filters prior to measurements of ORAC and ARS activity (cf. chapters 3.2.1 and 3.2.2).

3.4 Fractionation of processed AGE (pAGE)

3.4.1 Ultrafiltration of pAGE

An aliquot (1.0 g) of pAGE powder, prepared by 100 °C heating for 24 hours, was dissolved in 250 mL water, and the solution was filtrated using a 5000 Da cutoff membrane (polyethersulfone, Sartorius stedim biotech GmbH, Germany) and a device for ultrafiltration (Vivacell 250, Sartorius stedim biotech GmbH, Germany) under ambient temperatures. The filtrate and the residue were dried by lyophilization, and yields were 0.7 g and 0.3 g, respectively. Subsequently, the dried filtrate 480 mg was dissolved in 100 mL water, and the solution was subjected to a further ultrafiltration employing a 1000 Da cutoff membrane (regenerated cellulose, EMD Millipore Corporation, USA) and a device (Stirred Ultrafiltration Cells model 8400, EMD Millipore Corporation, USA) under ambient temperatures. The filtrate and the residue were dried through lyophilization, and yields were 225 and 241 mg, respectively. Finally, the following solutions (**Table 11**) were prepared based on natural ratios of the fractions in order to measure their ARS and ORAC activities (cf. chapter 3.2.1 and 3.2.2) and evaluate contribution degrees of activities of each fraction against the whole activities of pAGE power. The activities are expressed as ratios against that of pAGE powder.

Table 11. A list of preparations for measurements of antioxidant activities using fractionated pAGE powder by means of ultrafiltration.

	concentration (mg/mL)
1000 Da >	4.46
1000—5000 Da	4.79
5000 Da <	3.96
Recombination	*
pAGE	13.21

* This mixture was prepared using 4.46 mg (1000 Da >), 4.79 mg (1000—5000 Da) and 3.96 mg (5000 Da <) and filled up to 1 mL.

3.4.2 MPLC separation of pAGE and evaluation of antioxidative activities

The low molecular weight fraction (< 1000 Da) was fractionated by means of gradient medium pressure liquid chromatography (MPLC) with the following system (c.f chapter 3.10.1). Aliquots (500 mg) of the low molecular weight fraction was dissolved in water (10 mL) and separated into seventeen fractions. Yields of each fraction are shown below (**Table 12**).

Table 12. A list of yields obtained from MPLC separation of the low molecular weight fraction.

fraction No.	yields (mg)	fraction No.	yields (mg)	fraction No.	yields (mg)
1	260.0	7	7.1	13	2.2
2	63.9	8	6.2	14	1.8
3	40.1	9	6.5	15	2.0
4	47.8	10	6.2	16	4.0
5	13.1	11	4.5	17	4.0
6	9.7	12	2.1	total	481.2

All fractions which were dried through freeze-drying were dissolved in water (10 mL), respectively, and their antioxidant activities were measured using ORAC and ABTS radical scavenging assays (c.f chapters 3.2.1 and 3.2.2). Then, this separation was repeated several times to concentrate each fraction for further separations.

3.4.3 Isolation and structure elucidation of antioxidants obtained from MPLC fraction No.4

An aliquot (100 mg) of the fraction No.4 obtained by MPLC separation was further separated by means of semipreparative HPLC using the following system (c.f chapter 3.10.3, system 1). Nineteen fractions gained were concentrated under vacuum at 40 °C, then freeze-dried. Each fraction dried was dissolved in water (500 µL) again, and their antioxidative activities were measured using ORAC and ARS assays (c.f chapters 3.2.1 and 3.2.2). Six fractions (No.4—5, 6, 7, 8, 9 and 10) which showed relatively high UV absorbance at 290 nm and antioxidative activities were concentrated through the same HPLC runs and purified by further HPLC separations (**Table 13**), thus affording compounds **1—6**. Structure elucidation of **1—6** was achieved by means of 1D/2D-NMR and UPLC-TOF MS.

Table 13. A list of chromatographic conditions for purification of fractions obtained from MPLC fraction No.4.

fraction No.	purification
4—5	chapter 3.10.3, system 2, gradient 1
4—6	chapter 3.10.3, system 2, gradient 1
4—7	chapter 3.10.3, system 3 and 4
4—8	chapter 3.10.3, system 2, gradient 2
4—9	chapter 3.10.3, system 2, gradient 2
4—10	chapter 3.10.3, system 5, gradient 1

Spectroscopic data of obtained antioxidants from MPLC fraction No.4 (1—6, numbering refers to Figure 22): The numbering of the carbon atoms refers to the adjoining structures.

1,2,3-Butanetriol,4,4'-(2,5-pyrazinediyl)bis- (1)

UV/Vis (0.1% formic acid/methanol=99/1)

λ_{\max} =276 nm;

UPLC-TOF MS (ESI⁺):

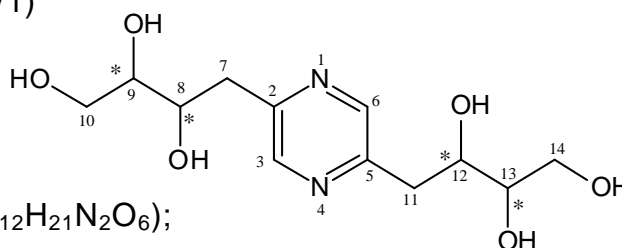
m/z 289.1412 ([M+H]⁺, measured),

m/z 289.1400 ([M+H]⁺, calculated for C₁₂H₂₁N₂O₆);

¹H NMR (400 MHz, D₂O/MeOD-*d*₄, 9:1, COSY): δ (ppm)

2.89 [dd, 1H, J =14.2, 9.4 Hz, H-C(7a, 11a)], 3.19 [dd, 1H, J =14.2, 3.1 Hz, H-C(7b, 11b)], 3.55 [td, 1H, J =6.5, 6.5, 3.8 Hz, H-C(9, 13)], 3.63 [dd, 1H, J =11.3, 6.3 Hz, H-C(10a, 14a)], 3.78 [dd, 1H, J =11.3, 3.9 Hz, H-C(10b, 14b)], 3.94 [ddd, 1H, J =9.5, 6.7, 3.0 Hz, H-C(8, 12)], 8.48 [s, 1H, H-C(3, 6)];

¹³C NMR (100 MHz, D₂O/ MeOD-*d*₄, 9:1, HSQC, HMBC): δ (ppm) 39.26 [CH₂, C(7, 11)], 64.57 [CH₂, C(10, 14)], 73.01 [CH, C(8, 12)], 76.14 [CH, C(9, 13)], 145.62 [CH, C(3, 6)], 154.14 [C, C(2, 5)].



1,2,3-Butanetriol,4,4'-(2,6-pyrazinediyl)bis- (2)

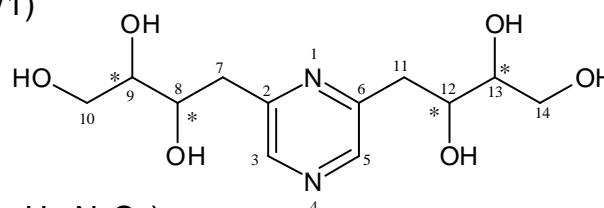
UV/Vis (0.1% formic acid/methanol=99/1)

λ_{\max} =276 nm;

UPLC-TOF MS (ESI⁺):

m/z 289.1412 ([M+H]⁺, measured),

m/z 289.1400 ([M+H]⁺, calculated for C₁₂H₂₁N₂O₆);



¹H NMR (500 MHz, D₂O/MeOD-*d*₄, 9:1, COSY): δ (ppm) 2.89 [dd, 1H, *J*=14.2, 9.4 Hz, H-C(7a, 11a)], 3.19 [dd, 1H, *J*=14.2, 3.1 Hz, H-C(7b, 11b)], 3.55 [td, 1H, *J*=6.5, 6.5, 3.8 Hz, H-C(9, 13)], 3.63 [dd, 1H, *J*=11.3, 6.3 Hz, H-C(10a, 14a)], 3.78 [dd, 1H, *J*=11.3, 3.9 Hz, H-C(10b, 14b)], 3.94 [ddd, 1H, *J*=9.5, 6.7, 3.0 Hz, H-C(8, 12)], 8.48 [s, 1H, H-C(3, 6)];

¹³C NMR (125 MHz, D₂O/MeOD-*d*₄, 9:1, HSQC, HMBC): δ (ppm) 38.74 [CH₂, C(7, 11)], 63.48 [CH₂, C(10, 14)], 72.33 [CH, C(8, 12)], 75.43 [CH, C(9, 13)], 143.58 [CH, C(3, 5)], 155.18 [C, C(2, 6)].

α-{{2-Formyl-5-hydroxymethyl}pyrrol-1-yl}arginine (3)

UV/Vis (0.1% formic acid/methanol=85/15)

λ_{max}=296 nm;

UPLC-TOF MS (ESI⁺):

m/z 283.1403 ([M+H]⁺, measured),

m/z 283.1406 ([M+H]⁺, calculated for C₁₂H₁₉N₄O₄);

¹H NMR (500 MHz, DMSO-*d*₆, COSY): δ (ppm)

1.01 [tt, 1H, *J*=11.6, 11.6, 5.7, 5.7 Hz, H-C(8a)],

1.42 [tt, 1H, *J*=11.3, 11.3, 5.5, 5.5 Hz, H-C(8b)],

1.86 [ddt, 1H, *J*=15.1, 10.9, 5.7, 5.7 Hz, H-C(7a)], 2.43 [m, 1H, H-C(7b)], 2.95

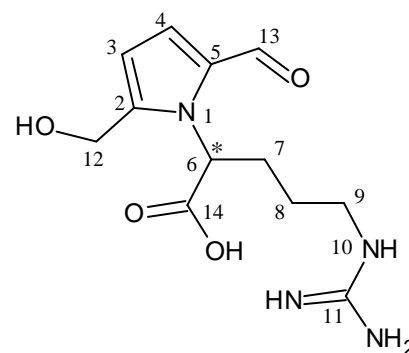
[m, 1H, H-C(9a)], 3.07 [m, 1H, H-C(9b)], 4.41 [d, 1H, *J*=13.9 Hz, H-C(12a)] 4.47

[d, 1H, *J*=13.9 Hz, H-C(12b)], 5.59 [br, 1H, H-C(6)], 6.20 [d, 1H, *J*=4.0 Hz,

H-C(4)], 6.89 [d, 1H, *J*=3.9 Hz, H-C(3)], 9.11 [br, 1H, H-N(10)], 9.44 [s, 1H,

H-C(13)];

¹³C NMR (125 MHz, DMSO-*d*₆, HSQC, HMBC): 26.24 [CH₂, C(8)], 30.35 [CH₂, C(7)], 40.27 [CH₂, C(9)], 55.71 [CH₂, C(12)], 60.30 [CH, C(6)], 109.91 [CH, C(3)], 122.78 [CH, C(4)], 132.37 [C, C(5)], 144.73 [C, C(2)], 157.08 [C, C(11)], 173.27 [C, C(14)], 179.30 [C, C(13)].



4-[7-Hydroxy-6-(hydroxymethyl)-7,8-dihydro-6*H*-pyrano[2,3-*b*]pyrazine-3-yl]-butane-1,2,3-triol (4)

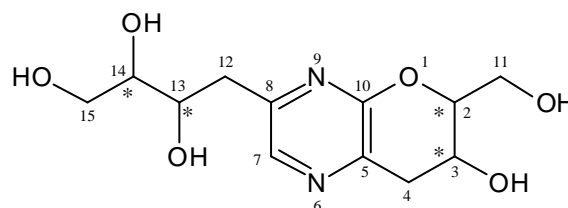
UV/Vis (0.1% formic acid/methanol

=92/8) λ_{max}=216, 304 nm;

UPLC-TOF MS (ESI⁺):

m/z 287.1252 ([M+H]⁺, measured),

m/z 287.1243 ([M+H]⁺, calculated for C₁₂H₁₉N₂O₆);



¹H NMR (400 MHz, DMSO-*d*₆, COSY): δ (ppm) 2.50 [dd, 1H, *J*=13.9, 9.5 Hz, H-C(12a)], 2.80 [dd, 1H, *J*=18.9, 6.4 Hz, H-C(4a)], 2.90 [dd, 1H, *J*=13.9, 2.9 Hz, H-C(12b)], 3.08 [dd, 1H, *J*=16.9, 4.7 Hz, H-C(4b)], 3.34 [m, 1H, H-C(14)], 3.38 [m, 1H, H-C(15a)], 3.55 [dd, 1H, *J*=10.4, 3.4 Hz, H-C(15b)], 3.66 [m, 2H, H-C(11)], 3.74 [m, 1H, H-C(13)], 4.07 [m, 1H, H-C(3)], 4.12 [m, 1H, H-C(2)], 7.99 [s, 1H, H-C(7)];

¹³C NMR (100 MHz, DMSO-*d*₆, HSQC, HMBC): δ (ppm) 34.95 [CH₂, C(4)], 38.03 [CH₂, C(12)], 60.74 [CH₂, C(11)], 61.66 [CH, C(3)], 63.25 [CH₂, C(15)], 71.23 [CH, C(13)], 74.90 [CH, C(14)], 81.45 [CH, C(2)], 135.39 [C, C(5)], 137.03 [CH, C(7)], 151.71 [C, C(8)], 155.84 [C, C(10)].

4-[6-(1,2-Dihydroxyethyl)-6,7-dihydrofuro[2,3-*b*]pyrazin-3-yl]butane-1,2,3-triol (5)

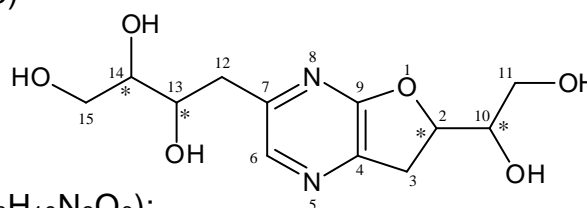
UV/Vis (0.1% formic acid/methanol=92/8)

λ_{\max} =220, 312 nm;

UPLC-TOF MS (ESI⁺):

m/z 287.1252 ([M+H]⁺, measured),

m/z 287.1243 ([M+H]⁺, calculated for C₁₂H₁₉N₂O₆);



¹H NMR (400 MHz, DMSO-*d*₆, COSY): δ (ppm) 2.55 [dd, 1H, *J*=13.9, 9.6 Hz, H-C(12a)], 2.88 [dd, 1H, *J*=13.8, 2.9 Hz, H-C(4a)], 3.22 [m, 2H, H-C(3)], 3.32 [m, 1H, H-C(14)], 3.39 [m, 1H, H-C(15a)], 3.41 [m, 2H, H-C(11)], 3.55 [dd, 1H, *J*=10.7, 3.6 Hz, H-C(15b)], 3.71 [m, 1H, H-C(13)], 3.83 [m, 1H, H-C(10)], 4.99 [ddd, 1H, *J*=10.0, 7.0, 3.5 Hz, H-C(2)], 7.80 [s, 1H, H-C(6)];

¹³C NMR (100 MHz, DMSO-*d*₆, HSQC, HMBC): δ (ppm) 28.17 [CH₂, C(3)], 38.25 [CH₂, C(12)], 62.03 [CH₂, C(11)], 63.26 [CH, C(15)], 71.23 [CH, C(13)], 71.88 [CH, C(10)], 74.90 [CH, C(14)], 81.20 [CH, C(2)], 135.64 [CH, C(6)], 143.23 [C, C(4)], 150.87 [C, C(7)], 161.86 [C, C(9)].

2,3-Dihydro-3,5-dihydroxy-6-methyl-4(*H*)-pyran-4-one (6)

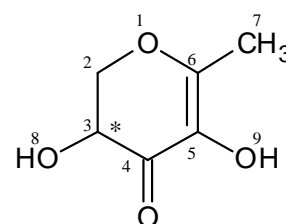
UV/Vis (0.1% formic acid/methanol=80/20)

λ_{\max} =296 nm;

UPLC-TOF MS (ESI⁺):

m/z 145.0495 ([M+H]⁺, measured),

m/z 145.0501 ([M+H]⁺, calculated for C₆H₉O₄);



¹H NMR (500 MHz, DMSO-*d*₆, COSY): δ (ppm)

1.94 [s, 3H, H-C(7)], 4.01 [m, 1H, H-C(2a)], 4.02 [m, 1H, H-C(3)], 4.24 [m, 1H, H-C(2b)], 5.78 [br, 1H, H-O(7)], 7.50 [br, 1H, H-O(9)];

¹³C NMR (125 MHz, DMSO-*d*₆, HSQC, HMBC): δ (ppm) 15.28 [CH₃, C(7)], 67.36 [CH, C(3)], 71.30 [CH₂, C(2)], 131.28 [C, C(5)], 157.67 [C, C(6)], 187.32 [C, C(4)].

3.4.4 Isolation and structure elucidation of antioxidants obtained from MPLC fraction No.5

An aliquot (100 mg) of fraction No.5 obtained by MPLC separation was further separated by means of semipreparative HPLC using the following system (c.f chapter 3.10.3, system 6). Twenty-five fractions gained were concentrated under vacuum at 40 °C, and then freeze-dried. Each fraction dried was dissolved in water (500 μL), and their antioxidative activities were measured using ORAC and ARS assays (c.f chapters 3.2.1 and 3.2.2). Five fractions (No.5—7, 9, 10, 11 and 13), which showed relatively high UV absorbance at 270 nm and moderate antioxidative activities, were concentrated through iterative HPLC runs and purified by further HPLC separations (**Table 14**). This separation step afforded compounds **6—10**. Structure elucidation of **6—10** was achieved by means of 1D/2D-NMR and UPLC-TOF MS.

Table 14. A list of chromatographic conditions for purification of fractions obtained from MPLC fraction No.5.

fraction No.	purification
5—7	chapter 3.10.3, system 5, gradient 1
5—9	chapter 3.10.3, system 8, gradient 1
5—10	chapter 3.10.3, system 9
5—11	chapter 3.10.3, system 10
5—13	chapter 3.10.3, system 10

Spectroscopic data of obtained antioxidants from MPLC fraction No.5 (7—10, numbering refers to **Figure 32, **6** is shown before.):** The numbering of the carbon atoms refers to the adjoining structures.

1,2,3-Butanetriol-4-(6-methyl-2-pyrazinyl) (7)

UV/Vis (0.1% formic acid/acetonitrile=95/5)

λ_{\max} =276 nm;

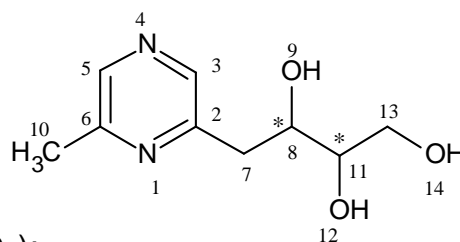
UPLC-TOF MS (ESI⁺):

m/z 199.1091 ([M+H]⁺, measured),

m/z 199.1083 ([M+H]⁺, calculated for C₉H₁₅N₂O₃);

¹H NMR (400 MHz, DMSO-*d*₆, COSY): δ (ppm) 2.45 [s, 3H, H-C(10)], 2.69 [dd, 1H, J =13.8, 9.7 Hz, H-C(7a)], 3.04 [dd, 1H, J =13.8, 2.9 Hz, H-C(7b)], 3.35 [m, 1H, H-C(11)], 3.39 [m, 1H, H-C(13a)], 3.57 [m, 1H, H-C(13b)], 3.75 [ddt, 1H, J =9.5, 6.4, 2.9 Hz, H-C(8)] 4.42 [t, 1H, J =5.5, 5.5 Hz, H-O(14)], 4.60 [d, 1H, J =6.4 Hz, H-O(9)], 4.68 [d, 1H, J =5.0 Hz, H-O(12)], 8.30 [s, 1H, H-C(3)], 8.32 [s, 1H, H-C(5)];

¹³C NMR (100 MHz, DMSO-*d*₆, HSQC, HMBC): δ (ppm) 21.05 [CH₃, C(10)], 38.71 [CH₂, C(7)], 63.22 [CH₂, C(13)], 71.32 [CH, C(8)], 74.99 [CH, C(11)], 141.38 [CH, C(5)], 142.32 [CH, C(3)], 152.34 [C, C(6)], 154.86 [C, C(2)].



5-Hydroxymethyl-2-furancarboxylic acid (8)

UV/Vis (0.1% formic acid/acetonitrile=95/5)

λ_{\max} =256 nm;

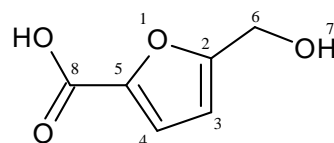
UPLC-TOF MS (ESI⁻):

m/z 141.0192 ([M-H]⁻, measured),

m/z 141.0188 ([M-H]⁻, calculated for C₆H₅O₄);

¹H NMR (500 MHz, DMSO-*d*₆, COSY): δ (ppm) 4.44 [s, 2H, H-C(6)], 5.42 [br, 1H, H-O(7)], 6.45 [d, 1H, J =3.3 Hz, H-C(3)], 7.13 [s, 1H, J =3.5 Hz, H-C(4)];

¹³C NMR (125 MHz, DMSO-*d*₆, HSQC, HMBC): δ (ppm) 55.79 [CH₂, C(6)], 108.90 [CH, C(3)], 118.41 [CH, C(4)], 144.00 [C, C(5)], 159.34 [C, C(8)], 159.61 [C, C(2)].



5-Hydroxymethyl-2-furaldehyde (9)

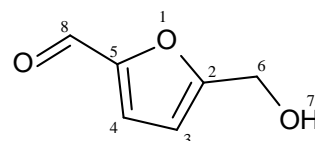
UV/Vis (0.1% formic acid/methanol=80/20)

λ_{\max} =284 nm;

UPLC-TOF MS (ESI⁺):

m/z 127.0396 ([M+H]⁺, measured),

m/z 127.0395 ([M+H]⁺, calculated for C₆H₇O₃);



¹H NMR (400 MHz, DMSO-*d*₆, COSY): δ (ppm) 4.50 [s, 2H, H-C(6)], 5.56 [br, 1H, H-O(7)], 6.60 [d, 1H, *J*=3.5 Hz, H-C(3)], 7.49 [s, 1H, *J*=3.5 Hz, H-C(4)], 9.54 [s, 1H, H-C(8)];

¹³C NMR (100 MHz, DMSO-*d*₆, HSQC, HMBC): δ (ppm) 55.94 [CH₂, C(6)], 109.71 [CH, C(3)], 124.48 [CH, C(4)], 151.75 [C, C(5)], 162.20 [C, C(2)], 178.00 [C, C(8)].

Thymidine (10)

UV/Vis (0.1% formic acid/methanol=50/50)

λ_{\max} =268 nm;

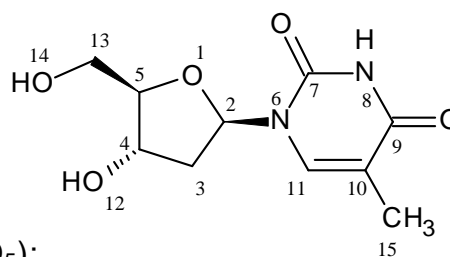
UPLC-TOF MS (ESI⁻):

m/z 241.0833 ([M-H]⁻, measured),

m/z 241.0824 ([M-H]⁻, calculated for C₁₀H₁₃N₂O₅);

¹H NMR (400 MHz, DMSO-*d*₆, COSY): δ (ppm) 1.77 [d, 3H, *J*=1.2 Hz, H-C(15)], 2.09 [m, 2H, H-C(3)], 3.54 [dd, 1H, *J*=11.8, 3.9 Hz, H-C(13a)], 3.59 [dd, 1H, *J*=11.8, 3.7 Hz, H-C(13b)], 3.75 [q, 1H, *J*=3.6, 3.6, 3.5 Hz, H-C(5)], 4.23 [dt, 1H, *J*=5.8, 3.1, 3.1 Hz, H-C(4)], 5.02 [s, 1H, H-O(14)], 5.23 [s, 1H, H-O(12)], 6.16 [dd, 1H, *J*=7.5, 6.2 Hz, H-C(2)], 7.69 [d, 1H, *J*=1.2 Hz, H-C(11)], 11.27 [br, 1H, H-N(8)];

¹³C NMR (100 MHz, DMSO-*d*₆, HSQC, HMBC): δ (ppm) 12.29 [CH₃, C(15)], 39.43 [CH₂, C(3)], 61.37 [CH₂, C(13)], 70.46 [CH, C(4)], 83.76 [CH, C(2)], 87.27 [CH, C(5)], 109.40 [C, C(10)], 136.15 [CH, C(11)], 150.50 [C, C(7)], 163.78 [C, C(9)].



3.4.5 Isolation and structure elucidation of antioxidants obtained from MPLC fraction No.6

An aliquot (88 mg) of fraction No.6 obtained by MPLC separation was further separated by means of semipreparative HPLC using the following system (c.f chapter 3.10.3, system 7, gradient 1). Thirty-four fractions gained were concentrated under vacuum at 40 °C, and then freeze-dried. Each fraction dried was dissolved in water (500 μL), and their antioxidative activities were measured using ORAC and ARS assays (c.f chapters 3.2.1 and 3.2.2). Six fractions (No.6—7, 11, 13, 14, 15 and 26) were concentrated by repeated HPLC runs and purified by further HPLC steps for structure determination (**Table 15**) affording compounds **6**, **9**, **11—15**. Structure elucidation for the compounds was

achieved by means of 1D/2D-NMR and UPLC-TOF MS. The absolute configuration of **15** was determined using CD spectroscopy.

Table 15. A list of chromatographic conditions for purification of subfractions obtained from MPLC fraction No.6.

fraction No.	purification
6—7	chapter 3.10.3, system 5
6—11	chapter 3.10.3, system 10
6—13	chapter 3.10.3, system 8, gradient 2
6—14	chapter 3.10.3, system 8, gradient 3
6—15	chapter 3.10.3, system 11, gradient 1
6—26	chapter 3.10.3, system 12

Spectroscopic data of obtained antioxidants from MPLC fraction No.6 (11—15, numbering refers to Figure 38, compounds 6 and 9 are shown before.):
The numbering of the carbon atoms refers to the adjoining structures.

α -{(2-Formyl-5-hydroxymethyl)pyrrol-1-yl}aspartic acid (**11**)

UV/Vis (0.1% formic acid/methanol=90/10)

λ_{\max} =296 nm;

UPLC-TOF MS (ESI⁻):

m/z 240.0972 ([M-H]⁻, measured),

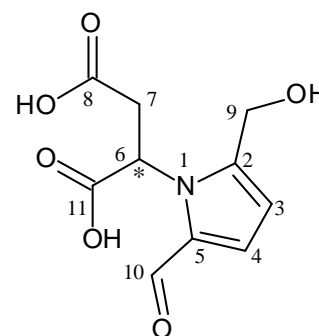
m/z 240.0978 ([M-H]⁻, calculated for C₁₀H₁₀NO₆);

¹H NMR (400 MHz, D₂O/MeOD-*d*₄, 9/1, COSY):

δ (ppm) 2.81 [dd, J =16.9, 7.7 Hz, 1H, H-C(7a)],

3.30 [m, 1H, H-C(7b)], 4.55 [s, 2H, H-C(9)], 5.48 [m, 1H, H-C(6)], 6.20 [d, 1H, J =3.9 Hz, H-C(3)], 7.05 [d, J =4.0 Hz, 1H, H-C(4)], 9.33 [s, 1H, H-C(10)];

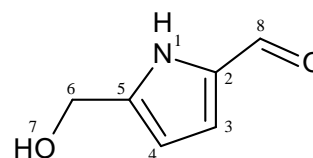
¹³C NMR (100 MHz, DMSO-*d*₆, HSQC, HMBC): δ (ppm) 37.13 [CH₂, C(7)], 54.83 [CH, C(6)], 55.26 [CH₂, C(9)], 109.21 [CH, C(3)], 125.88 [CH, C(4)], 131.64 [C, C(5)], 144.58 [C, C(2)], 170.17 [C, C(8)], 172.02 [C, C(11)], 178.41 [CH, C(10)].

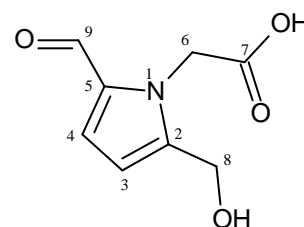


5-Hydroxymethyl-1*H*-pyrrole-2-carbaldehyde (**12**)

UV/Vis (0.1% formic acid/methanol=90/10)

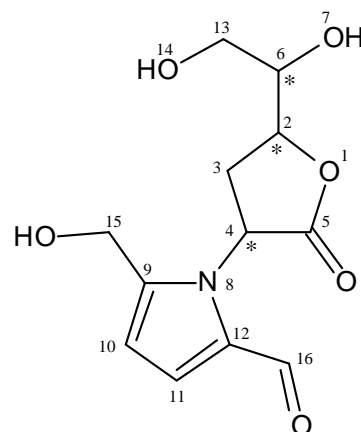
λ_{\max} =296 nm;



UPLC-TOF MS (ESI⁺):*m/z* 126.0554 ([M+H]⁺, measured),*m/z* 126.0555 ([M+H]⁺, calculated for C₆H₇NO₂);**¹H NMR** (500 MHz, DMSO-*d*₆, COSY): δ (ppm) 4.43 [s, 2H, H-C(6)], 5.13 [br, 1H, H-O(7)], 6.16 [m, 1H, H-C(4)], 6.89 [m, 1H, H-C(3)], 9.38 [s, 1H, H-C(8)], 11.87 [br, 1H, H-N(1)];**¹³C NMR** (125 MHz, DMSO-*d*₆, HSQC, HMBC): δ (ppm) 56.13 [CH₂, C(6)], 108.81 [CH, C(4)], 120.95 [CH, C(3)], 132.12 [C, C(2)], 142.48 [C, C(5)], 178.64 [CH, C(8)].**α-(2-Formyl-5-hydroxymethyl)pyrrol-1-ylglycine (13)****UV/Vis** (0.1% formic acid/methanol=80/20) λ_{\max} =296 nm;**UPLC-TOF MS (ESI⁻):***m/z* 182.0452 ([M-H]⁻, measured),*m/z* 182.0453 ([M-H]⁻, calculated for C₈H₈NO₄);**¹H NMR** (500 MHz, DMSO-*d*₆, COSY): δ (ppm)4.45 [s, 2H, H-C(8)], 5.06 [s, 2H, H-C(6)], 6.21 [d, 1H, *J*=4.0 Hz, H-C(3)],6.98 [d, 1H, *J*=4.0 Hz, H-C(4)], 9.43 [s, 1H, H-C(9)];**¹³C NMR** (125 MHz, DMSO-*d*₆, HSQC, HMBC): δ (ppm) 46.80 [CH₂, C(6)], 54.81 [CH₂, C(8)], 109.38 [CH, C(3)], 123.70 [CH, C(4)], 132.07 [C, C(5)], 143.49 [C, C(2)], 169.69 [C, C(7)], 179.62 [CH, C(9)].**1-{5-(1,2-Dihydroxyethyl)-2-oxotetrahydrofuran-3-yl}-5-(hydroxymethyl)-1H-pyrrole-2-carbaldehyde (14)****UV/Vis** (0.1% formic acid/methanol=90/10) λ_{\max} =260, 296 nm;**UPLC-TOF MS (ESI⁺):***m/z* 270.0980 ([M+H]⁺, measured),*m/z* 270.0978 ([M+H]⁺, calculated for C₁₂H₁₆NO₆);**¹H NMR** (500 MHz, DMSO-*d*₆, COSY): δ (ppm)

2.27 [m, 1H, H-C(3a)], 2.67 [m, 1H, H-C(3b)],

3.38 [m, 2H, H-C(13)], 3.78 [m, 1H, H-C(6)],



4.51 [s, 2H, H-C(15)], 4.79 [m, 1H, H-C(2)], 5.00 [m, 1H, H-O(7)], 5.49 [t, 1H, $J=10.2$, 10.2 Hz, H-C(4)], 6.27 [d, 1H, $J=3.9$ Hz, H-C(10)], 7.12 [d, 1H, $J=3.9$ Hz, H-C(11)], 9.36 [s, 1H, H-C(16)];

^{13}C NMR (125 MHz, DMSO- d_6 , HSQC, HMBC): δ (ppm) 27.92 [CH₂, C(3)], 54.36 [CH, C(4)], 54.95 [CH₂, C(15)], 61.84 [CH₂, C(13)], 72.01 [CH, C(6)], 78.10 [CH, C(2)], 109.92 [CH, C(10)], 125.77 [CH, C(11)], 131.02 [C, C(12)], 144.42 [C, C(9)], 172.86 [C, C(5)], 179.03 [CH, C(16)].

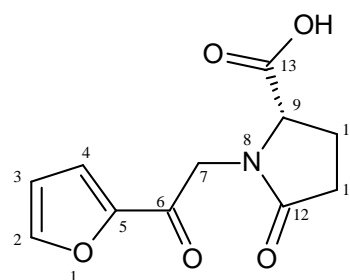
(2S)-1-[2-(Furan-2-yl)-2-oxoethyl]-5-oxopyrrolidine-2-carboxylic acid (**15**)

UV/Vis (0.1% formic acid/methanol=90/10)

$\lambda_{\text{max}}=212, 296$ nm;

CD (50% methanol, 0.844 mmol/L):

$\lambda_{\text{max}} (\Delta\epsilon)=310 (+3.5), 274 (-12.0), 241 (-0.1),$
 $236 (-0.8), 206 (+29.5)$



UPLC-TOF MS (ESI⁻):

m/z 236.0561 ([M-H]⁻, measured),

m/z 236.0559 ([M-H]⁻, calculated for C₁₁H₁₀NO₅);

^1H NMR (400 MHz, DMSO- d_6 , COSY): δ (ppm)

2.03 [m, 1H, H-C(10a)], 2.32 [m, 2H, H-C(11)],

2.39 [m, 1H, H-C(10a)], 4.22 [dd, 1H, $J=8.7, 4.6$ Hz, H-C(9)], 4.29 [d, 1H, $J=18.0$ Hz, H-C(7a)], 4.86 [d, 1H, $J=18.0$ Hz, H-C(7b)], 6.73 [dd, 1H, $J=3.6, 1.6$ Hz, H-C(3)], 7.56 [dd, 1H, $J=3.6, 0.7$ Hz, H-C(4)], 8.02 [dd, 1H, $J=1.6, 0.7$ Hz, H-C(2)];

^{13}C NMR (100 MHz, DMSO- d_6 , HSQC, HMBC): δ (ppm) 22.67 [CH₂, C(10)], 28.71 [CH₂, C(11)], 47.38 [CH₂, C(7)], 59.55 [CH, C(9)], 112.60 [CH, C(3)], 118.98 [CH, C(4)], 148.10 [CH, C(2)], 150.26 [C, C(5)], 173.31 [C, C(13)], 174.98 [C, C(12)], 182.83 [C, C(6)].

4.4.6 Isolation and structure elucidation of antioxidants obtained from MPLC fraction No.7

An aliquot (90 mg) of fraction No.7 obtained by MPLC separation was further separated by means of semipreparative HPLC using the following system (c.f chapter 3.10.3, system 7, gradient 2). Thirty-six fractions gained were concentrated under vacuum at 40 °C, followed by freeze-dried. Each fraction dried was dissolved in water (550 μL), and their antioxidative activities were

measured using ORAC and ARS assays (c.f chapter 3.2.1 and 3.2.2). Among the fractions, seven fractions (No.7—5, 8, 12, 13, 16, 17 and 23) were further concentrated and purified by repeated HPLC steps for structure determination (**Table 16**), thus yielding compounds **6**, **9**, **14—26**. Their structure elucidation were achieved by means of 1D/2D-NMR and UPLC-TOF MS. The absolute configuration of **20** was determined using CD spectroscopy.

Table 16. A list of chromatographic conditions for purification of subfractions obtained from MPLC fraction No.7.

fraction No.	purification
7—5	chapter 3.10.3, system 5
7—8	chapter 3.10.3, system 10
7—12	chapter 3.10.3, system 8, gradient 4
7—13	chapter 3.10.3, system 11, gradient 2
7—16	chapter 3.10.3, system 13
7—17	chapter 3.10.3, system 8, gradient 5
7—23	chapter 3.10.3, system 12

Spectroscopic data of obtained antioxidants from MPLC fraction No.7 (16—26, numbering refers to Figure 47, compounds 6, 9, 14 and 15 are shown before.): The numbering of the carbon atoms refers to the adjoining structures.

5-Hydroxy-3,4-dimethylfuran-2(5*H*)-one (**16**)

UV/Vis (0.1% formic acid/acetonitrile=75/25) λ_{\max} =220 nm;

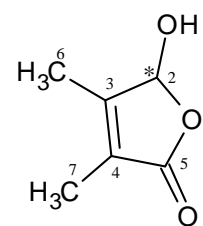
UPLC-TOF MS (ESI⁺): m/z 129.0551 ([M+H]⁺, measured),

m/z 129.0552 ([M+H]⁺, calculated for C₆H₉O₃);

¹H NMR (500 MHz, DMSO-*d*₆, COSY): δ (ppm)

1.72 [m, 3H, H-C(7)], 1.91 [m, 3H, H-C(6)], 5.85 [s, 1H, H-C(2)];

¹³C NMR (125 MHz, DMSO-*d*₆, HSQC, HMBC): δ (ppm) 8.19 [CH₃, C(7)], 11.22 [CH₃, C(6)], 98.33 [CH, C(2)], 123.79 [C, C(3)], 157.06 [C, C(4)], 171.85 [C, C(5)].



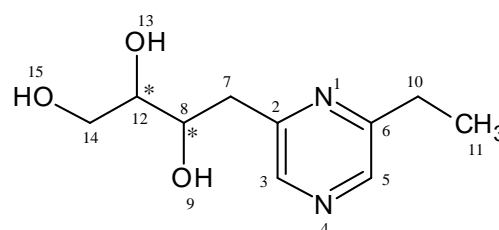
1,2,3-Butanetriol-4-(6-ethyl-2-pyrazinyl) (**17**)

UV/Vis (0.1% formic acid/acetonitrile=80/20)

λ_{\max} =276 nm;

UPLC-TOF MS (ESI⁺):

m/z 213.1242 ([M+H]⁺, measured),



m/z 213.1239 ($[M+H]^+$, calculated for $C_{10}H_{17}N_2O_3$);

1H NMR (500 MHz, DMSO- d_6 , COSY): δ (ppm) 1.23 [t, 3H, $J=7.6$, 7.6 Hz, H-C(11)], 2.75 [q, 2H, $J=8.0$, 2.7 Hz, H-C(10)], 2.70 [m, 1H, H-C(7a)], 3.05 [dd, 1H, $J=13.8$, 2.9 Hz, H-C(7b)], 3.36 [m, 1H, H-C(12)], 3.39 [m, 1H, H-C(14a)], 3.57 [dd, 1H, $J=10.7$, 3.8 Hz, H-C(14b)], 3.75 [m, 1H, H-C(8)], 4.34 [br, 1H, H-O(15)], 4.62 [br, 1H, H-O(9)], 4.68 [br, 1H, H-O(12)], 8.32 [s, 1H, H-C(3)], 8.34 [s, 1H, H-C(5)];

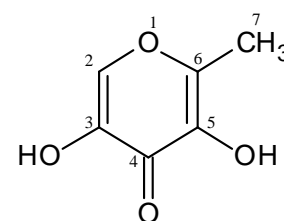
^{13}C NMR (125 MHz, DMSO- d_6 , HSQC, HMBC): δ (ppm) 13.45 [CH_3 , C(11)], 27.79 [CH_2 , C(10)], 38.77 [CH_2 , C(7)], 63.20 [CH_2 , C(14)], 71.31 [CH, C(8)], 74.98 [CH, C(12)], 140.63 [CH, C(5)], 142.66 [CH, C(3)], 154.85 [C, C(2)], 156.91 [C, C(6)].

5-Hydroxymaltol (18)

UV/Vis (0.1% formic acid/acetonitrile=75/25)

λ_{max} =288, 260 nm;

UPLC-TOF MS (ESI $^+$): m/z 143.0348 ($[M+H]^+$, measured),
 m/z 143.0344 ($[M+H]^+$, calculated for $C_6H_7O_4$);



1H NMR (500 MHz, DMSO- d_6 , COSY): δ (ppm)

2.22 [s, 3H, H-C(7)], 7.93 [s, 1H, H-C(2)];

^{13}C NMR (125 MHz, DMSO- d_6 , HSQC, HMBC): δ (ppm) 14.39 [CH_3 , C(7)], 138.96 [CH, C(2)], 141.37 [C, C(5)], 144.24 [C, C(3)], 149.24 [C, C(6)], 168.48 [C, C(4)].

α -{(2-Formyl-5-hydroxymethyl)pyrrol-1-yl}glutamic acid (19)

UV/Vis (0.1% formic acid/methanol=70/30)

λ_{max} =296 nm;

UPLC-TOF MS (ESI $^-$):

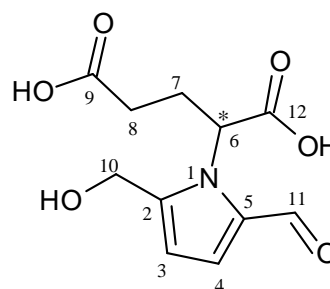
m/z 254.0663 ($[M-H]^-$, measured),

m/z 254.0665 ($[M-H]^-$, calculated for $C_{11}H_{12}NO_6$);

1H NMR (400 MHz, $D_2O/MeOD-d_4, 9/1$, COSY):

δ (ppm) 1.83 [ddd, 1H, $J=15.0$, 9.0, 5.7 Hz, H-C(8a)],

2.01 [dt, 1H, $J=15.8$, 8.0, 8.0 Hz, H-C(8b)], 2.30 [m, 1H, H-C(7a)], 2.54 [dddd, 1H, $J=13.7$, 8.9, 7.3, 4.4 Hz, H-C(7b)], 4.64 [m, 2H, H-C(10)], 6.41 [d, 1H, $J=4.1$ Hz, H-C(3)], 7.19 [d, 1H, $J=4.1$ Hz, H-C(4)], 9.30 [s, 1H, H-C(11)];



¹³C NMR (100 MHz, D₂O/MeOD-*d*₄, 9/1, HSQC, HMBC): δ (ppm) 29.72 [CH₂, C(7)], 35.06 [CH₂, C(8)], 56.51 [CH₂, C(10)], 61.38 [CH, C(6)], 111.69 [CH, C(3)], 128.10 [CH, C(4)], 132.93 [C, C(5)], 145.42 [C, C(2)], 178.00 [C, C(12)], 181.70 [CH, C(11)], 182.76 [C, C(9)].

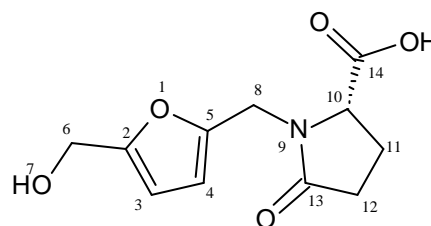
(*S*)-1-[(5-Hydroxymethyl)furan-2-yl)methyl]-5-oxopyrrolidine-2-carboxylic acid
(**20**)

UV/Vis (0.1% formic acid/methanol=85/15)

λ_{\max} =216 nm;

CD (50% methanol, 0.418 mmol/L):

λ_{\max} ($\Delta\epsilon$)=221 (+62.0)



UPLC-TOF MS (ESI⁻):

m/z 238.0721 ([M-H]⁻, measured),

m/z 238.0715 ([M-H]⁻, calculated for C₁₁H₁₂NO₅);

¹H NMR (500 MHz, DMSO-*d*₆, COSY): δ (ppm) 1.93 [m, 1H, H-C(11a)], 2.29 [m, 1H, H-C(11b)], 2.30 [m, 2H, H-C(12)], 3.95 [d, 1H, *J*=15.6 Hz, H-C(8a)], 3.97 [m, 1H, H-C(10)], 4.33 [s, 2H, H-C(6)], 4.77 [d, 1H, *J*=15.6 Hz, H-C(8b)], 5.17 [m, 1H, H-O(7)], 6.20 [d, 1H, *J*=3.2 Hz, H-C(3)], 6.21 [d, 1H, *J*=3.2 Hz, H-C(4)];

¹³C NMR (125 MHz, DMSO-*d*₆, HSQC, HMBC): δ (ppm) 22.35 [CH₂, C(11)], 28.98 [CH₂, C(12)], 37.74 [CH₂, C(8)], 55.64 [CH₂, C(6)], 58.20 [CH, C(10)], 107.61 [CH, C(3)], 109.31 [CH, C(4)], 148.72 [C, C(5)], 155.48 [C, C(2)], 173.20 [C, C(14)], 174.12 [C, C(13)].

3-Hydroxy-1*H*-[5-(hydroxymethyl)furan-2-yl)methyl]-2,5-dioxo-3-pyrrolidine-acetic acid (**21**)

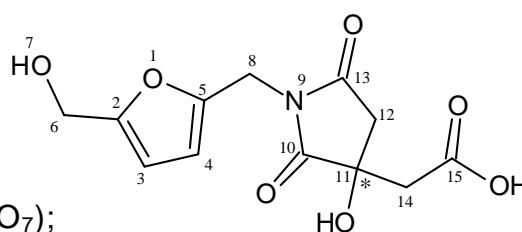
UV/Vis (0.1% formic acid/acetonitrile=85/15)

λ_{\max} =220 nm;

UPLC-TOF MS (ESI⁻):

m/z 282.0619 ([M-H]⁻, measured),

m/z 282.0615 ([M-H]⁻, calculated for C₁₂H₁₂NO₇);



¹H NMR (400 MHz, DMSO-*d*₆, COSY): δ (ppm)

2.65 [d, 1H, *J*=18.2 Hz, H-C(12a)], 2.81 [d, 1H, *J*=16.9 Hz, H-C(14a)], 2.90 [d, 1H, *J*=17.0 Hz, H-C(14b)], 3.05 [d, 1H, *J*=18.2 Hz, H-C(12b)], 4.32 [s, 2H, H-C(6)], 4.52 [d, 1H, *J*=15.8 Hz, H-C(8a)], 4.56 [d, 1H, *J*=15.8 Hz, H-C(8b)], 5.15 [br, 1H, H-O(7)], 6.18 [d, 1H, *J*=3.2 Hz, H-C(3)], 6.20 [d, 1H, *J*=3.2 Hz,

H-C(4)];

¹³C NMR (100 MHz, DMSO-*d*₆, HSQC, HMBC): δ (ppm) 34.95 [CH₂, C(8)], 40.55 [CH₂, C(14)], 42.01 [CH₂, C(12)], 55.59 [CH₂, C(6)], 71.70 [C, C(11)], 107.79 [CH, C(3)], 108.33 [CH, C(4)], 148.01 [C, C(5)], 154.08 [C, C(2)], 171.46 [C, C(15)], 174.41 [C, C(13)], 177.85 [C, C(10)].

(*E*)-4-(5-Methylpyrazin-2-yl)but-3-ene-7,2-diol (**22**)

UV/Vis (0.1% formic acid/acetonitrile=85/15)

λ_{max}=240, 304 nm;

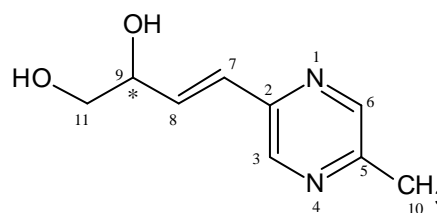
UPLC-TOF MS (ESI⁺):

m/z 181.0979 ([M+H]⁺, measured),

m/z 181.0977 ([M+H]⁺, calculated for C₉H₁₃N₂O₂);

¹H NMR (500 MHz, DMSO-*d*₆, COSY): δ (ppm) 2.55 [s, 3H, H-C(10)], 3.39 [m, 2H, H-C(11)], 4.20 [m, 1H, H-C(9)], 6.69 [dd, 1H, *J*=15.9, 1.3 Hz, H-C(7)], 6.86 [dd, 1H, *J*=15.9, 4.9 Hz, H-C(8)], 8.45 [s, 1H, H-C(6)], 8.53 [d, 1H, *J*=1.5 Hz, H-C(3)];

¹³C NMR (125 MHz, DMSO-*d*₆, HSQC, HMBC): δ (ppm) 20.86 [CH₃, C(10)], 65.72 [CH₂, C(11)], 71.80 [CH, C(9)], 125.32 [CH, C(7)], 137.22 [CH, C(8)], 141.86 [CH, C(3)], 143.77 [CH, C(6)], 147.62 [C, C(2)], 151.62 [C, C(5)].



α-((2-Formyl-5-hydroxymethyl)pyrrol-1-yl)alanine (**23**)

UV/Vis (0.1% formic acid/methanol=50/50)

λ_{max}=296 nm;

UPLC-TOF MS (ESI⁻):

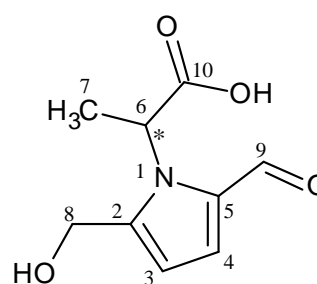
m/z 196.0613 ([M-H]⁻, measured),

m/z 196.0610 ([M-H]⁻, calculated for C₉H₁₀NO₄);

¹H NMR (400 MHz, D₂O/MeOD-*d*₄, 9/1, COSY):

δ (ppm) 1.51 [s, 3H, H-C(7)], 4.64 [d, 1H, *J*=14.0 Hz, H-C(8a)], 4.69 [d, 1H, *J*=13.9 Hz, H-C(8a)], 5.24 [br, 1H, H-C(6)], 6.38 [d, 1H, *J*=4.1 Hz, H-O(3)], 7.15 [d, 1H, *J*=4.1 Hz, H-O(4)], 9.30 [s, 1H, H-C(9)];

¹³C NMR (100 MHz, D₂O/MeOD-*d*₄, 9/1, HSQC, HMBC): δ (ppm) 18.97 [CH₃, C(7)], 56.23 [CH₂, C(8)], 57.32 [CH, C(6)], 111.75 [CH, C(3)], 127.67 [CH, C(4)], 132.55 [C, C(5)], 144.21 [C, C(2)], 178.74 [C, C(10)], 181.62 [CH, C(9)].

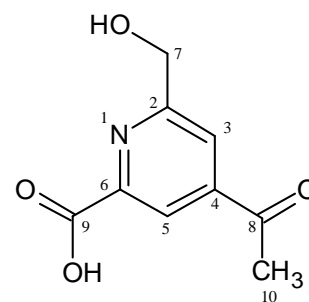


4-Acetyl-6-(hydroxymethyl)picolinic acid (**24**)**UV/Vis** (0.1% formic acid/acetonitrile=85/15) λ_{\max} =204, 292 nm;**UPLC-TOF MS** (ESI⁻): m/z 194.0457 ([M-H]⁻, measured), m/z 194.0453 ([M-H]⁻, calculated for C₉H₈NO₄);**¹H NMR** (500 MHz, DMSO-*d*₆, COSY): δ (ppm)

2.68 [s, 3H, H-C(10)], 4.71 [s, 2H, H-C(7)],

8.07 [d, 1H, J =1.5 Hz, H-C(3)], 8.25 [d, 1H, J =1.5 Hz, H-C(5)];**¹³C NMR** (125 MHz, DMSO-*d*₆, HSQC, HMBC): δ (ppm) 27.08 [CH₃, C(10)],63.83 [CH₂, C(7)], 120.33 [CH, C(5)], 120.75 [CH, C(3)], 144.47 [C, C(4)],

148.90 [C, C(6)], 163.72 [C, C(2)], 165.79 [C, C(9)], 197.68 [C, C(8)].

*(E)*-4-(6-Methylpyrazin-2-yl)but-3-ene-1,2-diol (**25**)**UV/Vis** (0.1% formic acid/acetonitrile=85/15) λ_{\max} =228, 300 nm;**UPLC-TOF MS** (ESI⁺): m/z 181.0982 ([M+H]⁺, measured), m/z 181.0977 ([M+H]⁺, calculated for C₉H₁₃N₂O₂);**¹H NMR** (500 MHz, DMSO-*d*₆, COSY): δ (ppm) 2.47 [s, 3H, H-C(11)], 3.41 [m,

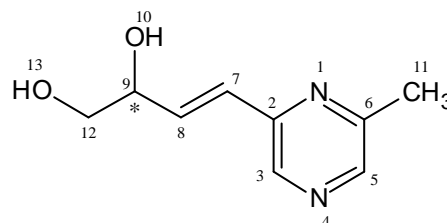
2H, H-C(12)], 4.22 [m, 1H, H-C(9)], 4.74 [br, 1H, H-O(13)], 5.09 [br, 1H,

H-O(10)], 6.69 [dd, 1H, J =15.8, 1.6 Hz, H-C(7)], 6.92 [dd, 1H, J =15.8, 4.9 Hz,

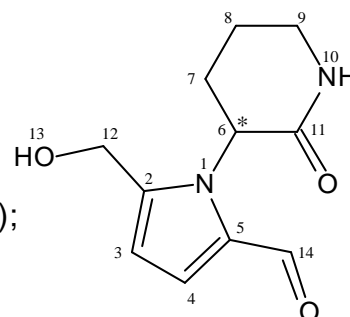
H-C(8)], 8.35 [s, 1H, H-C(5)], 8.45 [s, 1H, H-C(3)];

¹³C NMR (125 MHz, DMSO-*d*₆, HSQC, HMBC): δ (ppm) 21.21 [CH₃, C(11)],65.69 [CH₂, C(12)], 71.78 [CH, C(9)], 125.35 [CH, C(7)], 138.31 [CH, C(8)],

140.11 [CH, C(3)], 142.35 [CH, C(5)], 149.26 [C, C(2)], 152.92 [C, C(6)].

5-(Hydroxymethyl)-1-(2-oxopiperidin-3-yl)-1*H*-pyrrole-2-carbaldehyde (**26**)

trivial name: codyrrole A

UV/Vis (0.1% formic acid/acetonitrile=85/15) λ_{\max} =264, 296 nm;**UPLC-TOF MS** (ESI⁺): m/z 243.0903 ([M+Na]⁺, measured), m/z 245.0902 ([M+Na]⁺, calculated for C₁₁H₁₄N₂O₃Na);

¹H NMR (500 MHz, DMSO-*d*₆, COSY): δ (ppm) 1.85 [m, 2H, H-C(8)], 2.11 [m, 2H, H-C(7)], 3.16 [m, 1H, H-C(9a)], 3.41 [m, 1H, H-C(9b)], 4.50 [s, 2H, H-C(12)], 4.84 [dd, 1H, *J*=10.7, 7.2 Hz, H-C(6)], 5.34 [br, 1H, H-O(13)], 6.19 [d, 1H, *J*=4.0 Hz, H-C(3)], 7.00 [d, 1H, *J*=4.0 Hz, H-C(4)], 7.50 [br, 1H, H-N(10)], 9.30 [s, 1H, H-C(14)];

¹³C NMR (125 MHz, DMSO-*d*₆, HSQC, HMBC): δ (ppm) 22.70 [CH₂, C(8)], 29.45 [CH₂, C(7)], 41.70 [CH₂, C(9)], 55.54 [CH₂, C(12)], 56.63 [CH, C(6)], 109.49 [CH, C(3)], 125.39 [CH, C(4)], 132.09 [C, C(5)], 144.46 [C, C(2)], 168.39 [C, C(11)], 178.51 [C, C(14)].

3.5 Model reactions for generation of sulfur-containing compounds, spiro-alkaloids and a new pyrrole derivative (27—35)

3.5.1 Preparation of reaction matrices for screening study

D-(+)-glucose (125 mM) and SAC (62.5 mM) as well as only glucose or SAC were dissolved in phosphate buffer (1.5 mL, 100 mM, pH 6.0). The solutions were freeze-dried to obtain reaction samples in amorphous state, then they were packed in closed glass vials and heated (1 h, 100 °C) in a laboratory oven. Thereafter, each heated sample was dissolved with 20% MeCN and analyzed by means of HPLC (c.f chapter 3.10.2).

3.5.2 Extraction and isolation of target compounds

D-(+)-glucose (125 mM) and SAC (62.5 mM) were dissolved in the phosphate buffer (1.05 L), then dried matrices were prepared and heated as above. Subsequently, the heated sample was dissolved with 20% MeCN, and repeatedly extracted using ethyl acetate (sample:ethyl acetate=1:2 v/v, 6x). Ethyl acetate was removed from the combined organic layers under vacuum, and the residue was taken up in 30% MeCN, then the six fractions (GS—A, B, C, D, F and G) were separated by means of preparative HPLC (c.f chapter 3.10.3, system 14, gradient 1), collected repeatedly, concentrated under reduced pressure and at last freeze-dried.

3.5.3 Purification and structure elucidation of compounds 27—35

Each fraction was further purified by means of the following semi-preparative HPLC (**Table 17**), thus affording compounds **27—35**. After the HPLC separation,

solvents of compounds **27**–**35** except **32** were immediately removed through freeze-drying, while pH value of a solution of compound **32** was adjusted to 7.0 using sodium hydroxide, followed by lyophilization. Structural elucidation of the compounds was conducted by means of 1D/2D-NMR and UPLC-TOF MS, and the absolute configurations of **27**–**33** were determined using optical analyses (specific optical rotation or CD spectroscopy) comparing to literature data.

Table 17. A list of chromatographic conditions for purification of fractions obtained from HPLC separation of model reaction matrices

fraction No.	purification
GS—A	chapter 3.10.3, system 8, gradient 6
GS—B	chapter 3.10.3, system 8, gradient 6
GS—C	chapter 3.10.3, system 15
GS—D	chapter 3.10.3, system 15
GS—E	chapter 3.10.3, system 5, gradient 2
GS—F	chapter 3.10.3, system 5, gradient 3

Spectroscopic data of obtained antioxidants from the model system (27—35, numbering refers to Figure 65): The numbering of the carbon atoms refers to the adjoining structures.

Acortatarin A (**27**)

UV/Vis (0.1% formic acid/acetonitrile=85/15) λ_{\max} =300 nm;

$[\alpha]^{24}_{\text{D}} +295.9$ (c 0.028, MeOH);

UPLC-TOF MS (ESI⁺): m/z 254.1030 ([M+H]⁺, measured),
 m/z 254.1030 ([M+H]⁺, calculated for C₁₂H₁₆NO₅);

¹H NMR (400 MHz, DMSO-*d*₆, COSY): δ (ppm)

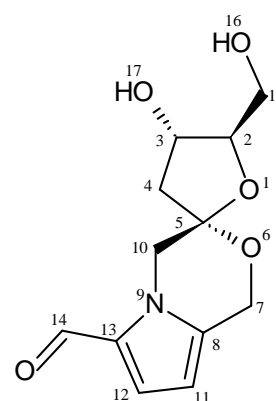
1.97 [dd, 1H, J =13.9, 3.4 Hz, H-C(4a)],

2.30 [dd, 1H, J =13.9, 8.5 Hz, H-C(4b)],

3.44 [m, 1H, H-C(15a)], 3.54 [m, 1H, H-C(15b)],

3.88 [td, 1H, J =5.0, 5.0, 3.1 Hz, H-C(2)], 4.12 [m, 1H, H-C(3)], 4.17 [d, 1H, J =13.9 Hz, H-C(10a)], 4.44 [d, 1H, J =13.9 Hz, H-C(10b)], 4.74 [t, 1H, J =5.7, 5.7 Hz, H-O(16)], 4.85 [s, 2H, H-C(7)], 5.07 [d, 1H, J =4.8 Hz, H-O(17)], 6.08 [d, 1H, J =4.0 Hz, H-C(11)], 7.03 [d, 1H, J =4.0 Hz, H-C(12)], 9.42 [s, 1H, H-C(14)];

¹H NMR (500 MHz, CD₃OD, COSY): δ (ppm) 2.15 [dd, 1H, J =14.0, 2.6 Hz, H-C(4a)], 2.35 [dd, 1H, J =14.0, 8.3 Hz, H-C(4b)], 3.62 [dd, 1H, J =12.1, 4.9 Hz,



H-C(15a)], 3.71 [dd, 1H, $J=12.1, 3.3$ Hz, H-C(15b)], 4.07 [td, 1H, $J=4.7, 4.7, 3.3$ Hz, H-C(2)], 4.23 [d, 1H, $J=14.0$ Hz, H-C(10a)], 4.26 [ddd, 1H, $J=8.3, 4.6, 2.7$ Hz, H-C(3)], 4.59 [d, 1H, $J=14.0$ Hz, H-C(10b)], 4.86 [m, 1H, H-C(7a)], 5.02 [d, 1H, $J=15.8$ Hz, H-C(7b)], 6.08 [d, 1H, $J=4.2$ Hz, H-C(11)], 7.02 [d, 1H, $J=4.1$ Hz, H-C(12)], 9.37 [s, 1H, H-C(14)];

^{13}C NMR (100 MHz, DMSO- d_6 , HSQC, HMBC): δ (ppm) 44.51 [CH₂, C(4)], 50.75 [CH₂, C(10)], 57.16 [CH₂, C(7)], 61.08 [CH₂, C(15)], 69.89 [CH, C(3)], 87.54 [CH, C(2)], 102.38 [C, C(5)], 104.79 [CH, C(11)], 123.75 [CH, C(12)], 130.64 [C, C(13)], 135.04 [C, C(8)], 178.95 [CH, C(14)].

Pollenopyrroside A (28)

UV/Vis (0.1% formic acid/acetonitrile=85/15)

$\lambda_{\text{max}}=300$ nm;

$[\alpha]_{\text{D}}^{22} +122.7$ (c 0.04, MeOH);

UPLC-TOF MS (ESI⁺):

m/z 254.1021 ([M+H]⁺, measured),

m/z 254.1028 ([M+H]⁺, calculated for C₁₂H₁₆NO₅);

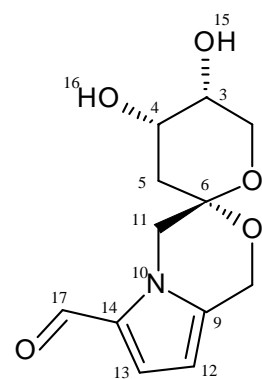
^1H NMR (500 MHz, DMSO- d_6 , COSY): δ (ppm)

1.88 [dd, 1H, $J=14.5, 3.9$ Hz, H-C(5a)],

2.03 [dd, 1H, $J=14.5, 3.8$ Hz, H-C(5b)], 3.37 [m, 1H, H-C(2a)], 3.56 [m, 1H, H-C(3)], 3.67 [t, 1H, $J=10.3$ Hz, H-C(2b)], 3.88 [m, 1H, H-C(4)], 3.96 [d, 1H, $J=13.9$ Hz, H-C(11a)], 4.28 [br, 1H, H-O(16)], 4.36 [d, 1H, $J=14.0$ Hz, H-C(11b)], 4.69 [d, 1H, $J=15.9$ Hz, H-C(8a)], 4.70 [br, 1H, H-O(15)], 4.85 [d, 1H, $J=15.9$ Hz, H-C(8b)], 6.06 [d, 1H, $J=4.1$ Hz, H-C(12)], 7.01 [d, 1H, $J=4.1$ Hz, H-C(13)], 9.41 [s, 1H, H-C(17)];

^1H NMR (500 MHz, CD₃COCD₃, COSY): δ (ppm) 2.07 [m, 1H, H-C(5a)], 2.22 [dd, 1H, $J=14.8, 3.4$ Hz, H-C(5b)], 3.54 [m, 1H, H-C(2a)], 3.70 [m, 1H, H-C(3)], 3.76 [m, 1H, H-C(2b)], 4.03 [d, 1H, $J=14.1$ Hz, H-C(11a)], 4.05 [m, 1H, H-C(4)], 4.46 [d, 1H, $J=14.2$ Hz, H-C(11b)], 4.84 [d, 1H, $J=15.8$ Hz, H-C(8a)], 4.90 [d, 1H, $J=15.7$ Hz, H-C(8b)], 6.06 [d, 1H, $J=3.9$ Hz, H-C(12)], 6.97 [d, 1H, $J=3.9$ Hz, H-C(13)], 9.46 [s, 1H, H-C(17)];

^{13}C NMR (125 MHz, DMSO- d_6 , HSQC, HMBC): δ (ppm) 37.46 [CH₂, C(5)], 50.99 [CH₂, C(11)], 56.94 [CH₂, C(8)], 60.06 [CH₂, C(2)], 65.54 [CH, C(4)], 65.94 [CH, C(3)], 93.36 [C, C(6)], 104.78 [CH, C(12)], 123.53 [CH, C(13)], 130.61 [C, C(14)], 134.69 [C, C(9)], 178.52 [CH, C(17)].

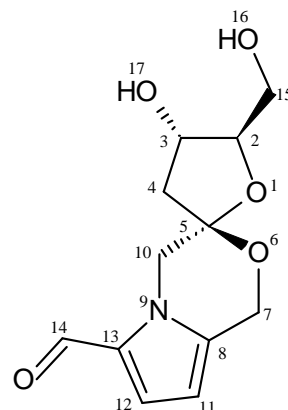
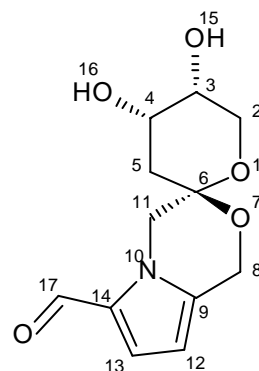


epi-Acortatarin A (29)**UV/Vis** (0.1% formic acid/acetonitrile=85/15) λ_{\max} =300 nm; $[\alpha]_D^{21}$ -138.9 (c 0.05, MeOH);**UPLC-TOF MS** (ESI⁺): m/z 254.1031 ([M+H]⁺, measured), m/z 254.1028 ([M+H]⁺, calculated for C₁₂H₁₆NO₅);**¹H NMR** (400 MHz, DMSO-*d*₆, COSY): δ (ppm)

2.00 [dd, 1H, J =13.4, 6.2 Hz, H-C(4a)], 2.34 [dd, 1H, J =13.4, 6.7 Hz, H-C(4b)], 3.40 [m, 1H, H-C(15a)], 3.49 [m, 1H, H-C(15b)], 3.86 [td, 1H, J =6.3, 4.8 Hz, H-C(2)], 4.17 [d, 1H, J =13.8 Hz, H-C(10a)], 4.23 [m, 1H, H-C(3)], 4.54 [d, 1H, J =13.8 Hz, H-C(10b)], 4.78 [m, 1H, H-O(16)], 4.82 [d, 1H, J =15.8 Hz, H-C(7a)], 4.95 [d, 1H, J =15.8 Hz, H-C(7b)], 5.22 [d, 1H, J =3.5 Hz, H-O(17)], 6.06 [d, 1H, J =4.1 Hz, H-C(11)], 7.03 [d, 1H, J =4.1 Hz, H-C(12)], 9.42 [s, 1H, H-C(14)];

¹H NMR (500 MHz, CD₃OD, COSY): δ (ppm) 2.09 [dd, 1H, J =13.3, 6.9 Hz, H-C(4a)], 2.35 [dd, 1H, J =13.3, 6.9 Hz, H-C(4b)], 3.61 [dd, 1H, J =11.7, 6.8 Hz, H-C(15a)], 3.70 [dd, 1H, J =11.7, 4.4 Hz, H-C(15b)], 4.01 [td, 1H, J =6.7, 4.7, 4.7 Hz, H-C(2)], 4.22 [d, 1H, J =14.0 Hz, H-C(10a)], 4.38 [td, 1H, J =6.9, 6.9, 5.1 Hz, H-C(3)], 4.67 [d, 1H, J =13.9 Hz, H-C(10b)], 4.81 [d, 1H, J =15.9 Hz, H-C(7a)], 5.09 [d, 1H, J =15.8 Hz, H-C(7b)], 6.06 [d, 1H, J =4.2 Hz, H-C(11)], 7.02 [d, 1H, J =4.1 Hz, H-C(12)], 9.37 [s, 1H, H-C(14)];

¹³C NMR (100 MHz, DMSO-*d*₆, HSQC, HMBC): δ (ppm) 44.32 [CH₂, C(4)], 51.41 [CH₂, C(10)], 57.75 [CH₂, C(7)], 62.27 [CH₂, C(15)], 70.22 [CH, C(3)], 88.40 [CH, C(2)], 102.41 [C, C(5)], 104.74 [CH, C(11)], 123.83 [CH, C(12)], 130.63 [C, C(13)], 135.05 [C, C(8)], 178.55 [CH, C(14)].

*Xylapyrroside* A (30)**UV/Vis** (0.1% formic acid/acetonitrile=80/20) λ_{\max} =300 nm; $[\alpha]_D^{23}$ -156.0 (c 0.09, MeOH);**UPLC-TOF MS** (ESI⁺): m/z 254.1024 ([M+H]⁺, measured), m/z 254.1028 ([M+H]⁺, calculated for C₁₂H₁₆NO₅);

¹H NMR (500 MHz, DMSO-*d*₆, COSY): δ (ppm) 1.75 [dd, 1H, *J*=12.8, 5.1 Hz, H-C(5a)], 1.85 [m, 1H, H-C(5b)], 3.62 [m, 2H, H-C(2)], 3.62 [m, 1H, H-C(3)], 3.88 [m, 1H, H-C(4)], 3.95 [d, 1H, *J*=14.0 Hz, H-C(11a)], 4.44 [d, 1H, *J*=13.9 Hz, H-C(11b)], 4.62 [d, 1H, *J*=15.8 Hz, H-C(8a)], 4.62 [m, 1H, H-O(15)], 4.75 [br, 1H, H-O(16)], 4.86 [d, 1H, *J*=16.0 Hz, H-C(8b)], 6.07 [d, 1H, *J*=4.1 Hz, H-C(12)], 7.02 [d, 1H, *J*=4.1 Hz, H-C(13)], 9.42 [s, 1H, H-C(17)];

¹H NMR (500 MHz, CDCl₃): δ (ppm) 1.91 [1H, dd, *J*=13.0, 11.4 Hz, H-C(5a)], 2.04 [dd, 1H, *J*=13.0, 5.4 Hz, H-C(5b)], 3.81 [dd, *J*=12.8, 1.7 Hz, H-C(2a)], 3.88 [dd, *J*=12.8, 2.2 Hz, H-C(2b)], 3.89 [m, 1H, H-C(3)], 4.02 [d, 1H, *J*=14.1 Hz, H-C(11a)], 4.17 [ddd, 1H, *J*=11.4, 5.3, 3.2 Hz, H-C(4)], 4.70 [d, 1H, *J*=14.2 Hz, H-C(11b)], 4.74 [d, 1H, *J*=15.6 Hz, H-C(8a)], 4.82 [d, 1H, *J*=15.4 Hz, H-C(8b)], 6.01 [d, 1H, *J*=4.1 Hz, H-C(12)], 6.91 [d, 1H, *J*=4.1 Hz, H-C(13)], 9.45 [s, 1H, H-C(17)];

¹³C NMR (125 MHz, DMSO-*d*₆, HSQC, HMBC): δ (ppm) 34.94 [CH₂, C(5)], 51.82 [CH₂, C(11)], 57.09 [CH₂, C(8)], 64.20 [CH, C(4)], 65.32 [CH, C(2)], 66.79 [CH, C(3)], 94.94 [C, C(6)], 104.83 [CH, C(12)], 123.28 [CH, C(13)], 130.59 [C, C(14)], 134.67 [C, C(9)], 178.63 [CH, C(17)].

5-Hydroxymethyl-1-[(5-hydroxymethyl-2-furanyl)methyl]-1*H*-pyrrole-2-carbaldehyde (**31**)

trivial name: HDFP;

UV/Vis (0.1% formic acid/acetonitrile=50/50)

λ_{\max} =228, 296 nm;

UPLC-TOF MS (ESI⁺):

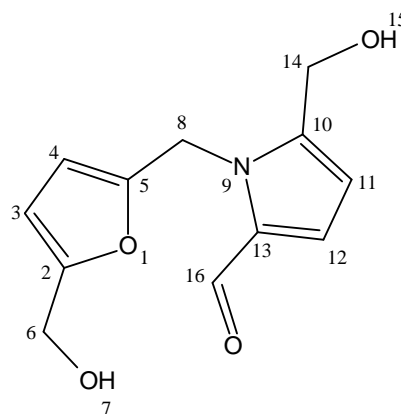
m/z 258.0739 ([M+Na]⁺, measured),

m/z 258.0742 ([M+Na]⁺, calculated for

C₁₂H₁₃NO₄Na);

¹H NMR (500 MHz, DMSO-*d*₆, COSY): δ (ppm)

4.30 [d, 2H, *J*=4.9 Hz, H-C(6)], 4.61 [d, 2H, *J*=4.5 Hz, H-C(14)], 5.17 [m, 1H, H-O(7)], 5.41 [t, 1H, *J*=5.5 Hz, H-O(15)], 5.58 [s, 2H, H-C(8)], 6.14 [d, 1H, *J*=3.2 Hz, H-C(4)], 6.17 [d, 1H, *J*=3.1 Hz, H-C(3)], 6.23 [d, 1H, *J*=4.0 Hz, H-C(11)], 6.98 [d, 1H, *J*=4.0 Hz, H-C(12)], 9.50 [s, 1H, H-C(16)];



^{13}C NMR (125 MHz, DMSO- d_6 , HSQC, HMBC): δ (ppm) 41.08 [CH₂, C(8)], 55.00 [CH₂, C(14)], 55.60 [CH₂, C(6)], 107.65 [CH, C(3)], 108.34 [CH, C(4)], 109.57 [CH, C(11)], 124.08 [CH, C(12)], 131.52 [C, C(13)], 143.69 [C, C(10)], 150.16 [C, C(5)], 155.23 [C, C(2)], 179.47 [CH, C(16)].

α -{(2-Formyl-5-hydroxymethyl)pyrrol-1-yl}S-allylcysteine (**32**)

trivial name: pyrrosac;

UV/Vis (0.1% formic acid/methanol=25/75)

λ_{max} =204, 296 nm;

UPLC-TOF MS (ESI⁻):

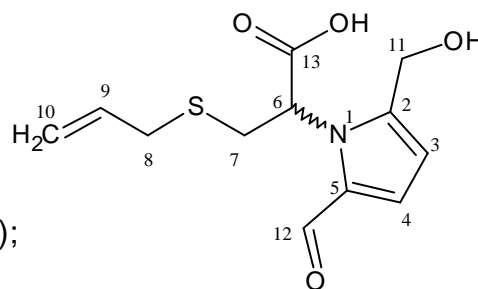
m/z 268.0642 ([M-H]⁻, measured),

m/z 268.0644 ([M-H]⁻, calculated for C₁₂H₁₄NO₄S);

^1H NMR (400 MHz, DMSO- d_6 , COSY): δ (ppm)

2.76 [dd, 1H, J =13.6, 7.0 Hz, H-C(8a)], 2.92 [m, 1H, H-C(8b)], 2.92 [m, 1H, H-C(7a)], 3.37 [m, 1H, H-C(7b)], 4.38 [d, 1H, J =13.9 Hz, H-C(10a)], 4.43 [d, 1H, J =13.6 Hz, H-C(10b)], 4.99 [m, 2H, H-C(11)], 5.63 [ddt, 1H, J =17.1, 10.3, 7.2, 7.2 Hz, H-C(9)], 6.19 [d, 1H, J =4.0 Hz, H-C(3)], 6.88 [d, 1H, J =4.0 Hz, H-C(4)], 9.30 [s, 1H, H-C(14)];

^{13}C NMR (100 MHz, DMSO- d_6 , HSQC, HMBC): δ (ppm) 33.42 [CH₂, C(8)], 34.06 [CH₂, C(7)], 55.74 [CH₂, C(11)], 60.84 [CH, C(6)], 110.18 [CH, C(3)], 116.97 [CH₂, C(10)], 123.40 [CH, C(4)], 132.77 [C, C(5)], 134.59 [CH, C(9)], 144.49 [C, C(2)], 170.95 [C, C(13)], 179.23 [CH, C(12)].



(4S)-4-(Allylthiomethyl)-3,4-dihydro-3-oxo-1H-pyrrolo[2,1-c][1,4]oxazine-6-carbaldehyde (**33**)

trivial name: pyrrosac ester;

UV/Vis (0.1% formic acid/methanol=20/80)

λ_{max} =204, 292 nm;

CD (50% MeOH, 0.398 mmol/L):

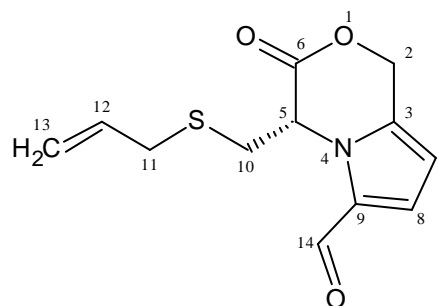
$\lambda_{\text{max}}(\Delta\epsilon)$ = 295 (+65.1), 247 (-20.6);

UPLC-TOF MS (ESI⁺):

m/z 252.0695 ([M+H]⁺, measured),

m/z 252.0694 ([M+H]⁺, calculated for C₁₂H₁₄NO₃S);

^1H NMR (500 MHz, DMSO- d_6 , COSY): δ (ppm) 2.62 [dd, 1H, J =13.6, 7.8 Hz, H-C(11a)], 2.96 [dd, 1H, J =13.6, 6.6 Hz, H-C(11b)], 3.16 [dd, 1H, J =14.8, 4.8 Hz,



H-C(10a)], 3.22 [dd, 1H, $J=14.8, 4.5$ Hz, H-C(10b)], 4.92 [dq, 1H, $J=16.9, 1.4, 1.4, 1.4$ Hz, H-C(13a)], 5.04 [m, 1H, H-C(13b)], 5.59 [m, 1H, H-C(5)], 5.59 [d, 1H, $J=15.2$ Hz, H-C(2a)], 5.77 [d, 1H, $J=14.8$ Hz, H-C(2b)], 5.78 [m, 1H, H-C(12)], 6.35 [d, 1H, $J=4.0$ Hz, H-C(7)], 7.23 [d, 1H, $J=4.0$ Hz, H-C(8)], 9.51 [s, 1H, H-C(14)];

^{13}C NMR (125 MHz, DMSO- d_6 , HSQC, HMBC): δ (ppm) 33.32 [CH₂, C(10)], 34.01 [CH₂, C(11)], 57.58 [CH, C(5)], 64.23 [CH₂, C(2)], 106.49 [CH, C(7)], 118.01 [CH₂, C(13)], 125.01 [CH, C(8)], 130.54 [C, C(9)], 132.60 [C, C(3)], 133.58 [CH, C(12)], 166.49 [C, C(6)], 179.46 [CH, C(14)].

(2*R*)-3-(Allylthio)-2-[(4*R*)-4-(allylthiomethyl)-6-formyl-3-oxo-3,4-dihydropyrrolo-[1,2-*a*] pyrazin-2(1*H*)-yl]propanoic acid (**34**)

trivial name: PSBS-A

UV/Vis (0.1% formic acid/methanol=30/70)

$\lambda_{\text{max}}=200, 296$ nm;

CD (50% MeOH, 0.538 mmol/L):

$\lambda_{\text{max}}(\Delta\epsilon) = 299 (-108.7), 252 (+49.6), 210 (-53.8)$;

UPLC-TOF MS (ESI⁻):

m/z 393.0949 ([M-H]⁻, measured),

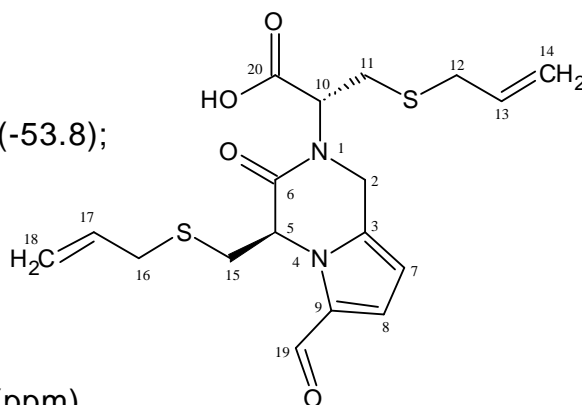
m/z 393.0943 ([M-H]⁻, calculated for

C₁₈H₂₁N₂O₄S₂);

^1H NMR (500 MHz, DMSO- d_6 , COSY): δ (ppm)

2.59 [dd, 1H, $J=13.6, 7.6$ Hz, H-C(16a)], 2.88 [dd, 1H, $J=13.6, 6.8$ Hz, H-C(16b)], 2.96 [dd, 1H, $J=14.2, 10.5$ Hz, H-C(11a)], 3.07 [m, 1H, H-C(11b)], 3.08 [m, 2H, H-C(15)], 3.12 [m, 2H, H-C(12)], 4.69 [d, 1H, $J=16.9$ Hz, H-C(2a)], 4.93 [d, 1H, $J=16.9$ Hz, H-C(2b)], 4.93 [m, 1H, H-C(18a)], 4.93 [m, 1H, H-C(10)], 5.01 [m, 1H, H-C(18b)], 5.10 [m, 2H, H-C(14)], 5.54 [m, 1H, H-C(5)], 5.55 [m, 1H, H-C(17)], 5.71 [ddt, 1H, $J=17.1, 10.0, 7.2, 7.2$ Hz, H-C(13)], 6.29 [d, 1H, $J=4.0$ Hz, H-C(7)], 7.20 [d, 1H, $J=4.0$ Hz, H-C(8)], 9.47 [s, 1H, H-C(19)];

^{13}C NMR (125 MHz, DMSO- d_6 , HSQC, HMBC): δ (ppm) 28.38 [CH₂, C(11)], 33.50 [CH₂, C(12)], 34.08 [CH₂, C(16)], 34.23 [CH₂, C(15)], 41.76 [CH₂, C(2)], 56.57 [CH, C(10)], 58.26 [CH, C(5)], 106.47 [CH, C(7)], 117.41 [CH₂, C(14)], 117.78 [CH₂, C(18)], 125.42 [CH, C(8)], 129.87 [C, C(9)], 133.89 [CH, C(17)], 134.25 [CH, C(13)], 134.69 [C, C(3)], 165.95 [C, C(6)], 170.08 [C, C(20)], 178.95 [CH, C(19)].



(2*R*)-3-(Allylthio)-2-[(4*S*)-4-(allylthiomethyl)-6-formyl-3-oxo-3,4-dihydropyrrolo-[1,2-*a*] pyrazin-2(1*H*)-yl]propanoic acid (**35**)

trivial name: PSBS-B;

UV/Vis (0.1% formic acid/methanol=30/70)

λ_{\max} =200, 296 nm;

CD (50% MeOH, 0.538 mmol/L):

$\lambda_{\max}(\Delta\epsilon)$ =299 (+139.3), 251 (-46.9), 240 (-38.5),

229 (-41.0), 207 (-11.2);

UPLC-TOF MS (ESI⁻):

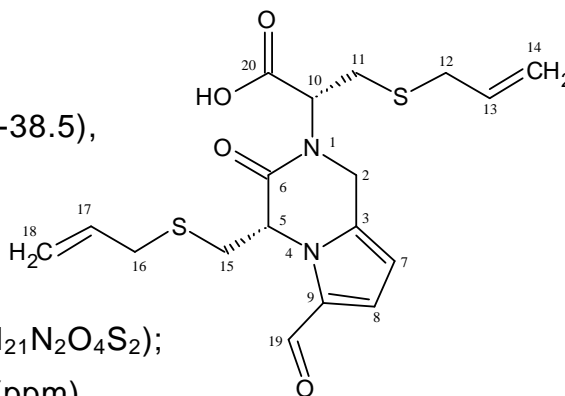
m/z 393.0948 ([M-H]⁻, measured),

m/z 393.0943 ([M-H]⁻, calculated for C₁₈H₂₁N₂O₄S₂);

¹H NMR (500 MHz, DMSO-*d*₆, COSY): δ (ppm)

2.52 [m, 1H, H-C(16a)], 2.83 [dd, 1H, J =13.6, 6.6 Hz, H-C(16b)], 2.92 [dd, 1H, J =14.2, 10.7 Hz, H-C(11a)], 3.09 [m, 2H, H-C(15)], 3.11 [m, 1H, H-C(11b)], 3.17 [m, 2H, H-C(12)], 4.55 [d, 1H, J =16.4 Hz, H-C(2a)], 4.81 [d, 1H, J =16.4 Hz, H-C(2b)], 4.90 [m, 1H, H-C(18a)], 4.98 [m, 1H, H-C(10)], 5.01 [m, 1H, H-C(18b)], 5.11 [m, 2H, H-C(14)], 5.54 [m, 1H, H-C(17)], 5.58 [m, 1H, H-C(5)], 5.74 [ddt, 1H, J =17.0, 10.0, 7.2, 7.2 Hz, H-C(13)], 6.31 [d, 1H, J =4.0 Hz, H-C(7)], 7.21 [d, 1H, J =4.0 Hz, H-C(8)], 9.48 [s, 1H, H-C(19)];

¹³C NMR (125 MHz, DMSO-*d*₆, HSQC, HMBC): δ (ppm) 28.67 [CH₂, C(11)], 33.53 [CH₂, C(12)], 34.15 [CH₂, C(15)], 34.19 [CH₂, C(16)], 42.35 [CH₂, C(2)], 56.06 [CH, C(10)], 58.32 [CH, C(5)], 106.58 [CH, C(7)], 117.56 [CH₂, C(14)], 117.73 [CH₂, C(18)], 125.19 [CH, C(8)], 130.04 [C, C(9)], 133.93 [CH, C(17)], 134.14 [CH, C(13)], 134.26 [C, C(3)], 165.84 [C, C(6)], 170.43 [C, C(20)], 179.05 [CH, C(19)].



3.5.4 Synthesis, purification and structure elucidation of decarboxylates of compounds **34** and **35**

In order to clarify the absolute configurations of compounds **34** and **35**, decarboxylated forms of them, as reference compounds possessing one chiral center for CD analysis, were synthesized through the following reaction. Compound **33** (178.82 mg) dissolved in acetone (2 mL) and SAC (343.9 mg) were mixed up adding the phosphate buffer (20 mL), followed by freeze-drying. Thereafter, the dried mixture was heated (100 °C, 50 min) in a laboratory oven using closed glass vials, and the heated mixture was dissolved with 50% MeCN

to apply HPLC separation (c.f chapter 3.10.3, system 14, gradient 2). In the HPLC separation, racemic decarboxylated forms (compounds **36**—**37**) eluted at 20.8 min, and simultaneously compounds **34** and **35**, generated in the reaction matrix, also eluted at 17.9 and 19.5 min, respectively. Yields of the racemic decarboxylates (**36+37**), **34** and **35** were 15.5, 10.2 and 17.1 mg, respectively. The relative structure of the racemate (**36+37**) was determined using UPLC-TOF MS and 1D/2D-NMR spectroscopy. Subsequently, chiral resolution of the racemic mixture was done employing the following system (c.f chapter 3.10.3, system 16), then enantiomers eluted at 11.2 (**36**) and 12.4 min (**37**).

Spectroscopic data of a racemic mixture of 36 and 37 (36—37, numbering refers to Figure 73): The numbering of the carbon atoms refers to the adjoining structures.

2-(Allylthioethyl)-4-(allylthiomethyl)-3-oxo-3,4-dihydropyrrolo[1,2-a]pyrazin-2(1*H*)-6-carbaldehyde [absolute configuration; **36**: (4*S*), **37**: (4*R*)]

UV/Vis (100% methanol) λ_{\max} =204, 296 nm;

CD of **36** (100% MeOH, 0.571 mmol/L):

$\lambda_{\max}(\Delta\epsilon)$ =296 (+172.1), 240 (-66.2), 206 (-7.6),

CD of **37** (100% MeOH, 0.571 mmol/L):

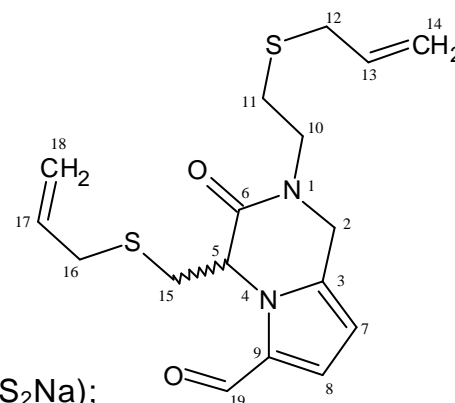
$\lambda_{\max}(\Delta\epsilon)$ =296 (-201.7), 237 (+77.1), 208 (+10.7);

UPLC-TOF MS (ESI⁺):

m/z 373.1021 ([M+Na]⁺, measured),

m/z 373.1020 ([M+Na]⁺, calculated for C₁₇H₂₂N₂O₂S₂Na);

¹H NMR (400 MHz, DMSO-*d*₆, COSY): δ (ppm) 2.41 [dd, 1H, *J*=13.6, 7.9 Hz, H-C(16a)], 2.68 [m, 2H, H-C(11)], 2.80 [dd, 1H, *J*=13.5, 6.5 Hz, H-C(16b)], 3.05 [dd, 1H, *J*=14.7, 4.1 Hz, H-C(15a)], 3.18 [m, 1H, H-C(15b)], 3.21 [m, 2H, H-C(12)], 3.58 [ddd, 1H, *J*=13.8, 8.2, 6.4 Hz, H-C(10a)], 3.66 [ddd, 1H, *J*=13.6, 8.2, 6.5 Hz, H-C(10b)], 4.73 [d, 1H, *J*=17.0 Hz, H-C(2a)], 4.87 [m, 1H, H-C(18a)], 4.90 [d, 1H, *J*=17.1 Hz, H-C(2b)], 5.00 [dt, 1H, *J*=10.0, 0.9, 0.9 Hz, H-C(18b)], 5.09 [dt, 1H, *J*=10.0, 0.9, 0.9 Hz, H-C(14a)], 5.18 [dq, 1H, *J*=17.0, 1.7, 1.7, 1.7 Hz, H-C(14b)], 5.51 [m, 1H, H-C(5)], 5.53 [m, 1H, H-C(17)], 5.76 [ddt, 1H, *J*=17.1, 9.9, 7.2, 7.2 Hz, H-C(13)], 6.29 [d, 1H, *J*=4.0 Hz, H-C(7)], 7.22 [d, 1H, *J*=4.0 Hz, H-C(8)], 9.45 [s, 1H, H-C(19)];



¹³C NMR (100 MHz, DMSO-*d*₆, HSQC, HMBC): δ (ppm) 26.25 [CH₂, C(11)], 33.39 [CH₂, C(12)], 34.04 [CH₂, C(16)], 34.73 [CH₂, C(15)], 44.60 [CH₂, C(2)], 45.84 [CH₂, C(10)], 58.12 [CH, C(5)], 106.41 [CH, C(7)], 117.42 [CH₂, C(14)], 117.75 [CH₂, C(18)], 125.62 [CH, C(8)], 129.73 [C, C(9)], 133.84 [CH, C(17)], 134.23 [C, C(3)], 134.31 [CH, C(13)], 165.06 [C, C(6)], 178.83 [CH, C(19)].

3.5.5 Model reactions using S-allyl-L-cysteine and S-allyl-D-cysteine

In order to determine the absolute configurations of the chiral center C(10) in compounds **34** and **35**, model reactions were performed using D-glucose and S-allyl-L-cysteine (SAC) or S-allyl-D-cysteine (SADC). D-(+)-glucose (125 mM) and SAC or SADC (62.5 mM) were dissolved in the phosphate buffer (1.5 mL), followed by freeze-drying. Thereafter, the freeze-dried mixtures were heated (1 h, 100 °C) in a laboratory oven, then each reaction mixture was dissolved in 20% MeOH (1.5 mL) and analyzed by means of HPLC (c.f chapter 3.10.2).

3.5.6 Identification of isolated compounds (27—37) in pAGE

pAGE (500 mg) was dissolved in water, and its volume was filled up to 5 mL, followed by filtration of the solution using 0.45 μm syringe filters. The filtrate was analyzed by means of UPLC-ESI-MS/MS with the following conditions (c.f chapter 3.11.3, system 1) to investigate the occurrence of isolated compounds **27—37** in the pAGE. Also, each reference compound was dissolved, diluted properly and analyzed as the same way, then retention times of the reference compounds were compared to those of chromatographic peaks eluted from the pAGE. MS/MS parameters of the compounds for the identification were tuned using IntelliStart of MassLnyx 4.1 software (Waters), then one optimal mass transition for detection of each compound was selected among four parameters in the individual compounds due to sensitivity and selectivity (**Table 18**).

Table 18. MS/MS parameters for identification of compounds **27—37** in pAGE.

compounds	mass transition (<i>m/z</i>)	cone (V)	collision (V)
Acortatarin A (27)			
Pollenopyrroside A (28)	254.223→206.090	4	10
<i>epi</i> -Acortatarin A (29)			
Xylapyrroside A (30)			
HDFP (31)	258.270→200.080	35	11
Pyrrosac (32)	268.160→193.948	20	8
Pyrrosac ester (33)	252.160→178.019	22	8
PSBS-A (34)			
PSBS-B (35)	395.223→279.010	30	14
decarboxylated PSBS-A (36)			
decarboxylated PSBS-A (37)	351.350→101.040	24	15

3.6 Model reactions for proposal of generation pathways on isolated compounds **8**, **15**, **20**, **21** and **26**

The following model reaction matrices (**Table 19**) were prepared using phosphate buffer (100 mM, pH 6.0, 1.5 mL). Each solution was freeze-dried and heated in closed vials employing a laboratory oven at 100 °C. Thereafter, the heated matrices were dissolved in water (1.5 mL), filtrated through syringe filters (0.45 µm), and analyzed by means of UPLC-ESI-MS/MS with the following analytical conditions (c.f chapter 3.11.3, system 2 and 6). MS/MS parameters for detection of compounds **8**, **15**, **20**, **21** and **26** were tuned using IntelliStart of MassLnyx 4.1 software (Waters) (**Table 20**).

Table 19. A list of preparations and heating times for model reactions.

labels	compounds	concentration [mM]	heating time [hour]
A	2-Keto-D-glucose	100	1
B	D-Glucose	100	1
	Glycine	100	
C	D-Glucose	100	1
	L-Glutamic acid	100	
D	D-Glucose	100	2
	L-Ornithine	100	
E	D-Glucose	200	18
	Glycine	200	
	Citric acid	100	

Table 20. MS/MS parameters for detection of compounds **8**, **15**, **20**, **21** and **26**.

compounds	mass transition (<i>m/z</i>)	cone (V)	collision (V)
5-Hydroxymethyl-2-furancarboxylic acid (8)	143.1→78.9	24	20
(2S)-1-[2-(Furan-2-yl)-2-oxoethyl]-5-oxo-pyrrolidine-2-carboxylic acid (15)	236.1→192.1	6	16
(2S)-1-[(5-(Hydroxymethyl)furan-2-yl)methyl]-5-oxopyrrolidine-2-carboxylic acid (20)	238.0→164.1	8	16
(3-Hydroxy-1 <i>H</i> -[5-(hydroxymethyl)furan-2-yl]methyl]-2,5-dioxo)-3-pyrrolidineacetic acid (21)	282.0→220.0	2	12
5-(Hydroxymethyl)-1-(2-oxopiperidin-3-yl)-1 <i>H</i> -pyrrole-2-carbaldehyde (26)	221.0→191.1	18	12

3.7 Identification of known antioxidative compounds in pAGE

Twenty-one antioxidative compounds (**38—58**), which had been identified in liquid AGE so far, were used to confirm their occurrences in pAGE by means of LC-MS/MS. Each compound was dissolved and diluted with water properly, and MS/MS parameters for identification of all compounds were tuned using IntelliStart of MassLynx 4.1 software (Waters). Subsequently, the pAGE powder (250 mg) was dissolved in water, and its volume was filled up to 5 mL, followed by filtration of the solution through 0.45 µm syringe filters. The filtrate and each reference compound were analyzed with the following MS/MS parameters (**Table 21**) and analytical conditions (c.f chapter 3.11.3, system 3).

Table 21. A list of MS/MS parameters for identification of compounds **38—58** in pAGE.

compounds	mass transition (<i>m/z</i>)	cone (V)	collision (V)
<i>N</i> α-(1-Deoxy-D-fructos-1-yl)-S-allyl-L-cysteine (38)	324.1→79.0	4	24
<i>N</i> α-(1-Deoxy-D-fructos-1-yl)-γ-glutamyl-S-allyl-L-cysteine (39)	453.0→435.1	28	12
<i>N</i> α-(1-Deoxy-D-fructos-1-yl)-L-phenylalanine (40)	328.1→120.1	6	28
<i>N</i> α-(1-Deoxy-D-fructos-1-yl)-L-tyrosine (41)	344.0→308.0	22	16
<i>N</i> α-(1-deoxy-D-fructos-1-yl)-L-tryptophan (42)	367.0→229.1	26	14
	367.0→349.1	26	10
<i>trans</i> -1-[(1 <i>R</i> ,2 <i>R</i> ,3 <i>S</i> ,4 <i>S</i>)-1,2,3,4,5-Pentahydroxypent-1-yl]-1,2,3,4-tetrahydro-β-carboline-3-carboxylic acid (43)	367.0→229.8	36	18
	367.0→247.1	36	14
<i>cis</i> -1-[(1 <i>R</i> ,2 <i>R</i> ,3 <i>S</i> ,4 <i>S</i>)-1,2,3,4,5-Pentahydroxypent-1-yl]-1,2,3,4-tetrahydro-β-carboline-3-carboxylic acid (44)	367.0→229.8	36	18
	367.0→247.1	36	14
1-Methyl-1,2,3,4-tetrahydro-β-carboline (45)	186.9→158.0	4	16
<i>N-trans</i> -Feruloyltyramine (46)	313.9→177.0	34	16
<i>N-trans</i> -Feruloylphenetyramine (47)	298.0→177.0	42	16
<i>N-trans</i> -Coumaroyltyramine (48)	284.0→147.0	36	14
<i>N-trans</i> -Coumaroylphenetyramine (49)	267.9→147.0	12	18
<i>N-trans</i> -Cinnamoylphenetyramine (50)	267.9→131.0	22	14
Ethyl ferulate (51)	223.1→145.0	2	18
Ethyl <i>p</i> -coumarate (52)	193.1→147.0	12	12
Ethyl vanilate (53)	197.1→125.0	2	12
Ethyl <i>p</i> -hydroxybenzoate (54)	167.1→121.0	2	16
(-)-(2 <i>R</i> ,3 <i>S</i>)-Dihydrodehydrodiconiferyl alcohol (55)	359.3→329.1	4	10
(+)-(2 <i>S</i> ,3 <i>R</i>)-Dehydrodiconiferyl alcohol (56)	357.3→309.2	8	28
	357.3→327.2	8	14
	357.3→339.2	8	10
<i>erythro</i> -Guaiacylglycerol-β-O-4'-conifery ether (57)	375.2→149.2	16	36
	375.2→165.0	16	24
	375.2→195.1	16	12
	375.2→327.2	16	10
<i>threo</i> -Guaiacylglycerol-β-O-4'-conifery ether (58)	375.3→150.0	6	30
	375.3→149.1	6	20
	375.3→195.1	6	10
	375.3→327.2	6	10

3.8 Quantitative analyses of identified compounds

3.8.1 Quantitative analysis of compounds 1—37 in processed and non-processed AGE powder

Well-purified compounds **1—37** were dissolved in water for quantitative analysis of compounds **1—26**, 20% acetonitrile for **38—42** and **45—55**, and 40% acetonitrile for compounds **27—37**. They were diluted properly to tune specific mass transitions for each compound employing IntelliStart of MassLynx 4.1 software (**Table 22**) and make their calibration curves (4 ng/mL—4 µg/mL, six points). Non-processed and processed AGE powder (pH 6.0, 100 °C, 24 hours) were dissolved and filled up to 5 mL (50 mg/mL) using same solvents to the target compounds, followed by filtration with 0.45 µm syringe filters. Dilutions of the reference compounds and the samples were analyzed by means of UPLC-MS/MS with the following analytical systems.

compounds	analytical condition
1, 2, 4—10	c.f 3.11.3, system 4
16—18, 22, 25, 26	c.f 3.11.3, system 5
3, 11, 13—15, 19—21, 23, 24, 26	c.f 3.11.3, system 6
12, 27—31	c.f 3.11.3, system 7
32—37	c.f 3.11.3, system 8

Table 22. A list of MS/MS parameters for quantitative analysis of compounds **1**–**55** in processed and non-processed AGE powder.

compounds	ionization	mass transition [<i>m/z</i>]	cone [V]	collision [V]
1,2,3-Butanetriol,4,4'-(2,5-pyrazinediyl)bis- (1)	ESI ⁺	289.3→107.0	2	30
1,2,3-Butanetriol,4,4'-(2,6-pyrazinediyl)bis- (2)				
α-((2-Formyl-5-hydroxymethyl)pyrrol-1-yl)arginine (3)	ESI ⁻	281.10→94.0	10	20
4-[7-Hydroxy-6-(hydroxymethyl)-7,8-dihydro-6 <i>H</i> -pyrano[2,3- <i>b</i>]pyrazine-3-yl]butane-1,2,3-triol (4)	ESI ⁺	287.3→269.1	22	16
4-[6-(1,2-Dihydroxyethyl)-6,7-dihydrofuro[2,3- <i>b</i>]pyrazin-3-yl]butane-1,2,3-triol (5)				
2,3-Dihydro-3,5-dihydroxy-6-methyl-4(<i>H</i>)-pyran-4-one (6)	ESI ⁺	145.1→99.0	22	12
1,2,3-Butanetriol-4-(6-methyl-2-pyrazinyl) (7)	ESI ⁺	199.2→163.0	34	14
5-Hydroxymethyl-2-furancarboxylic acid (8)	ESI ⁺	143.1→124.9	24	8
5-Hydroxymethyl-2-furaldehyde (9)	ESI ⁺	127.1→108.9	18	10
Thymidine (10)	ESI ⁺	243.2→127.0	38	10
α-((2-Formyl-5-hydroxymethyl)pyrrol-1-yl)aspartic acid (11)	ESI ⁻	240.0→124.0	30	14
5-Hydroxymethyl-1 <i>H</i> -pyrrole-2-carbaldehyde (12)	ESI ⁺	126.1→108.1	6	12
α-((2-Formyl-5-hydroxymethyl)pyrrol-1-yl)glycine (13)	ESI ⁻	182.0→108.0	2	16
1-{5-(1,2-Dihydroxyethyl)-2-oxotetrahydrofuran-3-yl}-5-(hydroxymethyl)-1 <i>H</i> -pyrrole-2-carbaldehyde (14)	ESI ⁻	268.1→93.9	42	24
(2 <i>S</i>)-1-[2-(Furan-2-yl)-2-oxoethyl]-5-oxopyrrolidine-2-carboxylic acid (15)	ESI ⁻	236.1→192.1	6	16
5-Hydroxy-3,4-dimethylfuran-2(5 <i>H</i>)-one (16)	ESI ⁺	129.1→83.0	6	12
1,2,3-Butanetriol-4-(6-ethyl-2-pyrazinyl) (17)	ESI ⁺	213.3→177.1	28	12
5-Hydroxymaltol (18)	ESI ⁺	143.1→69.0	24	20

Table 22. Continued

compounds	ionization	mass transition [<i>m/z</i>]	cone [V]	collision [V]
α -{(2-Formyl-5-hydroxymethyl)pyrrol-1-yl}glutamic acid (19)	ESI ⁻	254.1→124.0	2	16
(<i>S</i>)-1-{(5-Hydroxymethyl)furan-2-yl)methyl-5-oxopyrrolidine-2-carboxylic acid (20)	ESI ⁻	238.0→164.1	8	16
(3-Hydroxy-1 <i>H</i> -[5-(hydroxymethyl)furan-2-yl)methyl]-2,5-dioxo)-3-pyrrolidineacetic acid (21)	ESI ⁻	282.0→220.0	2	12
(<i>E</i>)-4-(5-Methylpyrazin-2-yl)but-3-ene-7,2-diol (22)	ESI ⁺	181.3→121.1	14	26
α -{(2-Formyl-5-hydroxymethyl)pyrrol-1-yl}alanine (23)	ESI ⁻	196.1→94.0	18	20
4-Acetyl-6-(hydroxymethyl)picolinic acid (24)	ESI ⁻	194.0→150.2	34	12
(<i>E</i>)-4-(6-Methylpyrazin-2-yl)but-3-ene-1,2-diol (25)	ESI ⁺	181.3→121.1	14	26
5-(Hydroxymethyl)-1-(2-oxopiperidin-3-yl)-1 <i>H</i> -pyrrole-2-carbaldehyde (26)	ESI ⁻	221.0→191.1	18	12
Acortatarin A (27)				
Pollenopyrroside A (28)	ESI ⁺	254.2→206.1	4	10
<i>epi</i> -Acortatarin A (29)				
Xylapyrroside A (30)				
HDFP (31)	ESI ⁺	258.3→200.1	35	11
Pyrrosac (32)	ESI ⁺	268.2→193.9	20	8
Pyrrosac ester (33)	ESI ⁺	252.2→178.0	22	8
PSBS-A (34)	ESI ⁺	395.2→279.0	30	14
PSBS-B (35)				
Decarboxylated PSBS-A (36)	ESI ⁺	351.4→101.0	24	15
Decarboxylated PSBS-B (37)				

Table 22. Continued

compounds	ionization	mass transition [<i>m/z</i>]	cone [V]	collision [V]
<i>N</i> α-(1-Deoxy-D-fructos-1-yl)-S-allyl-L-cysteine (38)	ESI ⁺	324.1→79.0	4	24
<i>N</i> α-(1-Deoxy-D-fructos-1-yl)-γ-glutamyl-S-allyl-L-cysteine (39)	ESI ⁺	453.0→435.1	28	12
<i>N</i> α-(1-Deoxy-D-fructos-1-yl)-L-phenylalanine (40)	ESI ⁺	328.1→120.1	6	28
<i>N</i> α-(1-Deoxy-D-fructos-1-yl)-L-tyrosine (41)	ESI ⁺	344.0→308.0	22	16
1-Methyl-1,2,3,4-tetrahydro-β-carboline (45)	ESI ⁺	186.9→158.0	4	16
<i>N-trans</i> -Feruloyltyramine (46)	ESI ⁺	313.9→177.0	34	16
<i>N-trans</i> -Feruloylphenetyramine (47)	ESI ⁺	298.0→177.0	42	16
<i>N-trans</i> -Coumaroyltyramine (48)	ESI ⁺	284.0→147.0	36	14
<i>N-trans</i> -Coumaroylphenetyramine (49)	ESI ⁺	267.9→147.0	12	18
<i>N-trans</i> -Cinnamoylphenetyramine (50)	ESI ⁺	267.9→131.0	22	14
Ethyl ferulate (51)	ESI ⁺	223.1→145.0	2	18
Ethyl <i>p</i> -coumarate (52)	ESI ⁺	193.1→147.0	12	12
Ethyl vanilate (53)	ESI ⁺	197.1→125.0	2	12
Ethyl <i>p</i> -hydroxybenzoate (54)	ESI ⁺	167.1→121.0	2	16
(-)-(2 <i>R</i> ,3 <i>S</i>)-Dihydrodehydrodiconiferyl alcohol (55)	ESI ⁻	359.3→329.1	4	10

3.8.2 Quantitative analysis of compounds 38—41 and 45—55 in processed and non-processed AGE powder

3.8.2.1 Quantitation of compounds 38—41 and 51—54

Amadori compounds **38—41** and ethyl esters **51—54** were quantified in processed and non-processed AGE powders by means of stable isotope dilution assays which had been developed in the chair institute so far. Briefly, $^{13}\text{C}_6$ -labeled internal standards for **38—41** and $^2\text{H}_5$ -labeled internal standards for **51—54** were used to perform the quantitation. The $^{13}\text{C}_6$ -compounds as well as the $^2\text{H}_5$ -labeled were mixed with own reference compounds, respectively, diluted into seven levels being in the ratio from 0.05 to 20.00 (reference/IS) using 20% methanol, and analyzed employing UPLC-MS/MS with the determined mass transitions (**Table 22**) and analytical systems (c.f 3.11.3 system 3). Non-processed and processed AGE powders were dissolved and filled up to 5 mL (50 mg/mL) using 20% methanol, followed by filtration with 0.45 μm syringe filters, then their proper dilutions were analyzed.

3.8.2.2 Quantitation of compounds 45—50 and 55

Seven compounds **45—50** and **55** were dissolved in 20% methanol and diluted into seven levels (**45—50**: 3 ng/mL—3 $\mu\text{g/mL}$, **55**: 600 ng/mL—60 $\mu\text{g/mL}$). The dilutions were analyzed by means of UPLC-MS/MS with the determined mass transitions (**Table 22**) and analytical systems (c.f 3.11.3 system 3). Non-processed and processed AGE powders were dissolved and filled up to 5 mL (50 mg/mL) using 20% methanol, followed by filtration with 0.45 μm syringe filters, then dilutions of the samples were analyzed with the same way as above.

3.8.3 Quantitative analysis of compounds 27—35 in garlic preparations

Raw garlic (28 g) was cut in about 1 mm slices and pan-fried at 250 °C for 8 min until its color reached light brown. Also, garlic powder (15 g) was pan-fried at 250 °C for 3 min. After cooling, the garlic samples heated as well as intact garlic samples for control were frozen in liquid nitrogen, ground, then mixed with water/acetonitrile (60/40, v/v; 30 mL), and, finally, filled up to 100 mL with the same solvent. After ultrasonication of each garlic suspension for 10 min, aliquots were taken, filtered using 0.45 μm syringe filters, and analyzed on compounds **27—35** by using the same way as above.

3.8.4 Quantitative analysis of compounds 1—35 in re-processed AGE powder

In order to investigate generation profiles of compounds 1—35, characteristic compounds in processed AGE, AGE powders of which pH values were controlled in three levels (4.0, 5.8 and 8.0) were processed again, then added in glass bials (2 g) with caps, respectively, and heated in a laboratory oven at 100 °C for 24 hours. Samplings were done at 0.5, 1.5, 3, 6, 9, 12, 18 and 24 hours since the heating started. Quantitative analysis of the compounds in the heated powders was performed as the same way as above.

3.9 Evaluation of identified compounds on antioxidative and taste activity, taste modulating effect, and pharmacological activity

All of compounds identified in pAGE were evaluated on antioxidative activity by means of ARS and ORAC assays. Compounds 27—35 gained with enough yields via the model system were further assessed on taste activity, taste modulating effect and pharmacological activity. As the pharmacological activity was evaluated by Wakunaga Pharmaceutical. Co. Ltd (JAPAN), methods for the assays are briefly shown below.

3.9.1 Evaluation of antioxidative activity

All compounds evaluated were dissolved in water and diluted in the phosphate buffer (pH 6.0) properly. The dilutions were measured in triplicate by means of ARS and ORAC assays (c.f chapters 3.2.1 and 3.2.2).

3.9.2 Evaluation of taste activity

3.9.2.1 Panel training

Seven subjects (4 women and 3 men, aged 25—41), who gave consent to participate in the sensory tests of the present investigation and have no history of known taste disorders, were trained to evaluate the taste of aqueous solutions of the following standard taste compounds in bottled water (pH 6.8): sucrose (50 mmol/L) for sweet taste, lactic acid (20 mmol/l) for sour taste, NaCl (20 mmol/L) for salty taste, caffeine (1 mmol/L) for bitter taste, monosodium L-glutamate (3 mmol/L) for umami taste, using the sip-and-spit method

(*Toelstede et al., 2008b*). Viscosity perception and kokumi activity (mouthfulness enhancement) were trained as reported earlier with a gelatin solution (0.5% in water) and a defined model broth spiked with glutathione (5.0 mmol/L) (*Ottinger et al., 2003, Toelstede et al., 2008a, Dunkel et al., 2009*). Prior to sensory analyses, purified compounds were analytically confirmed to be essentially free of solvents and buffer compounds (*Toelstede et al., 2008b, Ottinger et al., 2003*), and the purity of each tested compound was checked by ^1H NMR spectroscopy as well as high resolution mass spectrometry. To prevent cross-modal interactions with olfactory inputs, the panelists used nose clips and sensory sessions were performed at 22 °C in an air-conditioned room.

3.9.2.2 Bitter taste threshold

Detection thresholds of compounds **1—6** were determined in bottled water (pH 6.8) and of compounds **7—9** in bottled water containing 5% ethanol by means of a three-alternative forced choice test (*Dunkel et al., 2007*). Values between individuals and separate sessions differed not more than plus or minus one dilution step; that is, a threshold value of 20.0 $\mu\text{mol/L}$ for compound **34** represents a range of 10—40 $\mu\text{mol/L}$.

3.9.3 Evaluation of Kokumi-enhancement in a model broth

Taste-modulating activity of compound **32** was further assessed in a savory-tasting model broth consisted of monosodium glutamate monohydrate (1.9 g/L), yeast extract (2.1 g/L), maltodextrin (6.375 g/L) and sodium chloride (2.9 g/L) in bottled water (*Sonntag et al., 2010*). The pH value of the broth was adjusted to 5.9 using trace amounts of formic acid (0.1 mmol/L). Several concentrations of **32** in the broth were prepared. Sensory analysis was conducted by means of the three-alternative forced choice test with the trained panelists without nose clips.

3.9.4 Evaluation of pharmacological activity

3.9.4.1 Modulation effect on intracellular antioxidant system

Gene expressions of heme oxygenase-1 (HO-1) and glutamate-cysteine ligase modifier subunit (GCLM) were evaluated using Human umbilical vein endothelial cells treated with compounds **27—35**. Briefly, the cells plated at a density of 0.8×10^6 cells per 10 cm-dish were cultured using EGM-2 medium

containing vascular endothelial growth factor, basic fibroblast growth factor, insulin-like growth factor-1, epidermal growth factor, ascorbic acid, hydrocortisone, heparin and 2% fetal bovine serum at 37 °C in a 5% CO₂ humidified atmosphere. After 48 hours, the cells were treated with compounds **27–35** and S-allyl-L-cysteine (50 and 100 μM), respectively, for 4 hours. Thereafter, total RNA (25 ng each) extracted from each cell-batch using TRIzol reagent was converted to single-stranded cDNA using a PrimeScript RT reagent kit (Takara Bio, Otsu, Japan) in 5 μL of reaction volume. Diluted cDNA solutions (10-fold) were subjected to real-time PCR employing SYBR Premix Ex TaqII (Takara Bio, Otsu, Japan) and GAPDH as an internal control. The PCR study was performed in a PikoReal Real-Time PCR system (ThermoFisher Scientific, Waltham, MA, USA) by means of the following thermal program; pre-heating at 95 °C for 1 min, followed by 45 repeats of 95 °C for 10 seconds→56 °C for 10 seconds→72 °C for 15 seconds. The specific mRNA levels were calculated using the comparative CT ($\Delta\Delta$ CT) method (*Livak et al., 2001*). Primer sequences used were shown below;

HO-1: forward 5'-CAG GCA GAG AAT GCT GAG-3'

reverse 5'-GGC CAC ATA GAT GTG GTA-3'

GCLM: forward 5'-ACA CAG TTG GAA CAG CTG TA-3'

reverse 5'-CAA ATC TGG TGG CAT CAC AC-3'

GAPDH: forward 5'-GAG TCC ACT GGC GTC TTC A-3'

reverse 5'-GGG GTG CTA AGC AGT TGG T-3'

3.9.4.2 Modulation effect on immunoglobulin A (IgA) production in mouse lymphocytes

Peyers Patches and spleen obtained from sacrificed female C57BL/6N mice (9-week old) were crushed finely with a plunger in Hank balanced salt solution (HBSS) containing 5% fetal bovine serum (FBS). The red blood cells were lysed using BD lyse Pharm buffer. The cellular solution was passed through a 40 μm cell strainer to collect lymphocytes, followed by washing and resuspending in HBSS including 5% FBS. The isolated lymphocytes were plated at a density of 1×10^6 cells per well in 24-well plate, then cultured in RPMI-1640 containing 10% FBS, penicillin (100 U/mL), and streptomycin (100 μg/mL) with or without compounds **27–35** and S-allyl-L-cysteine (6.7–60 μM) in the presence of lipopolysaccharide (LPS) at 37 °C for 3 days. Thereafter, cells were removed

from each well via centrifugation at 400g for 5 min at 4 °C, obtaining supernatants for measurements of IgA concentration using Mouse IgA ELISA Quantification set (Bethyl Laboratories, Inc. Montgomery, AL, USA).

3.9.4.3 Modulation effect on interleukin 6 (IL-6) production in mouse lymphocytes

The mouse lymphocytes were cultured in the same way as described above using compounds **27—35** and S-allyl-L-cysteine (6.7—60 μM) under stimulation of LPS. After 24 hours, IL-6 was quantified in each culture medium using an ELISA kit (Mouse IL-6 Quantikine ELISA Kit, R&D SYSTEMS, Inc. USA).

3.10 Chromatographic methods

3.10.1 Gradient medium pressure liquid chromatography (MPLC)

p-AGE was separated through gradient medium pressure liquid chromatography (MPLC) with the following instruments and conditions.

pumps Büchi Pump Module C-605
sample injection Büchi Manual Reodyne Injector (25 mL loop)
UV detector Büchi UV Photometer C-635
pump manager Büchi Pump-Manager C-620
fraction collector Büchi Fraction Collector C-660
software Büchi Sepacore Record 1.0
[Every instrument is purchased from Büchi Labortechnik AG (Flawil, Switzerland)]

stationary phase Polypropylene cartridge (150 x 40 mm i.d.), filled with RP-18 material (LiChroprep, 25-40 mm (Merck KgaA, Darmstadt, Germany))

flow rate 40 mL/min

detection 220 nm (for p-AGE)
 290 nm (for model reaction products)

eluent A: aqueous formic acid (0.1%) B: methanol

gradient

time (min)	0	5	25	35
eluent A (%)	100	100	0	0
eluent B (%)	0	0	100	100

3.10.2 Analytical high performance liquid chromatography (HPLC)

pumps	PU-2080 plus
auto sampler	AS-2055 plus
degasser	DG-2080-53
detector	MD-2010 plus photodiode array detector
software	Chrompass

[Every instrument is purchased from Jasco (Gross-Umstadt, Germany).]

System

stationary phase	Luna Phenyl-Hexyl (250×4.6 mm, 5 μm, Phenomenex, Aschaffenburg, Germany)	
flow rate	0.9 mL/min	
eluent	A: 0.1% aqueous formic acid	B: methanol

gradient

time (min)	0	5	25	35	40
eluent A (%)	100	100	40	5	5
eluent B (%)	0	0	60	95	95

3.10.3 Semipreparative high performance liquid chromatography (semipreparative HPLC)

pumps	PU-2087 plus
gradient unit	LG-2080-02
degasser	DG-2080-53
detector	MD-2010 plus
software	Chrompass

[Every instrument is purchased from Jasco (Gross-Umstadt, Germany).]

System 1

stationary phase	Luna Phenyl-Hexyl (250×21.2 mm, 5 μm, Phenomenex, Aschaffenburg, Germany)
flow rate	18.0 mL/min

Materials and methods

detection UV 290 nm
eluent A: 0.1% aqueous formic acid B: methanol
gradient

time (min)	0	3	8	21	26
eluent A (%)	97	97	92	5	5
eluent B (%)	0	3	8	95	95

System 2

stationary phase ODS Hypersil (250 × 10 mm, 5 μm, Thermo)
flow rate 3.6 mL/min
detection UV 270 nm
eluent A: 0.1% aqueous formic acid B: acetonitrile
gradient 1

time (min)	0	10	13	17
eluent A (%)	99	99	5	5
eluent B (%)	1	1	95	95

elution compound **1** 7.7 min
compound **2** 8.4 min

gradient 2

time (min)	0	10	13	17
eluent A (%)	94	94	5	5
eluent B (%)	6	6	95	95

elution compound **4** 9.2 min
compound **5** 9.5 min

System 3

stationary phase Microsorb C18 MW 100-5 (250 × 21.2 mm, 5 μm, Varian, Darmstadt, Germany)
flow rate 20.0 mL/min
detection UV 290 nm
eluent A: 0.1% aqueous formic acid B: acetonitrile

gradient

time (min)	3	3	15	17	21
eluent A (%)	93	93	85	5	5
eluent B (%)	7	7	15	95	95

elution compound **3** 7.9 min (crude)System 4

stationary phase Synergi Polar-RP 80A (250×10 mm, 4 μm, Phenomenex, Aschaffenburg, Germany)

flow rate 3.8 mL/min

detection UV 290 nm

eluent A: 0.1% aqueous formic acid B: acetonitrile

gradient

time (min)	0	3	15	18	23
eluent A (%)	95	95	85	5	5
eluent B (%)	5	5	15	95	95

elution compound **3** 9.5 min (pure)System 5

stationary phase ODS Hypersil (250×10 mm, 5 μm, Thermo)

flow rate 4.0 mL/min

detection UV 290 nm

eluent A: 0.1% aqueous formic acid B: acetonitrile

gradient 1

time (min)	0	3	10.5	13.5	18
eluent A (%)	97	97	93	5	5
eluent B (%)	3	3	7	95	95

elution compound **6** 7.0 min

gradient 2

time (min)	0	3	20	25
eluent A (%)	60	60	20	20
eluent B (%)	40	40	80	80

elution compound **34** 11.4 min

Materials and methods

gradient 3

time (min)	0	3	20	25
eluent A (%)	70	70	20	20
eluent B (%)	30	30	80	80

elution compound **35** 14.9 min

System 6

stationary phase Synergi Polar-RP 80A (250×10 mm, 4 μm, Phenomenex, Aschaffenburg, Germany)

flow rate 3.8 mL/min

detection UV 270 nm

eluent A: 0.1% aqueous formic acid B: methanol

gradient

time (min)	0	15	18	23
eluent A (%)	88	88	5	5
eluent B (%)	12	12	95	95

System 7

stationary phase Synergi Polar-RP 80A (250×10 mm, 4 μm, Phenomenex, Aschaffenburg, Germany)

flow rate 3.8 mL/min

detection UV 290 nm

eluent A: 0.1% aqueous formic acid B: methanol

gradient 1

time (min)	0	3	23	26	31
eluent A (%)	85	85	75	5	5
eluent B (%)	15	15	25	95	95

gradient 2

time (min)	0	23	26	31
eluent A (%)	85	85	75	5
eluent B (%)	20	20	95	95

System 8

stationary phase ODS Hypersil (250×10 mm, 5 μm, Thermo)
 flow rate 3.8 mL/min
 detection UV 290 nm
 eluent A: 0.1% aqueous formic acid B: acetonitrile
 gradient 1

time (min)	0	3	13	15	19
eluent A (%)	95	95	8	50	50
eluent B (%)	5	5	10	50	50

elution compound **7** 8.5 min

gradient 2

time (min)	0	3	13	16	20
eluent A (%)	97	97	92	5	5
eluent B (%)	3	3	8	95	95

elution compound **11** 13.0 min
 compound **12** 13.9 min

gradient 3

time (min)	0	13	16	20
eluent A (%)	95	95	5	5
eluent B (%)	5	5	95	95

elution compound **13** 10.5 min

gradient 4

time (min)	0	13	16	20
eluent A (%)	92	92	5	5
eluent B (%)	8	8	95	95

elution compound **14** 9.0 min
 compound **16** 9.6 min
 compound **17** 10.6 min

Materials and methods

gradient 5

time (min)	0	13	16	20
eluent A (%)	90	90	5	5
eluent B (%)	10	10	95	95

elution compound **24** 9.0 min
 compound **25** 10.6 min
 compound **26** 12.2 min

gradient 6

time (min)	0	3	15	17.5	22.5
eluent A (%)	87.5	87.5	82	5	5
eluent B (%)	12.5	12.5	18	95	95

elution compound **27** 10.3 min
 compound **28** 11.4 min
 compound **29** 12.4 min
 compound **30** 13.3 min
 compound **31** 14.8 min

System 9

stationary phase ODS Hypersil (250×10 mm, 5 μm, Thermo)
flow rate 4.2 mL/min
detection UV 256 nm
eluent A: 0.1% aqueous formic acid B: acetonitrile
gradient

time (min)	0	3	15	17	22
eluent A (%)	92	92	90	50	50
eluent B (%)	8	8	10	50	50

elution compound **8** 10.0 min

System 10

stationary phase ODS Hypersil (250×10 mm, 5 μm, Thermo)
flow rate 4.2 mL/min
detection UV 270 nm
eluent A: 0.1% aqueous formic acid B: acetonitrile

gradient

time (min)	0	3	23	25	30
eluent A (%)	92	92	90	50	50
eluent B (%)	3	3	8	50	50

elution compound **9** 15.0 mincompound **10** 18.5 minSystem 11

stationary phase ODS Hypersil (250×10 mm, 5 μm, Thermo)

flow rate 3.8 mL/min

detection UV 260 nm

eluent A: 0.1% aqueous formic acid B: acetonitrile

gradient 1

time (min)	0	13	16	20
eluent A (%)	92	92	5	50
eluent B (%)	8	8	95	95

elution compound **14** 9.3 min

gradient 2

time (min)	0	3	13	16	20
eluent A (%)	95	95	5	5	5
eluent B (%)	5	5	10	95	95

elution compound **18** 12.2 mincompound **19** 14.9 minSystem 12

stationary phase ODS Hypersil (250×10 mm, 5 μm, Thermo)

flow rate 3.8 mL/min

detection UV 276 nm

eluent A: 0.1% aqueous formic acid B: acetonitrile

gradient

time (min)	0	13	16	20
eluent A (%)	90	90	5	5
eluent B (%)	10	10	95	95

elution compound **15** 8.8 min

System 13

stationary phase ODS Hypersil (250×10 mm, 5 μm, Thermo)
 flow rate 3.8 mL/min
 detection UV 236 nm
 eluent A: 0.1% aqueous formic acid B: acetonitrile
 gradient

time (min)	0	13	16	20
eluent A (%)	90	90	5	5
eluent B (%)	10	10	95	95

elution compound **20** 7.3 min
 compound **21** 8.1 min
 compound **22** 9.4 min
 compound **23** 10.1 min

System 14

stationary phase Luna Phenyl-Hexyl (250×21.2 mm, 5 μm)
 flow rate 15.0 mL/min
 detection UV 290 nm
 eluent A: 0.1% aqueous formic acid B: methanol
 gradient 1

time (min)	0	3	21	26
eluent A (%)	50	50	5	5
eluent B (%)	50	50	95	95

gradient 2

time (min)	0	3	23	28
eluent A (%)	30	30	95	95
eluent B (%)	70	70	95	95

elution compound **34** 17.9 min
 compound **35** 19.5 min
 compound **36** and **37** 20.8 min (racemic mixture)

System 15

stationary phase ODS Hypersil (250×10 mm, 5 μm, Thermo)

flow rate 4.2 mL/min
detection UV 290 nm
eluent A: 0.1% aqueous formic acid B: acetonitrile

gradient

time (min)	0	3	18	22
eluent A (%)	70	70	20	20
eluent B (%)	30	30	80	80

elution compound **32** 7.6 min
compound **33** 12.8 min

System 16

stationary phase Lux Cellulose-2 (4.6 × 250 mm, 5 μm, Phenomenex)
flow rate 0.8 mL/min
detection UV 290 nm
eluent A: 0.1% aqueous acetic acid B: methanol

gradient

time (min)	0	3	18	22
eluent A (%)	5	5	0	0
eluent B (%)	95	95	100	100

elution compound **36** 11.2 min
compound **37** 12.4 min

3.11 Spectroscopic methods

3.11.1 Nuclear magnetic resonance spectrometry (NMR)

NMR spectroscopic experiments were conducted on an Avance III 500 MHz spectrometer with a CTCI probe or an Avance III 400 MHz spectrometer with a BBO probe (Bruker, Rheinstetten, Germany). Samples were dissolved in D₂O, methanol-*d*₄, CDCl₃, aceton-*d*₆ or DMSO-*d*₆ (0.03% trimethylsilane (TMS)) (Euriso-Top, Saarbrücken, Germany), transferred to NMR tubes and analyzed at 300 K (500/125 MHz) or 295 K (400/100 MHz). The chemical shift is referenced against TMS, and TOPSPIN (version 1.2 and 2.1, Bruker, Rheinstetten, Germany) is used for data acquisition. ¹H-, ¹³C-, COSY-, HMQC- and HMBC-spectra are generated using standard pulse sequences of the Bruker software library. Interpretation of the obtained spectra is performed with MestReNova (version 5.1.0, Mestrelab Research S.L, Santiago de Compostella, Spain).

3.11.2 Time of flight - mass spectrometry (TOF-MS)

High resolution mass spectra of all the isolated compounds were measured on a Waters Synapt G2-S HDMS mass spectrometer (Waters, Manchester, UK) coupled to an Acquity UPLC core system (Waters, Milford, MA, USA). The measurements are performed with the following system (shown below), and obtained data are processed using MassLnyx 4.1 (Waters).

LC-pump	binary solvent manager, Acquity UPLC core system
LC-degasser	Acquity UPLC core system
LC-auto sampler	sample manager, Acquity UPLC core system
LC-column oven	Acquity UPLC core system
ionization	electrospray ionization (ESI)
calibration	sodium formate (0.5 mmol/L) in 2-propanol:water (9:1, v/v)
lock mass correction	leucine enkephaline ([M+H] ⁺ <i>m/z</i> 556.2771, [M-H] ⁻ <i>m/z</i> 554.2615)
capillary voltage	+2.5kV or -3.0kV
sampling cone	30
extraction cone	4.0
source temperature	150 °C

desolvation temperature	450 °C
cone gas	30L/h
desolvation gas	850L/h
column	BEH C18 (2 × 150 mm, 1.7 μm, Waters, Manchester, UK)
flow rate	0.4 mL/min
injection volume	1–4 μL
column temperature	40 °C
eluent	A: 0.1% formic acid in water B: 0.1% formic acid in acetonitrile

3.11.3 Tandem mass spectrometry (MS/MS)

All of LC-MS/MS experiments were carried out using the following instruments and conditions.

LC system	Acquity UPLC i-class core system (Waters, Milfold, USA)
LC-pump	binary solvent manager, Acquity UPLC core system
LC-degasser	Acquity UPLC core system
LC-auto sampler	sample manager, Acquity UPLC core system
LC-column oven	Acquity UPLC core system
MS-spectrometer	Xevo T-Q-S (Waters, Manchester, UK)
ionization	electrospray ionization (ESI)
scan type	MRM (multiple reaction monitoring)
stationary phase	ACQUITY UPLC BEH phenyl (2.0 × 150 mm, 1.7 μm, Waters, Eschborn, Germany)
capillary voltage	positive mode: 1.5-2.5 kV, negative mode:-2.5kV
sampling cone voltage	12-50 V
source offset	30-50 V
source temperature	150 °C
desolvation temperature	500-600 °C
cone gas	150 L/hour
desolvation gas	850-1000 L/hour
collision gas	0.15-0.25 mL/min
nebulizer gas	7.0 bar

The system 1 was used for identification of compounds **27—37** in pAGE.

System 1

polarity positive (for **27—31**, **33—37**) and negative (for **32**)
 flow rate 0.4 mL/min
 injection volume 1 μ L
 eluents A 0.1% formic acid in water
 B 0.1% formic acid in acetonitrile

gradients

for compounds **27—31**

time (min)	0	7	8	9
eluent A (%)	90	80	1	1
eluent B (%)	10	20	99	99

for compounds **32—37**

time (min)	0	4	4.2	4.8
eluent A (%)	70	40	1	1
eluent B (%)	30	60	99	99

The system 2 was used for identification on compound **8** in the model system.

System 2

polarity positive
 flow rate 0.4 mL/min
 injection volume 1 μ L
 eluents A 0.1% formic acid in water
 B 0.1% formic acid in acetonitrile

gradient

time (min)	0	4	4.1	4.9
eluent A (%)	99	93	1	1
eluent B (%)	1	7	99	99

The system 3 was used for identification on compounds **38—58** in pAGE.

System 3

polarity	positive (for 38—54) and negative (for 55—58)
flow rate	0.4 mL/min
injection volume	1 μ L
eluent	A 0.1% formic acid in water B 0.1% formic acid in acetonitrile

gradients

for compounds **38—41** and **51—54**

time (min)	0	7	8	9
eluent A (%)	99	60	1	1
eluent B (%)	1	40	99	99

for compounds **42—50**

time (min)	0	7	8	9
eluent A (%)	99	50	1	1
eluent B (%)	1	50	99	99

for compounds **55—58**

time (min)	0	9	9.1	9.6
eluent A (%)	88	60	1	1
eluent B (%)	12	40	99	99

The system 4 was used for quantitative analysis on compounds **1, 2, 4—10** in pAGE.

System 4

polarity	positive
flow rate	0.4 mL/min
injection volume	1 μ L
eluent	A 0.1% formic acid in water B 0.1% formic acid in Acetonitrile

gradient

time (min)	0	2.5	3	3.5	4.5
eluent A (%)	99	99	95	1	1
eluent B (%)	1	1	5	99	99

The system 5 was used for quantitative analysis on compounds **16—18**, **22** and **25—26** in pAGE.

System 5

polarity positive
 flow rate 0.4 mL/min
 injection volume 1 μ L
 eluents A 0.1% formic acid in water
 B 0.1% formic acid in acetonitrile

gradient

time (min)	0	3	3.5	4.5
eluent A (%)	95	92	1	1
eluent B (%)	5	8	99	99

The system 6 was used for quantitative analysis on compounds **3**, **11**, **13—15**, **19—21**, **23**, **24** and **26** in pAGE.

System 6

polarity negative
 flow rate 0.4 mL/min
 injection volume 1 μ L
 eluents A 0.1% formic acid in water
 B 0.1% formic acid in acetonitrile

gradient

time (min)	0	3.5	4	5
eluent A (%)	90	80	1	1
eluent B (%)	5	12	99	99

The system 7 was used for quantitative analysis on compounds **38—41** in pAGE.

System 7

polarity	positive
flow rate	0.4 mL/min
injection volume	1 μ L
eluent	A 0.1% formic acid in water B 0.1% formic acid in acetonitrile

gradient

time (min)	0	1	3	3.5
eluent A (%)	99	99	1	1
eluent B (%)	1	1	99	99

The system 8 was used for quantitative analysis on compounds **45—50** in pAGE.

System 8

polarity	positive
flow rate	0.4 mL/min
injection volume	1 μ L
eluent	A 0.1% formic acid in water B 0.1% formic acid in acetonitrile

gradient

time (min)	0	5.0	7.0
eluent A (%)	99	50	50
eluent B (%)	1	50	50

The system 9 was used for quantitative analysis on compounds **51—54** in pAGE.

System 9

polarity	positive
flow rate	0.4 mL/min
injection volume	1 μ L
eluent	A 0.1% formic acid in water B 0.1% formic acid in acetonitrile

gradient

time (min)	0	3.0	3.5
eluent A (%)	70	1	1
eluent B (%)	30	99	99

The system 10 was used for quantitative analysis on compound **55** in pAGE.

System 10

polarity	negative
flow rate	0.4 mL/min
injection volume	1 μ L
eluent A	0.1% formic acid in water
eluent B	0.1% formic acid in acetonitrile

gradient

time (min)	0	9.0	9.1	9.6
eluent A (%)	90	80	1	1
eluent B (%)	12	60	99	99

3.11.4 Circular dichroism spectrometry (CD)

Compounds **15**, **20**, **32—37** were dissolved in methanol or aqueous methanol, and their dilutions were analyzed by means of a Jasco J-810 Spectro polarimeter.

3.11.5 Specific optical rotation

Compounds **27—30** were dissolved in methanol, and their dilutions were analyzed by means of a P-2000 digital polarimeter (Jasco, Gross-Umstadt, Germany).

4. Summary

Controlling the levels of reactive oxygen species (ROS) plays a crucial role in maintaining cellular homeostasis and preventing oxidative stress related diseases like diabetes and cancer. Antioxidants, which are able to reduce elevated level of ROS, are, therefore, considered as crucial micronutrients to maintain health. Although aged garlic extract (AGE) is known for its antioxidative activity, the corresponding key molecules have not yet been fully investigated.

Preliminary studies on the impact of pH value, heating temperature and time, shows that thermal treatment of AGE powder containing 3.5% water at 100 °C for 1 day revealed a significantly increased antioxidant activity (ARS and ORAC tests). Subsequently, activity-guided fractionation of this processed AGE (pAGE) by means of ultrafiltration, MPLC and HPLC in combination with antioxidant testing (ARS, ORAC) was performed to locate, isolate and identify twenty-six antioxidants (compounds **1-26**) in pAGE. Based on an educated guess approach and combined with suitable *in vitro* reactions to model compound transformations in pAGE from the garlic precursors S-allyl-L-cysteine and D-glucose revealed four spiro-alkaloids (**27-30**), a pyrrole derivative (**31**), and six sulfur-containing compounds (**32-37**) as important antioxidants in pAGE. Furthermore, four Amadori compounds (**38-41**), a tetrahydro-carboline (**45**), a series of *N*-phenylpropenoic acid amides (**46-50**), four ethyl esters (**51-54**) and one dilignol (**55**) were confirmed as literature-known antioxidants in AGE by means of UPLC-MS/MS screening. Overall, 52 antioxidants were identified in pAGE, among which 18 antioxidants have not been previously reported (**Figure 97**).

Summary

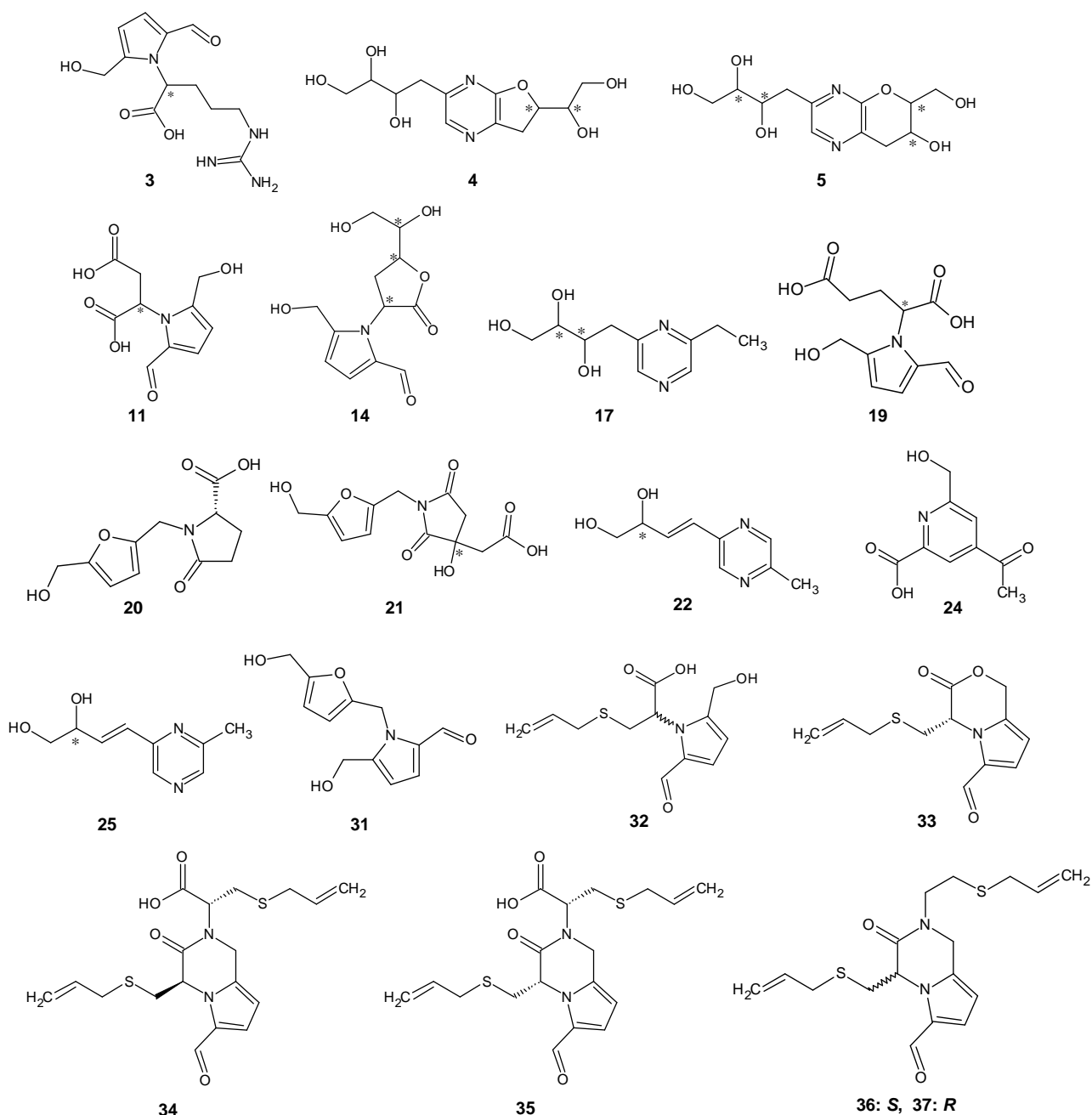


Figure 97. Chemical structures of new antioxidants identified in pAGE.

Among the isolated compounds **1**—**37**, 5-hydroxymaltol (**18**) showed the highest ARS activity ($0.49 \mu\text{mol TE}/\mu\text{mol}$) and ORAC activity ($3.50 \mu\text{mol TE}/\mu\text{mol}$), while the other compounds showed comparative weak ARS activities ($0.18 - 0.01 \mu\text{mol TE}/\mu\text{mol}$) and ORAC activity ($0.72 - 0.01 \mu\text{mol TE}/\mu\text{mol}$), respectively.

Quantitative analysis of the antioxidants in pAGE revealed that the highest concentration of $36090 \mu\text{mol}/\text{kg}$ for 2,3-dihydro-3,5-dihydroxy-6-methyl-4(*H*)-pyran-

4-one (**6**, **Figure 98**), followed by 5-(hydroxymethyl)-1-(2-oxopiperidin-3-yl)-1*H*-pyrrole-2-carbaldehyde (**26**, 7905 $\mu\text{mol/kg}$). Although *N*-phenylpropenoic acid amides (**46-50**) exhibited rather higher antioxidant activities, like as *N-trans*-coumaroyltyramine (**48**) with an ARS activity of 1.83 $\mu\text{mol TE}/\mu\text{mol}$ and an ORAC activity of 6.31 $\mu\text{mol TE}/\mu\text{mol}$, their concentrations in pAGE were rather low and in the range between 0.01 and 2.0 $\mu\text{mol/kg}$. Further quantitative analysis of the compounds **1—37** in pAGE powders heat-treated at various pH-values (pH 4.0, 6.0 and 8.0) revealed that concentrations of the major compounds **6** and **26** could be maximized when AGE was treated for 3h at pH 4 (159.6 mmol/kg) and 12h at pH 8 (12.1 mmol/kg), respectively.

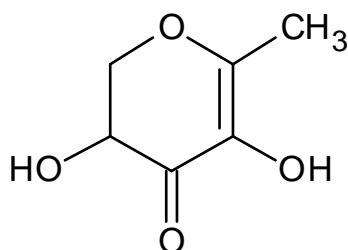


Figure 98. Chemical structure of 2,3-dihydro-3,5-dihydroxy-6-methyl-4(*H*)-pyran-4-one (compound **6**), a major antioxidant in pAGE.

Sensory studies on compounds **27—35** revealed an intrinsic bitter taste of the spiro-alkaloids **27-30** and the pyrrole **31** with taste recognition thresholds between 263 and 785 $\mu\text{mol/kg}$, which is comparable to that of caffeine. The lowest bitter threshold (0.5 $\mu\text{mol/kg}$) was found for (2*R*)-3-(allylthio)-2-[(4*S*)-4-(allylthiomethyl)-6-formyl-3-oxo-3,4-dihydropyrrolo-[1,2-*a*]pyrazin-2(1*H*)-yl] propanoic acid (**35**, **Figure 99**), while its diastereomer **34** were by a factor of 20 less active. As the concentration of compound **35** in pan-fried garlic powder (2.8 $\mu\text{mol/kg}$) were found to exceed its bitter taste threshold by a factor of 5, this antioxidant also was identified as a key contributor to the slight bitter taste of pan-fried garlic powder. While α -{(2-formyl-5-hydroxymethyl)pyrrol-1-yl}-*S*-allylcysteine (**32**) was tasteless in water, this compound enhanced the complexity, mouthfulness and richness of a savory model broth solution above a threshold concentration of 186 $\mu\text{mol/kg}$ (kokumi enhancement). This compound in pan-fried garlic powder exceeded its kokumi threshold by a factor of 4, **32** can be considered a taste modulating compound contributing to the well-known longlasting taste profile of heated garlic powder.

Summary

Moreover, (2*R*)-3-(allylthio)-2-[(4*R*)-4-(allylthiomethyl)-6-formyl-3-oxo-3,4-dihydropyrrolo[1,2-*a*]pyrazin-2(1*H*)-yl]propanoic acid (**34**, **Figure 99**) was found to upregulate gene expression of OH-1 and GCLM encoding antioxidant enzymes in cellular systems, accelerate IgA production in mouse lymphocytes, and suppress IL-6 production in mouse lymphocytes, thus giving first indication for antioxidant, immunomodulatory, and anti-inflammatory activity of compound **34**. In comparison, *S*-allyl-L-cysteine and the diastereomer (**35**) of **34** did not exhibit such biological effects in vitro, thus indicating the absolute configuration of the 2-keto-piperazine moiety in **34** to be crucial for the compound's activities. Compound **34** would be found in highest yields when the AGE was processed at pH 6.0 for 6 h at 100 °C.

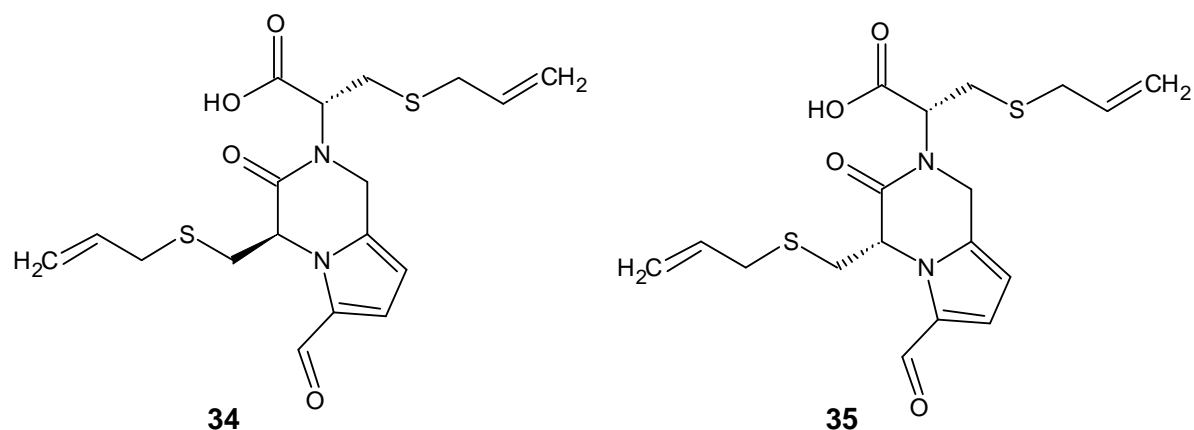


Figure 99. Chemical structures of pharmacologically active compounds **34** and taste active compound **35**.

In summary, 52 compounds have been identified in the pAGE, among which 18 have not been reported in literature before. The data obtained on the antioxidative activity and the activities on the cellular antioxidant system give first insight into potential biological activities of the Maillard-type compounds generated during thermal garlic processing.

5. Cited literature

Allison, G.L.; Lowe, G.M.; Rahman, K. Aged garlic extract and its constituents inhibit platelet aggregation through multiple mechanisms. *J. Nutr.* **2006**, 136 (Suppl), 782S—788S.

Amagase, H.; Petesch, B.L.; Matsuura, H.; Kasuga, S.; Itakura, Y. Intake of garlic and its bioactive components. *J Nutr.* **2001**, 131, 955S—62S.

Anderson, E.J.; Lustig, M.E.; Boyle, K.E.; Woodlief, T.L.; Kane, D.A.; Lin, C.T.; Price, J.W.; Kang, L.; Rabinovitch, P.S.; Szeto, H.H.; Houmard, J.A.; Cortright, R.N.; Wasserman, D.H.; Neufer, P.D. Mitochondrial H₂O₂ emission and cellular redox state link excess fat intake to insulin resistance in both rodents and humans. *J. Clin. Invest.* **2009**, 119, 573—581.

Bae, E.S.; Cho, Y.S.; Won, D.Y.; Lee, H.S.; Park, J.H. A comparative study of the different analytical methods for analysis of S-allylcysteine in black garlic by HPLC. *LWT* **2012**, 46, 532—535.

Bae, E.S.; Cho, Y.S.; Won, D.Y.; Lee, H.S.; Park, J.H. Changes in S-allyl cysteine contents and physicochemical properties of black garlic during heat treatment. *LWT* **2014**, 46, 397—402.

Bersuker, B.I.; Dimoglo, S.A.; Gorbachov, Y.M.; Greni, I.A.; Vysotskaya, E.L.; Mikhailova, V.T. Study of the electronic and structural properties of the chemical compounds in garlic aroma. *Die Nahrung.* **1989**, 33(5), 405—411.

Block, E.; Ahmad, S.; Jain, M.K.; Crecely, R.W.; Apritz-Castro, R.; Cruz, M.R. (*E,Z*)-Ajoene: a potent antithrombotic agent from garlic. *J. Am. Chem. Soc.* **1984**, 106, 8295—8296.

Block, E.; Ahmad, S.; Catalfamo, J.L.; Jain, M.K.; Apritz-Castro, R. The chemistry of alkyl thiosulfinate esters. 9 antithrombotic organosulfur compounds from garlic: structural, mechanistic, and synthetic studies. *J. Am. Chem. Soc.* **1986**, 108, 7045—7055.

Bloem, E.; Haneklaus, S.; Schnug, E. Influence of fertilizer practices on S-containing metabolites in garlic (*Allium sativum* L.) under field conditions. *J. Agric. Food Chem.* **2010**, 58, 10690—10696.

Borrero, N.V.; Aponick, A. Total synthesis of acortatarin A using a Pd(II)-catalyzed spiroketalization strategy. *J. Org. Chem.* **2012**, 77, 8410—8416.

Cao, G.; Alessio, H.M.; Cutler, R.G. Oxygen-radical absorbance capacity assay for antioxidants. *Free Radical Biol. Med.* **1993**, 14 (3), 303—311.

Cavallito, C.; Bailey, J. Allicin, the antibacterial principle of *Allium sativum*. L. Isolation, physical properties and antibacterial action. *J. Am. Chem. Soc.* **1944**, 66, 1950—1951.

Chen, X.M.; Kitts, D.D. Antioxidant activity and chemical properties of crude and fractionated Maillard reaction products derived from four sugar-amino acid Maillard reaction model systems. *Ann. N.Y. Acad. Sci.* **2008**, 1126, 220—224.

Chen, X.M.; Kitts, D.D. Correlating changes that occur in chemical properties with the generation of antioxidant capacity in difference sugar-amino acid maillard reaction models. *J. Food Sci.* **2011a**, 76(6), 831—837.

Chen, X.M.; Kitts, D.D. Anioxidant and anti-inflammatory ektivities of Maillard reaction products isolated from sugar-amino acid model systems. *J. Agric. Food Chem.* **2011b**, 59(20), 11294—11303.

Chen, X.M.; Kitts, D.D. Identification and quantification of α -dicarbonyl compounds produced in differencnt sugar-amino acid Maillard reaction model systems. *Food Res. Int.* **2011c**, 44(9), 2775—2782.

Chen, X.M.; Kitts, D.D. Characterization of antioxidant and anti-inflammatory activities of bioactive fractions recovered from a glucose-lysine Maillard reaction model system. *Mol. Cell. Biochem.* **2012**, 364, 147—157.

Chen, X.M.; Liang, N.; Kitts, D.D. Chemical properties and reactive oxygen and nitrogen species quenching activities of dry sugar-amino acid maillard reaction mixtures exposed to baking temperatures. *Food Res. Int.* **2015**, *76*, 618–625.

Colin-Gonzalez, A.L.; Santana, R.A.; Silva-Islas, C.A.; Chanez-Cardenas, M.E.; Santamaria, A.; Maldonado, P.D. The antioxidant mechanisms underlying the aged garlic extract- and S-allylcysteine-induced protection. *Oxid. Med. Cell. Longevity*, **2012**, Article ID 907162, 16 pages.

Das, I.; Khan, NS.; Sooranna, SR. Potent activation of nitric oxide synthase by garlic: a basis for its therapeutic applications. *Curr. Med. Res. Opin.* **1995**, *13*, 257–63.

Dittrich, R.; El-Massry, F.; Rinaldi, F.; Peich, C.C.; Beckmann, M.W.; Pischetsrieder, M. Maillard reaction products inhibit oxidation of human low-density lipoproteins in vitro. *J. Agric. Food Chem.* **2003**, *51*, 3900–3904.

Dunkel, A.; Koester, J.; Hofmann, T. Molecular and sensory characterization of γ -glutamyl peptides as key contributors to the kokumi taste of Edible beans. *J. Agric. Food Chem.* **2007**, *55*, 6712–6719.

Dunkel, A.; Hofmann, T. Sensory-directed identification of β -alanyl dipeptides as contributors to the thick-sour and white-meaty orosensation induced by chicken broth. *J. Agric. Food Chem.* **2009**, *57*, 9867–9877.

Edris, E. A.; Fadel, M. H. Investigation of the volatile aroma components of garlic leaves essential oil. Possibility of utilization to enrich garlic bulb oil. *Eur. Food Res. Technol.* **2002**, *214*, 105–107.

Fenwick, G.R.; Hanley, A.B. The genus *Alium*. Part 1. *Crit. Rev. Food Sci. Nutri.* **1985**, *22*, 199–271.

Floegel, A.; Kim, D.O.; Chung, S.J.; Koo, S.I.; Chun, O.K. Comparison of ABTS/DPPH assays to measure antioxidant capacity in popular antioxidant-rich US foods. *J. Food Comp. Anal.* **2011**, *24* (7), 1043–1048.

Frank, O.; Hofmann, T. Characterization of key chromophores formed by nonenzymatic browning of hexoses and L-alanine by using the colour activity concept. *J. Agric. Food Chem.* **2000**, 48, 6303—6311.

Gobert, J.; Glomb, M.A. Degradation of glucose: Reinvestigation of reactive α -dicarbonyl compounds. *J. Agric. Food Chem.* **2009**, 57, 8591—8597.

Guo, J.L.; Feng, Z.M.; Yang, Y.J.; Zhang, Z.W.; Zhang, P.C. Pollenopyrroside A and B, novel pyrrole ketohexoside derivatives from bee-collected *Brassica campestris* pollen. *Chem. Pharm. Bull.* **2010**, 58, 983—985.

Quiroz-Florentino, H.; Aguilar, R.; Santoyo, B.M.; Diaz, F.; Tamariz, J. Total syntheses of natural furan derivatives rehmanones A, B, and C. *Synthesis* **2008**, 7, 1023—1028.

Higuchi, O.; Tateshita, K.; Nishimura, H. Antioxidative activity of sulfur-containing compounds in *Allium* species for human low-density lipoproteine (LDL) oxidation in vitro. *J. Agric. Food Chem.* **2003**, 51, 7208—7214.

Hofmann, T.; Schieberle, P. Evaluation of the key odorants in a thermally treated solution of ribose and cysteine by aroma extract dilution. *J. Agric. Food Chem.* **1995**, 43, 2187—2194.

Hofmann, T.; Schieberle, P. Flavor contribution and formation of the intense roast-smelling odorants 2-propionyl-1-pyrroline and 2-propionyltetrahydropyridine in Maillard-type reactions. *J. Agric. Food Chem.* **1998**, 46, 2721—2726.

Hofmann, T.; Bors, W.; Stettmaier, K. Studies on radical intermediates in the early stage of the nonenzymatic browning reaction of carbohydrates and amino acids. *J. Agric. Food Chem.* **1999**, 47, 379—390.

Hofmann, T. Taste-active Maillard reaction products. The “tasty” world of nonvolatile Maillard reaction products. *Ann. N.Y. Acad. Sci.* **2005**, 1043, 20—29.

Hwang, I.G.; Kim, H.Y.; Woo, K.S.; Lee, S.H.; Lee, J.; Jeong, H.S. Isolation and identification of antioxidant DDMP from heated pear (*Pyrus pyrifolia Nakai*). *Prev. Nutr. Food Sci.* **2013**, *18*(1), 76–79.

Ichikawa, M.; Ryu, K.; Yoshida, J.; Ide, N.; Yoshida, S.; Sasaoka, T.; Sumi S. Antioxidant effects of tetrahydro-beta-carboline derivatives identified in aged garlic extract. *Biofactors* **2002**, *16* (3-4), 57–72.

Ide, N.; Lau, B.H. Aged garlic extract attenuates intracellular oxidative stress. *Phytomedicine* **1999**, *6* (2), 125–131.

Imai, J.; Ide, N.; Nagae, S.; Moriguchi, T.; Matsuura, H.; Itakura, Y. Antioxidant and radical scavenging effects of aged garlic extract and its constituents. *Planta Med.* **1994**, *60* (5), 417–420.

Jung, S.E.; Park, H.S.; Choi, K.E.; Ryu, H.B.; Park, H.B.; Kim, S.D.; Kim, G.Y.; Chae, W.S. Reduction of blood lipid parameters by a 12-wk supplementation of aged black garlic: A randomized controlled trial. *Nutrition* **2014**, *30*, 1034–1039.

Jadhav, H.; Pedersen, C.M.; Solling, T.; Bols, M. 3-Deoxy-glucosone is an intermediate in the formation of furfurals from D-glucose. *Chem. Sus. Chem.* **2011**, *4*, 1049–1051.

Kim, H.E.; Jung, Y.E.; Kang, H.D.; Chang, J.U.; Hong, H.Y.; Suh, J.H. Physical stability, antioxidative properties, and photoprotective effects of a functionalized formulation containing black garlic extract. *J. Photoch. Photobio. B* **2012**, *117*, 104–110.

Kim, M.O.; Baltes, W. On the role of 2,3-dihydro-3,5-dihydroxy-6-methyl-4(*H*)-pyran-4-one in the Maillard reaction. *J. Agric. Food Chem.* **1996**, *44*, 282–289.

Kim, S.B.; Chang, B.Y.; Hwang, B.Y.; Kim, S.Y.; Lee, M.K. Pyrrole alkaloids from the fruits of *Morus alba*. *Bioorg. Med. Chem. Lett.* **2014**, *24*(24), 5656–5659.

Kim, S.B.; Ahn, B.; Kim, M.; Ji, H.J.; Shin, S.K.; Hong, I.P.; Kim, C.Y.; Hwang, B.Y.; Lee, M.K. Effect of *Cordyceps militaris* extract and active constituents on metabolic parameters of obesity induced by high-fat diet in C58BL/6J mice. *J. Ethnopharmacol.* **2014**, *151*, 478–484.

Koch, H.P.; Lawson, L.D. Garlic: The science and therapeutic application of *Allium sativum* L. and related species. *Baltimore: Williams and Wilkins*, **1996**, second edition, pp.1–329.

Kosuge, T.; Tsuji, K.; Nukaya, H.; Terada, A.; Ochiai, M.; Wakabayashi, K.; Nagao, M.; Sugimura, T. 5-Hydroxymaltol, a mutagenic substance in glucose pyrolysate. *Agric. Biol. Chem.* **1983**, *47*(4), 881–883.

Kwon, K.B.; Yoo, S.J.; Ryu, D.G.; Yang, J.Y.; Rho, H.W.; Kim, J.S.; Park, J.W.; Kim, H.R.; Park, B.H. Induction of apoptosis by diallyl disulfide through activation of caspase-3 in human leukemia HL-60 cells. *Biochem. Pharmacol.* **2002**, *63*, 41–47.

Labuza, T.P.; Saltmarch, M. Kinetics of broqing and protein quality lose in whey powders during steady state and nonsteady state storage conditions. *J. Food Sci.* **1981**, *47*, 92–96.

Lancaster, J.E.; Shaw, M.L. γ -Glutamyl peptides in the biosynthesis of S-alk(en)yl-l-cysteine sulphoxides (flavour precursors) in *Allium*. *Phytochemistry* **1989**, *28* (2), 455–460.

Lee, R.Y.; Lee, K.Y.; Hwang, G.I.; Lee, J.Y.; Woo, S.K.; Han, S.C.; Kim, S.E.; Joeng, S.H. Optimization of the processing conditions for heated garlic juice by response surface methodology. *J. Food Sci. Nutr.* **2008**, *13*, 334–339.

Li, M.; Xiong, J.; Huang, Y.; Wang, L.J.; Tang, Y.; Yang, G.X.; Liu, X.H.; Wei, B.G.; Fan, H.; Zhao, Y.; Zhai, W.Z.; Hu, J.F. Xylapyrrosides A and B, two rare sugar-morpholine spiroketal pyrrole-derived alkaloids from *Xylaria nigripes*: isolation, complete structure elucidation, and total syntheses. *Tetrahedron* **2015**, *71*, 5285–5295.

Lindenmeier, M.; Faist, V.; Hofmann, T. Structural and functional characterization of pronyl-lysine, a novel protein modification in bread crust melanoidins showing in vitro antioxidative and phase I / II enzyme modulating activity. *J. Agric. Food Chem.* **2002**, 50, 6997—7006.

Livak, K.J.; Schmittgen T.D. Analysis of relative gene expression data using real-time quantitative PCR and the 2^{-ΔΔC(T)} method. *Methods* **2001**, 25, 402-408.

Magaletta, R.L.; Ho, C.H. Effect of roasting time and temperature on the generation of nonvolatile (polyhydroxyalkyl)pyrazine compounds in peanuts, as determined by high-performance liquid chromatography. *J. Agric. Food Chem.* **1996**, 44, 2629—2635.

Mitsukawa, K.; Sato, Y.; Yoshida, T.; Nagasawa, T. Oxidation of heterocyclic and aromatic aldehydes to the corresponding carboxylic acids by *Acetobacter* and *Serratia* strains. *Biotechnol. Lett.* **2004**, 26, 1643—1648.

Montano, A.; Casado, F.J.; de Castro, A.; Sánchez, A.H.; Rejano, L. Vitamin content and amino acid composition of pickled garlic processed with and without fermentation. *J. Agric. Food Chem.* **2004**, 52, 7324—7330.

Nakagawa, S.; Kasuga, S.; Matsuura, H. Prevention of liver damage by aged garlic extract and its components in mice. *Phytother. Res.* **1989**, 3 (2), 50—53.

Nakagawa, S.; Masamoto, K.; Sumiyoshi, H.; Kunihiro, K.; Fuwa, T. Effect of raw and extracted-aged garlic juice on growth of young rats and their organs after peroral administration. *J. Toxicol. Sci.* **1980**, 5 (1), 91—112.

Niki, E.; Noguchi, N.; Tsuchihashi, H.; Gotoh, N. Interaction among vitamin C, vitamin E, and β-carotene. *Am. J. Clin. Nutr.* **1995**, 62, 1322S—6S.

Niki, E. Assessment of antioxidant capacity in vitro and in vivo. *Free Radic. Biol. Med.* **2010**, 49, 503—515.

Nishimura, H.; Fujiwara, K.; Mizutani, J.; Obata, Y. Volatile flavor components of caucas. *J. Agric. Food Chem.* **1971**, *19*, 992—994.

Omar, S.H.; Ai-Wabel, N.A. Organosulfur compounds and possible mechanism of garlic in cancer. *Saudi Pharm. J.* **2010**, *18* (1), 51—58.

Olsson, K.; Pernemalm, P.; Theander, O. Formation of aromatic compounds from carbohydrates. VII. Reaction of D-glucose and glycine in slightly acidic aqueous solution. *Chem. Informationsdienst.* **1978**, *9*, 249—256.

Ottinger, H.; Hofmann, T. Identification of the taste enhancer alapyridaine in beef broth and evaluation of its sensory impact by taste reconstitution experiments. *J. Agric. Food Chem.* **2003**, *51*, 6791—6796.

Ou, B.; Hampsch-Woodill, M.; Prior, R.L. Development and validation of an improved oxygen radical absorbance capacity assay using fluorescein as the fluorescent probe. *J. Agric. Food Chem.* **2001**, *49* (10), 4619—4626.

Owusu-Ansha, E.; Banerjee, U. Reactive oxygen species prime *Drosophila* hematopoietic progenitors for differentiation. *Nature* **2009**, *461*, 537—541.

Papageorgiou, C.; Corbet, J.P.; Menezes-Brandao, F.; Pecegueiro, M.; Benezra, C. Allergic contact dermatitis to garlic (*Allium sativum* L.). Identification of the allergens: the role of mono-, di-, and trisulfides present in garlic. A comparative study in man and animal (guinea-pig). *Arch. Dermatol. Res.* **1983**, *275* (4), 229—234.

Packer, J.E.; Slater, T.F.; Willson, R.L. Direct observation of a free radical interaction between vitamin E and vitamin C. *Nature* **1979**, *278*, 737-745.

Qidwai, W.; Qureshi, R.; Hasan, S.N.; Azam, S.I. Effects of dietary garlic (*Allium Sativum*) on blood pressure in humans: a pilot study. *J Pak. Med. Assoc.* **2000**, *50*, 204—7.

Re, R.; Pellegrini, N.; Proteggente, A.; Pannala, A.; Yang, Min.; Catherine, R.E. Antioxidant activity applying an improved ABTS radical cation decolorization assay. *Free Radic. Biol. Med.* **1999**, 26, 1231—1237.

Rystov, L.; Chadwick, R.; Krock, K.; Wang, T. Simultaneous determination of Maillard reaction impurities in memantine tablets using HPLC with charged aerosol detector. *J. Pharm. Biomed. Anal.* **2011**, 56, 887—894.

Ryu, K.; Ide, N.; Matsuura, H.; Itakura, Y. $N\alpha$ -(1-Deoxy-D-fructos-1-yl)-L-arginine, an antioxidant compound identified in aged garlic extract. *J. Nutr.* **2001**, 131 (3), 972S—976S.

Sakai, K.; Matsumoto, K.; Nishikawa, T.; Suefuji, M.; Nakamaru, K.; Hirashima, Y.; Kawashima, J.; Shirotani, T.; Ichinose, K.; Brownlee, M.; Araki, E. Mitochondrial reactive oxygen species reduce insulin secretion by pancreatic beta-cells. *Biochem. Biophys. Res. Commun.* **2003**, 300, 216—222.

Sasaki, J.; Lu, C.; Machiya, E.; Tanahashi, M.; Hamada, K. Processed black garlic (*Allium sativum*) extracts enhance anti-tumor potency against mouse tumors. *Med. Aromat. Plant Sci. Biotechnol.* **2007**, 1, 278—281.

Sato, E.; Kohno, M.; Hamano, H.; Niwano, Y. Increased anti-oxidative potency of garlic by spontaneous short-term fermentation. *Plant Food Hum. Nutr.* **2006**, 61, 157—160.

Sendl, A.; Schliack, M.; Loser, R.; Stanislaus, F.; Wagner, H. Inhibition of cholesterol synthesis in vitro by extracts and isolated compounds prepared from garlic and wild garlic. *Atherosclerosis* **1992**, 94, 79—85.

Sonntag, T.; Kunert, C.; Dunkel, A.; Hofmann, T. Sensory-guided identification of N-(1-methyl-4-oxoimidazolidin-2-ylidene)- α -amino acids as contributors to the thick-sour and mouth-drying orosensation of stewed beef juice. *J. Agric. Food Chem.* **2010**, 58, 6341—6350.

Souci Fachmann Kraut, 1991, Wissenschaftliche Verlagsgesellschaft GmbH Stuttgart

Stark, T.D.; Matsutomo, T.; Loesch, S.; Boakye, P.A.; Balemba, O.B.; Pasilis, S.P.; Hofmann, T. Isolation and structure elucidation of highly antioxidative 3,8"-linked biflavanones and flavanone-C-glycosides from *Garcinia buchananii* bark. *J. Agric. Food Chem.* **2012**, 60, 2053—2062.

Stark, T.D.; Mathias, S.; Flank, O.; Balemba, O.B.; Wakamatsu, J.; Hofmann, T. Isolation and structure elucidation of highly antioxidative 3,8"-linked biflavanones and flavanone-C-glycosides from *Garcinia buchananii* bark. *J. Nat. Prod.* **2015**, 78, 234—240.

Steiner, M.; Kham, A.H.; Holbert, D.; Lin, R. A double-blind crossover study in moderately hypercholesteremic men that compared the effect of aged garlic extract and placebo administration on blood lipids. *Am. J. Clin. Nutr.* **1996**, 64 (6), 866—870.

Sudhakar, G.; Kadam, V.D.; Bayya, S.; Pranitha, G.; Jagadeesh, B. Total synthesis and stereochemical revision of acortatarins A and B. *Org. Lett.* **2011**, 13(20), 5452—5455.

Sumiyoshi, H.; Kanezawa, A.; Masamoto, K.; Harada, H.; Nakagami, S.; Yokota, A.; Nishikawa, M.; Nakagawa, S. Chronic toxicity test of garlic extract in rats. *J. Toxicol. Sci.* **1984**, 9 (1), 61—75.

Sumiyoshi, H.; Wargovich, M.J. Chemoprevention of 1,2-dimethylhydrazine induced colon cancer in mice by naturally occurring organosulfur compounds. *Cancer Res.* **1990**, 50 (16), 5084—5087.

Surmont, R.; Verniest, G.; Kimpe, N.D. Short synthesis of the seed germination inhibitor 3,4,5-trimethyl-2(5H)-furanone. *J. Org. Chem.* **2010**, 75(16), 5750—5753.

Sundaram, S. G.; Milner, J. A. Diallyl disulfide suppresses the growth of human colon tumor cell xenografts in athymic nude mice. *J. Nutr.* **1996a**, 126, 1355–1361.

Sundaram, S. G.; Milner, J. A. Diallyl disulfide inhibits the proliferation of human tumor cells in culture. *Biochim. Biophys. Acta.* **1996b**, 1315, 15–20.

Szatrowski, T.P.; Nathan, C.F. Production of large amounts of hydrogen peroxide by human tumor cells. *Cancer Res.* **1991**, 51, 794–798.

Tahara, EB.; Navarete, FD.; Kowaltowski, AJ. Tissue-, substrate-, and sitespecific characteristics of mitochondrial reactive oxygen species generation. *Free Radical Biol. Med.* **2009**, 46(9), 1283-1297.

Tate, S.; Meister, A. Glutamyl transpeptidase: catalytic, structural and functional aspects. *Mol. Cell Biochem.* **1981**, 39, 357–368.

Toelstede, S.; Hofmann, T. Sensomics mapping and identification of the key bitter metabolites in Gouda cheese. *J. Agric. Food Chem.* **2008a**, 56, 2795–2804.

Toelstede, S.; Hofmann, T. Quantitative studies and taste reengineering experiments toward the decoding of the nonvolatile sensometabolome of Gouda cheese. *J. Agric. Food Chem.* **2008b**, 56, 5299–5307.

Tong, X.G.; Zhou, L.L.; Wang, Y.H.; Xia, C.; Wang, Y.; Liang, M.; Hou, F.F.; Cheng, Y.X. Acortatarin A and B, two novel antioxidative spiroalkaloids with a naturally unusual morpholine motif from *Acorus tatarinowii*. *Org. Lett.* **2010**, 12, 1844–1847.

Ueda, Y.; Sakaguchi, M.; Hirayama, K.; Miyajima, R.; Kimizuka, A. Characteristic flavor constituents in water extract of garlic. *Agric. Biol. Chem.* **1990**, 54(1), 163–169.

Ueda, Y.; Tsubuku, T.; Miyajima, R. Composition of sulfur-containing components in onion and their flavor characters. *Bosci. Biotech. Biochem.* **1994**, 58(1), 108—110.

Voigt, M.; Glomb, M.A. Reactivity of 1-deoxy-D-erythro-hexo-2,3-diulose: A key intermediate in the maillard chemistry of hexoses. *J. Agric. Food Chem.* **2009**, 57, 4765—4770.

Voigt, M.; Smuda, M.; Pfahler, C.; Glomb, M.A. Oxygen-dependent fragmentation reactions during the degradation of 1-deoxy-D-erythro-hexo-2,3-diulose. *J. Agric. Food Chem.* **2010**, 58, 5685—5691.

Volk, G.M.; Henk, A.D.; Richards, C.M. Genetic diversity among US garlic clones as detected using AFLP method. *J. Am. Soc. Hortic. Sci.* **2004**, 129 (4), 559—569.

Wang, D.; Feng, Y.; Liu, J.; Yan, J.; Wang, M.; Sasaki, J. Black garlic (*Allium sativum*) extracts enhance the immune system. *Med. Aromat. Plant Sci. Biotechnol.* **2010**, 4, 37—40.

Wang, Y.C.; Zhang, Y.W.; Zheng, L.H.; Bao, Y.L.; Wu, Y.; Yu, C.L.; Huang, Y.X.; Sun, L.G.; Zhang, Y.; Jia, X.J.; Li, Y.X. Four new alkaloids from the fermentation broth of *Armillaria mellea*. *Helv. Chim. Acta.* **2013**, 96, 330—337.

Wang, P.; Kong, F.; Wei, J.; Wang, Y.; Wang, W.; Hong, K.; Zhu, W. Alkaloids from the mangrove-derived actinomycete *Jishengella endophytica* 161111. *Mar. Drugs* **2014**, 12, 477—490.

Weinberg, D.S.; Manier, M.L.; Richardson, M.D.; Haibach, F.G. Identification and quantification of organosulfur compliance markers in a garlic extract. *J. Agric. Food Chem.* **1993**, 41 (1), 37—41.

West, A.P.; Brodsky, I.E.; Rahner, C.; Woo, D.K.; Erdjument-Bromage, H.; Tempst, P.; Walsh, M.C.; Choi, Y.; Shadel, G.S, Ghosh, S. TLR signalling augments macrophage bactericidal activity through mitochondrial ROS. *Nature*. 2011, 472, 476—480.

Yaylayan, V.A.; Keyhani, A. Origin of carbohydrate degradation products in L-alanine/D-[13C]glucose model systems. *J. Agric. Food Chem.* **2000**, 48, 2415-2419.

Yeh, Y.Y.; Liu, L. Cholesterol-lowering effect of garlic extracts and organo-sulfur compounds: human and animal studies. *J. Nutr.* **2001**, 131 (3), 989S—993S.

Yehye, W.A.; Rahman, N.A.; Ariffin, A.; Abd Hamid, S.B.; Alhadi, A.A.; Kadir, F.A.; Yaeghoobi, M. Understanding the chemistry behind the antioxidant activities of butylated hydroxytoluene (BHT): A review. *Eur. J. Med. Chem.* **2015**, 101, 295—312.

Yoshimura, Y.; Iijima, T.; Watanabe, T.; & Nakazawa, H. Antioxidative effect of Maillard reaction products using glucose glycine model system. *J. Agric. Food Chem.* **1997**, 45, 4106—4109.

Xiao, Y.; Wang, Y.L.; Gao, S.X.; Sun, C.; Zhou, Z.Y. Chemical composition of *Hydrilla verticillata* (L.f.) royle in Taihu lake. *Chinese J. Chem.* **2007**, 25, 661—665.

Yu, Z.; Zhao, M.; Liu, F.; Zeng, S.; Hu, J. Identification of 2,3-dihydro-3,5-dihydroxy-6-methyl-4H-pyran-4-one as a strong antioxidant in glucose-histidine Maillard reaction products. *Food Res. Int.* **2013**, 51, 397—403.

Zhang, J.; Perry, G.; Smith, M.A.; Robertson, D.; Olson, S.J.; Graham, D.G.; Montine, T.J. Parkinson's disease is associated with oxidative damage to cytoplasmic DNA and RNA in substantia nigra neurons. *Am. J. Pathol.* **1999**, 154, 1423—1429.

Cited literature

Other references

imnews. Available from

http://imnews.imbc.com/replay/nwtoday/article/2778803_5782.html.

Accessed 15.01.11.

Production and trade statistics. Rome, Italy: FAO, **2013**.